THE NATIONAL PRECIPITATION RESEARCH PROGRAMME

FINAL REPORT
1990 - 1992

by

G. K. Mather
CloudQuest (Pty) Ltd

and

D. E. Terblanche
South African Weather Bureau

Report to the
Water Research Commission
Pretoria

March, 1993

WRC Report No. 133/8/93
ISBN 1 874858 96 9

THE NATIONAL PRECIPITATION RESEARCH PROGRAMME

FINAL REPORT
1990 - 1992

by

G. K. Mather
CloudQuest (Pty) Ltd

and

D. E. Terblanche
South African Weather Bureau

Report to the
Water Research Commission
Pretoria

March, 1993

WRC Report No. 133/8/93
ISBN 1 874858 96 9

TABLE OF CONTENTS

LIST OF TABLES

LIST OF FIGURES

1. EXECUTIVE SUMMARY

The central objective of the research carried out by the National Precipitation Research Programme (NPRP) has been to evaluate the potential for beneficial modification of summertime convective rainfall. It has been estimated that local water demand will exceed the total available supply around the year 2020. Rainfall augmentation, if feasible, has been identified as an attractive source of good quality water.

The search for rainfall augmentation opportunities must begin with a comphrehensive study of the natural rainfall processes. This has been accomplished in the study areas using sophisticated meteorological radars and instrumented aircraft. These studies have recognized that many of the region's convective storms are inefficient in terms of rainfall production, i.e. only about 30 percent of the atmospheric water vapour entering the storms reaches the ground as precipitation. Thus, the search for augmentation opportunities has centred around a means of increasing rainfall production efficiency. The research has also recognized the efficiency of rainfall formation via a collision-coalescence process which has been shown to occur in certain storms in both the Carolina and Bethlehem study areas. Observations in storms growing over a Kraft paper mill west of Nelspruit raised the possibility that coalescence could be enhanced or accelerated by the addition of hygroscopic nuclei into the storm updraft at cloud base. To investigate the efficiency of hygroscopic nuclei, a hygroscopic cloud seeding flare was designed and manufactured by Swartklip Products, Cape Town. Racks for the flares were designed, constructed and mounted on the aft end of the engine nacelles of one of the project's Commander 690s. Each rack holds a total of 10 flares, which are electrically ignited from switches in the cockpit. Initial seeding trials were so promising that a formal randomized seeding experiment was designed with the aid of the Applied Statistics group at UNISA after one season of trials.

At this point, the strong prospect that pursuit of the hygroscopic seeding approach might accelerate progress towards the goal of developing a viable cloud seeding technology, caused the discontinuation of experiments with dry ice as a seeding material. The dry ice pulse seeding experiment, designed to confirm elements of seeding hypotheses based on previous research at Bethlehem and Nelspruit, had by then produced only promising but as yet inconclusive results.

The results of the hygroscopic randomized seeding experiment show statistically significant increases in radar-measured rainfall after just one experimental season. To our knowledge, no formal convective cloud seeding experiment has ever shown significant increases in rainfall after a single season's experimentation. We believe this new approach to convective cloud seeding can be hailed as a breakthrough in the field of weather modification.

Verifying the efficiency of the new hygroscopic seeding flare required the coordination and application of skills and knowledge that have taken years to develop. The complete report contains many examples of the application of these skills. Coordinating two aircraft, the seeding and the cloud physics sampling aircraft on an experimental storm within range of a project radar is but one example of the exercise of these skills. The knowledge required to analyse and interpret the acquired radar data and cloud physics measurements is another. The in-house skills required to maintain, and when required, to update the hardware and software that is the core of the data gathering capability is yet another. It is the acquired depth of this knowledge and these skills that has bred the confidence required to embark on a novel and, we believe, a more appropriate approach to cloud seeding in South Africa.

The hygroscopic seeding hypothesis which has been formulated should be relatively easily verified by a combination of microphysical and radar measurements supported by numerical cloud models. An additional season of the randomized cloud seeding experiment should supply sufficient additional experiments to reinforce the conclusions of the statistical studies.

The primary objectives set by the contract covering the past 3 years of research were to:

- investigate both natural and artificially modified precipitation process in multicellular convective clouds and to gain a better understanding of the physical mechanisms of precipitation development in the larger cloud systems

- use the knowledge gained to identify those conditions in which precipitation efficiency may be increased by intervention

- develop a viable technology that can be applied operationally to artificially enhance rainfall.

The first two of these objectives have been addressed with a considerable measure of success. Results to date support the contention that, with the new hygroscopic approach to convective cloud modification, the third objective also is well on the way to being accomplished. The ultimate test of the viability of this new technology will be an area experiment in which the first deliberate attempts to produce more rainfall on the ground will be objectively evaluated.

The planning of this next stage should start immediately, and should proceed in parallel with the seeding experiment and further observational and modelling studies. Many of the methodologies required for an area experiment are already in place, having been developed through the NPRP as well as independent research. For instance, rapid progress is being made

with the accurate measurement of rainfall over an area with a calibrated meteorological radar. Catchment modelling studies geared to assessing the impacts of cloud seeding on water resources are well under way. Societal impact studies are indicating that a major public relations effort in and around a chosen experimental area should be an integral part of early planning for the area experiment.

The users of a potentially successful rain augmentation technology must be drawn into the planning from the outset. These include Forestry, Water Affairs and Agriculture. Their participation will be required in the design of the experiment, to specify the measurements (rain gauges, stream flow, radar etc) and the confidence levels that they will require before recommending the use of the technology as an effective means of augmenting South Africa's water resources.

2.0 THE NATIONAL PRECIPITATION RESEARCH PROGRAMME

2.1 Introduction - a historical review

The purpose of this historical review is to place in perspective the aims, procedures and achievements of the National Precipitation Research Programme (NPRP) during the contract period 1990 to 1992. Consolidation of rainfall augmentation research in South Africa was achieved in early 1990 by the amalgamation of the Bethlehem and Nelspruit research projects under the NPRP banner.

Research at Bethlehem and Nelspruit had since 1983 been focussed on the search for a rain augmentation hypothesis, which if successfully tested, would lead to the ability to augment South Africa's water resources by putting more water on the ground. Initially, the research was led by results from major research programmes overseas, mainly in the United States. These well-designed projects were evaluated by a combination of physical measurements and sophisticated experimental techniques using the randomized allocation of treatment. The experimental hypotheses dictated the anticipated outcome, which was clearly stated before the experiment commenced. Any statistical result had to be supported by physical measurements, using instrumented aircraft and radars. There were two favoured hypotheses. The Florida Area Cumulus Experiment (FACE) was based on the dynamic seeding concept, the theory that massive seeding of convective clouds with artificial ice nuclei, in this case silver iodide, would lead to increased buoyancy through the sudden release of the heats of fusion, deposition and condensation, thereby producing taller, wider and longer lasting clouds (Simpson, 1980).

The second hypothesis rested on the assumption that there are insufficient precipitation embryos in the supercooled regions of convective clouds, which results in an inefficient natural precipitation formation process. The introduction of additional precipitation embryos via glaciogenic seeding was expected to redress this deficiency. This hypothesis was thoroughly tested in isolated cumulus congestus clouds in the HIPLEX I experiment in the United States (Mielke et al., 1984) and at Bethlehem in South Africa (Kraus et al., 1987). In both experiments, massive increases in ice crystals were documented, but the linkage between increases in precipitation embryos and more rainfall at cloud base was missing. Measurements in the experimental clouds showed that the available supercooled water was being lost to entrainment (cloud air mixing with dry environmental air) before the artificially produced precipitation embryos had reached their riming threshold, i.e. grown large enough to collect the available supercooled water droplets. Both experiments concluded that future convective cloud experiments should move upscale to the larger, isolated convective complexes where entrainment would not be such an impediment.

The Nelspruit dry ice seeding experiment commenced 1 October, 1984, (Programme for Atmospheric Water Supply, 1990) and chose the isolated convective complex as the experimental unit. Since it was not clear what response to seeding (if any) could be expected from convective complexes, the Nelspruit experiment was designed to test for radar-measured differences between seeded and control storms. In this sense, the experiment was exploratory, since response variables were not specified before the experiment commenced.

There are two mechanisms which produce precipitation embryos, or graupel in the supercooled regions of convective clouds. The first involves the growth of ice crystals via vapour diffusion followed by riming growth, the freezing of supercooled water droplets on the surfaces of the ice crystals. This mechanism was well documented in both the HIPLEX and Bethlehem experiments. In the second, drizzle drops grow by coalescence, which is the collection of smaller cloud droplets via collisions with a few larger drops. If these freeze, then growth continues via the riming process. This second mechanism can be a more efficient precipitation growth process than the ice crystal mechanism because of the greater density of the frozen drop (0.9 g/cm^3 versus 0.2 for ice crystals). The presence and importance of the coalescence growth mechanism was recognized and documented using the cloud physics Learjet at Nelspruit and a simple classification technique developed, based upon cloud base temperature and potential cloud buoyancy, which appears to adequately separate clouds in which ice crystal growth dominates from those in which precipitation is initiated via the coalescence or coalescence-freezing mechanism (Mather et al., 1986). This thermodynamic classification technique was used to stratify the storms collected during the Nelspruit dry ice seeding experiment, eliminating those storms from the radar data base which were unlikely to develop precipitation via the coalescence process. The analysis with this partitioned data set revealed significant and physically realistic differences between the seeded and control storm groups. These differences were consistent with a seeding hypothesis based on an observation by Braham (1964) that drops growing via coalescence will grow faster by riming if they can be frozen by the seeding. The design, analysis and results of the Nelspruit dry ice seeding experiment are fully reported in Mather (1991).

The next step was to run a confirmatory dry ice seeding experiment at Nelspruit, in which the anticipated response variables were specified in advance. This experiment was interrupted after the Review Workshop on Rainfall Stimulation Research in South Africa, held in the Kruger Park in August 1989. Expert overseas scientists at this workshop asserted that unless the physical mechanisms responsible for the apparent radar-inferred increases in rainfall were understood, the results of any number of confirmatory experiments would not be accepted. It was at this stage that the Nelspruit and Bethlehem research groups were amalgamated and the research continued under the

banner of the NPRP, the aims of which are set out below (Section 2.2). The Nelspruit and Bethlehem research bases remained unaltered, operations being conducted from whichever base showed the most potential for storm development. The combined group has made good progress, including the in-house development of hardware and software for radar and aircraft systems. One of the major initial thrusts of the NPRP was to attempt to clarify certain of the postulated mechanisms whereby dry ice seeding led to apparently enhanced precipitation development. For this purpose, the pulse seeding experiments were designed and executed in 1989/90 and 1990/91. More specifically, this was an attempt to resolve the links in the chain of events between the creation of massive amounts of ice crystals at seeding levels and more rainfall on the ground.

The experiment yielded interesting, but inconclusive results. Regretfully, the experiment was abandoned prematurely in favour of an intensive research effort in what was proving to be a much more promising direction; the possible early enhancement of precipitation growth via coalescence through hygroscopic seeding. This alteration of the course of rain augmentation research by the NPRP was prompted by a chance event on 20 December 1988. A storm selected during the normal course of the dry ice seeding experiment departed so radically from what experience had taught us to expect, that some explanation had to be found for the apparent anomalous behaviour of this storm. Huge drops were encountered at the penetration level ($-10^{o}C$), indicating an active coalescence precipitation formation mechanism. Subsequent analyses showed that this unusual storm was growing over a Kraft paper mill west of Nelspruit. Follow-on measurements in cumuli growing near the paper mill showed a broadening of the cloud-drop spectra caused by the hygroscopic material in the emissions from the mill stacks. It was the broadening of the spectra at cloud base that was leading to the enhanced coalescence observed at the $-10^{o}C$ level (Mather, 1991). These observations led to the development of a hygroscopic seeding flare. The idea was to free the research from the geographical restraints of the paper mill, allowing experiments on selected clouds anywhere within the experimental area. Although the flare output is small compared to the paper mill, the hope was that placing the hygroscopic material at exactly the right place and at the right time would compensate for this deficit.

Trial seeding experiments with the new flares commenced in October 1990. These trials were so promising that a randomized experiment was designed and initiated just a year later in October 1991. This experiment was designed and evaluated with the help of the Centre of Applied Statistics at UNISA. The anticipated response variable, rain flux, was specified in advance. A total of 51 experiments were conducted, 21 in the Bethlehem area and 30 around Carolina. This experiment reached acceptable levels of statistical significance in a single season! Contrast this result with that of the dry ice seeding experiment which took three seasons to reach acceptable levels of

statistical significance and then only after the radar data had been partitioned using the coalescence criterion. It was the excitement generated by these results that led to the termination of the dry ice pulse seeding experiment.

The hygroscopic seeding hypothesis is already on firmer ground than the dry ice seeding equivalent. Future work will concentrate on filling in the remaining gaps in this new hypothesis and on strengthening the statistical analysis by continuing with the randomized seeding experiment.

In summary, work at Nelspruit and Bethlehem identified the inefficient rainfall formation process in the convective storms that bring most of the rainfall to the eastern Transvaal and Free State. To redress this inefficiency, attempts have been focussed on placing more and larger precipitation embryos into the strong updraft regions of these storms, to collect more of the available supercooled water before it is swept up into the large anvil clouds that are a characteristic of the summertime skies in the region. At this stage, the most promising method of increasing precipitation efficiency appears to be the addition of hygroscopic nuclei to the updraft feeding the storm at cloud base.

For this reason, it was generally agreed by all those directly involved with the NPRP that the decision to prematurely terminate experimentation with dry ice and concentrate on hygroscopic seeding was fully justified. The results achieved during the course of the dry ice pulse seeding experiments will nevertheless be documented in Section 4.

2.2 Aims of the NPRP

The primary objectives of the rainfall stimulation research project are:

(a) To investigate both natural and artificially modified precipitation processes in multicellular convective clouds and to attain a better understanding of the physical mechanisms of precipitation development in the larger cloud systems.

(b) To use the knowledge gained in (a) to identify those environmental (synoptic) conditions in which the precipitation efficiency of larger cloud systems may be increased by human intervention, should there be any reason to believe that the natural processes are inefficient at times.

To achieve these objectives the following broad research avenues have been identified:

1. Comprehensive field studies to document the fundamental cause and effect relationships during each step of the physical chain of events, in natural and artificially modified clouds, in order to quantify the physical processes and develop an adequate physical understanding of such processes.

2. Numerical cloud modelling to provide a framework for comparisons between observations and theory, and to test and/or refine an underlying hypothesis. Computer technology is now available to develop sophisticated models to test the concepts of rainfall stimulation. Laboratory, theoretical and numerical modelling studies should go hand-in-hand with the field studies.

3. Development and application of technology, instrumentation and data handling systems to ensure that measurements and analytical capabilities are adequate for needed field and modelling studies. Since research is at the forefront of science, developments overseas will have to be monitored diligently and where necessary, incorporated locally with the minimum of delay. For this reason, it is extremely important for the relatively small local research team to interact regularly with researchers in other parts of the world.

4. Development of local expertise in every facet of the research should be a primary goal at all stages of the research effort.

2.3 Personnel

The personnel employed at each site are listed in Tables 2.0 and 2.1. The many skills and disciplines that are required to pursue the programme's objectives become evident after a quick scan of these tables. Meteorological skills must be supplemented by knowledge of radars, computers and sophisticated measuring systems including laser imaging probes. Software must be developed to analyse the outputs from the radars and aircraft measuring systems. These data must be processed and stored in easily accessible data bases.

Statistical techniques must then be employed to assess the significance of the measurements. The assistance of Professor Francois Steffens at UNISA has been elicited for this purpose. The group at UNISA is also consulted about the design of any experiments, especially those that include randomization in their design.

A qualitative rather than a quantitative advantage of the consolidation of the two projects has emerged. The youthful and enthusiastic Bethlehem group blends well with the older, more experienced Nelspruit group. Also, a comparison of past research efforts indicates that both groups have been moving in roughly the same direction. This sharing of common goals has meant that the combined group has been able to agree on plans for future research with much more confidence.

Table 2.0 List of Bethlehem Personnel

Personnel		Responsibilities
D. Terblanche	-	project leader and research director
F. Adam	-	assistant project leader
E. Loftus	-	pilot and aircraft data
F. Hiscutt	-	aircraft and radar systems development
S. Edwards	-	aircraft instrumentation, calibration and development
K. de Waal	-	computers and system software
Z. Botha	-	software development
H. Pienaar	-	radar and radar data
G. van de Hoven	-	forecasting, mesonetwork, surface and upper air observations
H. Ihlenfeldt		
D. Wannenburg		
R. Bindeman		
J. McKerry		
E. Visser		
T. Maseko		
A. Navarro	-	administration
L. Masangana	-	assistant
I. Malan	-	rainfall
S. Mokoena	-	assistant
G. Corroyer	-	aircraft maintenance
P. Mokoena	-	assistant

Table 2.1 List of Nelspruit Personnel

Personnel		Responsibilities
G. Mather	-	project leader and pilot
R. Parsons	-	deputy project leader, pilot, radar analysis software and data base
F. van der Westhuizen	-	chief pilot, surface rain gauge network
C. Wightman	-	pilot, aircraft analysis software and data bases
K. Young	-	electronics engineer, project radars and computers
P. McNaught	-	electronics technician, project radars
I. Ross	-	electronics technician, aircraft instrumentation systems
E. Botha	-	Nelspruit-Weather Bureau computer link, rain gauge data collection, software development
M. Schormann	-	temporary assistant, software development, radar and aircraft
M. Dreyer	-	secretary and comptroller
J. Segage	-	driver
P. Ngobeni	-	site maintenance

2.4 Equipment

The combined equipment of both projects makes an impressive list, making the NPRP one of the best equipped convective cloud research group in the world. A partial list of this equipment follows:

- Learjet 24, instrumented for cloud physics research, has a dry ice seeding capability

- turboprop Aero Commander 690 (JRA), instrumented for cloud physics research and rainfall measurements at cloud base

- turboprop Aero Commander 690 (JRB), instrumented for cloud physics research, has a dry ice seeding capability and is equipped with wing racks for end-burning flares

- Aero Commander 500S (IZN) instrumented for making measurements of rainfall at cloud base, also has an isokinetic particle sampling capability

- twin Commanche, at this stage used for communication flights

- 5 cm meteorological radar with a 1^{o} beam width and volume scan capabilities (Bethlehem)

- a second 5 cm meteorological radar with 1.6^{o} beam width, volume and sector scan capabilities (Carolina)

- mesoscale network of rain gauges and automatic weather stations

- upper air sounding equipment at both sites

- aircraft maintenance and hangar facilities.

Each radar is supported by a computer system which displays, digitizes and records the reflected radar signals. Each radar tracks the project aircraft, displaying (for purposes of control) and recording the position of the aircraft. Each aircraft is equipped with a computer which displays and records the aircraft measurements. Both the radar and aircraft data must be further processed and stored in data bases by large computers. The data bases are accessed for study purposes by cloud physicists at both sites. In the process, valuable analysis software is created.

During the course of experiments, measurements from the data bases are extracted and sent to statisticians at UNISA for analysis.

These data bases are a valuable scientific asset for South Africa since they describe in detail the radar and microphysical climatology of clouds in the Bethlehem and Nelspruit areas.

(a) The Bethlehem Radar

The 5 cm Enterprize radar at Bethlehem was converted to PC based antenna control, data acquisition and storage during the past three years. The prototype designs in this system were upgraded during the past year and the present system is summarized below.

The upgrade to a PC based system was done to replace the Enterprize DVIP for the acquisition real-time display and storage of data by a more flexible system. The hardware based antenna scan sequence was also replaced with a flexible software controlled system and data storage moved from 9 track tapes to miniature video cassettes. The whole system is an improvement on the original system as it uses the latest high speed digital technology, and it is easily upgradable and flexible.

The PC based system and its interfaces with the radar are shown schematically in Figure 2.0.

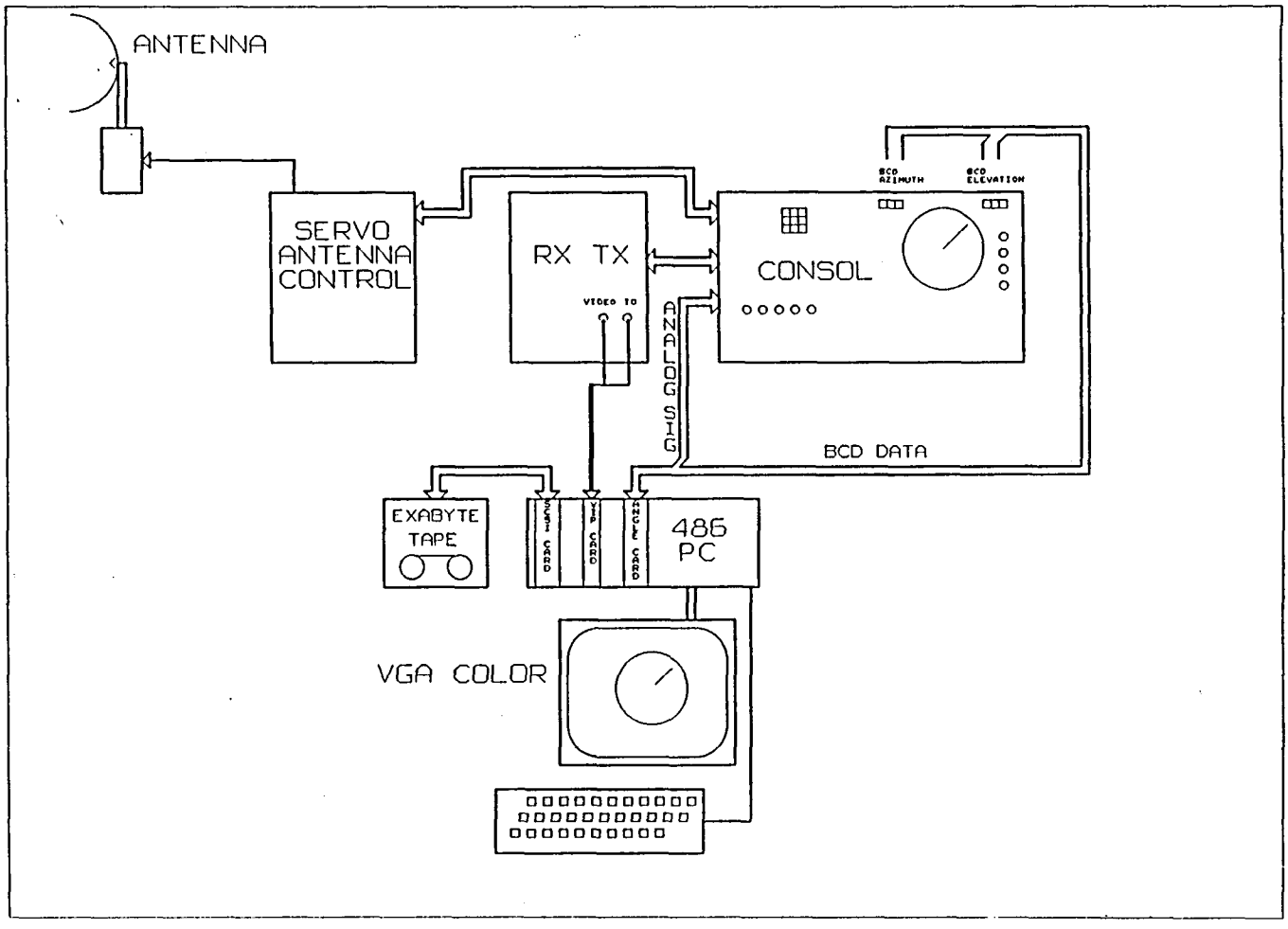

Fig.2.0 PC based system and its interfaces with the radar.

(i) DVIP board

The DVIP interface is a high speed 16 bit ISA bus DSP based Digital Video Integrator Processor card customized for acquisition of radar video data.

The card is capable of a sample rate of up to 1.25 mHz of 12 bit data and performs a real-time integration in range and azimuth producing a 16 bit averaged Bin buffer.

The card is fully user programmable and configurable for sample rate, bin size, integrations per bin and other setup parameters via a 16 bit port between the PC and DSP bus. High speed memory chips and FIFO buffers are implemented to store and prepare the Bin data for downloading to the PC bus.

The card accepts a TRIGGER and VIDEO Input signal from the radar system. The DVIP digitizes the video signal in sync with the master trigger from the radar and when a full buffer of integrated data is available an interrupt is generated signalling the PC to unload the data. The card has 32k words of memory and 4k words of FIFO buffering organized in a ping-pong fashion.

An on-card communications chip allows direct connection to external systems such as Transputers and other DSP based systems. The card uses only 4 I/O ports on the PC bus and makes use of interrupts and I/O to signal when data are ready for unloading into PC memory.

The interface can occupy any expansion slot in a PC AT 286, 386 or 486 compatible computer enclosure and is jumper and dip switch configurable allowing several cards in one system.

A simplified diagram of this card is shown in Figure 2.1.

(ii) Angle board

This PC based interface makes use of a closed loop digital to analogue system which allows the main programme to position the radar antenna to an accuracy of 0.1^{o} in elevation. The present azimuth and elevation position in BCD is read into the PC via this card. The card outputs an analogue signal to the servo driver of the antenna.

The amplitude of this analogue signal is determined by the difference between the present elevation position and the required elevation position. This results in a fast slew in antenna elevation with minimal overshoot. After reaching the required elevation the closed loop system maintains this elevation without main programme intervention.

Figure 2.2 shows the main features of this card.

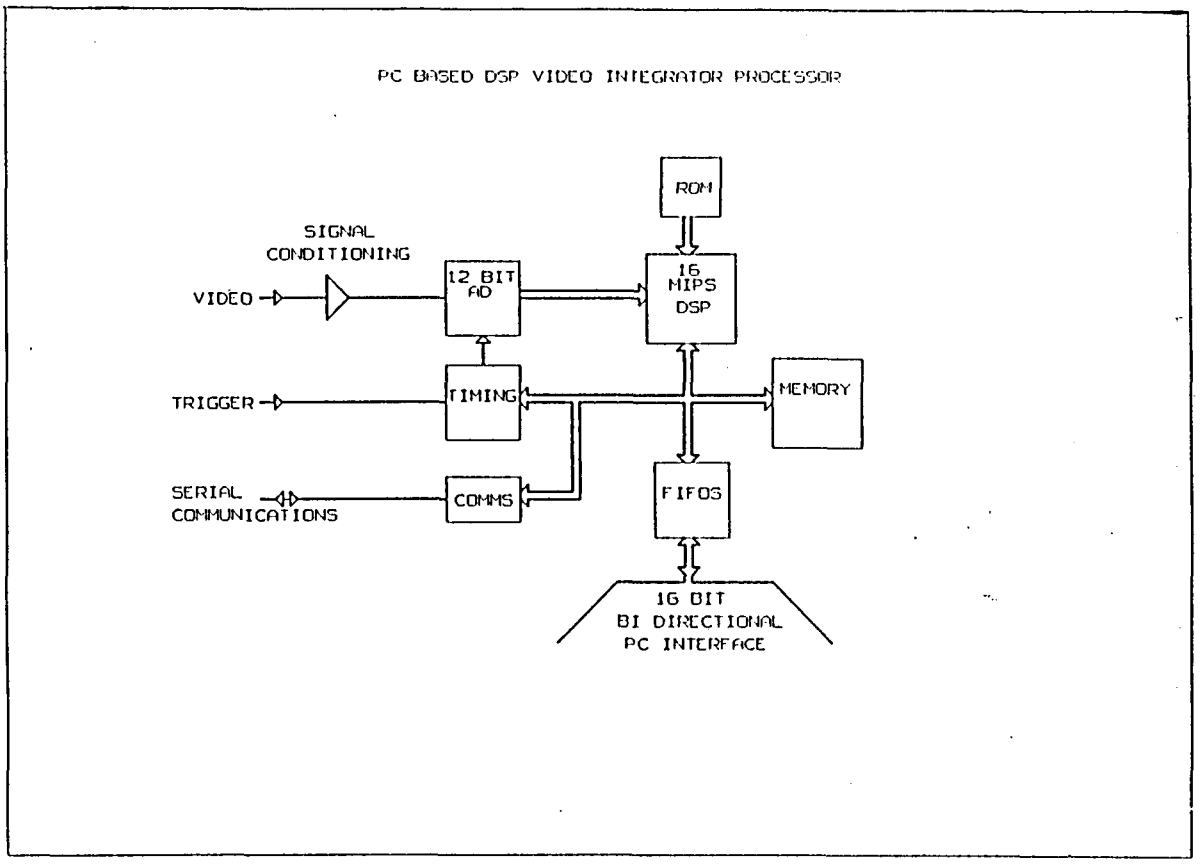

Fig. 2.1 Simplified diagram of DVIP board.

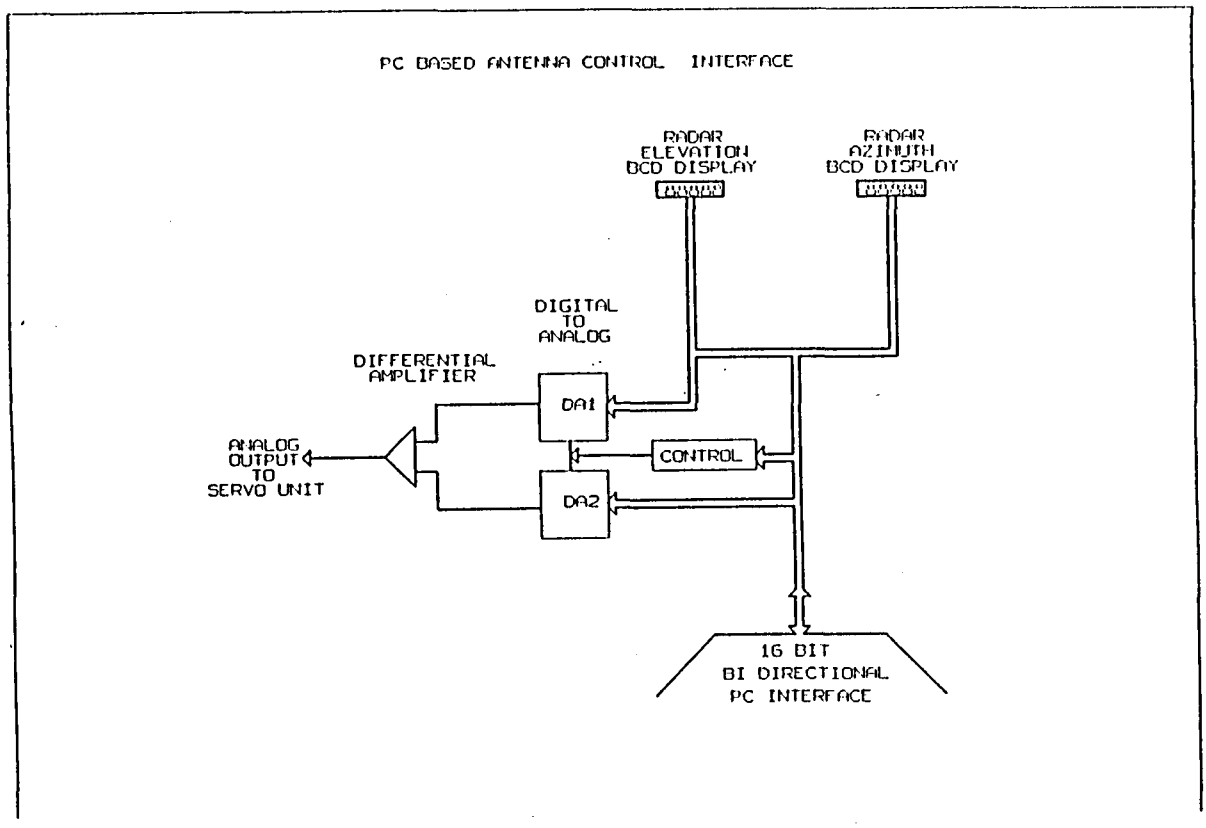

Fig. 2.2 Simplified diagram of angle board.

(iii) Data storage

Data are stored in real-time on miniature video cassette tape by a helical scanning technique on an Exabyte Cassette Tape System. Each cassette can store 2.3 Gigabytes of data allowing extended sustained operation. The Exabyte is interfaced to the PC via a Small Computer System Interface.

As drivers are not commercially available, they were developed to enable real-time data transfer from the PC to Exabyte and error monitoring.

(iv) General

Upon initiation the main radar programme reads a configuration file to set up all the site specific parameters and uploads configuration parameters to the DVIP card for sample rate, bin size, number of bins and number of integrations per bin.

The main programme sends the base scan elevation to the angle board which slews the antenna to this elevation. As soon as this elevation is reached, the main programme starts the DVIP process. Once the DVIP has collected 8 rays (8 PRF pulses) of data it generates an interrupt signalling to the PC that data are available for unloading. The PC will then unload the data into memory and onto Exabyte tape. These data are stored with a header containing date, time, elevation, azimuth, etc. The data in memory are processed for display purposes by the main program.

While the PC is processing and storing the data the DVIP card accumulates the next block of data resulting in a multi-tasking acquisition system which prevents data loss.

The antenna rotation speed is set such that 8 rays of bin data represents 1° of rotation. Once data from 360° have been collected the main program puts the DVIP card in a hold state and slews the antenna via the angle board to the next elevation in the configuration file. This whole process is repeated until the maximum required elevation is reached. On completion of this elevation, the antenna is slewed down to the base scan. This process, producing a complete volume scan, takes about 4 minutes.

(b) The Carolina Radar

Repairing the Carolina radar and site after the fire in early January, 1991 proved to be a major effort. All electronic equipment had to be removed and taken to Johannesburg for cleaning because of smoke damage. Advantage was taken of an opportunity to purchase a full set of critical spare parts for the Carolina radar from a sister radar that was being scrapped in the United States. This will significantly prolong the useful life of this radar.

The Carolina radar was off line from January 14 to March 4, 1991. The combined resources of the NPRP meant that the research could continue, shifting to the Bethlehem area, using the Bethlehem radar, which became operational at the beginning of January, 1991.

(c) Radar software

New software was developed for controlling the Bethlehem radar (in azimuth and elevation), for recording antenna position, radar and aircraft returns on an Exabyte tape recorder. Also developed was software for displaying the low level scan and project aircraft tracks on a colour VGA monitor in almost real time. As the antenna steps up from the lowest scan, the display of this scan is held on the VGA monitor, but the positions of the aircraft are updated each scan so the radar operator has a history of all aircraft tracks. The display is refreshed each time the radar completes a volume scan.

The basic operating, recording and display software are in place. Future plans included manufacturing common boards for both radars and implementing a real-time storm tracking scheme.

The Nelspruit radar analysis software was transferred to Bethlehem. Initially, the first part of the analysis was completed and recorded on magnetic tape at Bethlehem. This tape was then sent to Nelspruit for storm track analysis and display and storage in a radar database. By mid 1991 all storm analyses and displays could be accomplished at Bethlehem. Identical radar data bases for both radars are currently held at both sites. Plans for updating this software include the use of new storm tracking software that is being developed at NCAR by Mike Dixon who was also responsible for installing the original tracking software at Nelspruit in 1983.

(d) Aircraft measuring systems

The new PC based aircraft instrumentation system was installed in both JRA and JRB. New permanent racks to house the hardware, built locally, were installed. It should be emphasized that this system, which includes boards for the laser probes (an FSSP board and a 2D board), analogue to digital converters, a computer, an Exabyte tape recorder, analogue filters and surge protectors and displays has been designed and built in-house. Fig. 2.3 shows the results of a test in which the output from the FSSP probe was fed to the new interface and to the PMS data acquisition system in parallel. There is no discernable difference between the two outputs. These achievements mean that the NPRP has achieved a major goal; almost complete self-sufficiency in terms of hardware and software. Products in use that need outside support receive this support locally. All aircraft will eventually be converted to this new instrumentation

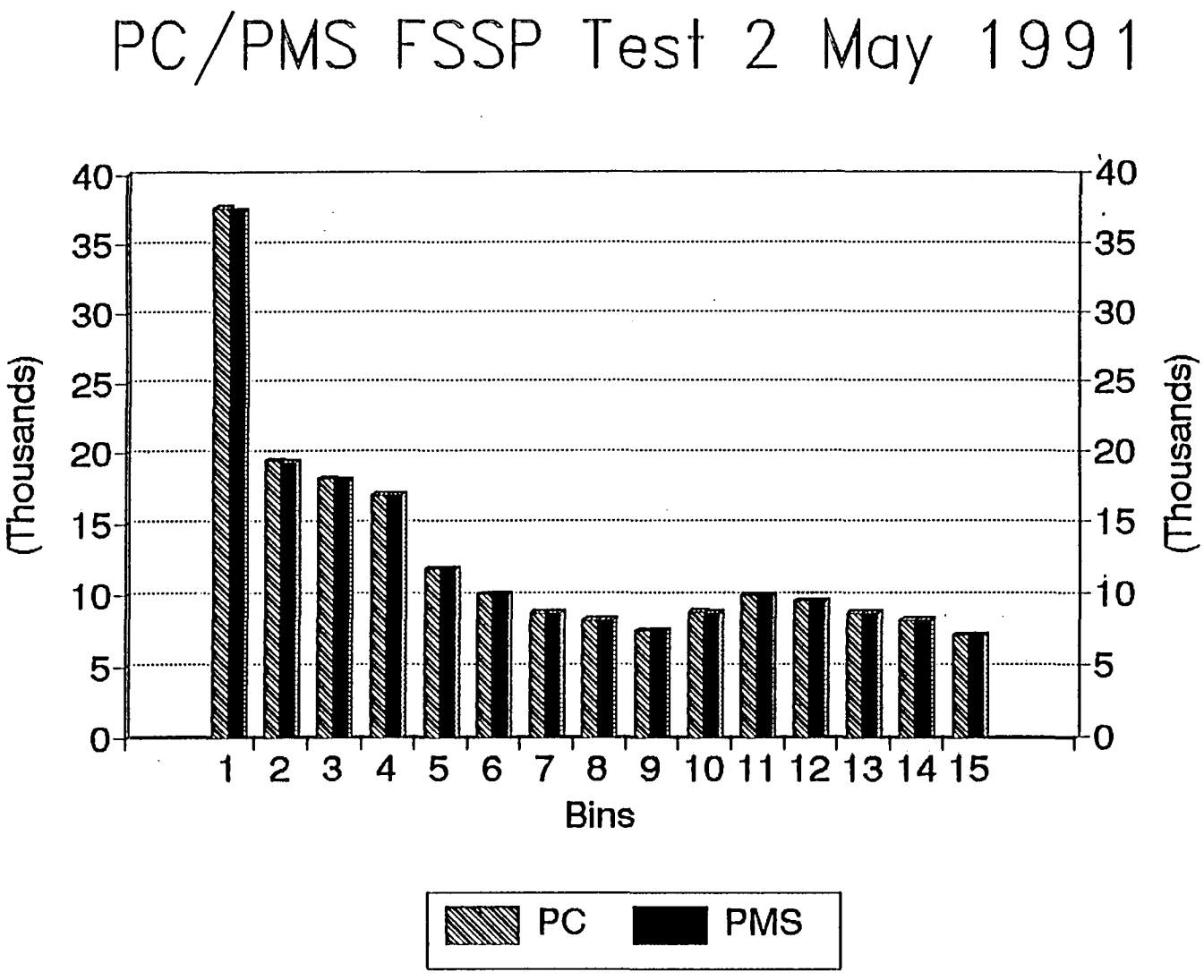

Fig. 2.3 Results from a test in which the output from an FSSP probe was fed in parallel into a PMS commercial data acquisition system and an interface developed in-house. Comparisons in all 15 bins are excellent.

system. A detailed description of aircraft measurements is provided in Appendix 1.

The new hardware requires new software. Software has been developed for recording and displaying in real time chosen variables measured by the aircraft system. Aircraft data analysis and display software is being developed at Bethlehem. At this stage, there are large differences between the aircraft analysis and display hardware at Bethlehem and Nelspruit. These differences are expected to blur as time passes but it is unlikely that the software will ever become identical, since the aircraft measure different variables with different instruments.

(e) Mesoscale network

The Bethlehem mesoscale network of 50 automatic weather stations has been reduced to 12, which are kept operational for monitoring surface conditions in the project area and for transferring data to Central Forecasting. The reasons for this reduction are :

- the 10 year old Diel data loggers and several of the sensors have reached the stage where spares are no longer available

- the NPRP has defined other priorities and staff transfers had to be made

- the limited use of data from the network no longer warranted the cost of its upkeep.

3.0 RADAR/RAIN GAUGE COMPARISONS OF RAINFALL MEASUREMENTS

(a) Introduction

There is a need to begin to consider the design of an area rainfall augmentation experiment, in anticipation of a successful outcome from the current seeding experiments. It is unlikely that an area rainfall experiment will be conducted over an area of less than 10 000 km^2. The most likely statistical design will be random seeding of the target area using the rainfall day or part of a rainfall day as the evaluation unit, or a design using two areas with highly correlated rainfalls for the experiment, choosing randomly one of the areas for treatment and using the other as a control. In any event, the measurement of rainfall, upon which the evaluation of the experiment will depend, will have to be measured as accurately as possible. There are two accepted methods of measuring rainfall over an area; with recording rain gauges, or using a well-calibrated meteorological radar. The problem with gauges is the number required to adequately measure rainfall over an area of 10^4 km^2. Work in Florida (Woodley et al., 1975) indicates that a gauge density of 143 km^2 per gauge would be required to measure the rainfall over an area of that size, i.e. roughly 70 evenly spaced gauges. The logistics of setting up, servicing and taking readings from a gauge network of this size would be formidable.

The use of radar also presents problems, but of a different sort. It seems necessary to prove that rainfall measured aloft by radar corresponds closely to rainfall measured on the ground. This is the purpose of this study.

Studies over the past 30 years have all shown poor correlations between radar and gauge measurements of precipitation. These correlations also seem to be relatively insensitive to the rain rate (R) to reflectivity (Z) relationships used in the analyses. It should be clear by now that these poor correlations are not going to be solved by a 'better' Z-R relationship. What is required is the following:

- accept the low correlation in comparisons of radar and gauge estimates of rainfall as an inherent characteristic of such comparisons

- try to understand the origins and properties of the variability

- develop approaches for handling the comparisons based upon this understanding (Smith and Cain, 1983).

Hodson (PAWS - Phase 2, 1987-1989 Vol. 3) has thoroughly studied this subject and concludes that agreement between measurements aloft and gauge measurements at the ground is only possible when the area-time integral of the rain is compared aloft and at the ground.

This approach is followed here, in a four-season comparison between radar and rain gauge measurements of rainfall from a 1000 km^2 area west of Ermelo.

(b) Measurements

Fig. 3.0 shows the location of the network and its distance from radar. Fig. 3.1 is a close-up of the 20 gauge network. Each gauge is assumed to adequately sample the rainfall for each area shown and each area is about 50 km^2 for a total network area of 1000 km^2. The gauges have a resolution of 0.25 mm (one tip) and total tips are recorded at 5 minute intervals on solid state recorders mounted inside the gauge housing.

(c) Results

The results of measurements over four seasons are summarized in Table 3.0. The familiar Marshall-Palmer relationship was used to convert the measurement of effective radar reflectivity, Z_e, into rainfall,

where $Z_e = 200\ (R)^{1.6}$
R = rain rate (mm/hr)
Z_e = effective radar reflectivity (mm^6/m^3).

The unit used in the following comparisons is a partial rain day. It started when the radar was turned on and ended when the radar was turned off. The biggest discrepancy between the gauges and the radar occurred on December 1, 1989. Cumulative totals of gauge/radar rainfall amounts up to this day are within 100 ktons of each other (28360 versus 28453). A scan-by-scan analysis of December 1 shows that the discrepancy between the gauge and radar measurements of rainfall was caused by attenuation of the radar beam by storms between the radar and the gauge network. Successive lines of storms on this day moving in from the southwest moved over the gauge network, then between the gauge network and the radar, blocking the radar view over the gauges. For example, Fig. 3.2 (a) shows the low level (1.5^o) scan for 15:31. Fig. 3.2 (b) shows the rain rates recorded by the network between 15:25 and 15:30. Only those equivalent radar reflectivities that are greater than 30 dBz are displayed. Rain rates of 3, 6 and 9 mm/hr correspond to reflectivities of 30.6, 35.5 and 38.3 dBz respectively using the Marshall-Palmer relationship of $Z = 200\ (R)^{1.6}$. While the correspondence between radar echo and rainfall looks reasonable over the northern edge of the network, there is a complete absence of echo over the southwestern part of the network, where rain rates of 5 mm/hr (35.5 dBz) were recorded by the gauges. The radar was not seeing storms that were breaking out over the network behind the squall line.

Cumulative gauge totals are commenced again on December 4, 1989. The cumulative totals are close until December 6, 1990 when another attenuation event takes place. The exercise is repeated

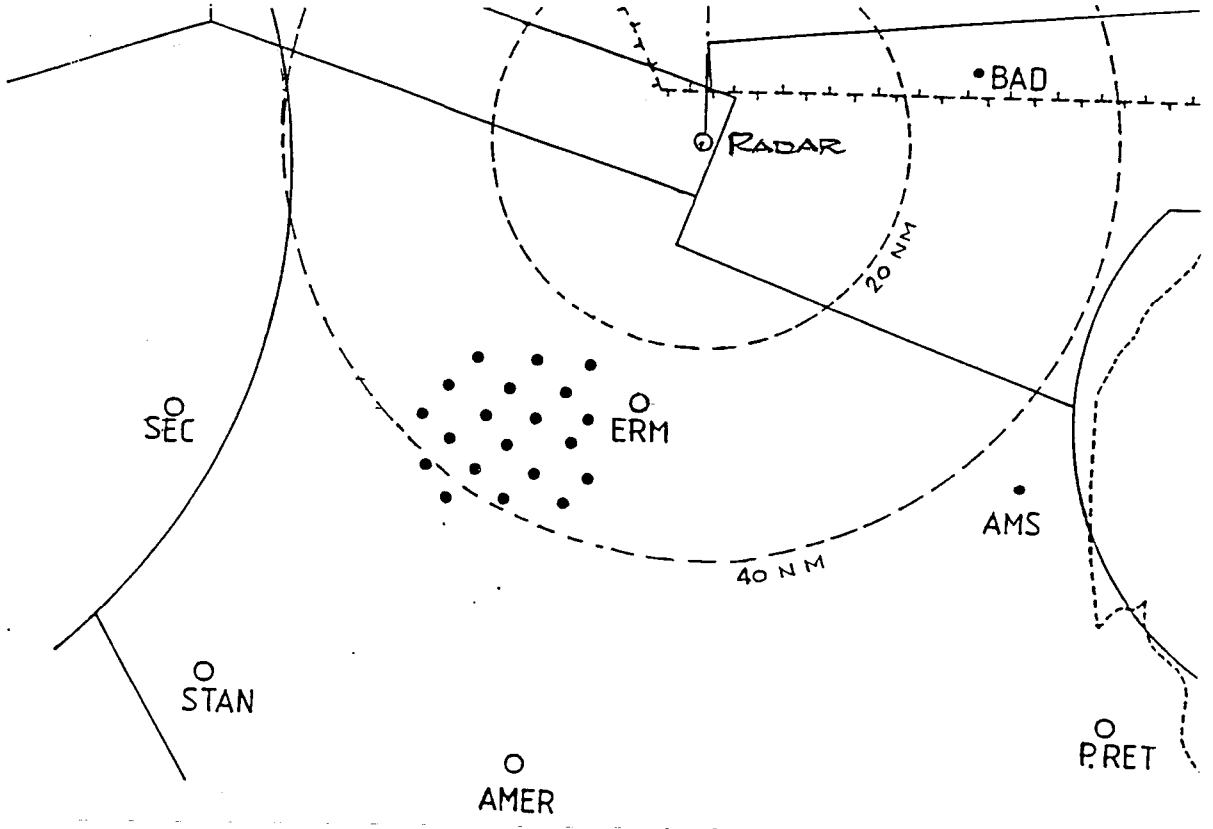

Fig. 3.0 Location of rain gauge network west of Ermelo in relation to the 5 cm radar at Carolina.

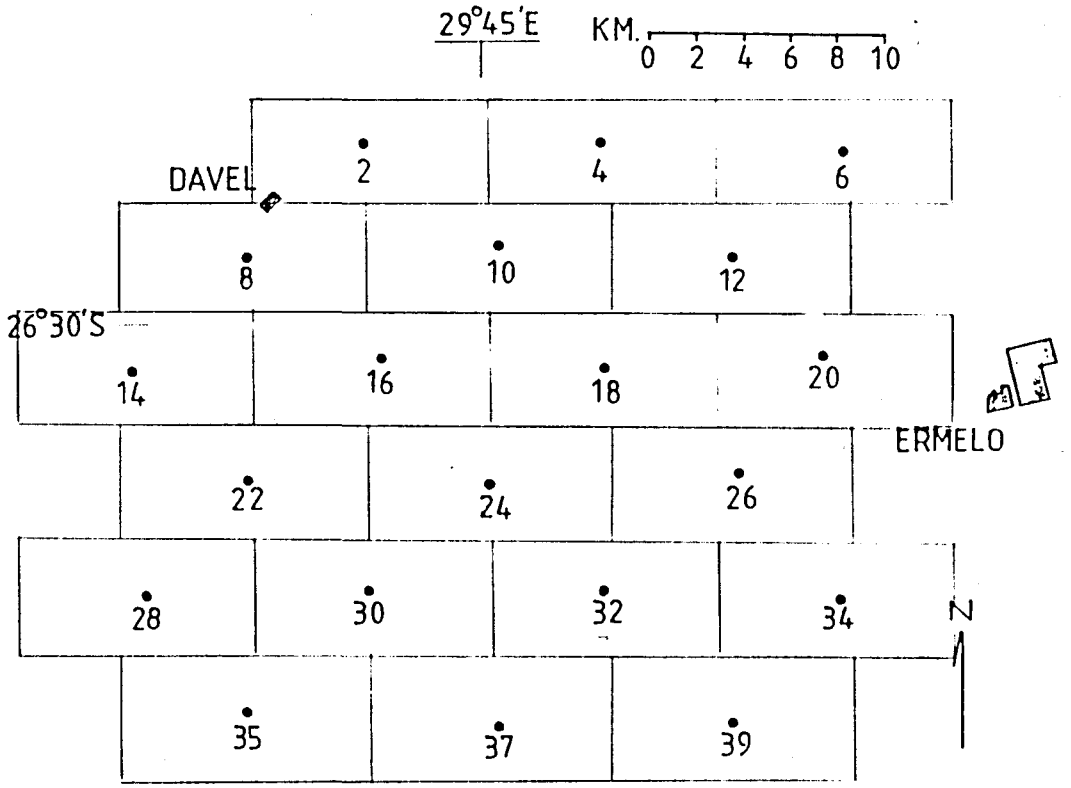

Fig. 3.1 A close up of the network. Each rain gauge is assumed to adequately sample the rain falling in each area shown in the figure.

Table 3.0 Comparison of radar/rain gauge measurements of rainfall.

Date	Time	Gauges (KTONS)	Radar (KTONS)	Cum. Gauges (KTONS)	Cum. Radar (KTONS)	Log G/R
3/11/88	1042/1654	1988	1983	1998	1983	0.001
9/11/88	1314/1730	683	2868	2681	4851	-0.623
26/11/88	1128/1714	1688	2302	4369	7153	-0.135
28/11/88	1038/1554	554	638	4923	7791	-0.061
5/12/88	1101/1519	3303	3796	8226	11587	-0.060
12/12/88	1129/1604	0	2	8226	11589	-
15/12/88	1137/1605	29	1	8255	11590	1.462
20/12/88	1316/1803	0	20	8255	11610	-
21/12/88	1100/1726	384	791	8639	12401	0.314
9/01/89	1223/1851	5221	3641	13850	16042	0.156
10/01/89	1230/1822	15	1	13865	16043	1.176
11/01/89	1158/1608	117	274	13982	16317	-0.369
14/02/89	1051/1449	189	48	14171	16365	0.595
1/03/89	1612/1747	607	492	14778	16857	0.091
2/03/89	0955/1801	24	8	14802	16865	0.477
13/03/89	1252/1559	171	345	14973	17210	-0.305
19/10/89	1204/1542	114	709	15087	17919	-0.794
25/10/89	1304/1638	934	804	16021	18723	0.065
10/11/89	1429/1759	6034	5749	22055	24472	0.021
29/11/89	1338/1520	1016	1140	23071	25612	-0.050
30/11/89	1133/1650	5289	2841	28360	28453	0.270
1/12/89	1051/1620	14768	3584	43128	32037	0.615
4/12/89	1319/1631	145	333	143	333	-0.361
9/01/90	1320/1627	317	0	462	333	-
10/01/90	1434/1641	930	1001	1392	1334	-0.032
20/01/90	1247/1647	23	8	1415	1342	0.459
23/01/90	1153/1521	1235	1454	2650	2796	-0.071
27/01/90	1227/1443	0	4	2650	2800	-
30/10/90	1136/1729	1254	1141	3904	3941	0.041
5/11/90	1408/1539	903	733	4807	4674	0.091
20/11/90	1223/1523	0	362	4807	5036	-
21/11/90	1121/1805	317	457	5124	5493	-0.159
22/11/90	1314/1651	660	587	5784	6080	0.051
5/12/90	1159/1539	456	944	6240	7024	-0.316
6/12/90	1429/1600	4712	1144	10952	8168	0.615
12/12/90	1200/1732	10244	8067	21196	16235	0.104
15/12/90	1118/1414	0	7	21196	16242	-
1/03/91	1448/1646	0	57	21196	16299	-
4/03/91	1217/1545	65	0	21261	16299	-
21/03/91	1142/1555	2804	1384	24065	17683	0.307
5/03/91	1528/1816	498	966	24563	18649	-0.288

Continuation of Table 3.0

Date	Time	Gauges (KTONS)	Radar (KTONS)	Cum. Gauges (KTONS)	Cum. Radar (KTONS)	Log G/R
31/10/91	1224/1555	73	191	73	191	-.418
1/11/91	1116/1545	1077	1434	1150	1625	-.124
11/11/91	1243/1706	52	227	1202	1852	-.640
12/11/91	1037/1617	302	196	1504	2048	.188
13/11/91	1127/1356	399	678	1903	2726	-.230
19/11/91	1304/1643	37	153	1940	2879	-.616
21/11/91	1115/1448	0	120	1940	2999	-
26/11/91	1233/1611	209	635	2149	3634	-.483
28/11/91	1148/1542	15	133	2164	3767	-.949
29/11/91	1129/1634	13	7	2177	3774	.269
2/12/91	1315/1603	922	557	3099	4331	.219
11/12/91	1530/1807	3601	2966	6700	7297	.084
13/12/91	1316/1546	5017	3330	11717	10627	.178
16/12/91	1153/1558	986	481	12703	11108	.312
6/01/92	1103/1611	2373	2150	15076	13258	.043
10/01/92	1248/1801	2224	2622	17300	15880	-.071
14/01/92	1535/1849	1085	1134	18385	17014	-.019
15/01/92	1057/1818	0	4	18385	17018	-
17/01/92	1249/1716	0	2	18385	17020	-
21/01/92	1050/1747	1788	3823	20173	20843	-.330
24/01/92	1251/1559	12	498	20185	21341	-1.618
30/01/92	1340/1824	2820	2370	23005	23711	-.076
3/02/92	1238/1759	3819	3909	26824	27620	-.010
4/02/92	1338/1657	473	238	27297	27858	0.298
13/02/92	1320/1615	0	143	27297	28001	
20/03/92	1254/1559	184	138	27481	28139	.125
23/03/92	1243/1651	106	366	27587	28505	-.538
17/02/92	1236/1532	2123	1294	29710	29799	.215
21/02/92	1203/1527	829	631	30539	30430	.119
2/03/92	1356/1508	4852	1781	35391	32211	.435
18/03/92	1305/1559	602	800	35993	33011	-.123

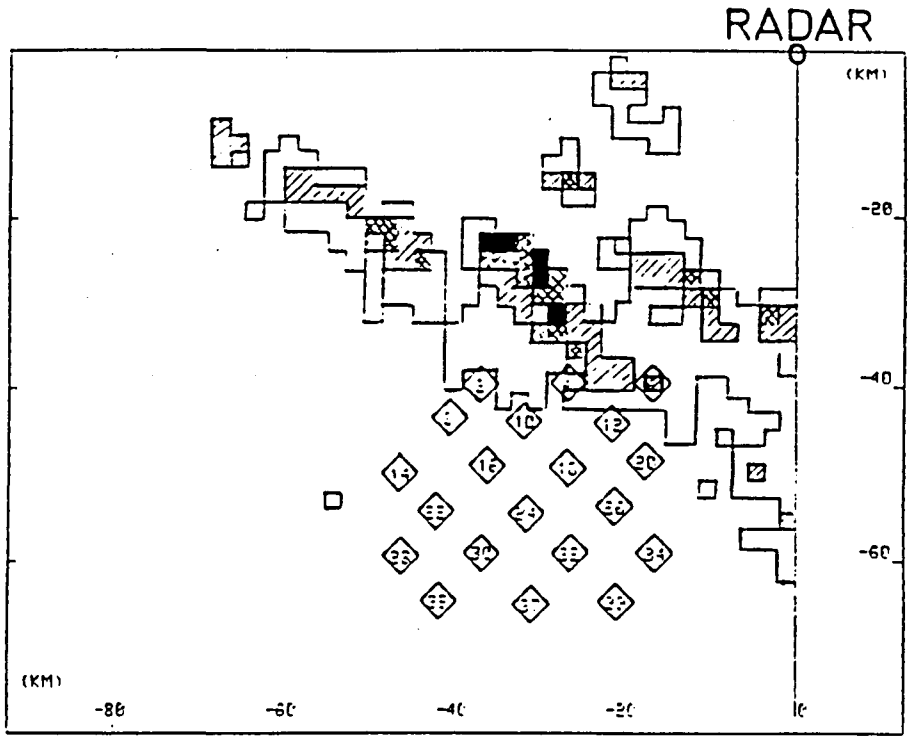

Fig. 3.2 (a). Schematic of radar echo over the rain gauge network at 15:31.

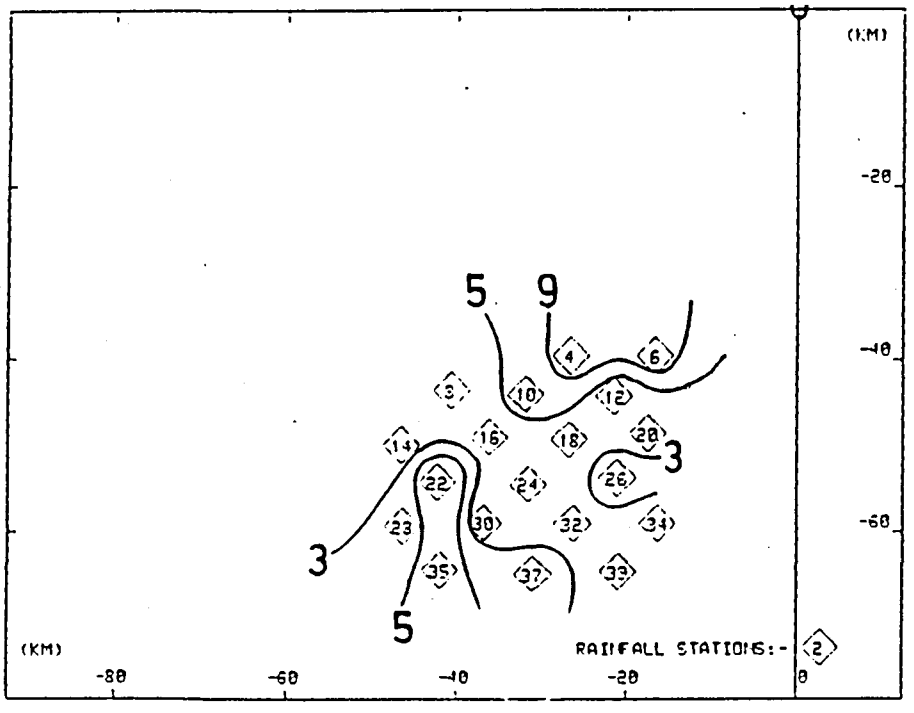

Fig. 3.2 (b). Contours of rain rates measured by the rain gauge between 15:25 and 15:30. Units are in millimeters per hour.

yet again, commencing on October 31, 1991. Here, the comparison between the two measurements is excellent until March 2, 1992 when attenuation again affects the radar measurement of rainfall over the gauge network. Attenuation of the radar beam at 5 cm wavelength is the single biggest source of error between the radar and gauge measurements. This type of error can be eliminated by careful attention to radar patterns, or perhaps an algorithm could be developed for objectively eliminating such events.(The best cure, of course, would be to use a 10 cm radar).

The two measurements of rainfall are compared by analysing the ratios of the log of the gauge rainfalls to the log of the radar measurements (log G/R). Studies have shown that this ratio has a normal distribution (Smith and Caine, 1983), which permits the use of normal distribution statistics. The agreement between gauges and radar can be improved by eliminating the smaller rainfall events. Table 3.1 lists the mean and standard deviations of log G/R for all gauge measurements and those measurements that exceed 100, 250, 500 and 1000 ktons. The 3 attenuation events, underlined in Table 3.0, have been omitted for these comparisons.

There are two features from this table that should be noted:

- for all values of rain events, mean gauge and radar measurements of rainfall are very similar. For instance, for those events over the network that exceed 250 ktons, the two estimates differ by about 2% (antilog of 0.010)

- the standard error of log (G/R) or log G - log R decreases almost exponentially at first, then more gradually as the rain over the network increases. This is not a new result. The Florida work (Woodley et al., 1975) showed that the accuracy of gauge measurement of rainfall is a function of the gauge density and the size of the rain event.

For those gauge measurements that exceed 250 ktons, the standard error of 0.198 corresponds to a factor of difference between the daily gauge/rainfall measurements of $10^{.198}$ which equals 1.58. Another way of stating this is that the radar and gauge measurements differ by less than 58 percent for 66 percent of the comparisons (plus and minus 1 standard error). Most studies show about a factor of difference of about 2 in radar and gauge comparison studies (Wilson, 1970).

Table 3.1 Comparsion of radar/rain gauge rainfall estimates in terms of log G/R for all measurements, those gauge events larger than 100, 250, 500 and 1000 Ktons. The 3 attenuation cases, underlined in Table 3.0, have been omitted for this comparison.

Class	Mean	Standard Error	Cases
All	-0.037	0.456	57
> 100 Ktons	-0.037	0.267	50
> 250 Ktons	0.010	0.198	42
> 500 Ktons	0.018	0.180	35
> 1000 Ktons	0.023	0.146	24

For our purposes, the mean of log G/R is of most importance, since in an area experiment, seeded and control rainfall will be compared whether measured by gauges or radar. Here, after 4 seasons, the gauge and radar measurements for those cases that exceed 250 ktons differ by just 2 percent. This convergence of the two estimates is a result of the long integration period, and indicates that the scatter of the individual (daily) gauge and radar measurements of rainfall are random. Other studies (Woodley et al., 1975) indicate that gauge errors of about 25 percent are likely with a gauge density of one per 50 km^2 for network events that exceed 250 ktons and a radar error of around 25 percent seems reasonable (leaving only 8 percent unaccounted for). We wish to stress here that there is no evidence of systematic errors in these measurements. No amount of "fine tuning" of the Z-R relationship will improve this analysis.

(d) Conclusions

A four season comparison of rain gauge and radar measurements of rainfall in a 1000 km^2 area west of Ermelo has shown that:

- the biggest single source of error is attenuation of the 5 cm wavelength radar beam. This may restrict an area experiment relying on radar measurements of rainfall to isolated storms, eliminating squall lines and fronts from the experiment

- although the daily gauge/radar measurements of rainfall show scatter around a perfect correlation (1 to 1), summing of these events over time leads to almost perfect agreement between the mean radar and gauge measurements of rainfall, provided that attenuation events are avoided and the analysis is restricted to looking at the bigger rain events over the network. Since it appears that radar can measure rainfall over an area within a few percent of gauge readings, radar rainfall measurements, summed over time can be used in an area experiment

- these results show that there were no systematic biases in either measurement and clearly indicate the success of the area-time integral approach to gauge/rainfall comparisons.

Perhaps the best compromise for an area experiment will be to nest a manageable rain gauge network (about 20 gauges) within the experimental area(s). This might satisfy the need for "ground truth" rainfall measurements. Another reason for some sort of a gauge network is the possibility that seeding may change the rain drop spectra at cloud base. Because equivalent radar reflectivities are proportional to the sixth power of drop diameters, it is possible to imagine a redistribution of drop diameters which causes an increase in radar reflectivity without a concomitant increase in rain mass.

4.0 CONTINUATION OF RESEARCH ON DRY ICE SEEDING

4.1 The Pulse Seeding Experiment

The concept of the pulse seeding experiment was to seed a large turret growing on the flank of a multicell storm (convective complex) only once with dry ice, then to try to trace the resulting physical changes (if any) from the time of seeding to the appearance of rainfall at cloud base. Changes were monitored by the seeding aircraft which penetrated the target turret while seeding (pre-seed pass) and attempted to repenetrate the seeded volume some 3 to 6 minutes later (post-seed pass). The target cloud was within range of a ground based radar (at Carolina or Bethlehem) operating in volume scan mode. A second aircraft at cloud base made serial passes through the precipitation falling from the target cloud for a period of 30 minutes after the seeding run. The experiment was randomized so that the significance of any measured changes could be assessed.

The experiment was designed to thoroughly test the seeding hypotheses that had been formulated at Bethlehem and Nelspruit. These hypotheses can be stated as follows:

Two hypotheses were formulated for the Bethlehem area; the so called "static" and "dynamic" modes of cloud seeding. Briefly stated, the first assumes that an injection of a moderate amount of seeding material leads to the formation of earlier and more precipitation. The latter intends to invigorate clouds by altering their water and heat budgets through the injection of large amounts of glaciogenic material (Kraus et al., 1987).

The seeding hypothesis under test at Nelspruit proposed that the early freezing of drops by glaciogenic seeding would speed up the precipitation growth process, since frozen drops would grow faster by rimming than unfrozen drops via collision and coalescence.

The significance of the rainfall measurements at cloud base cannot be overemphasized. Both hypotheses, if correct, should result in a change in rainfall, brought about by an increase in rain drop concentration and/or size, i.e. an increase in <u>rain rate</u>.

The design of the pulse seeding experiment was arrived at after exploratory seeding trials, conducted during the 1989/90 season. The randomized experiment commenced with the 1990/91 season.

(a) Seeding trials

Only once during the 1989/90 trials was the cloud base aircraft successfully manoeuvred beneath a test cloud chosen for a pulse seed experiment. A case study of this experiment follows:

(1) Pulse seeding case study - 12 January 1990.

The atmospheric sounding for 12 January 90 showed some positive buoyancy, 1.2 degrees at 500 mb, and a warm cloud base, 12.8^{o}C, the type of sounding that experience has shown leads to a coalescence and/or a coalescence freezing precipitation formation process.

A relatively small storm, radar cloud tops about 5500 m above sea level, was chosen and seeded at 14:00 SAST. The time history of the penetration indicated that the seeded turret was almost 7 km across. The total cloud water mixing ratio (10.7 g/kg) was close to the cloud base mixing ratio of 12.1 g/kg, indicating an adiabatic (unmixed) cloud core. The seeding time was 39 seconds for a total of 7.8 kg of dry ice (0.2 kg/s seeding rate).

(i) Microphysical measurements

Averages of measurements made on the first (seed) and second (post seed) pass through the cloud selected for an experiment on January 12 are listed in Table 4.0. Pertinent observations from the table are:

- weak updraft, consistent with the weak thermal buoyancy (4)

- King liquid water content decreased slightly between first and second pass (6)

- cloud water mixing ratio decreased (7)

- radar reflectivity increased

- particle concentrations increased but diameters decreased between passes (9 and 11)

- assuming that all 2D images are water, the mass of this water increased (12)

- the cloud was large and almost symmetrical as shown by the lengths of the two almost orthogonal passes (13 and 14).

Table 4.0 Cloud physics measurements from the passes made through the test cloud - 12 January 1990.

Measurement	1st Pass	2nd Pass	Units
1 Time	14:00	14:06	SAST
2 Pressure	469.3	482.2	mb
3 Temperature	-10.9	-9.6	^{o}C
4 Updraft	2.3	2.4	m/s
5 True air speed	164.1	150.8	m/s
6 King LW mix ratio	3.9	3.2	g/kg
7 Engine CW mix ratio	7.1	5.9	g/kg
8 Radar reflectivity	10.8	14.9	dBz
9 2D Total conc.	0.9	5.7	l^{-1}
10 2D > 1068 µm	0.02	0.04	l^{-1}
11 2D MW Mean dia.	1.48	1.05	mm
12 2D liquid water	0.19	0.46	g/kg
13 Pass length	6878	7075	m
14 Heading	081	190	^{o}M

There is no strong evidence that the Lear intercepted the seeded plume in this comparison. While concentrations increased from 0.9 to 5.7 l^{-1}, the mass-weighted mean diameter decreased from 1.48 to 1.05 mm, a result not consistent with the Nelspruit seeding hypothesis, which calls for rapid growth in particle diameters following seeding.

This illustrates one of the problems of post-seed sampling using aircraft. The volume sampled by the aircraft is so small compared to the storm volume that it is unrealistic to expect consistent interception of the seeded volume. This problem becomes more acute when dealing with the larger storm complexes. Tracing microphysical changes much past 10 minutes after seeding cannot be accomplished with any regularity using aircraft sampling at seeding levels. The use of additional aircraft is of little value because of the co-ordination problem in a multicell storm environment.

A total of 13 pulse seed experiments took place from January to mid April 1990. The in-cloud measurements from these experiments (13 first and 13 second passes) were stored in a prototype microphysical data base. Averages of some of these measurements are listed in Table 4.1.

Table 4.1 In-cloud averages of measurements from first (pre-seed) and second (post-seed) passes from 13 exploratory pulse seed experiments. Second pass was 3 to 6 minutes after 1st pass.

Measurement	1st Pass	2nd Pass	Units
1 Pressure	462.4	459.8	mb
2 Temperature	-10.2	-10.2	^{o}C
3 Updraft	3.2	4.1	m/s
4 True Airspeed	143.1	138.7	m/s
5 King LW mix ratio	3.4	2.5	g/kg
6 Engine CW mix ratio	5.5	4.9	g/kg
7 Radar reflectivity	12.5	17.8	dBz
8 2D Total conc	63	206	l^{-1}
9 2D > 1068 μm	0.5	1.3	l^{-1}
10 2D MW mean dia.	0.566	0.745	mm
11 2D LW mix ratio	4.5	14.3	g/kg
12 Cloud dimension	3916	3846	m

Note from this table that, on average:

- updrafts have increased slightly (dynamic effect?) between first and second passes (3)

- liquid water measurements by the King hot wire have decreased (5)

- total cloud water mixing ratios have also decreased but not as much as cloud liquid water (6)

- radar reflectivities have increased by about 5 dBz (7)

- particle concentrations measured by the laser imaging probe have increased (8)

- mass-weighted mean diameters have increased (10)

- assuming a particle density of one (water), precipitation mass in the cloud has increased dramatically (11)

- the average diameter of the clouds selected for this experiment was around 4 km (12).

The cloud physics measurements from this short experiment are promising. Both the Nelspruit and Bethlehem seeding hypotheses require an increase in particle diameters following seeding. On average, this seems to be occurring. Clearly, it is not possible to assess the significance of the trends shown in Table 4.1 without recourse to a randomized experiment.

(ii) Radar measurements

The experiment on 12 January was conducted within about 45 km of the 5 cm radar at Carolina. The radar was placed in a sector scan mode shortly before seeding so that a complete volume scan of the storm was acquired every 3.5 minutes. Three relevant storm track properties are plotted in Fig. 4.0. Some 30 minutes before the cloud was seeded, the radar storm top exceeded 8 km and the rain flux 300 m^3/s. Recall that this storm was seeded at 14:00. Some 26 minutes after seeding, the rain flux again peaked around 300 m^3/sec, but this time, radar storm tops barely exceeded 6 km.

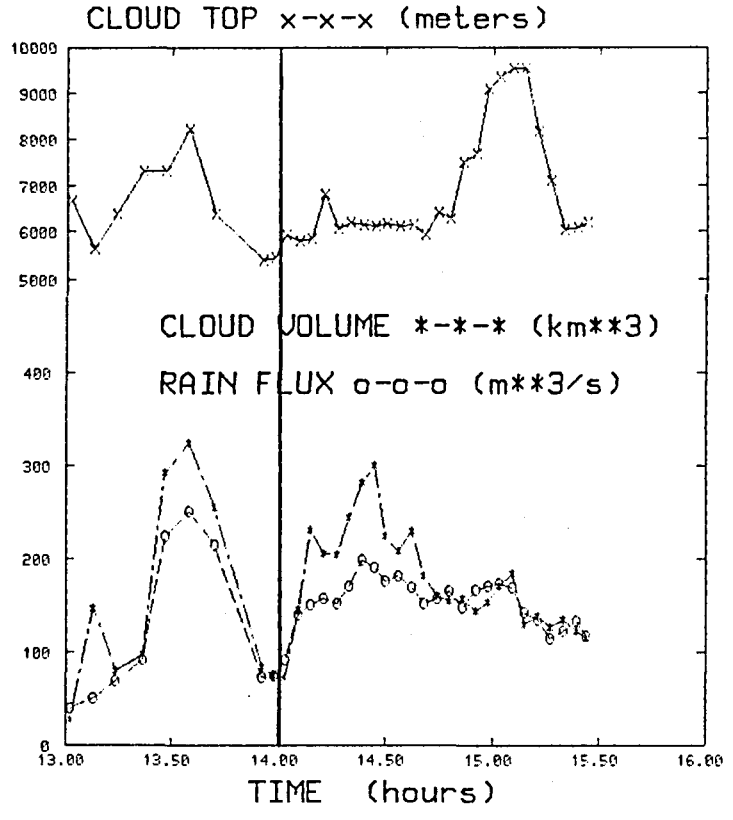

Fig. 4.0. Plot of cloud top height, volume and rain flux versus time measured by radar. This cloud was seeded once at 14:00.

If the additional rain following seeding was caused by the treatment, it was coming from a cloud whose observed top rose only slightly after seeding, indicating a microphysical rather than a dynamical enhancement of the rainfall process.

Another type of analysis that may be useful in a pulse seeding experiment uses time-height plots of peak radar reflectivity. Such a plot is depicted in Fig. 4.1. The positive slope of the peak reflectivity contours after seeding (time = 0) may be indicative of heightened particle trajectories caused by the freezing, then rapid riming, of small drops, a crucial part of the Nelspruit seeding hypothesis.

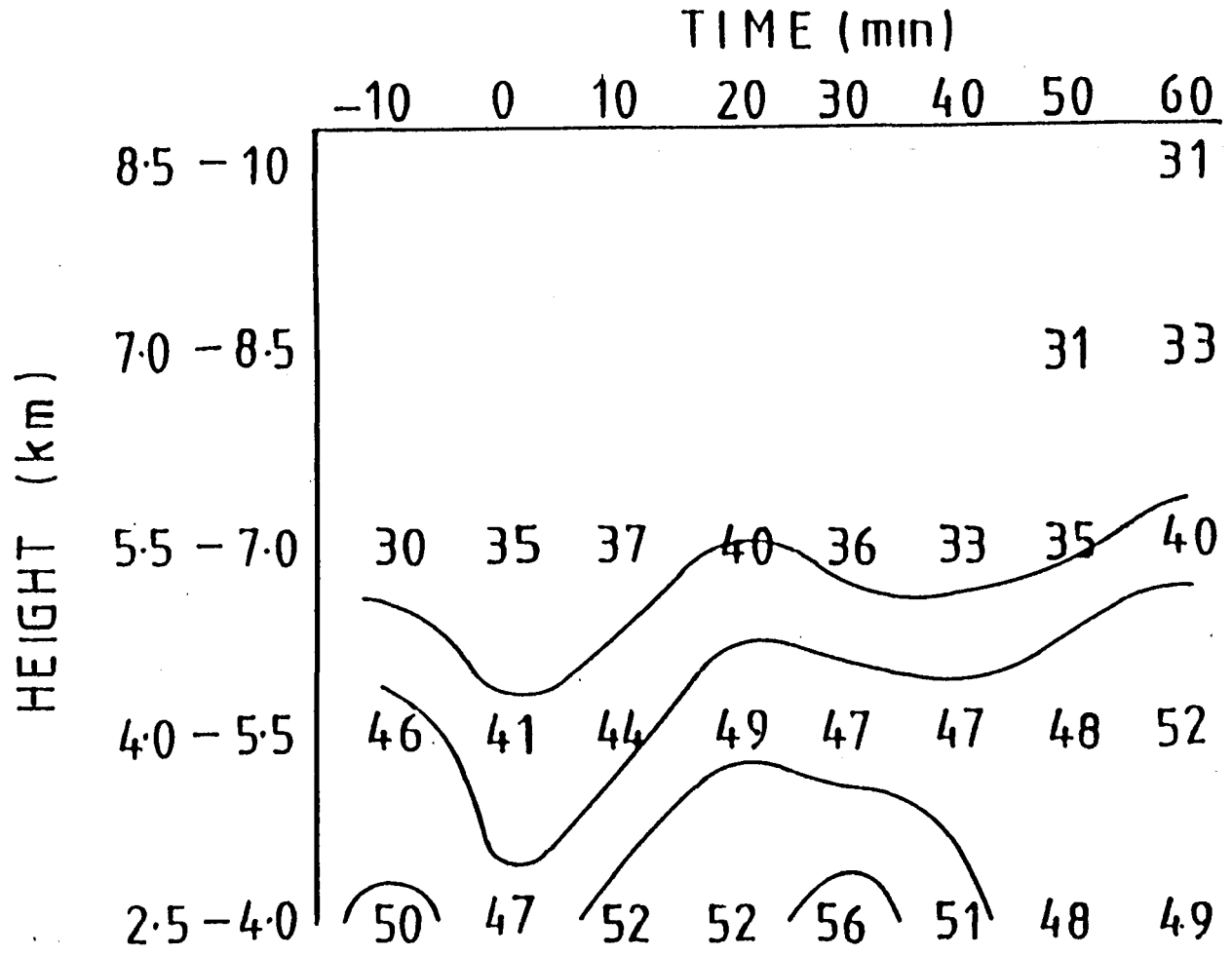

Fig. 4.1. Time-height plots of peak reflectivity of "pulse" seeded storm, 12 January 1990. Contours are fitted by eye.

(iii) Rainfall measurements at cloud base

On January 12, 1990 the cloud base aircraft (ZS-IZN) was positioned underneath a test cloud. Orthogonal penetrations commenced at 14:10 (ten minutes after seeding). Figure 4.2 shows time histories of the rain rates calculated from the 2D-P drop images, corrected for large drop distortion and up and downdrafts. A sudden increase in rain rate appears on the 14:27 panel. Rates increased to more than twice the values recorded before or after this event and persisted for about 1.2 km. A comparison of the aircraft (Table 4.2) and radar measurements (Table 4.3) of rainfall for this event follows.

The storm was located 45 km from the radar. The beam width at this range is 1.3 km wide. The precipitation shaft of interest was about 1.2 km in diameter, assuming symmetry, so there was a beam filling problem that would lead to an underestimation of the radar return. The best radar measurement for detecting such a small scale feature is the maximum reflectivity measured in the scan closest to the event. In fact, the maximum reflectivity jumped almost 4 dB between 14:26 and 14:30. The maximum recorded radar reflectivity at 14:30, 56.4 dBz is within about 2 dB of the average reflectivity calculated from the 2D-P probe measurements through the intense rain shaft (58.3 dBz). However, both measurements fall far short of the calculated rain rates that take into account the downdraft that was associated with the intense shower. The average rain rate calculated for this event, 435 mm/hr, corresponds to an equivalent radar reflectivity of 65.2 dBz, using the Marshall-Palmer reflectivity-rain rate relationship. Clearly, it was the inability of the radar to "see" the downdraft that led to the radar underestimating the rain rate in this study. If the event was caused by the seeding, then this result has implications in terms of using only a radar to evaluate the results of a seeding experiment.

Of additional interest because of its possible bearing on the seeding hypothesis was the approximate doubling of the particle concentrations measured in the precipitation shaft without a noticeable increase in mass-weighted mean diameters.

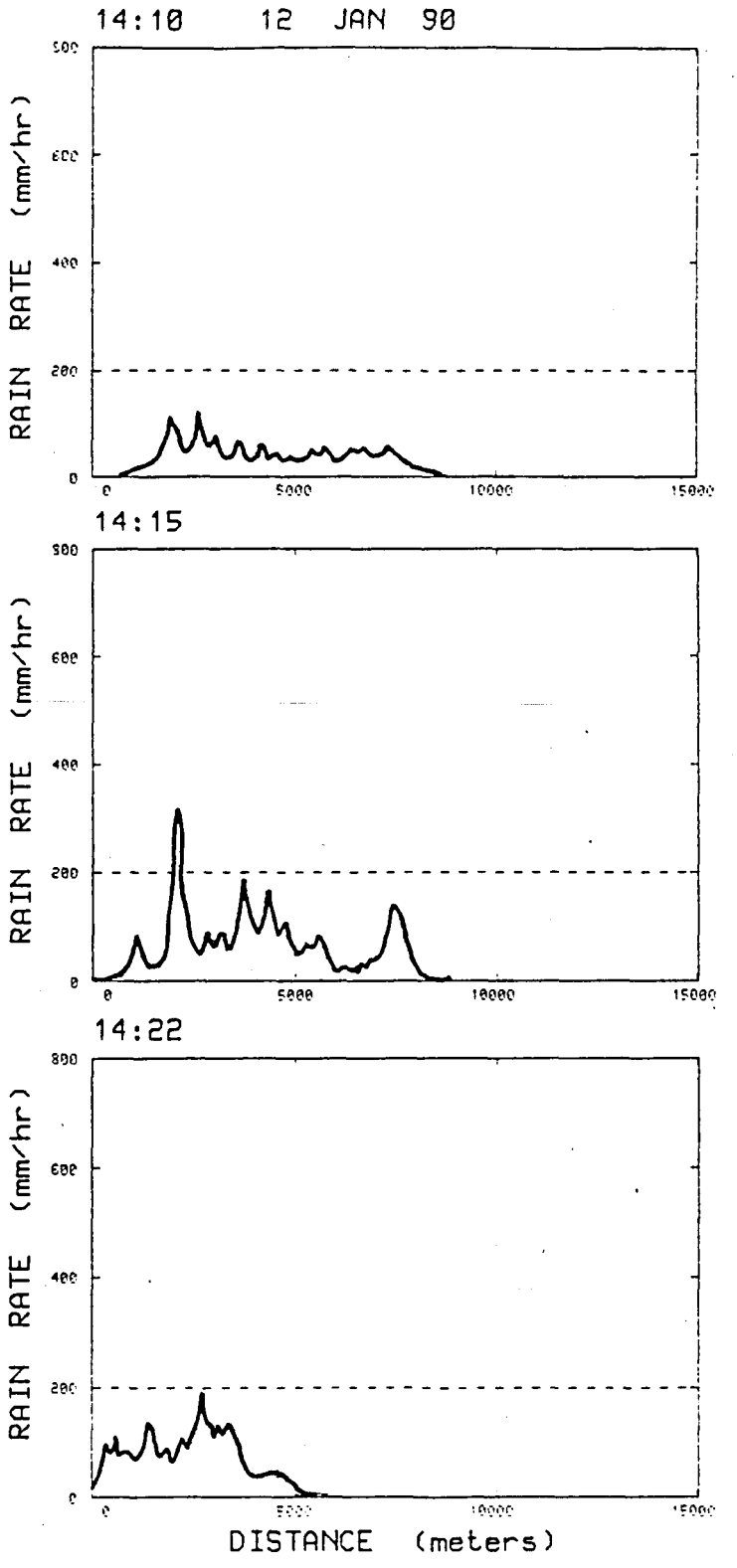

Fig. 4.2 Time histories of rain rates measured with the 2D-P probe on the cloud base aircraft. The cloud was seeded at 14:00.

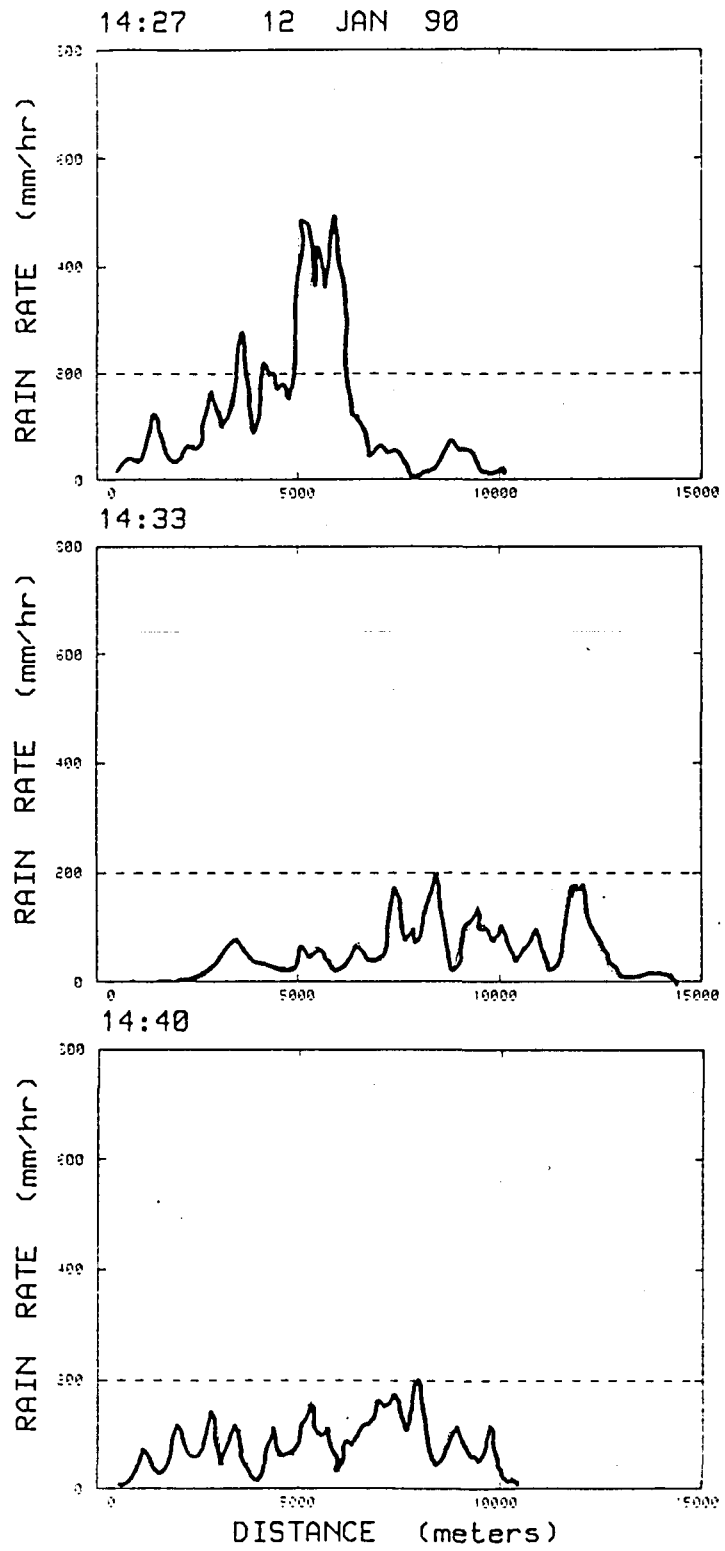

Fig. 4.2 Continued.

Table 4.2 Detailed aircraft measurements through rain shaft, 12 January 1990.

Time	Rain rate (mm/hr)	Reflectivity (dBz)	MWD (mm)	Conc (m^{-3})	Distance (m)	Vertical wind (m/sec)
	140	52.9	2.4	5842		.5
	206	50.6	2.1	4020		- .7
	235	56.9	2.9	4333		-1.8
	85	46.4	1.8	3470		- .7
	197	55.8	2.9	5446		-1.7
	240	56.0	2.9	4997		- .9
	96	50.1	2.2	4413		-1.6
	84	43.3	0.8	4700		-1.4
14:29	254	57.5	3.2	5053	5806	-2.8
	694	61.7	3.4	8533		-4.7
	451	55.2	2.5	6643		-5.1
	581	57.8	2.6	*		-4.1
	101	42.4	1.3	8527		-4.8
	513	64.0	4.5	9327		-4.3
	577	59.2	2.8	*		-5.1
	396	59.7	2.9	8912		-1.9
	103	41.2	1.2	8781		-3.3
	610	58.1	2.8	7545		-4.5
	568	55.0	2.2	*		MSG
	446	52.7	2.0	*		-7.2
	447	57.2	2.7	8521		-7.3
14:29:12	353	56.8	2.7	7181	6977	-5.0
	198	45.5	1.5	8393		-6.2
	107	47.5	2.2	2726		-5.5
	76	42.0	1.5	3675		-6.1
MEAN	435	58.3	2.6			-4.6

Table 4.2 Notes:

1. MWD is the mass-weighted mean diameter
2. * in concentrations column indicates that the drop concentrations have exceeded 10 000 m^{-3}
3. Means are calculated across the precipitation shaft, from 14:29 to 14:29:12.

Table 4.3 Track properties computed from the radar data acquired for the experimental storm - 12 January 1990.

Time (SAST)	Volume (km^3)	1.5^o Area (km^2)	Rain Flux (m^3/s)	R (mm/hr)	Ze max (dBz)
14:02	92	35.2	74	7.6	44.8
14:05	140	56.4	146	9.3	50.3
14:09	151	70.1	231	11.9	51.8
14:12	158	65.7	206	11.3	52.4
14:16	152	60.2	204	12.2	53.9
14:19	171	70.3	245	12.6	52.1
14:23	199	81.0	282	12.5	53.2
14:26	191	91.1	300	11.8	52.9
14:30	177	72.7	225	11.1	56.4

4.2 The randomized pulse seed experiment

The 1989/90 exploratory seeding trials were sufficiently encouraging to lead to the design and execution of a randomized experiment that commenced at the beginning of the 1990/91 season.

The design of the experiment was as follows. Two sets of cards containing randomized seed/no-seed instructions were prepared by UNISA; one set for the Bethlehem area, the other for the Carolina area. The seeding aircraft, in this case the Learjet, held a set of cards for the Carolina and Bethlehem areas. The Learjet crew would select a suitable test case, an isolated multicell convective storm and declare an experiment (decision time). The respective radar operator would open an envelope and instruct the crew to seed or not to seed. The Lear crew would then open the envelope that corresponded to that test case and area (Bethlehem or Carolina). The envelope would contain either a "yes" or "no" instruction. The instructions and actions appear below.

RADAR	LEARJET	ACTION
Seed	No	No-Seed
Seed	Yes	Seed
No-Seed	Yes	No-Seed
No-Seed	No	Seed

The procedure in the event of a seed decision was to penetrate and seed an active turret growing on the flank of a selected target storm. A second sampling penetration would take place 3 to 6 minutes later, if possible orthogonal to the seeding run. For no-seed outcomes, the Lear merely simulated the seeding pass and the subsequent sampling run, keeping clear of all cloud. This procedure kept both the radar operator and the aircraft sampling the rain at cloud base "blind" as to treatment, preventing any biases from creeping into the collection of the radar and rainfall measurements.

The pulse seed missions are summarized in Table 4.4. All of the early experiments took place in the Carolina area because the Bethlehem radar was not fully serviceable until the middle of January, 1991. A total of 31 experiments were conducted. Good radar data were acquired on all experiments except for the first Bethlehem experiment (16 January 1991). Measurements of rainfall at cloud base were not made in a consistent manner and led to an inadvertent bias towards the number of seed cases. Of 10 measurements of rainfall below cloud base, 7 were seed cases and just 3 were no-seed. Since just three no-seed storms were sampled, it may not be possible to judge the significance of these events.

Table 4.4 Summary of Pulse Seed Experiments 1990/91

Carolina Area

Exp No	Cloudbase a/c	Date	D.T.	Treatment
P.S. 1	-	30 Oct 90	13:13	S
2	-	" "	13:30	S
3	IZN	3 Nov	14:55	NS
4	-	21 Nov	16:21	NS
5	-	5 Dec	13:03	NS
6	IZN	" "	13:26	S
7	-	" "	13:50	S
8	IZN	12 Dec	13:02	S
9	-	" "	13:32	S
10	-	" "	13:47	NS
11	IZN	5 Mar 91	16:16	S
12	-	" "	16:35	NS
13	IZN	21 Mar	13:36	S
14	-	21 Mar	14:48	S
15	-	31 Oct	13:14	NS
16	-	31 Oct	13:47	NS
17	-	11 Nov	13:38	S
18	-	11 Nov	14:06	NS
19	-	11 Nov	14:26	S
20	JRA	12 Nov	12:43	S
21	JRA	13 Nov	12:48	S
22	JRA	13 Nov	13:26	NS
23	IZN	19 Nov	15:08	NS

Bethlehem Area

1	JRA	16 Jan 91	14:11	S
2	-	23 Jan	15:18	NS
3	2D-Probe U/S	7 Feb	13:12	S
4	-	14 Feb	12:14	S
5	-	14 Feb	13:05	NS
6	-	" "	16:30	NS
7	-	15 Feb	13:11	NS
8	-	8 Mar	12:10	S

(a) Gushers or unusual rainfall events

A "gusher" is defined as an unusually heavy rain rate, usually associated with a downdraft, encountered at cloud base by either of the instrumented aircraft (IZN, JRA). The first such event was recorded in the seeding trials on 12 Jan 1990.

Table 4.5 summarizes the gusher events to date. Recall that all these clouds were seeded once and once only with dry ice. The gusher events occur between 15 and 27 minutes after decision time, i.e. in the time range in which the effects of seeding at cloud top might be expected to appear at cloud base.

The most impressive event occurred on December 5, 1990. Fig. 4.3 shows the computed rain rates (unsmoothed) captured by the 2D-P probe. The downdraft that was associated with this event is shown in the same figure.

It is again instructive to compare the cloud base aircraft and radar measurements. Table 4.6 lists some of the pertinent radar measurements collected during this experiment, with the radar in sector/volume scan mode. Rain flux divided by storm area (column 5) is a measure of average storm rain rate. Note that this radar-measured variable does peak at 13:51 (the scan closest to the aircraft pass at 13:52), but the relative magnitude of the increase is small compared to the aircraft measurements. However, a peak reflectivity of 62 dBz corresponds to a rain rate of 273 mm/hr (using $Z = 200\ (R)^{1.6}$) which would be a pretty good average for the gusher depicted in Fig. 4.3.

Listed in column 6 is another ratio; rain flux divided by storm volume. This can be viewed as a measure of rainfall "efficiency", i.e. the rain flux per unit storm volume. This ratio also peaks at 13:51.

The rain rates measured by the instrumented aircraft are summarized in Fig. 4.4, for the 7 seed and 3 no-seed cases. Four out of the 7 seeded cases show rain rates that exceed 100 mm/hr some 15 to 26 minutes after decision time (t=0). None of the no-seed cases exceeds this threshold.

In summary, unusual rainfall events have been recorded by instrumented aircraft beneath seeded storms. These events are characterised by sudden increases in rain rate, often associated with a strong downdraft. It is too early to state that these events are unique to seeded storms, but if further measurements prove this to be true, this is the sort of "strong" seeding signature that experimenters search for.

Since the radar does not "see" downdrafts, radar measurements underestimate the rain rates associated with these events, a result that should be considered when designing rain augmentation experiments.

Table 4.5 Summary of Gusher Statistics

Date	D.T.	Time	Conc (m^{-3})	MWD (mm)	R (mm/hr)
12/1/90	14:00	14:10	443	2.69	18
		14:15	873	2.33	25
	(:27)	14:22	1150	2.19	23
		14:27	1851	2.84	61
		14:33	767	2.34	22
		14:40	1437	2.40	42
5/12/90	13:26	13:38	1687	0.82	42
		13:45	1351	0.76	30
	(:26)	13:52	12202	3.05	128
12/12/90	13:02	13:06	1420	4.41	53
	(:16)	13:18	1489	4.33	74
		13:24	680	3.27	28
		13:33	937	2.84	28
		13:36	800	3.64	32
		13:41	1280	3.79	51
16/1/91	14:10	14:14	512	1.72	9
		14:17	1625	1.74	18
		14:20	1054	1.73	14
	(:19)	14:25	1528	2.00	26
		14:29	3609	1.91	81
		14:35	2071	1.94	37
		14:40	2812	1.86	49
21/3/91	13:36	13:36	1255	1.02	42
		13:43	2150	1.85	58
	(:15)	13:51	4521	2.20	99
		13:58	1080	1.36	17
		14:05	1667	1.93	23
		14:13	1928	1.76	20
		14:21	1066	0.77	22

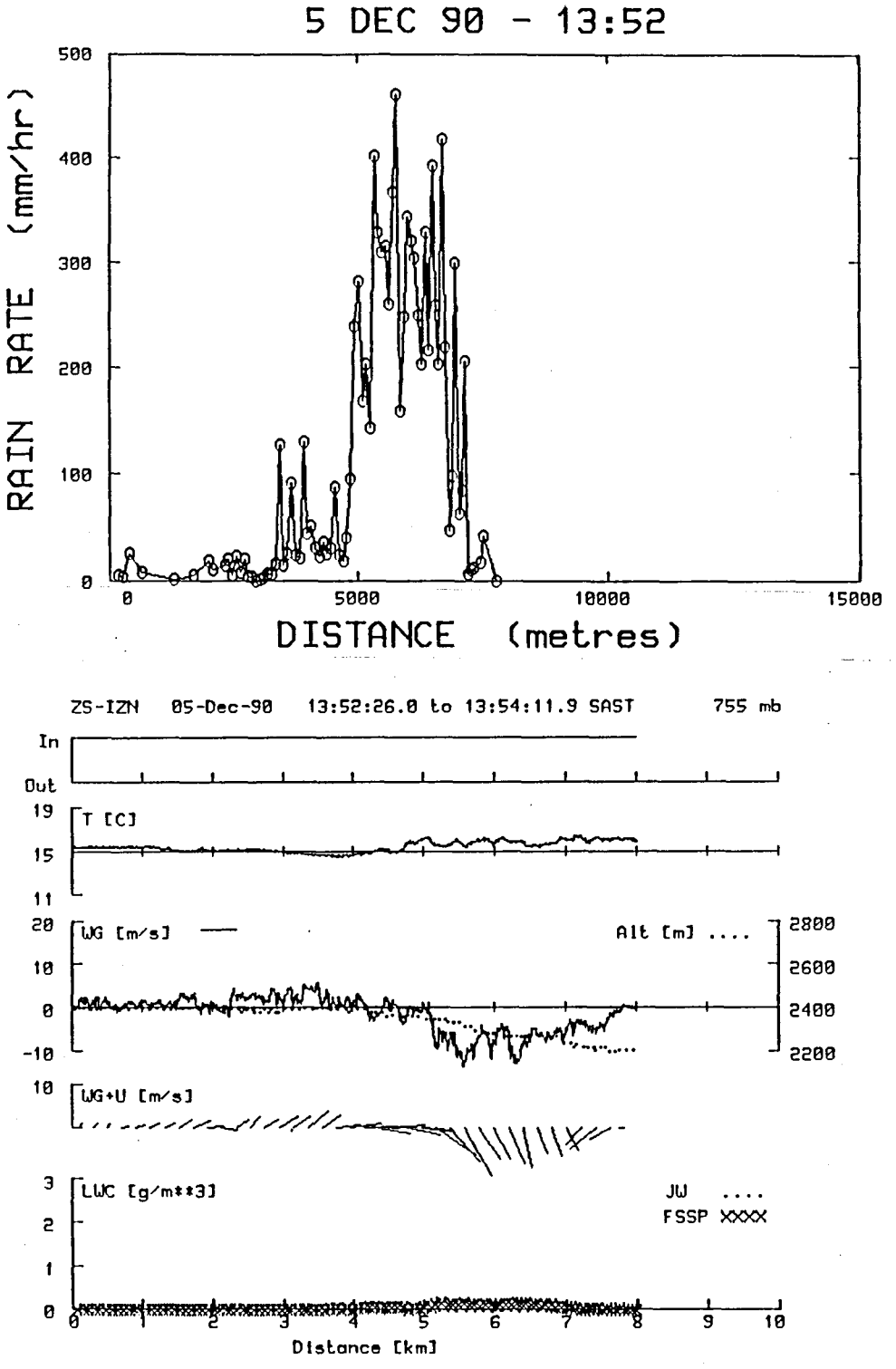

Fig. 4.3 Measurements of rain rates by the cloud base aircraft (IZN) on December 5, 1990. Note the downdraft measured by the aircraft in the lower portion of the figure.

Table 4.6 Radar data - 5 December 1990
Decision time - 13:26

Scan time	Storm Area (km^2)	Rain Flux (m^3/s)	Peak Ze (dBz)	Flux / Area	Flux / Vol
13:25	107	395	57	3.70	0.9
13:29	98	442	53	4.53	1.1
13:32	112	517	55	4.60	1.2
13:36	117	501	55	4.27	1.1
13:40	121	585	56	4.83	1.2
13:44	120	467	60	3.89	1.0
13:47	135	598	59	4.41	1.3
13:51	123	645	62	5.25	1.5
13:55	108	486	57	4.49	1.3
13:59	94	304	52	3.24	0.8

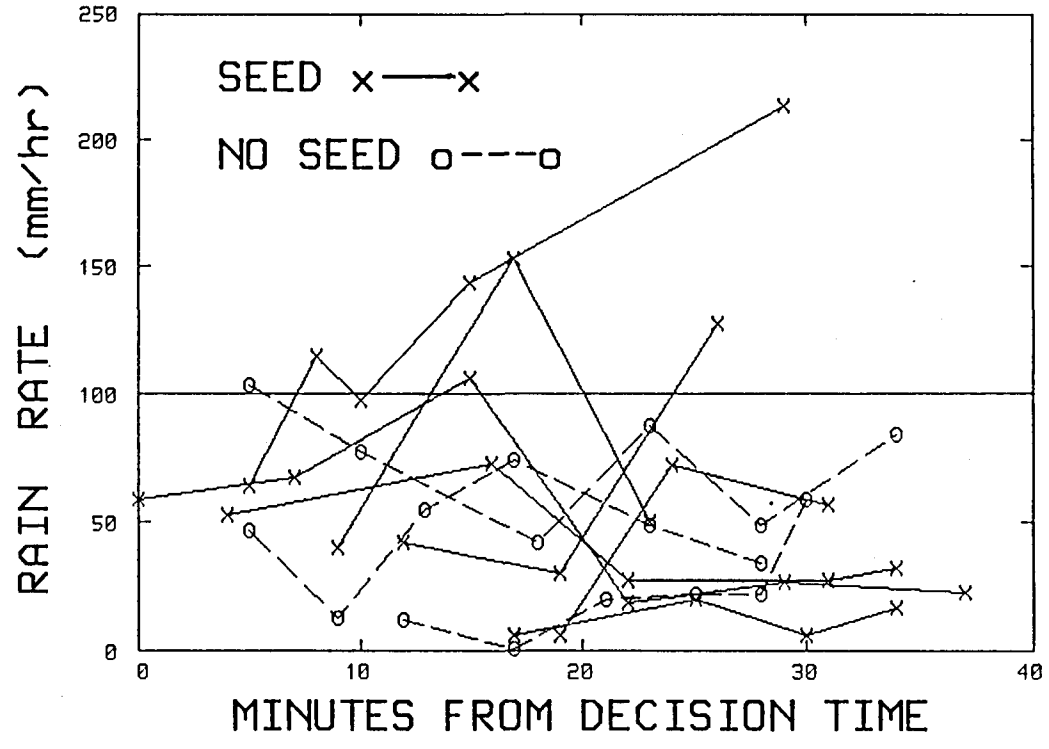

Fig. 4.4 Time histories of average rain rates measured at cloud base in the randomized pulse seed experiment - 7 seed and 3 no-seed cases.

(b) Statistical results

Of the 31 pulse seeding experiments, radar data were not available for one of the cases (16 Jan 91) and two failed to fall within the range limitations (10 - 90 km radius from the radars). Past experience has shown that 28 cases is not sufficient for the type of analysis used here - an examination and comparison of storm track characteristics in 10 minute time windows from decision time. The analysis is presented here for two reasons. First, it is unlikely that the pulse seed experiment will continue, since the results from the seeding experiments using the hygroscopic flares are showing more promise than the dry ice seeding experiments. Second, the analysis shows what can go wrong with an experiment having too few cases. In our experience, the statistics acquire stability (admittedly a subjective judgement) when case numbers reach about 50.

The results of the statistical analyses, using a re-randomization or a permutation analysis are listed in Table 4.7 and show an apparent decrease in rainfall 20 to 30 minutes after decision time. Listed in Table 4.8 are the individual rain masses from each experiment calculated over 10 minute time intervals from decision time (t = 0). Track 10, a no-seed case, increases its rain mass 16 times by the third time interval, completely dominating the analysis. This track merged with a large storm mass shortly after decision time. If this track is deleted from the analysis and arithmetic means computed (including zeros) both seed and no-seed cases show about a 10 percent decrease in rain mass 20 to 30 minutes after decision time. The only other feature of note in this analysis is that more of the no-seed cases dissipate than in the seeded case.

(c) Aircraft microphysical measurements

The Lear samples the characteristics of the treated cloud on the seeding pass and then penetrates the same cloud some 3 to 6 minutes later. In this experiment, no-seed cases are not sampled, because of the concern that aircraft-produced ice particles (APIPS) may affect the unseeded clouds. Thus Table 4.9 is a summary of microphysical measurements from the Lear database for the seeded cases from the 1990/91 experimental season and, for purposes of comparison, the results from the previous season's exploratory seeding trials.

The microphysical implications of these observed gushers are important. Under what thermodynamic conditions do they occur? Does the time between treatment and appearance of the gusher at cloud base have any significance?

Table 4.5 suggests that the increases in rain rates are caused by increases in both drop concentrations and diameters. This observation impacts upon the formulation of a seeding hypothesis. For instance, if the dry ice seeding is freezing drops that are already present which now proceed to grow faster as graupel, how does one explain the increase in concentrations? Is it possible that some of the drops that are frozen would have been collected via coalescence in an untreated cloud? These and other matters must be settled with further observations. The pulse-seeding experiment appears to have taken us a lot closer to one of our goals - a seeding hypothesis validated through observations.

Table 4.7 Results of statistical analysis of the pulse seed experiment

	MINUTES		
GEOM. MEAN OF:	0 - 10 Seed/No-Seed	10 - 20 S/NS	20 - 30 S/NS
Volume (km^3)	258/186	244/327	214/547
Area (km^2)	53/41	60/76	54/119
Rain Mass (ktons)	97/56	94/107	83/253
1.5^o			
Rain flux (m^3/s)	172/97	177/226	141/422
Rain mass (ktons)	62/35	38/62	35/154
6 km			
Rain flux (m^3/sec)	103/61	72/131	58/258

% DIFFERENCE (SEED - NO-SEED/NO-SEED) x 100			
	%	%	%
Volume (km^3)	39	- 25	- 61
Area (km^2)	29	- 21	- 54
Rain mass (ktons)	75	- 12	- 67
1.5^o			
Rain flux (m^3/s)	77	- 22	- 67
Rain mass (ktons)	75	- 38	- 77
6 km			
Rain flux (m^3/s)	68	- 45	- 77

Table 4.8 Rain Masses (ktons) @ 1.5°

Track No.	0 - 10	10 - 20	20 - 30
	SEED CASES (N = 15)		
26	264	350	272
43	37	53	49
201	285	315	346
35	182	76	86
114	208	92	36
229	80	93	88
28	24	18	0
183	42	80	22
6	26	20	5
5	203	44	0
45	207	197	392
48	330	363	273
99	300	254	368
244	391	545	380
150	2	8	6
ARITH MEAN	172	167	155
	NO-SEED CASES (N = 13)		
10	59	296	952
205	573	467	549
133	143	128	171
217	18	0	0
72	2	0	0
243	1	0	0
27	8	1	0
226	157	23	0
1	354	357	259
32	289	269	274
68	180	217	273
83	129	190	140
41	57	58	69
ARITH MEAN	159	142	144

Table 4.9 Microphysical measurements - Pulse Seeding Experiment

	1989/90		1990/91		
Measurement	1st Pass	2nd Pass	1st Pass	2nd Pass	Units
Pass length	3916	3846	3085	3110	m
Pressure	462	460	455	451	mb
Temperature	-10.2	-10.2	-10.8	-11.0	^{o}C
Updraft	3.2	4.1	4.3	11.3	m/s
True air speed	143	139	143	141	m/s
Radar reflectivity	12.5	17.8	15	19	dBz
King LW mix ratio	3.4	2.5	2.2	1.6	g/kg
La CW mix ratio	2.1	2.3	5.7	5.3	g/kg
E.T. CW mix ratio	5.5	4.9	4.9	5.0	g/kg
2D LW mix ratio	4.5	14.3	1.9	3.4	g/kg
2D Total conc	63	206	16	85	l^{-1}
2D > 1068 µm	0.5	1.3	.2	0.3	l^{-1}
2D MWD	566	745	718	818	µm
Temp @ CCL	12.8		10.9		^{o}C
ΔT_{500}	3.8		4.3		^{o}C

Notes from Table 4.9

- updraft increases between pass 1 and 2 in both seasons; possible dynamic reaction from the release of the latent heat of freezing

- radar reflectivity increases about 4-5 dB between pass 1 and 2, both seasons; an increase in particle size and/or number

- King LW decreases between pass 1 and 2, both seasons; depletion of cloud liquid water by growing hydrometeors

- La and E.T. cloud water (CW) contents stay roughly the same between passes in both seasons; no decrease in cloud water contents, which is the sum of supercooled cloud water and precipitation particles. (La values are low; there were problems with this instrument during the 1989/90 season).

- 2D calculated liquid water contents (precipitation) increase; expectations are for increases after seeding

- 2D concentrations go the right way, showing large average increases by the second pass after seeding

- large particles (> 1 mm) show an increase in concentrations in the first season, but on average, remain constant in the second; expectations are for increases

- mass-weighted mean diameters (MWD) increase from passes 1 to 2;

Generally, the statistics are showing increases in the expected variables in the expected directions. What plagues all measurements of this sort is the inescapable sample volume limitations of all aircraft microphysical measurements; the clouds are so big and the aircraft is so small.

(d) Summary

The pulse seed experiment, designed to validate the Bethlehem and Nelspruit dry ice seeding hypotheses, was not conclusive. Intriguing observations of gushers, or sudden increases in rain rates at cloud base were observed in some of the seeded cases. Because of the inability to obtain reliable measurements of rainfall at cloud base using instrumented aircraft, the significance of this observation cannot be assessed. We were warned that a single dry ice seeding run would not produce a sufficient signal to be detected by radar in the noisy convective storm environment. This appears to be the case, as the radar analysis of the 15 seed and 13 no-seed cases does not detect a seeding effect.

The statistical analysis was useful in the sense that an apparent negative result was shown to be the result of a single case which completely dominated the routine analysis, a circumstance encountered all to often in convective cloud experiments.

This experiment, while constructive, was not carried through to a conclusion. Hopefully, the reasons for the early termination of the experiment are adequately expounded in the historical review that introduces this report.

5.0 NEW HYGROSCOPIC SEEDING FLARES

(a) Introduction

In an attempt to mimic the effects of the Kraft paper mill on storms, an experimental hygroscopic flare was designed and subsequently manufactured by Swartklip Products in Cape Town. Initially a batch of 25 flares was ordered, each flare about the size of a beer can, containing 500g of the seeding mixture (see Fig. 5.0).

The flare racks originally used for silver iodide end-burning flares on the Commander JRB were modified to accept 4 of the new hygroscopic flares on each rack (for a total of 8). Since both flares were fired electrically, the original firing mechanism was used.

Tests performed on the combustion products of the new flares were carried out by Dr. Mark van der Riet at the engineering laboratory at ESKOM. These tests determined the chemical composition of combustion products and provided some information on particle sizes (spectra). Further static tests were conducted at Nelspruit. An FSSP-100 probe was positioned behind JRB and a flare was lit while the engine was running. Airborne tests at Bethlehem cast doubts on the spectra obtained from the ground runs. Additional ground runs were performed collecting particles in the plume on sticky glass slides. Particles of over 100 μm in diameter were collected on these tests, supporting the airborne measurements. The particles collected on the glass slides were analysed at the University of the Witwatersrand, using a scanning electron microscope and an X-ray diffractometer.

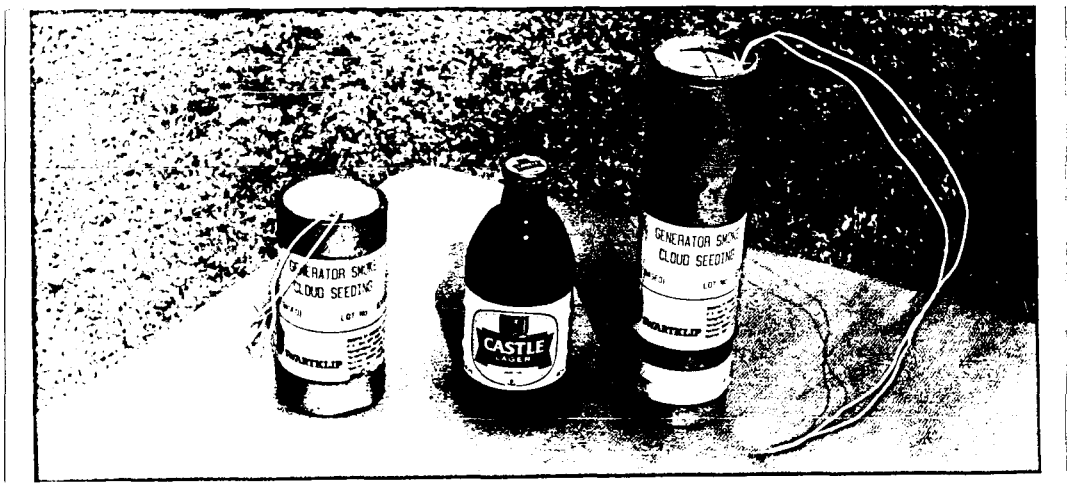

Fig. 5.0 The two sizes of hygroscopic seeding flares manufactured in Cape Town by Swartklip Products (Pty) Limited.

The first test of these new flares on a relatively small convective storm produced spectacular results. Observational systems used in this test (October 9, 1990) were the Learjet and the 5 cm radar at Carolina in sector scan mode. This test is described in detail in a later section. This and a second test were sufficiently encouraging to warrant the placing of an order for additional flares. The second version of the flare was twice as long, containing around 1 kg of the seeding mixture. A total of 200 of the longer version was ordered.

Further seeding tests with the longer flares, both at Nelspruit and at Bethlehem were very encouraging. On most tests, a solid radar and/or microphysical signature was detected shortly after seeding commenced, and the signals were commensurate with the seeding hypothesis which states that the coalescence rainfall formation process can be enhanced by the introduction of hygroscopic materials into the storm updraft at cloud base. This clearly represents a breakthrough in weather modification. Based upon a solid knowledge of the microphysics of the local precipitation mechanisms, a seeding device, designed to increase the efficiency of the precipitation process by encouraging (accelerating) coalescence, has been manufactured and subsequent tests have indicated that the new device achieves the desired effect.

(b) Analyses of combustion products

(1) ESKOM tests

A flare was supplied to ESKOM for an investigation into the combustion residue (chemical composition and particle size distribution). The composition of the flare, according to the manufacturer was:

- 65% potassium perchlorate ($KClO_4$)
- 10% sodium chloride (NaCl)
- 2% lithium carbonate ($Li_2\ CO_3$)
- 5% Magnesium (Mg)
- 18% hydrocarbon binder

The mixture was combusted in 3 ways. The method closest to actual flight conditions was the use of a wind tunnel. The residues from the wind tunnel tests were analysed by a scanning electron microscope. The chemical composition is similar to the one deduced by Hindeman (1978).

	Hindeman (%)	Eskom (%)
Sodium chloride (NaCl)	19	21
Potassium chloride (KCl)	65	67
Lithium Carbonate (Li_2CO_3)	1	-
Magnesium oxide (MgO)	15	12

It is of interest to note that no trace of lithium was detected in any of the measurements.

The particle size measurements were probably not representative. Following combustion in the wind tunnel, the residue was collected on a filter paper and some agglomeration occurred. Undoubtably, agglomeration also occurred during the cooling phase, before the particles struck the filter face. Ultrasonic vibration was used to attempt to disperse the impacted agglomerates and leave the "fused" agglomerates intact. Unfortunately no experimental technique can disperse one type of agglomerate to the total exclusion of the other.

(2) Nelspruit and Bethlehem ground and airborne tests

The FSSP probe on the wing of IZN was placed about 2 m behind the flare rack mounted on the rear end of JRB's engine nacelle. JRB's engine was started and, when a suitable RPM had been reached, the flare was ignited. Airflow past the FSSP was measured using a pitot tube that was connected to IZN's pitot-static system. Knowing the speed of the flow past the FSSP ($\sim$37 m/s), the approximate diameter of the plume ($\sim$ 30 cm) and the length of the burn (220 s), particle concentrations measured by the FSSP (120 cm^{-3}) could be used to estimate the total number of particles produced by the flare. This estimate produced a total particle production of around 10^{11}, or about 10^{8} particles per gram of flare mix.

The largest particle sensed by the FSSP was 13 μm in diameter. This result was somewhat contradicted by airborne tests conducted at low level early in the morning in calm conditions and relative humidities exceeding 80%. The first Commander (JRB) was trailed by the second Commander (JRA) equipped with an FSSP-100 probe and a 2D cloud probe. Two flares were ignited, and JRA trailing JRB by about 30 to 40 m, made measurements in the plume. Unexpectedly, the 2D probe recorded images of what appeared to be drops with diameters between 80 and 300 μm in concentrations of about 8 l^{-1} (Fig 5.1).

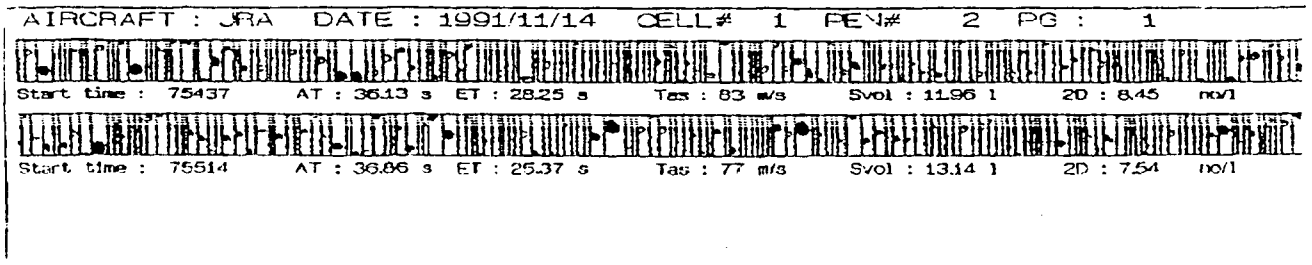

Fig. 5.1 2D images recorded by an aircraft flying in the plume from 2 flares burning on the seeding aircraft. Vertical time bars are 800 microns long.

A second ground run was conducted in which sticky glass slides were used to collect particles in the plume of a burning flare. The slides were examined by Mrs. Pat Sterling at the University of the Witwatersrand, using a scanning electron microscope and X-ray diffraction. These tests identified the elements potassium and chlorine in some of the particles whose diameters exceed 100 µm (see Fig 5.2), confirming the presence of large particles in the plume that were detected in the airborne tests. The small sample volume of the FSSP 100 may explain why this probe missed the larger particles.

The ground and airborne tests are compared in Fig. 5.3, and agree within an order of magnitude. Differences between the measurements can be attributed to:

- underestimation of the concentrations in the airborne tests, since it was not possible to keep probes in the plume from the flares at all times

- the deliquescence of the larger hygroscopic particles causing the "knee" in the airborne spectrum.

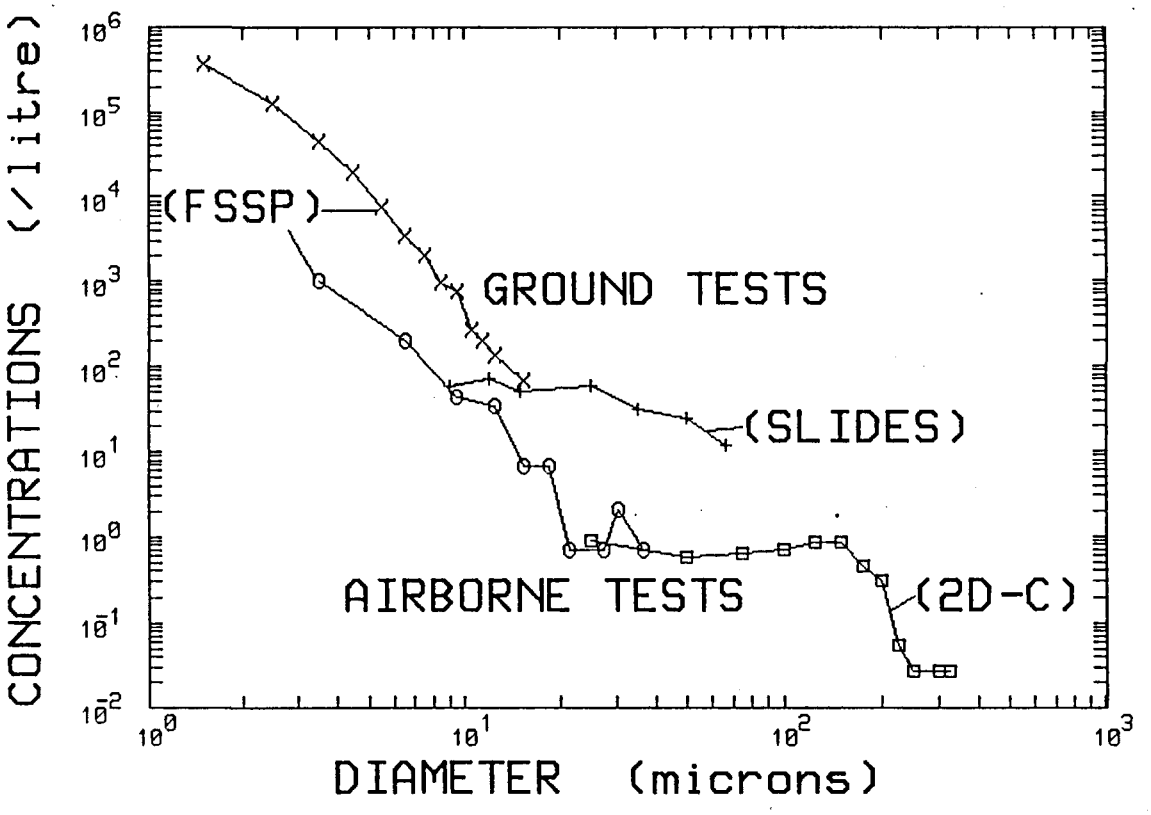

Fig. 5.3 Measured dry particle combustion spectra from ground and airborne tests of hygroscopic flares. See text for details.

(c) Cloud seeding tests

The first trial on clouds took place on October 9, 1990. Observational systems used were the Learjet and the 5 cm radar in volume scan mode. The flares, mounted on the Aero Commander, were ignited at cloud base under a small isolated storm at 15:56. The Learjet had commenced sampling cloud turrets rising on the northwestern flank of this storm at 15:54. Updraft speed was measured at 8.2 m/s. The second pass was at 15:58, and an updraft speed of 9.4 m/s was measured. The Learjet first encountered the seeded plume at 16:02, some six minutes after seeding commenced. This is clearly shown in Table 5.0 and illustrated in Fig. 5.4. The Commander was seeding at about 3000 m and the Lear was sampling at 5900 m, an altitude difference of 2900 m. To reach the altitude of the Lear in the available 6 minutes, the seeding material would have to travel vertically at a speed of 8 m/s which is close to the observed updraft speeds.

There is a dramatic difference in FSSP measurements between pass 2 and 3, most pronounced in the 1 km averages around the updraft maxima. The number of drops with diameters greater than 32 um increases almost seven times from 0.55 to 3.68 cm^{-3}. Note that the mean particle diameter decreases but the mass-weighted mean diameter increases (Table 5.0). Fig. 5.4 portrays time histories of FSSP concentrations and updraft profiles for passes 2 to 4. The tick marks on the X axes are 1 km apart. The spectra show the size distributions of water mass up to the probe size limit of 47 μm. The second spectrum in each group (2) is the 1 km average around the updraft maximum. It is this spectrum that changes radically from pass 2 to pass 3. The updraft peak coincides with the peak in concentrations >32 μm confirming that the updraft is carrying the seeding material. By 16:06, the material appears to be pretty well spread throughout the cloud. The mass density spectra around the liquid water and updraft maxima look similar. Concentrations have almost doubled (Table 5.0) and computed liquid water contents peak on this pass. By 16:10, values have fallen back to pre-treatment levels.

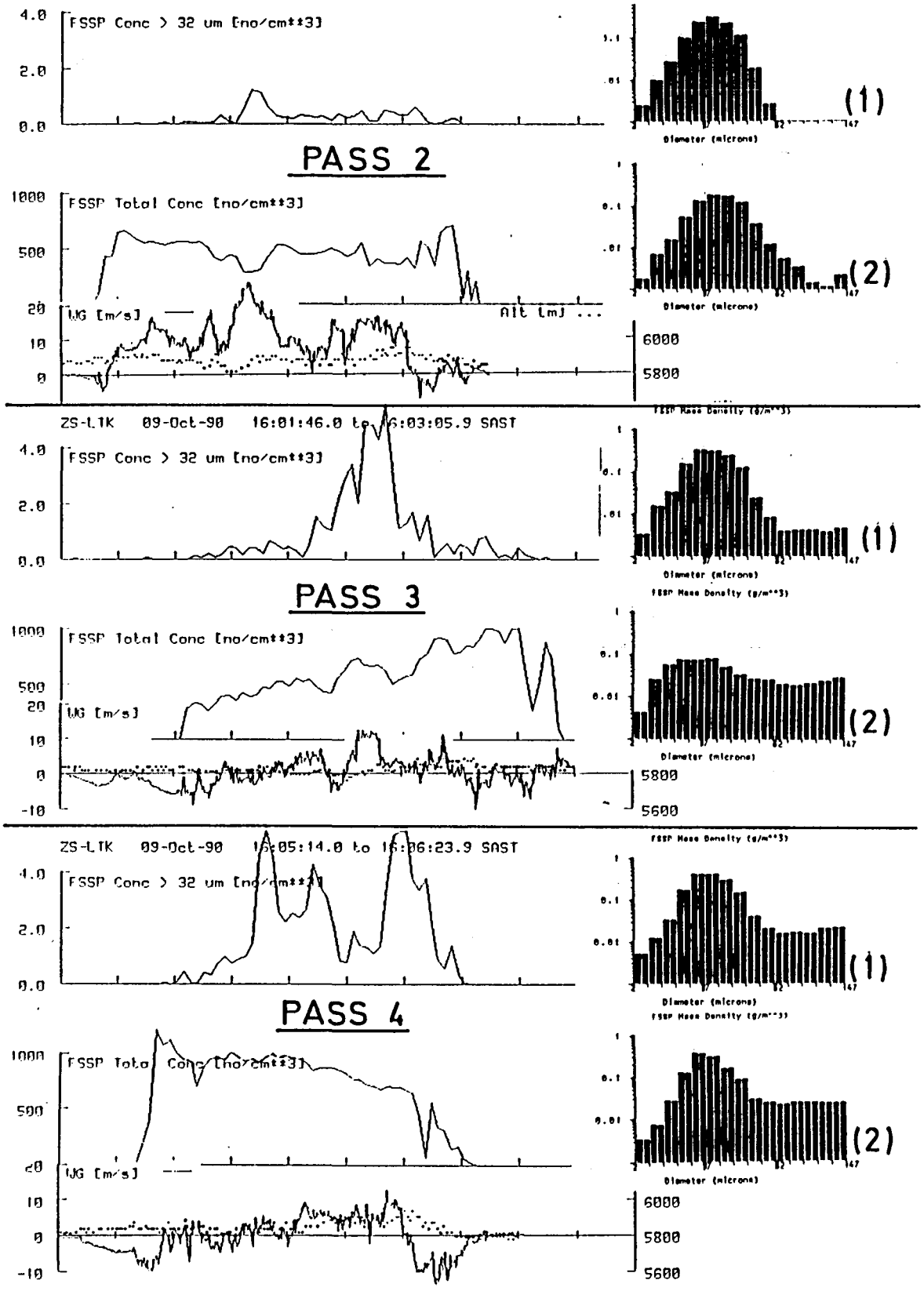

Fig. 5.4 Time histories of FSSP concentrations, FSSP concentrations of droplets >32 μm and vertical velocities measured on 3 passes through a cloud seeded with hygroscopic flares, October 9, 1990. The spectra show how the mass of water is distributed between 2 and 47 μm and is measured over a distance of 1 km around the maximum concentrations (1) and the maximum updrafts (2).

Table 5.0 Comparisons of 1 km averages of FSSP measurements around the maximum liquid water content and the maximum updraft speed.

		Pass:	1	2	3	4	5
		Time:	15:54	15:58	16:02	16:06	16:10
1 km averages around max. FSSP	conc (cm^{-3})		470	589	808	965	595
	conc >32 μm (cm^{-3})		0.20	.02	0.70	3.00	1.13
	LWC (g/m^3)		0.92	1.00	1.26	1.63	1.00
	mean dia. (μm)		13.20	12.30	11.90	12.00	12.30
	MW mean dia.(μm)		19.10	18.40	18.40	19.50	18.70
1 km averages around max updraft	conc (cm^{-3})		413	393	649	703	391
	conc >32 μm(cm^{-3})		0.39	0.55	3.68	3.77	0.57
	LWC (g/m^3)		0.76	0.77	0.57	1.22	0.58
	mean dia. (μm)		12.70	12.60	8.50	12.20	11.60
	MW mean dia. (μm)		19.00	19.90	21.80	19.90	18.20

Aircraft tracks and returns from the target storm were recorded by the project's 5 cm radar, operating in volume scan mode. Objective storm tracking software is used to process the raw radar data. Thus storms are described or characterized in terms of their track properties. Time-height plots of peak equivalent reflectivities appear to be one of the most revealing ways of presenting storm time histories. This technique is used here and portrayed in Fig. 5.5. The trajectory of the seeding material, released at time = 0, arcing up into the cloud to produce a maximum aloft (46 dBz at t+10), the downward cascade of the growing precipitation particles reaching cloud base at t+20 (51 dBz); these can easily be visualized when presented in this manner.

We believe that this seeding event has been well documented; from the release of the material at cloud base to the first interception of the plume by the Learjet to the formation of a reflectivity maximum aloft to rainfall, at least at cloud base. These observations are completely consistent with a seeding-induced acceleration of the coalescence process leading to the early development of large precipitation particles (recall the spreading of the FSSP spectra) in a cloud that might otherwise not have rained at all.

The exploratory seeding trials that were conducted during the 1990/91 season are listed in Table 5.1. Data from the Bethlehem radar was not retrievable until after 16 January 1991. "No data" under aircraft response refers to instrument failure.

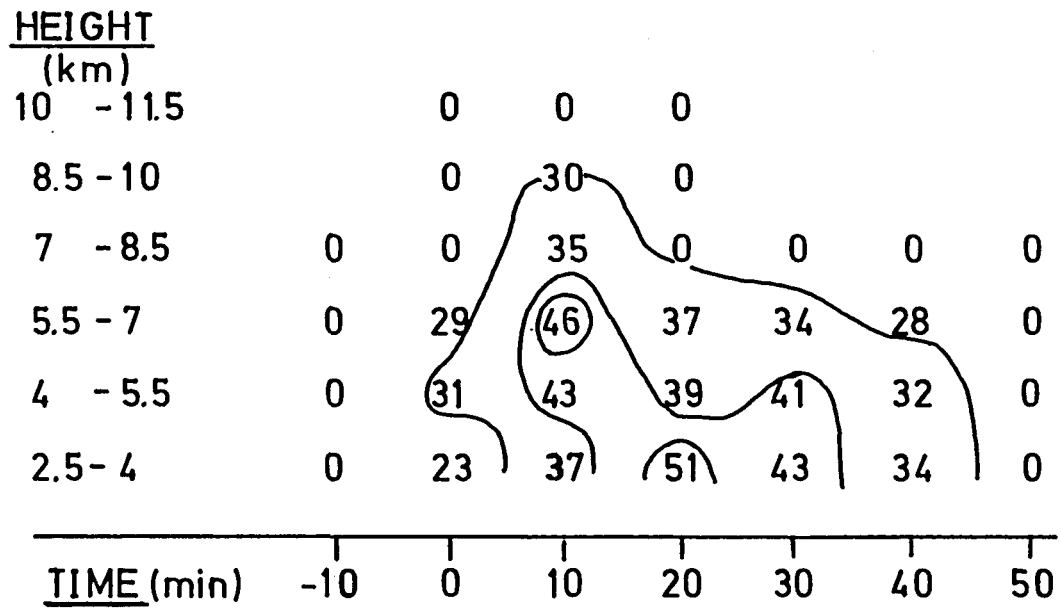

Fig. 5.5 Height-time profile of peak reflectivities measured in a small storm treated with hygroscopic flares on October 9, 1990. The numbers in this figure are in dBz. Contours were drawn by hand.

On December 13, a storm was seeded at cloud base with 7 flares. This storm located just west of the Braam Raubenheimer dam, produced 80 mm of rain in less than an hour, but no hail, despite the fact that the 45 dBz contours exceeded 9000 m (Mather et al., 1976). The time-height profile of this storm is presented in Fig. 5.6. Note the behaviour of the maximum reflectivity profile between about 14:50 and 15:07. Treatment of this storm commenced at 14:20.

Table 5.1 Summary of Flare Tests

Date	Exp	Fired	Radar response	Cloud response
9 Oct	F1	2(S)	Yes *	Yes *
13 Oct	F2	5(S)	Yes	No
20 Nov	F3	2	No, small storm	No
21 Nov	F5	4	Yes *	No
28 Nov	F6(B)	1	No radar	No
13 Dec	F7	6	Yes *	No
15 Dec	F8	4	Yes	Possible
	F9	1	No, small storm	No
4 Jan	F10	4	No data	No data
	F11	4	No data	No data
5 Jan	F12	8	Yes	Yes *
16 Jan	F13(B)	4	No data	Yes *
	F14(B)	2	No data	No data
14 Feb	F15(B)	3	No	No
	F16(B)	2	No	No
	F17(B)	8	No	Yes *
15 Feb	F18	6	No	Yes *
1 Mar	F19	7	Yes *	No
4 Mar	F20	4	Yes	Yes *
	F21	4	No	No
8 Mar	F22(B)	4	Yes	Yes *
	F23(B)	4	Yes	Yes *

NOTES:

1. (S) refers to short flare.
2. (B) experiments conducted at Bethlehem.
3. * further analyses in text and tables.

Two examples of storm track alterations that may have been caused by the seeding are presented next. A storm was seeded east of Carolina on a day when winds at storm steering levels were light. Fig. 5.7 shows all the storm tracks recorded by the Carolina radar on that day. Only one storm exhibits any significant movement (the circled storm). Fig. 5.8 is a blowup of the storm track and the storm time-height profile. Seeding commenced at 15:23 and the last two flares were ignited at 15:38. The first significant jump of the storm position westward occurred between 15:33 and 15:40, some 10 to 15 minutes after seeding commenced. The storm stopped its westward propagation between 16:15 and 16:22, about 30 minutes after the last flare was extinguished. Note the now familiar arc in the time-height plot of maximum reflectivity in Fig. 5.8. Assuming that this traces the seeding effect, the altered precipitation should be reaching the ground some 20 minutes after seeding commences, which coincides closely with commencement of the storm's westward

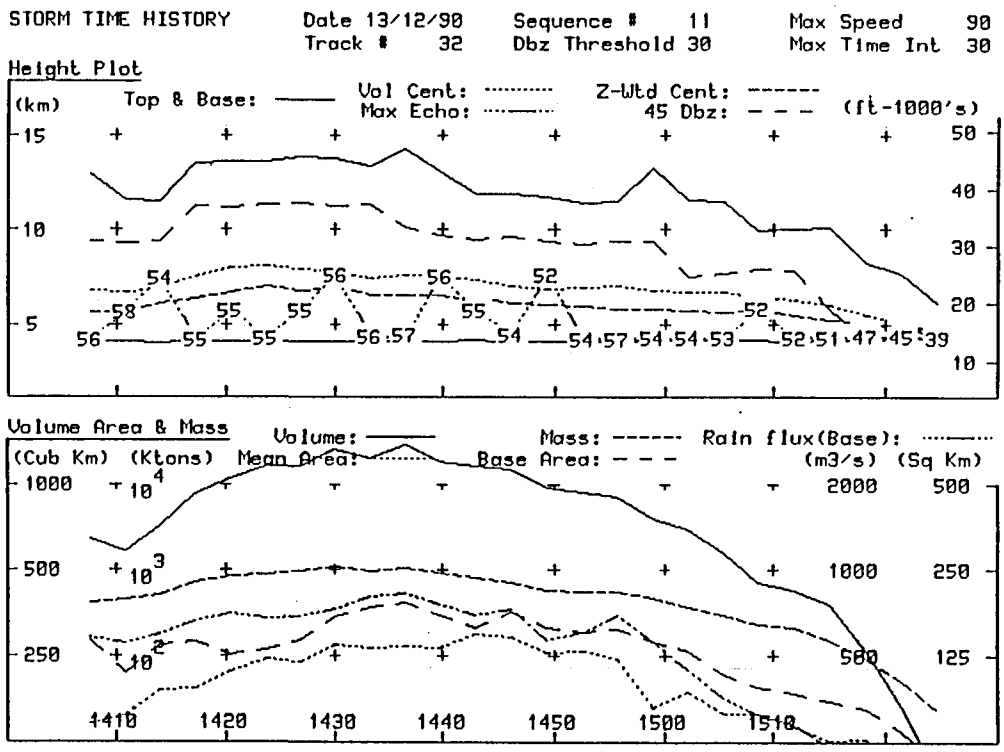

Fig. 5.6 Storm seeded with hygroscopic flares at 14:20 on December 13, 1991. Note the height of the 45 dBz contour (exceeds 10 km). There were no traces of hail from this storm.

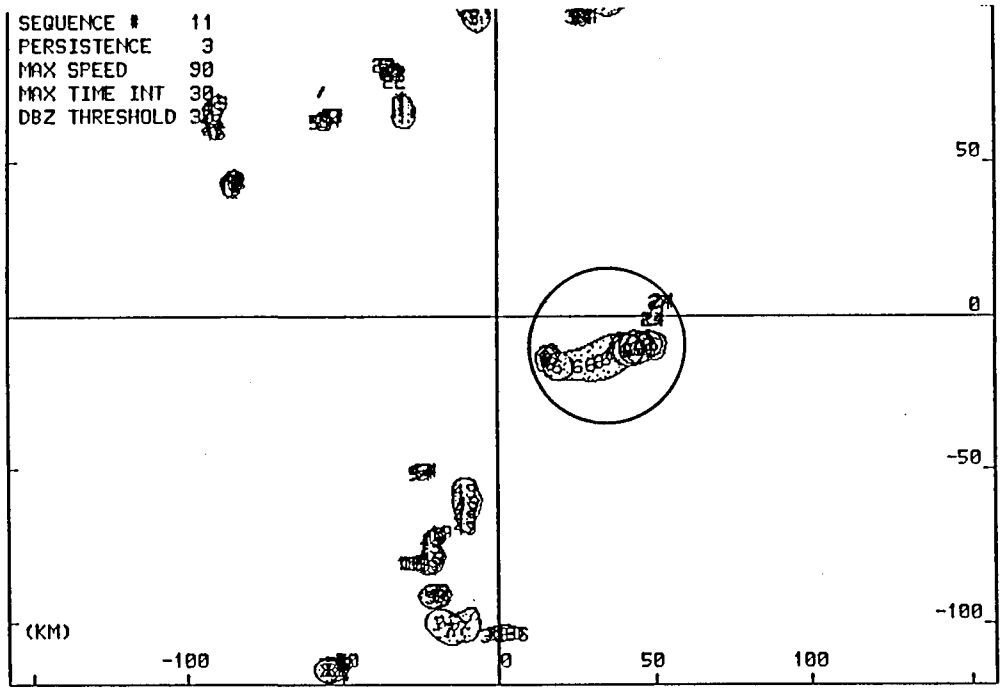

Fig. 5.7 Map of storms tracked on March 1, 1991 within a 120 km radius of the Carolina radar. Note lack of movement except for the storm directly ESE of the radar.

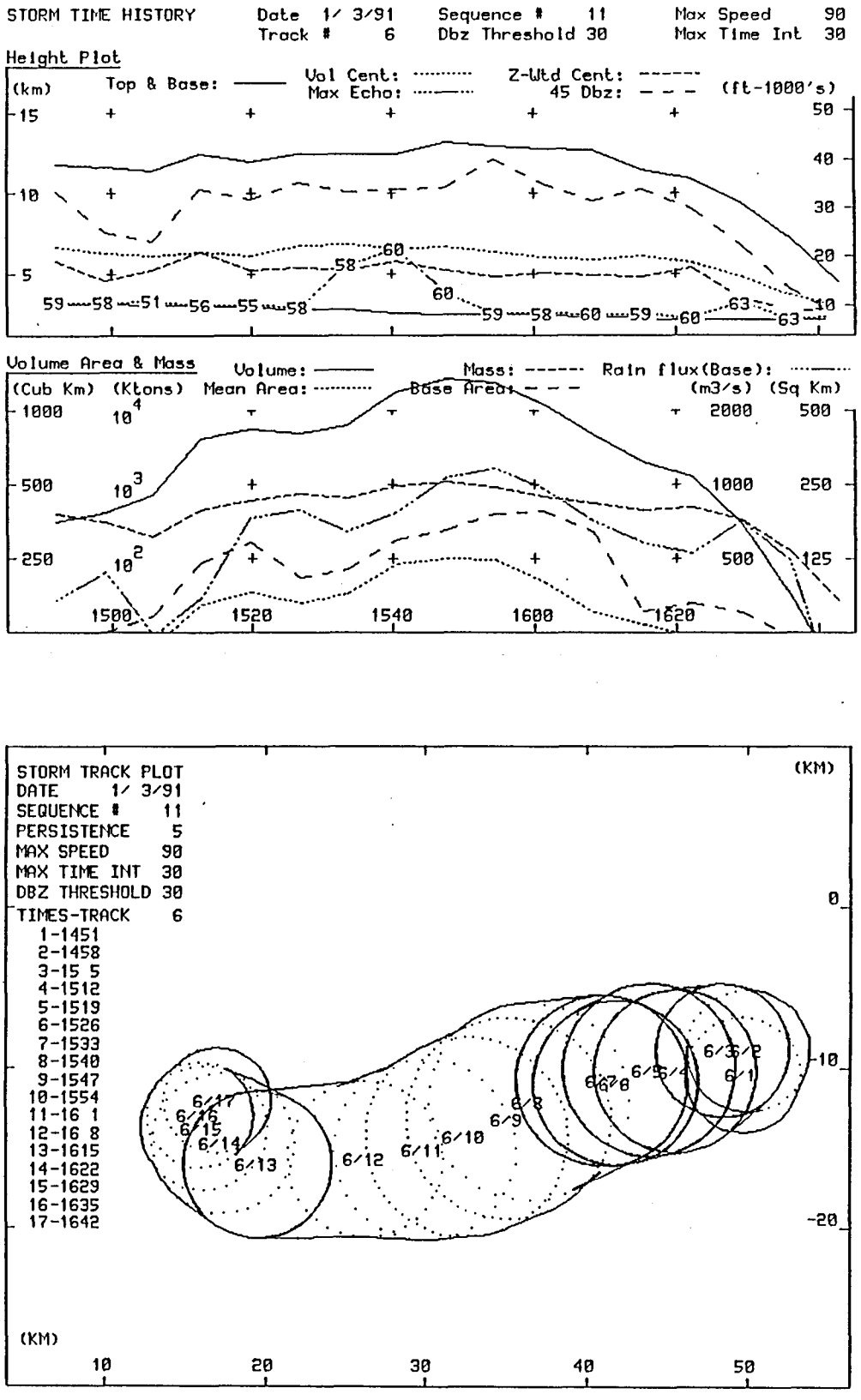

Fig. 5.8 Track and height-time profile of storm seeded on March 1, 1991. Note trajectory of max reflectivity between 15:20 and 16:00 (top).

propagation.

A flare seeding mission in Bethlehem on March 8, 1991 produced curious results. Two adjacent storms were seeded and both exhibited a " dog leg" in their plotted storm tracks which coincided with the seeding. Fig. 5.9 is a plot of storm tracks acquired by the Bethlehem radar on that day. Most of the storms are tracking smoothly to the southeast, except for two tracks, track 46 and 90 which exhibit a sudden lurch westward before continuing their southeast bound tracks. This "lurch" occurs shortly after seeding commences on both tracks. Fig. 5.10 shows the seeding track of JRB and the two apparently altered storm tracks. Fig. 5.11 shows the time-height profiles of both storms. The familiar maximum reflectivity signature is evident in the profile of storm track 90 after seeding commences. Track 46 appears to reflect the commencement of seeding in an upward pulse in the height of the 45 dBz contour (around 13:20).

In summary then, from the exploratory seeding conducted to date, the radar seeding signature appears to be:

- a parabolic trajectory described by the time-height plots of the maximum reflectivities. The trajectory reaches its peak height about 10 minutes after seeding commences

- possible changes in storm tracks, especially notable in light storm steering wind conditions.

The last observation is most intriguing. Microphysical changes of sufficient magnitude to affect the rainfall are likely to have dynamic consequences. Intuitively any significant changes in storm dynamics are most likely to show up as changes in storm track behaviour.

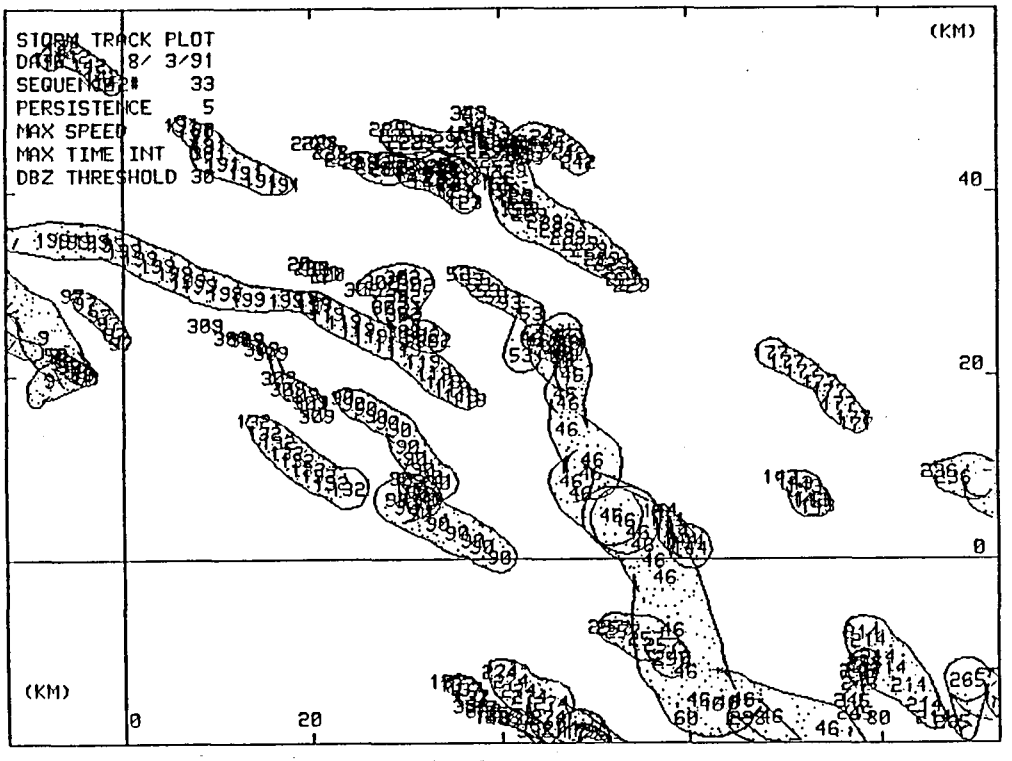

Fig. 5.9 Storms tracked by the Bethlehem radar on March 8, 1991.

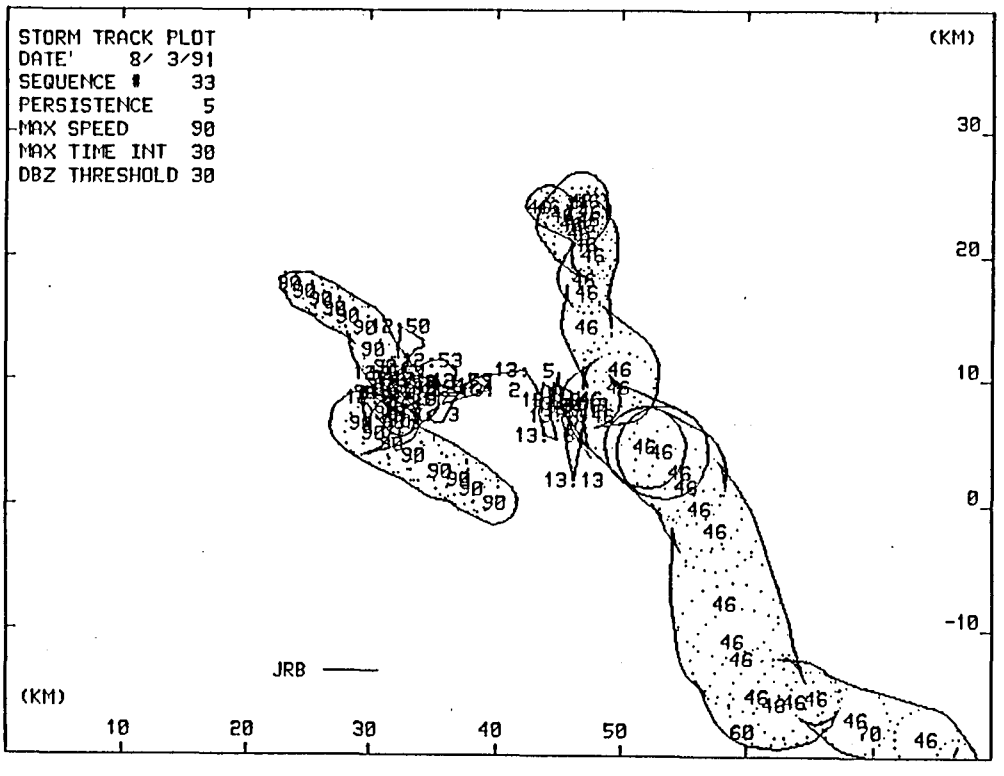

Fig. 5.10 Tracks of storms seeded on March 8, 1991 with hygroscopic flares. The track of the seeding aircraft (JRB) is also shown in this figure. Note that the seeding locations coincide with the storm track shifts westward.

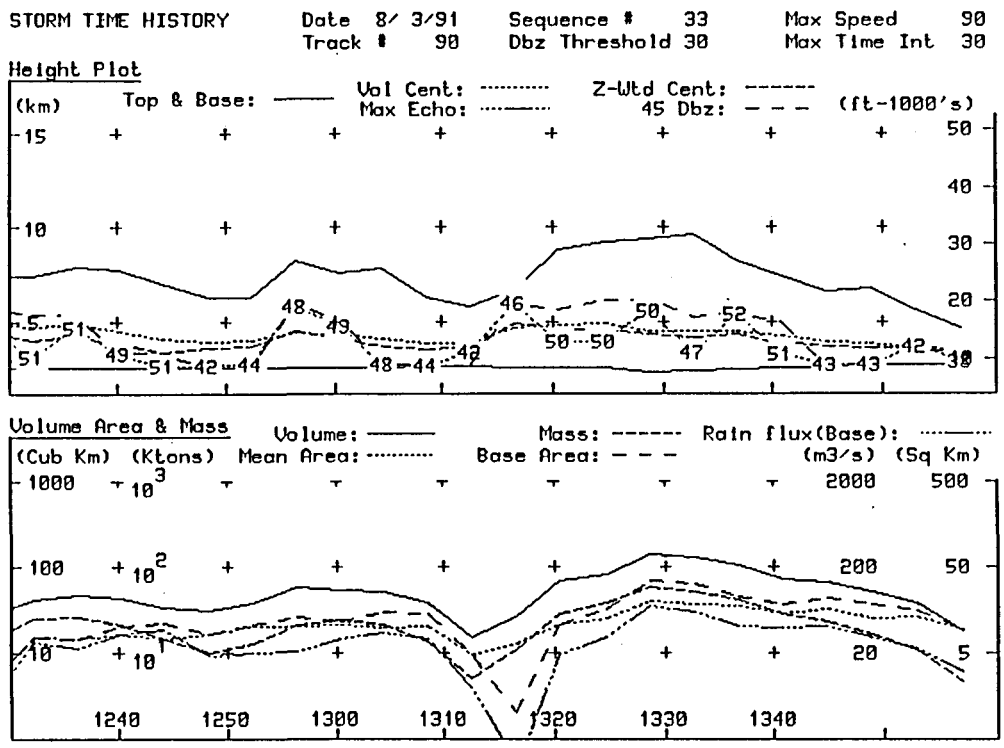

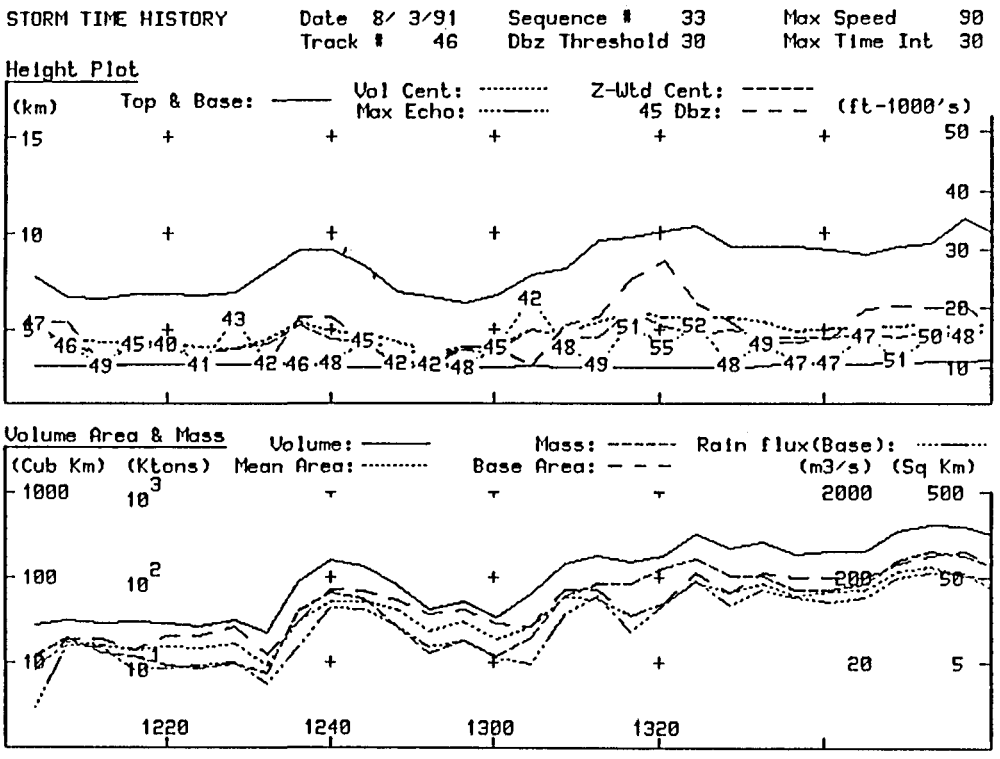

Fig. 5.11 Height-time profiles of the 2 storms seeded with hygroscopic seeding flares in the Bethlehem area on March 8, 1991. Storm track 90 (top) was seeded at 12:50 and track 46 at 13:06.

(d) Microphysical evidence

Table 5.2 is a summary of Lear measurements from clouds judged to be showing a response to hygroscopic seeding. Listed are the times of the sampling pass, the mean 2D-C particle concentrations and mass-weighted mean diameters, the mean and maximum equivalent reflectivities recorded by the aircraft radar and an estimated particle density based on a comparison of reflectivity computed from the 2D-C measurements to that measured by the aircraft radar (Mather, 1989).

Consider January 5, 1991 from Table 5.2. Seeding commenced at cloud base at 13:52. The Lear started sampling at 13:58. Although some ice was present, mass-weighted mean diameters (MWD) are small and radar reflectivities are barely above noise levels. All this changed at 14:07. Particle concentrations jump and MWD increase by almost a factor of 10. Radar reflectivities jump to a mean of 24 and a maximum of 40 dBz. Radar and 2D-C calculated reflectivities match best if the sampled particles are assumed to be water drops.

The 2D-C images from 2 passes on February 14 (Table 5.2) are presented to illustrate the development of drops, frozen drops and dense graupel, presumably as a result of the seeding, in a storm in the Bethlehem area. Fig. 5.12(a) is a pass through a cloud unaffected by the seeding. The images show "streaking" (caused by water running off the probe) and some small images less than 300 μm in diameter, probably small ice crystals. The line of pass-averaged variables, immediately above the images indicate a high liquid water content and a poor "conversion efficiency", i.e. very little of the cloud water has been converted to precipitation at the sampling level. Contrast Fig. 5.12(a) with (b) which shows images of large frozen drops and graupel. The line of pass-averaged variables for this figure indicates that in this case, 57 percent of the cloud water has been converted into precipitation. The engine temperature measurement of cloud water content, which is the water content in the precipitation plus the cloud supercooled liquid water content (measured by the King hot wire), has been used in the conversion efficiency computation (Morgan et al., 1989).

In summary then, both the radar and the microphysical measurements in many of the clouds that have been seeded experimentally with the new hygroscopic seeding flares are showing strong signatures that are compatible with the seeding hypothesis. (Hygroscopic seeding at cloud base should produce more and larger particles sooner in the life cycle of the treated storm, thereby harvesting more of the available supercooled water, i.e. increasing the efficiency of the rainfall process).

Table 5.2 Summary of Lear Measurements

Time (SAST)	2D-C CONC (l^{-1})	2D-C MWD (mm)	Radar MEAN (dBz)	Radar MAX (dBz)	Est. Density (g/cm^3)	Remarks
			5 JANUARY 1991 - NELSPRUIT			
13:58	13.5	0.14	6	13	-	Flares
14:02	7.7	0.12	4	7	-	2 x 13:52
14:07	37.1	1.14	24	40	1.0	2 x 13:56
14:10	15.2	0.89	21	36	-	2 x 14:02
14:14	8.3	0.28	14	28	-	2 x 14:08
14:21	11.8	0.44	12	25	-	
14:28	48.5	0.33	15	26	1.0	
14:34	20.3	1.30	18	33	0.2	
			16 JANUARY 1991 - BETHLEHEM			
13:36	2.1	0.06	3	4	-	2 x 13:35
:38	0.9	0.12	3	4	-	
:41	5.6	0.40	6	14	0.2	
:44	2.5	0.18	4	6	0.8	2 x 13:44
:49	25.7	1.41	20	37	1.0	
:51	5.8	0.23	24	34	1.0	
			14 FEBRUARY 1991 - BETHLEHEM			
15:37	38.4	0.95	13	21	0.4	2 flares
15:42	2.3	0.18	4	5	-	
15:46	2.2	0.57	6	13	-	2 flares
15:52	13.3	1.56	17	30	0.8	2 flares
15:54	4.4	0.29	6	18	-	
15:56	17.5	1.07	10	23	0.2	
15:59	13.0	0.85	12	24	0.4	2 flares
16:06	16.8	1.56	24	32	1.0	
16:12	9.3	2.18	24	40	-	Drops
			15 FEBRUARY 1991 - BETHLEHEM			
13:24	1.7	0.26	6	14	-	2 x 13:22
13:31	2.6	0.27	5	11	0.2	2 x 13:26
13:36	1.3	0.71	14	24		2 x 13:38

- abandoned because of generator failure

Table 5.2 continued/

Time (SAST)	2D-C CONC (l^{-1})	2D-C MWD (mm)	Radar MEAN (dBz)	Radar MAX (dBz)	Est. Density (g/cm^3)	Remarks
			4 MARCH 1991 - NELSPRUIT			
13:29	0.3	0.35	3	4	-	2 x 13:35
13:42	0.9	0.09	4	4	-	2 x 13:41
13:44	3.9	2.57	21	30	1.0	
13:51	20.4	1.40	25	35	-	
			8 MARCH 1991 - BETHLEHEM			
12:51	1.9	1.28	6	31	0.6	2 x 12:50
	9.2	0.77	16	27	0.4	
12:56	14.2	1.67	19	30	1.0	2 x 12:56
12:59	48.1	0.51	27	34	0.8	
13:02	1.0	0.08	3	5	-	
			8 MARCH 1991 - BETHLEHEM			
13:04	1.7	0.33	4	7	0.8	
	2.2	0.35	6	9	0.6	
13:06	1.4	0.21	7	14	-	2 x 13:06
13:09	17.0	1.02	29	40	1.0	2 x 13:10
13:12	27.7	1.12	31	45	-	
13:15	4.7	1.56	15	25	-	
13:18	36.5	0.91	28	36	1.0	

Fig. 5.12(a)

Time (SAST)	Alt (m)	Temp (^{o}C)	Updraft (m/s)	King La (g/kg)		E.T.	C.E. (%)
15:42	5905	-6.0	5.1	4.32	5.43	4.78	10

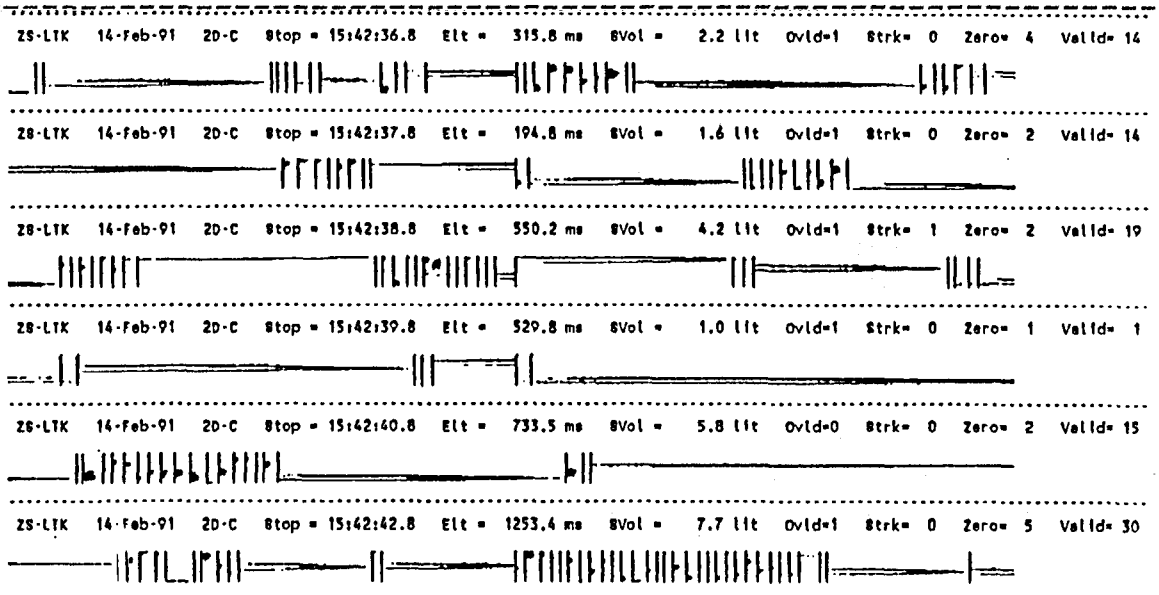

Fig. 5.12(b)

Time (SAST)	Alt (m)	Temp (^{o}C)	Updraft (m/s)	King La (g/kg)		E.T.	C.E. (%)
16:12	5844	-7.0	3.0	2.03	7.29	4.77	57

Notes: (1) Vertical time bars separating images are 1.2mm long
(2) C.E. is defined as (1 - King/E.T.) x 100.

The results from this one season of experimental seeding justified the design and execution of a randomized seeding experiment, which was conducted during the 1991/92 season.

6.0 THE RANDOMIZED HYGROSCOPIC CLOUD SEEDING EXPERIMENT

(a) Introduction

The decision to conduct a randomized seeding experiment was based upon the promising results of the 1990/91 seeding trials. The experiment was proposed only after the NPRP researchers had achieved confidence in their seeding hypothesis.

Flare racks were built by Atlas Aircraft Corporation to carry ten 1 kg flares mounted behind each engine nacelle. These were electrically fired from a selector switch and a firing button in the aircraft cockpit. First tests of the racks (Oct 3, 1991) indicated that flow reversal around the rear of the nacelles was burning the plastic connectors holding the ignition wires. The racks were returned to Atlas for modification. The first randomized seeding experiment took place on October 15. Two flares were ignited on the left hand rack. These set alight the rest of the flares in the rack. The resulting conflagration severely damaged the seeding rack. At this stage, Atlas proposed a completely new design. Each flare receptacle was mounted on a small pylon which placed the burning flare well above the boundary layer into the air flow around the nacelle. To ensure streamline flow, the nacelle rear faring was replaced.

The new flare racks were successfully tested on November 14, and no further troubles were encountered with the new system.

(b) Experimental design

The experimental design was worked out in conjunction with Professor F E Steffens and his team at UNISA.

1. Two sets of paired envelopes were prepared at UNISA, one for Bethlehem experiments, the second for Nelspruit. One set of the pairs was held at the Carolina and Bethlehem radars. Matching pairs were held in the seeding aircraft (JRB).

2. Launch criterion was the appearance on radar of two separate echoes that simultaneously exceeded 40 dBz.

3. The seeding aircraft was directed to the storm of interest by radar. The cloud top sampling aircraft, either the Learjet or the other Commander, was directed to the same storm.

4. JRB's pilot chose the experimental storm on the basis of a seedable updraft before declaring an experiment (decision time).

5. An experiment was performed if

- JRB's transponder was visible on radar
- the storm was clearly identified on radar
- the cloud top aircraft was in position. However, experiments were permitted in the absence of an available cloud top aircraft.

Once JRB's pilot declared an experiment, and it was determined that the above conditions were fulfilled, the radar operator opened the appropriate envelope, broadcast the decision to JRB who then opened his matching envelope. The combinations and outcomes were as follows:

RADAR	JRB	ACTION
Seed	No	No-seed
Seed	Yes	Seed
No-seed	Yes	No-seed
No-seed	No	Seed

Since the pilot did not announce his action, and stayed with the chosen storm for 15 minutes whatever the outcome (seed or no-seed), both the radar operator and the cloud top aircraft were "blind" as to treatment. This prevented any biases creeping into the collection of the radar and microphysical observations.

JRB was equipped with 20 flares of which a maximum of 10 were used per experiment (storm). Since two successive cases could both be "seed", no more than 2 experiments took place per flight, thus preserving blindness as to treatment. A second experimental storm had to be at least 20 km distant from the first case.

Daily forecasts of the best area for operations were made by the Bethlehem group. Telephone briefings took place each day at 10:30 and operations were planned based upon the forecast and equipment availability (aircraft, radars).

(c) The experiment

The design of the experiment remained unchanged throughout the season. The breakdown of case numbers by month and area are shown in Table 6.0.

Table 6.0 Experiments tabulated by month and area.

Month	Bethlehem		Nelspruit	
Oct			201	(1)
Nov	501	(1)	202 - 209	(8)
Dec	502 - 504	(3)	210 - 214	(5)
Jan	505 - 506	(2)	215 - 225	(11)
Feb	507 - 514	(8)	226	(1)
Mar	515 - 521	(7)	227 - 230	(4)
	Totals	21		30

Most of the Bethlehem storms were acquired in the last two months of the season, whereas the experiments at Nelspruit took place in the first four months of the season.

At a farmers meeting in Carolina on February 4, 1992, it was agreed to suspend operations in that area for one month (Feb 4 to Mar 4). This accounts for the sudden drop off in experiments in that area.

The 1991/92 season was one of the driest summers on record, resulting in fewer storms and the usual public relations problems attendant with droughts. This may also have affected storm characteristics in other ways (smaller storms, higher cloud bases, etc). Comparison of results from future experimental seasons will be needed to resolve this question.

The radar data were collected by the Bethlehem and Carolina 5 cm radars operating in volume scan mode. Both radars used identical software to collect storm reflectivities. Calibration of both radars was checked on a daily basis. Initially the radar tapes at Bethlehem were processed using Nelspruit software and the "storms" file sent to Nelspruit for storm track analyses. By the end of the season, the storm tracking software had been implemented on the Bethlehem computer, and track identification and analysis could be carried out at both sites. This had the advantage of allowing all personnel to participate in the track selection process, thereby increasing our confidence in the correct selection of case tracks. For details on the storm and track analysis software, see Programme for Atmospheric Water Supply, Volume 4, (1986). All tracks from all experimental days are stored on both computers, so it would be possible for the analysis to be re-run by individuals that were unaware of treatment. Here, most of the tracks were selected by staff who were aware of the treatment.

(d) Results

The core of the statistical analysis of the experiment is being carried out at UNISA by Professor Steffens and his group, and results to date are included as appendices to this report (Appendix 2 and 3). Presented here is a brief analysis of the experiment carried out at Nelspruit using the re-randomization software that is available in our radar software package. This analysis differs from UNISA's since geometric rather than arithmetic means were used in the storm track property comparisons. However, the results of the two analyses are almost identical. In both, storm track properties are averaged over 10 minute segments from decision time (t=0). This follows the procedure that was developed to analyse the Nelspruit dry ice seeding experiment, which led to insights into physical mechanisms that could have led to the observed increases in radar-measured rainfall. Table 6.1 is a summary of the relevant mean storm track properties.

Table 6.1 Mean storm track properties

Property	0 - 10 Seed/No-seed	10 - 20 Seed/No-Seed	20 - 30 Seed/No-seed	30 - 40 Seed/No-seed	
Mean storm:					
Volume	203/222	171/239	211/250	319/224	(km^3)
Area	45/48	41/48	49/60	69/55	(km^2)
Rain flux (1.5^o)	106/126	91/123	111/143	172/166	(m^3/s)
Rain mass (1.5^o)	63/73	49/60	57/72	101/46	(ktons)
Rain mass (6 km)	29/39	23/32	36/27	65/16	(ktons)
Rain mass (6 km) / Rain mass (1.5^o)	0.46/0.53	0.47/0.53	0.63/0.38	0.64/0.35	
CASES	24/24	25/24	22/20	16/17	

PERCENTAGE DIFFERENCES $\frac{\text{SEED - NO-SEED}}{\text{NO-SEED}} \times 100$

Mean Storm:	%	%	%	%
Volume	- 9	- 28	- 16	42
Area	- 6	- 16	- 18	27
Rain flux (1.5^o)	- 25	- 26	- 22	48
Rain flux (6 km)	- 25	- 33	30	185
Rain mass (1.5^o)	- 14	- 19	- 20	117
Rain mass (6 km)	- 27	- 28	35	298

Pertinent observations from this table are :

1. The radar data from Bethlehem and Nelspruit have been combined since this is a relatively small data set. The combined geometric means show a negative bias (against a seeding effect) which is dramatically reversed in the 30 - 40 minute time interval.

2. All the data have been used. No attempts were made to stratify the data on the basis for example, of cloud base temperature, location etc. The only restriction was that the average storm positions had to be contained in a range interval of between 10 and 90 km from the radars. All case tracks passed this restriction.

3. The statistics are well behaved. For example, the average seed versus no-seed rain masses parallel each other for the first 3 time windows. Only in the fourth (30 - 40 minutes after seeding commences) do they diverge, the average seeded storm rain mass exceeding the no-seed by 117 percent.

4. Of great importance here is that the first seed/no-seed differences appear in the third time window (20 - 30 min) at 6 km. Radar-measured changes between the seeded and control group of storms are appearing first aloft, then later at the surface (more correctly at 6 km then on the low level scan). This observation is depicted in Fig. 6.0 and perfectly matches the seeding hypothesis.

5. The ratio of the seeded rain mass at 6 km to that at 1.5^{o} becomes significantly greater than the unseeded storm mass ratio 20 to 30 minutes after decision. This ratio was previously used to stratify those storms allegedly altered by the Kraft paper mill west of Nelspruit from other storms in the area (Mather, 1991). This previous study showed that certain storms growing close to the paper mill were showing enhanced growth of drops aloft, interpreted as clear evidence of an accelerated or amplified coalescence growth process presumably caused by the hygroscopic emissions from the mill. Table 6.1 shows this ratio jumping from 0.47 to 0.63 from the second to the third time window for the seeded storms, whereas the control group mean drops from 0.53 to 0.38 over the same period. This top heavy structure revealed by the radars is believed to be a characteristic of storms in which precipitation formation via coalescence dominates.

6. Remarkably, this experiment has reached acceptable levels of statistical significance in a single season, without the use of covariates or data stratification. Given the noisy environment characteristic of convective cloud research, this means that the seeding signal is a strong one.

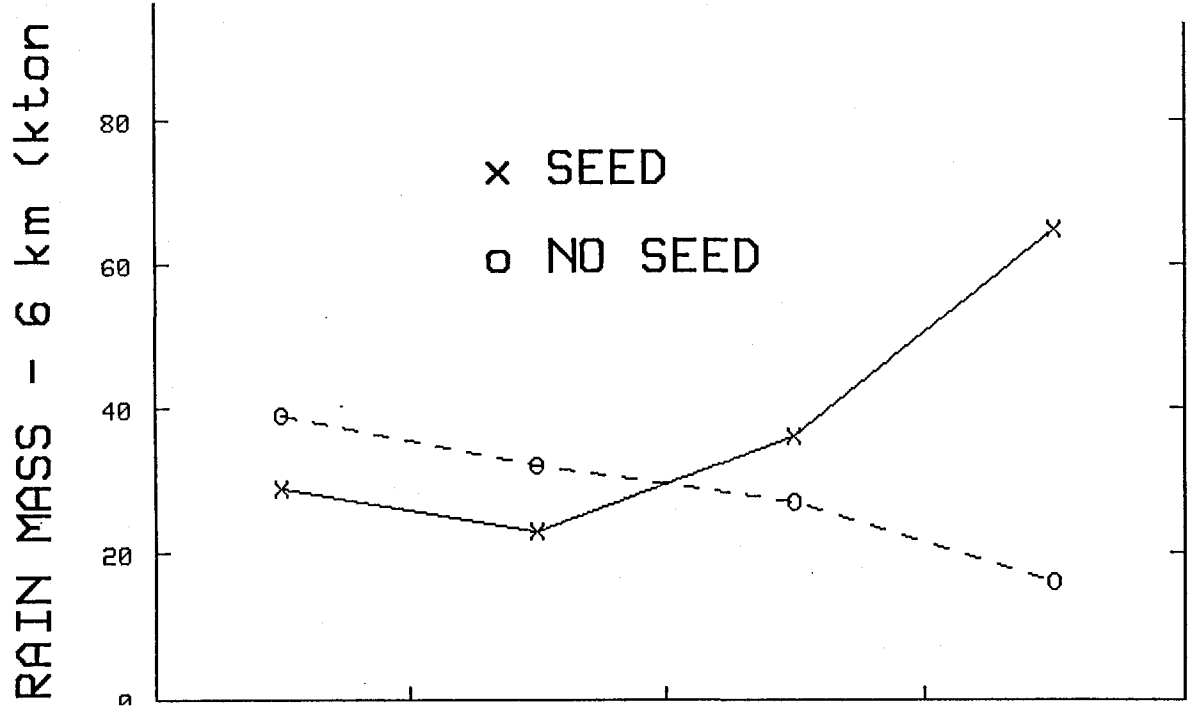

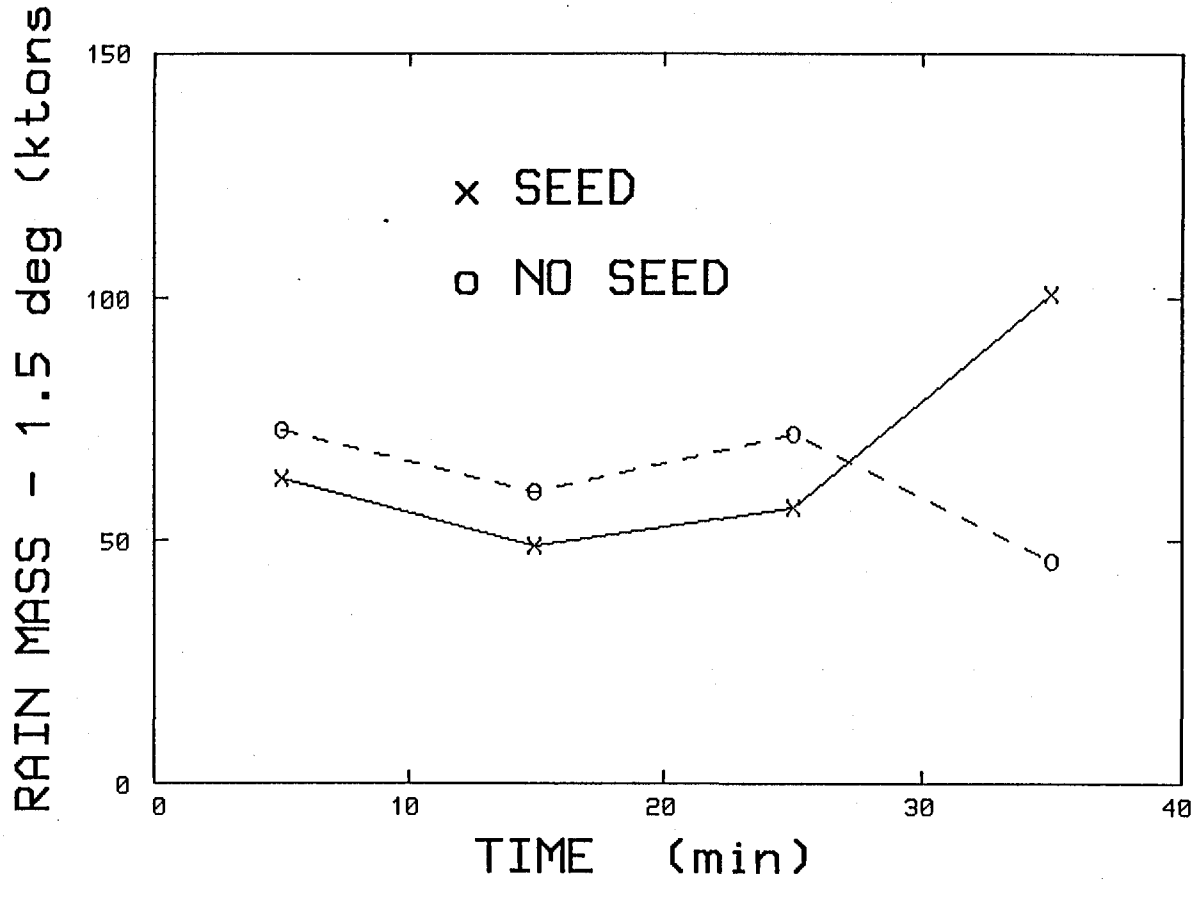

Fig. 6.0. Comparison of seed versus no-seed rain mass in 10 minute time windows from decision time (t=0) at 6 km and lowest scan (1.5°).

It is prudent to examine the distributions of the key variables to make sure that the results are not dependent upon outliers or some other quirk in the data. A comparison of relative frequency distributions is one of the best ways of obtaining a feel for the way the variables are behaving. Fig. 6.1 compares the relative frequency distributions of seed versus no-seed radar-estimated storm rain mass at 6 km. In the first time window, there is a clear bias here in favour of the control storms. As time passes, the no-seed distributions show only minor changes whereas the seeded distributions increase steadily, overtaking then surpassing the control distribution.

The radar-measured increases in rainfall from seeded storms are coming from an increase in storm area and rainfall rate. Average rain rates can be obtained by dividing the rain flux by storm area and multiplying by 3.6 (units of mm/hr)

Table 6.2 Comparative average rain rates

	0 - 10 Seed/no-seed	10 - 20 S/NS	20 - 30 S/NS	30 - 40 min S/NS
Rain rates (mm/hr)	8.5/9.4	8.0/9.2	8.2/8.6	9.0/7.6

Both the seeded and control storms are showing decreases in rain rates in the second time window. The unseeded storms continue this trend whereas the seeded storms begin an increase in the third time window which is carried through to the 30 - 40 min. time interval. Convective storms all have a finite life span, and normal behaviour after selection would be a decrease in intensity with time. The dry ice experiment suggested that seeding led to a reduction in this rate of decline. Initial results from this experiment show a reversal of this trend; apparent increases in storm sizes. Corroboration of this result from an extended experimental data set would provide convincing indications of storm invigoration through alterations of storm dynamics.

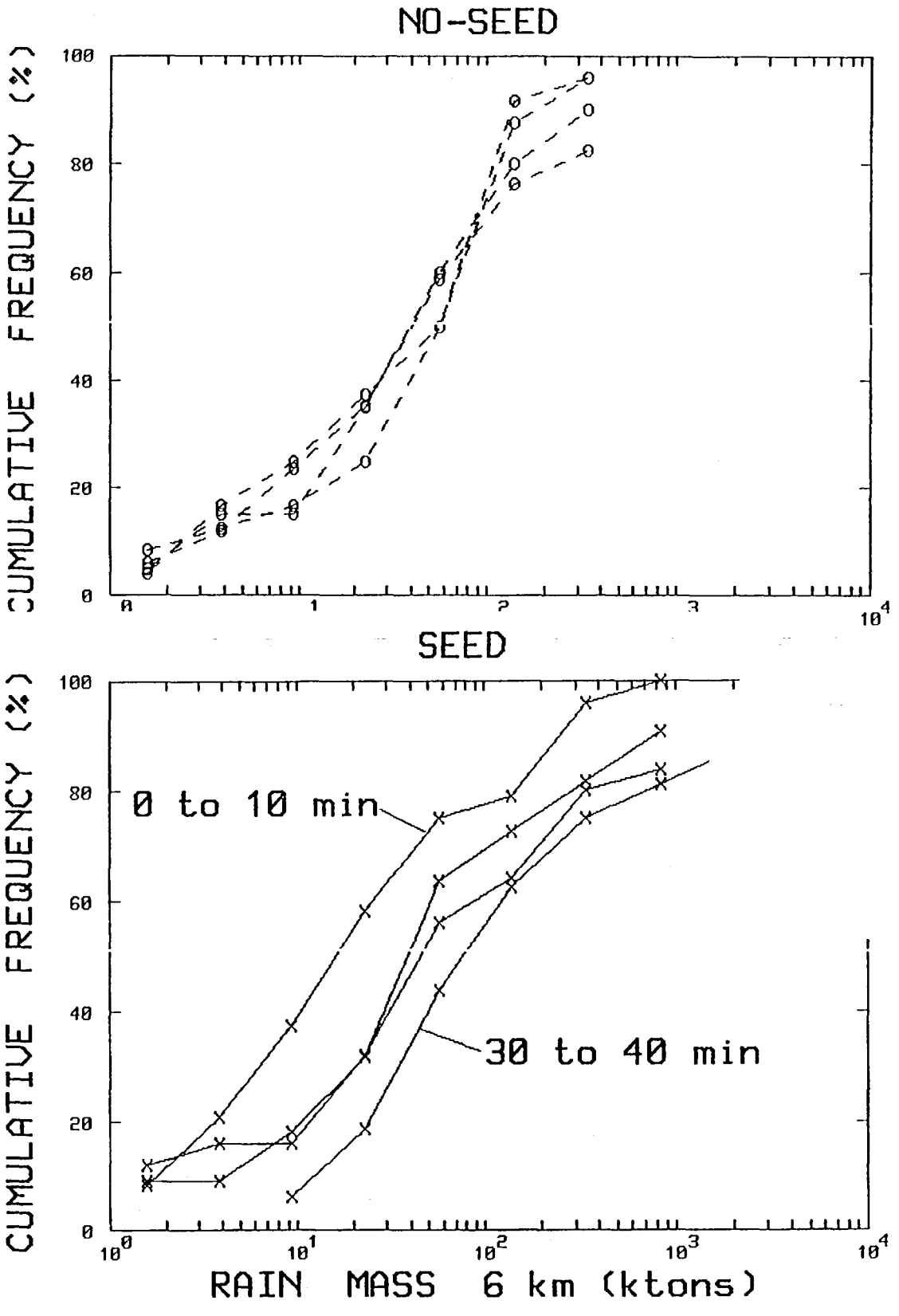

Fig. 6.1. Cumulative frequency distribution of storm rain mass at 6 km for seeded and control storms in four 10 minute time windows from decision time.

7.0 RADAR CLIMATOLOGY

(a) Introduction

With the Nelspruit storm tracking software implemented on the Bethlehem radar, it now becomes possible to compare the storm climatology of the two areas. This comparison serves two purposes; it checks on the performance of the radars, determining for example range limitations (how far from the radars can an experiment take place), and it compares the characteristics of the storms in the two areas.

(b) Analysis methods and results

Volume scan data from the 2 radars were analysed in the following manner. The average storm track positions for the 1991/92 season were stratified into 20 km annuli as shown in Table 7.0. Because of different scan angle sequences determined by the different radar beam widths (Bethlehem 1.0 deg, Nelspruit 1.6 deg.) the analysis at Nelspruit starts 10 km from the radar, while the Bethlehem analysis commences at 20 km. The normalized tracks (normalized by dividing the track numbers by the number of tracks in the first annulus) are compared to the normalized areas (divided by the area of the first annulus). Based upon geometry alone, these two normalized values should compare closely and do up to about a range of 80 km from both radars. Thereafter, the normalized track values decrease even though the areas of the annuli are increasing. We believe that this behaviour is caused by attenuation of the radar signal by storms in the inner annuli.

Storms only partially filling the radar beam, leading to overestimation of storm volumes, areas and rain masses, is apparent after about 80 km from both radars. This effect should begin to appear at a greater range at Bethlehem because of the narrower beam width, but is probably offset by the smaller storms that were recorded in this area. The averages (storm volumes, areas and rain masses) shown in Table 7.0 are all geometric means except for the values shown in parenthesis under "Averages" at the bottom of this table. These arithmetic averages indicate that Bethlehem storms are 3 to 4 times smaller on average than the storms acquired by the Carolina radar over the period in which this study took place. It is interesting to compare the arithmetic averages of the storms chosen as cases for the randomized seeding experiment. Although larger than the rain mass averages in the climatic study, the ratio of about 4 (Carolina rain mass/Bethlehem rain mass) found in the climatology study is preserved in the experiment. This suggests that the cases chosen for experiments in both areas are representative of the overall storm populations.

The relation between radar-estimated rain masses (R_b and R_c) and area-time-integrals is listed at the bottom of Table 7.0, and is similar for both areas (and both radars). Storms with area-time-integrals larger than 2 km^2.hr on average produce more

rainfall in the Carolina area than in Bethlehem. Also, larger storms in the Carolina area rain harder (a Bethlehem exponent of 1.10 versus 1.16 for Carolina).

This study will have an impact upon future planning of an area experiment, given that the sample used in this study is representative of the average storm climatologies in both areas.

Table 7.0 Bethlehem and Carolina radar comparisons

CAROLINA

Range Annulus	10/30	20/40	30/50	40/60	50/70	60/80	70/90	80/100	90/110 km
Mean Range	20	30	40	50	60	70	80	90	100
TRACKS	385	593	790	937	1069	1053	928	834	717
NORM AREA	1	1.5	2.0	2.5	3.0	3.5	4.0	4.5	5.0
NORM TRACKS	1	1.7	2.1	2.4	2.8	2.7	2.4	2.2	1.9
MEAN:									
Echo top (m)	6519	6368	6095	5913	5905	6094	6359	6533	6703
Volume(km^3)	26	28	26	24	23	25	29	34	38
Area(km^2)	6.9	8.7	9.8	10.3	10.3	10.5	11.6	12.4	14.5
Rain Mass(1.5^o)	17	19	19	17	16	16	16	19	21
Rain Mass (6.0km)	4	4	3	4	4	5	6	6	10
dBz (1.5^o)	37.1	36.4	35.6	34.9	34.5	34.4	34.3	34.6	34.6

BETHLEHEM

Range Annulus	20/40	30/50	40/60	50/70	60/80	70/90	80/100	90/110 km
Mean Range	30	40	50	60	70	80	90	100
TRACKS	286	323	414	489	520	508	441	411
NORM.AREA	1	1.3	1.7	2.0	2.3	2.7	3.0	3.3
NORM. TRACKS	1	1.1	1.4	1.7	1.8	1.8	1.5	1.4
MEAN:								
Echo top (m)	6187	6239	6196	6203	6172	6377	6873	7235
Volume(km^3)	21	20	19	18	18	21	28	33
Area (km^2)	4.5	5.1	5.2	5.6	6.2	6.9	8.1	9.1
Rain Mass (1.5^o)	8	9	8	9	9	10	11	12
Rain Mass (6km)	2	2	2	2	3	4	5	7
dBz(1.5^o)	34.7	34.7	34.4	34.8	34.2	34.1	34.5	34.4

AVERAGES

Mean	Bethlehem (1456 tracks)		Nelspruit (3172 tracks)	
Echo Tops (m)	6257		6160	
Volume (km^3)	20	(45)	26	(132)
Area (km^2)	5.7	(10.6)	10.0	(31.3)
Rain mass (1.5^o)	9	(43)	17	(160)
Rain mass (6km)	3	(31)	5	(95)
dBz (1.5^o)	34.3		35.1	

$$R_B = 5.04\ (ATI)^{1.10} \qquad R_N = 4.88\ (ATI)^{1.16}$$

Randomized experiment

Rain mass (1.5^o)	(58)	(225)

7.1 Radar storm characteristics at and above the 30 dBz level in the Bethlehem area during December 1991 and January 1992.

(a) Introduction

During the summer of 1991/1992 the National Precipitation Reseach Programme's (NPRP) Bethlehem section participated in a satellite/radar/rainfall study whereby the Enterprize radar was operated on a continuous basis. This study is funded by the Water Research Commission and is known as RASRAIN (RAdar and Satelite RAINfall). The Weather Bureau, the University of Pretoria and the Department of Water Affairs are the participants in this ongoing study.

Steyn and Bruintjes (1990) reported on the characteristics of 3345 echoes observed during during 33 days in the summer of 1988/1989. They concentrated on echoes at and above the 10 dBz level in contrast with the higher reflectivity storms that are considered in the present study.

The radar data collected as part of the RASRAIN project were used to study the storm properties of all storms between 20 and 80 km from Bethlehem at or above the 30 dBz level. The aim of this study is to summarize the characteristics of the more significant clouds which are representative of the experimental units in the present precipitation research effort of the NPRP. An objective tracking procedure was used to calculate storm properties of 826 storms with lifetimes greater than 16 minutes.

(b) Equipment and data

Steyn and Bruintjes (1990) summarized the Enterprize radar's technical specifications. Since 1990 this radar has been upgraded to computer based data assimilation, storage and control of the antenna. The radar is programmed to operate in an 18 step volume scan which takes about 4 minutes to complete. A base scan elevation of 1.5 degrees was chosen. The elevation step size was determined using an optimization scheme which assures constant resolution between steps at the furthest radar bin of interest. Therefore the step sizes at higher elevations are larger than those at low elevations.

The raw video and pulse repetition frequency (PRF) signals are fed directly into the same computer where integration and processing takes place. Thereafter the data are stored on 2.3 Gigabyte Exabyte cassettes for analysis and at the same time a selected elevation is displayed. In addition to the above, the raw IFF (Identify Friend or Foe) position signals of the research aircraft's transponders are processed, displayed and stored by the same system. Parameters including radar bin size (600m), number of integrations per bin (8), and number of elevation steps with the required elevation values, are all software controlled and therefore easily changeable. All the hardware and software

used in this system was developed inhouse by the technical team of the NPRP. Daily calibrations to check the stability of transmitter power and receiver linearity were done.

An objective tracking programme originally devised by Mader (1979) and adapted by Dixon and Mather (1986) to take the three dimensional structure of echoes into account, was used to track the centroids of storms. Thresholds of 30 dBz minimum intensity and 750 km^3 maximum initial echo volume were applied. The translation speed between volume scans was limited to less than 90 kmh^{-1}. Only echoes with lifetimes longer than five consecutive volume scans (+- 16 minutes) were considered. This package is also used routinely to determine storm properties of interest in the precipitation research experiment.

The periods of data collection were between 2 and 19 December 1991 and between 5 and 23 January 1992. The December period was characterized by good convective development. Towards the end of the January period activity decreased and a serious drought set in over most of South Africa, including the Bethlehem area. Although the results of this study cannot be seen as a general climatology, it is characteristic of normal to below normal rain periods over the area of interest. In Table 7.0, a summary of the echo properties is given on a day to day basis. As echo activity reaches a minimum in the morning a day is defined as the 24 hour period ending at 08:00. The date used is that of the day in which the 24 hour period started. On average 29.5 individual 30+ dBz echoes occurred per day excluding the eight days with no activity and one day which was classified as a general rain day.

The absolute maximum reflectivity in the period under investigation was 57.3 dBz on 9 December 1991, a day on which serious hail damage was reported. The maximum 30 dBz echo top of 15 864 m above ground occurred on 2 December.

(c) Storm development and lifetimes

The diurnal distribution of first 30+ dBz echo development is shown in Figure 7.0. The effect of the diurnal cycle in surface heating in the development of convective clouds can be seen. After 12:00 there is a rapid increase in the number of 30+ dBz echoes that develop. The maximum number of storms (17%) developed between 15:00 and 16:00 whereafter a gradual decrease in echo development occurred. About 75% of first development occurred between 14:00 and 20:00. These results agree with the findings of Steyn and Bruintjes although they found a more gradual increase in activity between early morning and maximum activity. Also shown in this figure is the diurnal distribution for storms that developed in the different sectors. First development occurred in the 150 to 180 degree sector with the other sectors lagging and the latest development starting in the sectors to the west.

Table 7.1 Summary of storm echo properties.

DATE	# OF TRACKS	AVG. MAX. dBZ	MEAN VOLUME km^3	AVG. DIR.	AVG. SPEED $km.h^{-1}$	AVG. LIFE
2/12/91	70	43.6	70.7	73.2	9.5	27.5
3/12/91	39	42.5	33.8	114.9	5.6	27.8
4/12/91	11	43.8	109.2	81.5	16.2	22.9
5/12/91	NO WEATHER					
6/12/91	NO WEATHER					
7/12/91	1	40.8	21.0	166.3	11.5	16.9
8/12/91	34	42.7	49.0	128.5	17.5	28.1
9/12/91	3	48.5	24.3	66.4	8.1	40.4
10/12/91	60	43.3	51.0	127.8	9.9	28.2
11/12/91	32	44.9	61.5	102.7	19.4	35.6
12/12/91	33	43.5	46.5	112.8	10.6	28.6
13/12/91	12	43.4	21.2	54.6	5.9	22.7
14/12/91	49	43.8	38.7	91.3	8.8	30.6
15/12/91	33	43.8	44.2	104.8	6.4	26.4
16/12/91	26	46.8	42.6	161.5	5.1	30.1
17/12/91	36	43.6	32.0	67.5	7.9	33.7
18/12/91	44	44.1	39.6	210.0	4.9	32.4
19/12/91	GENERAL RAIN CONDITION					
5/1/92	11	39.8	12.2	103.8	11.3	28.2
6/1/92	54	44.3	78.8	58.1	10.2	31.3
7/1/92	2	42.6	23.0	62.1	8.1	29.2
8/1/92	20	44.1	70.4	85.2	7.9	28.2
9/1/92	33	42.5	23.7	100.3	11.5	23.1
10/1/92	18	44.1	78.6	143.1	10.4	28.6
11/1/92	21	46.5	307.6	107.4	17.0	31.9
12/1/92	45	43.7	43.7	91.2	14.9	29.9
13/1/92	78	44.3	75.2	125.5	12.9	24.3
14/1/92	NO WEATHER					
15/1/92	3	43.8	40.7	91.1	17.1	27.8
16/1/92	5	43.3	15.6	111.8	20.7	27.6
17/1/92	NO WEATHER					
18/1/92	NO WEATHER					
19/1/92	NO WEATHER					
20/1/92	35	45.2	81.1	101.7	20.8	26.6
21/1/92	NO WEATHER					
22/1/92	NO WEATHER					
23/1/92	18	42.5	33.3	92.3	15.2	26.3
AVERAGES	29.5	43.9	59.7	107.2	11.2	28.5

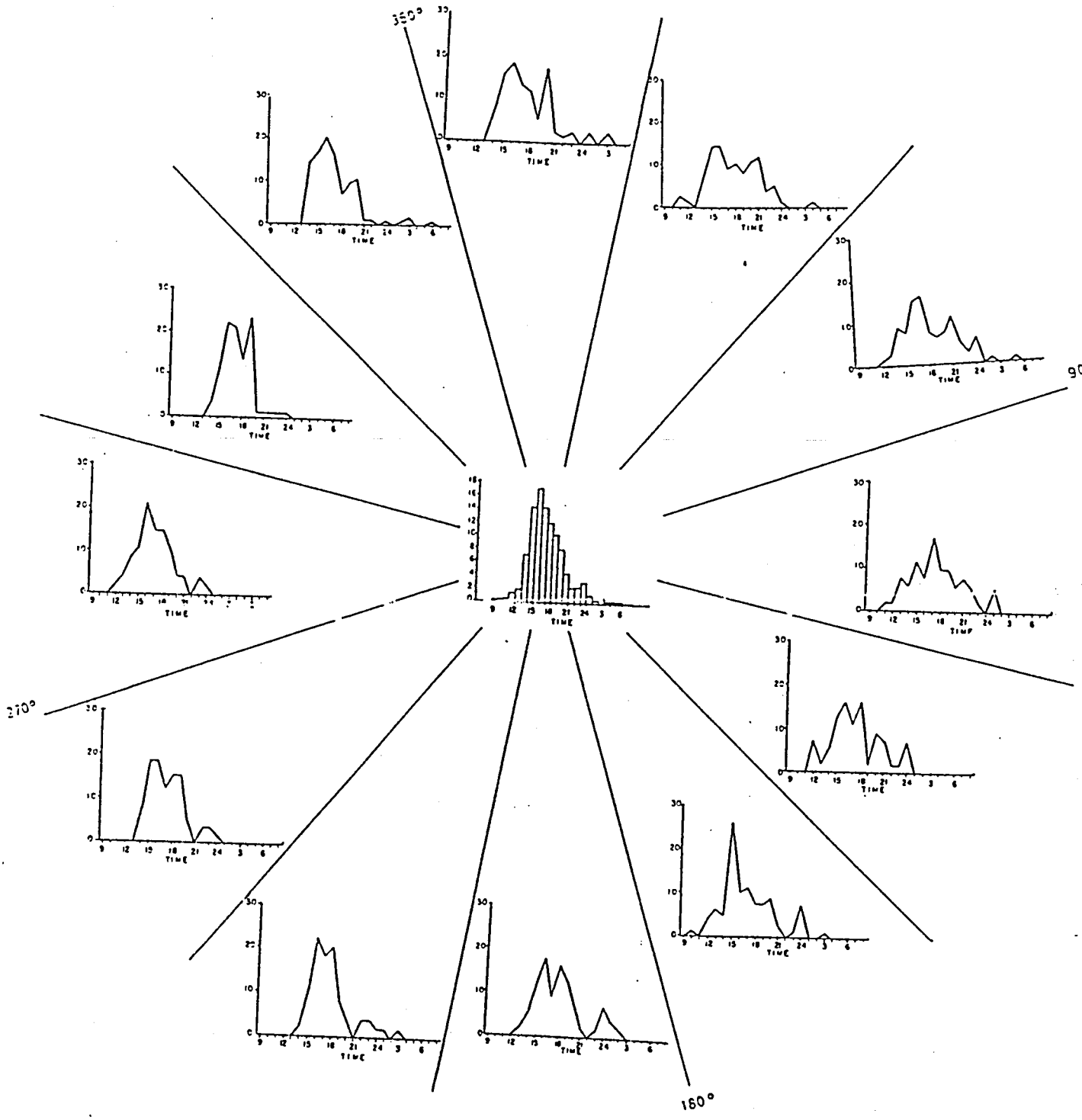

Fig. 7.0 Diurnal distribution of first echo development (inner diagram) and diurnal distribution of first echoes for different sectors.

Figure 7.1 shows the frequency of 30+dBz echo development in the different sectors. The development between 300 and 360 degrees is the most prominent. In contrast to the findings of Steyn and Bruintjes (1990) a marked decrease in development is evident in the south west.

A histogram of the frequency of storm lifetimes is displayed in Figure 7.2 where it is clear that in the period under investigation the 30+ dBz echoes were generally shortlived. Only a quarter of the echoes had lifetimes of more than 30 minutes. Also shown in the figure are the lifetime frequencies of storms in the different sectors. From this it is apparent that storms tend to have longer lifetimes in the eastern sectors.

(d) Storm translation

The average direction of storm movement was generally from west to east as depicted in Figure 7.3. Also shown is the direction of movement of storms that developed in the different sectors.

Of all the storms studied, about 75% had tracks of less than 15 km and only 3.5% of the tracks were longer than 30 km. As shown in Table 1, the average translation speed of all the storms was 11.2 kmh^{-1}.

(e) Echo volumes

The distribution of echo volumes above the 30 dBz threshold is shown in Figure 7.4. It is clear that about half of the storms that occurred during the period under investigation had volumes of less than 25 km^3.

(f) Maximum echo intensities and heights

Figure 7.5 displays the distribution of maximum echo intensity in all the storms under investigation. It is of interest that storms which develop above the 30 dBz level on average tend to develop further into significant storms.

The maximum height of the 30 dBz intensity level in each cloud was investigated. The peak occurrence (20%) was between 9 and 10 km above ground. In only 14% of the cases did the 30 dBz intensity level peak at above 12 km.

(g) Conclusions

This study summarizes the properties of 826 individual 30+ dBz echoes in the Bethlehem radar area that were observed during December 1991 and January 1992. The majority of the storms developed between 14:00 and 20:00 with initial development in the south eastern sector. The north western sector was the area with the most frequent development. Only a quarter of all the echoes had lifetimes of more than 30 minutes and about half of the echoes had volumes of less than 25 km^3. The storms generally

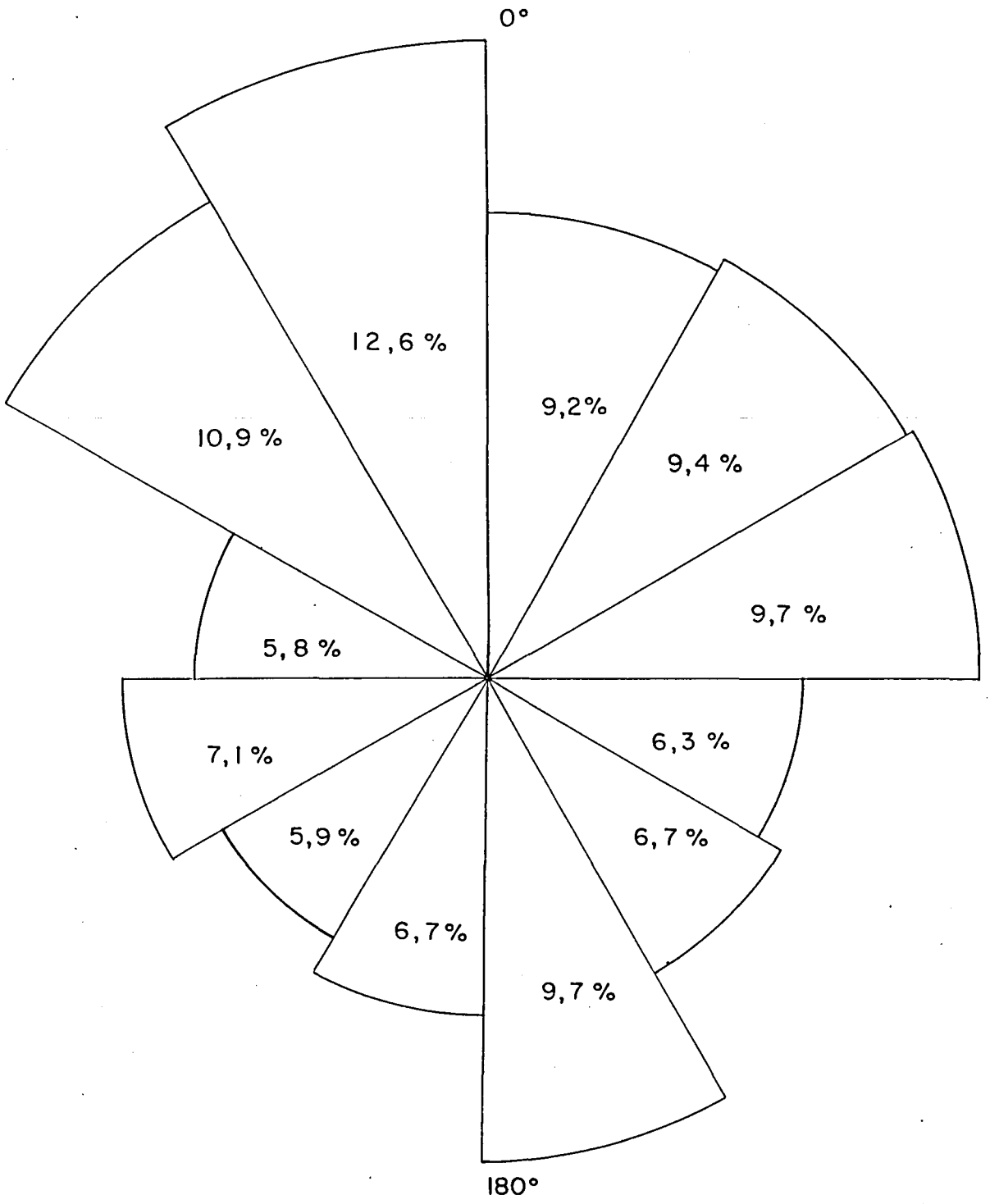

Fig. 7.1 Percentage of first echo development in sectors.

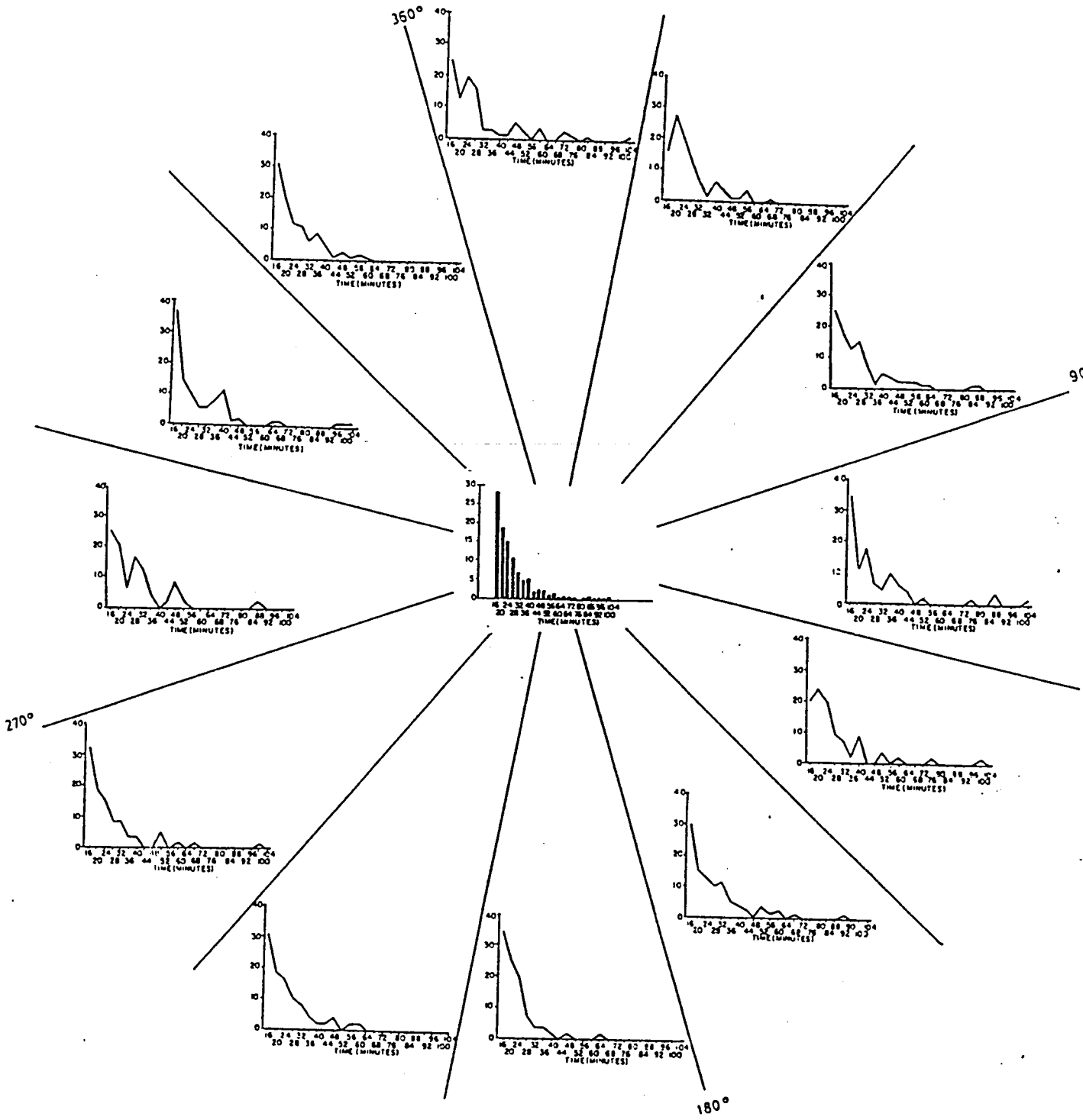

Fig. 7.2 Distribution of storm lifetimes (inner diagram) and the distribution for each sector.

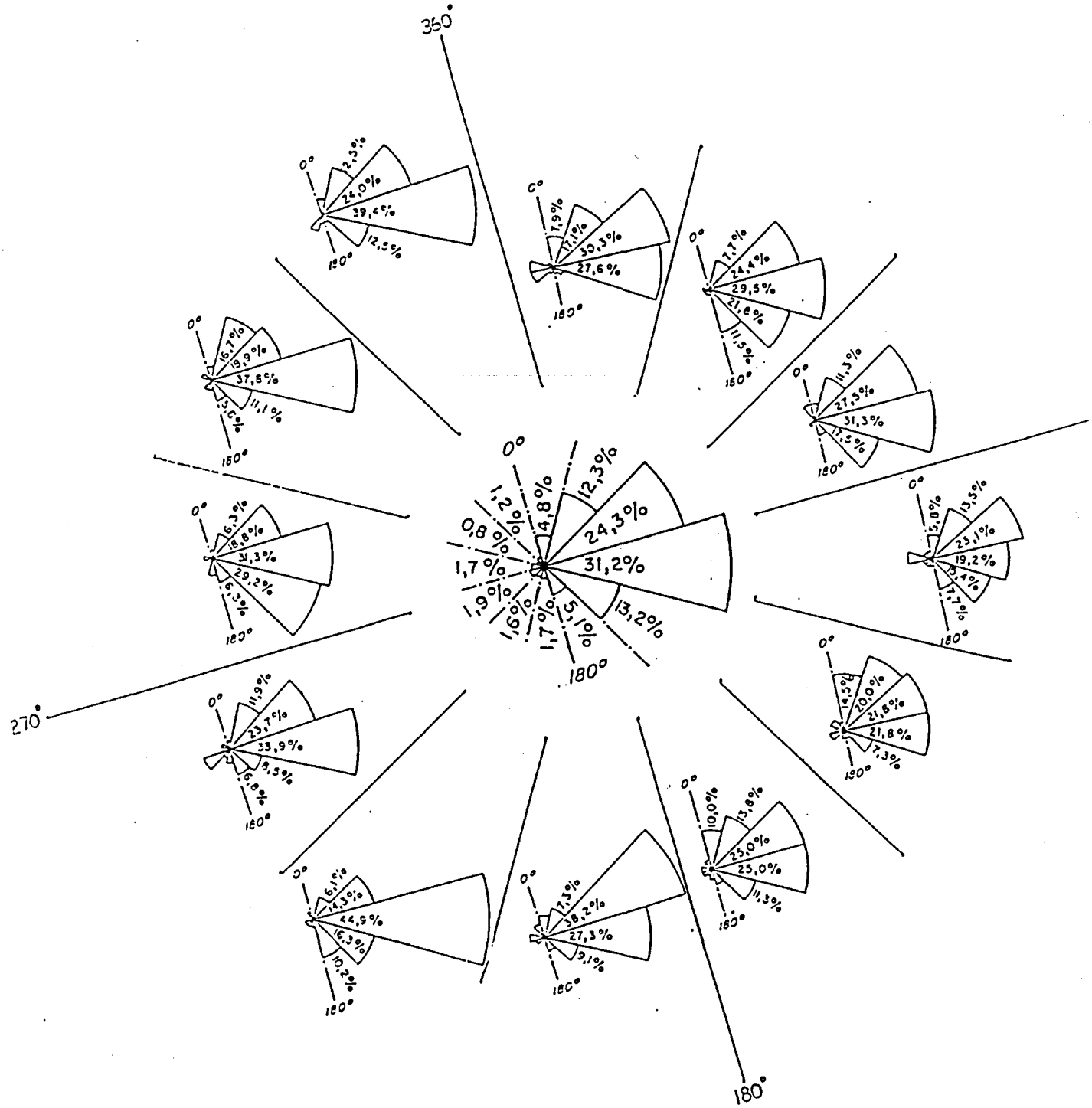

Fig. 7.3 Distribution of storm movement (inner diagram) and the distribution for each sector.

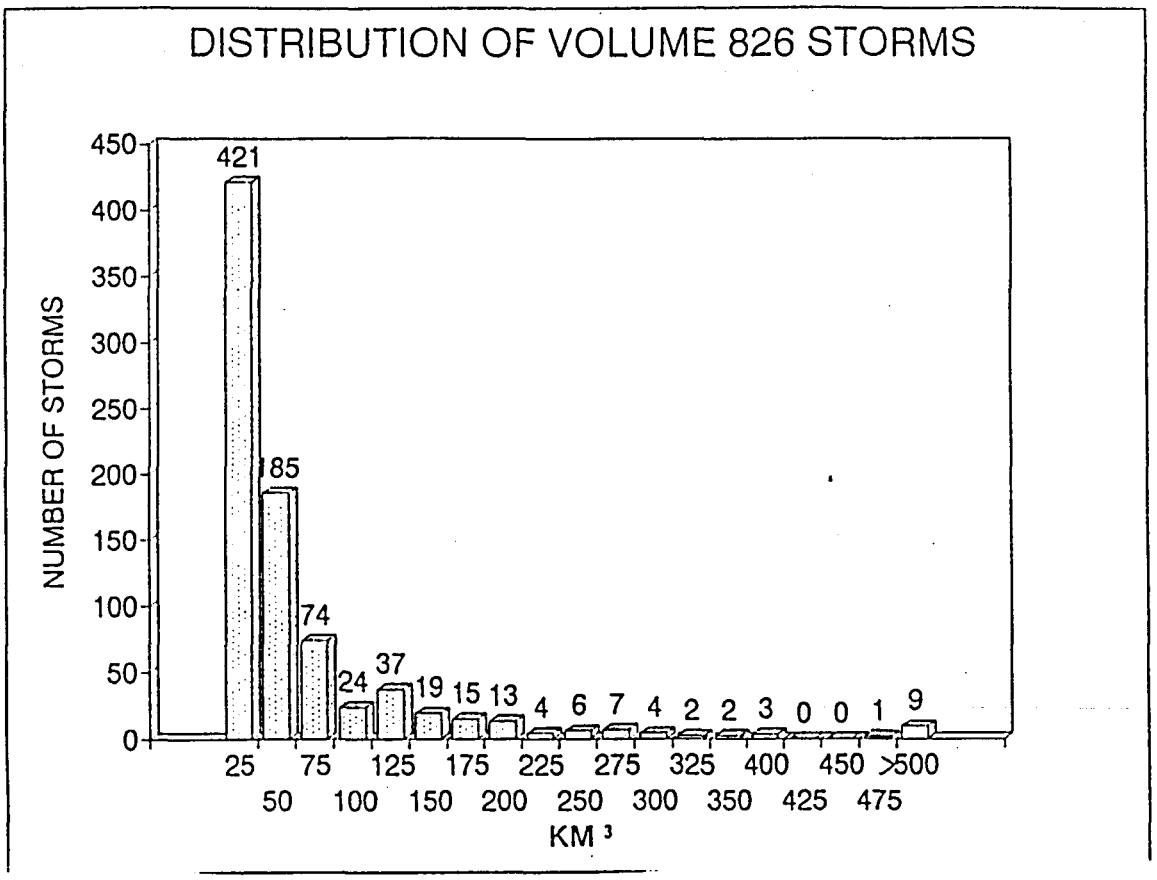

Fig. 7.4 Volume distribution of storms.

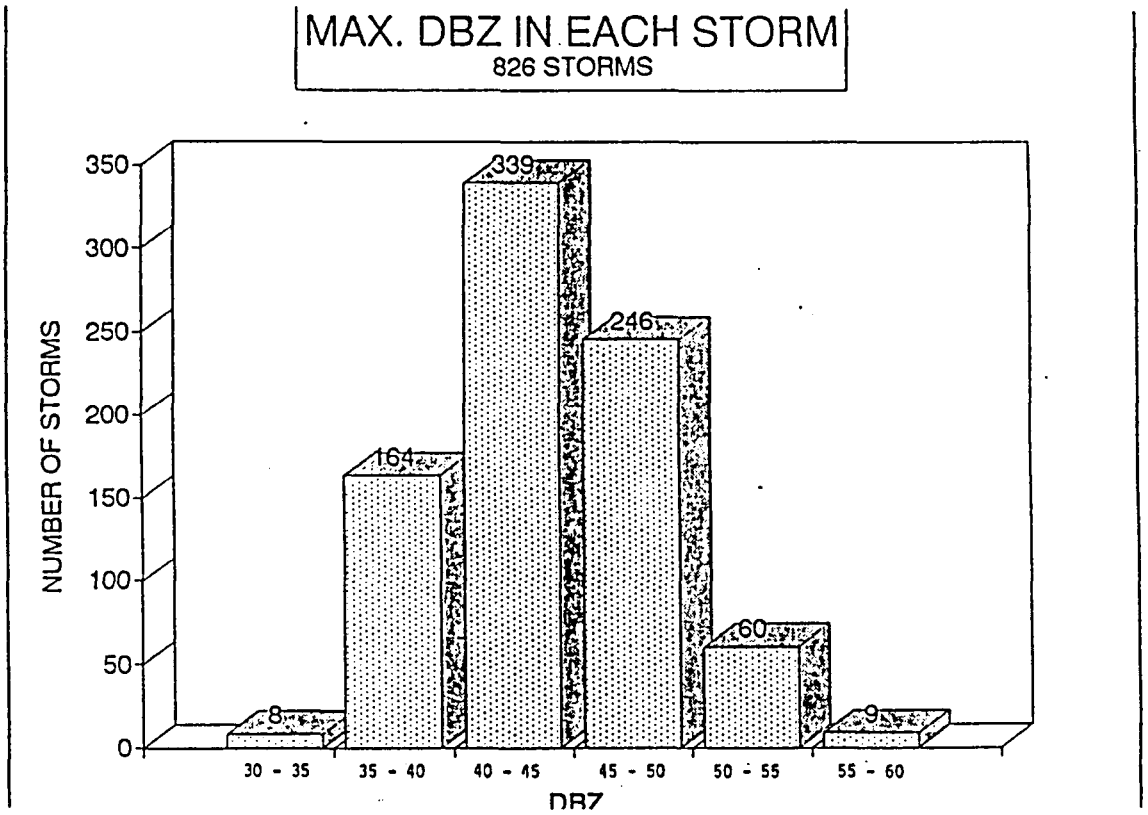

Fig. 7.5 Distribution of maximum dBz.

moved from west to east at an average speed of 11.2 km^{-1}. Storms which developed above the 30 dBz level and lived for longer than 16 minutes generally tended to develop further.

The results show the importance of fast reaction times during aircraft operations, especially in droughts. It is clear that although the clouds are shortlived, there is adequate cloud development above the threshold of interest.

8.0 HYGROSCOPIC MODELLING STUDIES

(a) Deliquescence and initial diffusional growth

A hygroscopic particle exposed to humidity conditions above the value at which solution formation starts, is subject to a process known as deliquescence. During this process vapour from the environment is absorbed, the hygroscopic material goes into solution and the particle grows. This process continues until all the hygroscopic material is in solution. Up to this point the solution part of the particle can be treated as a saturated solution but thereafter dilution takes place.

It has been found that particles exposed to slowly increasing humdities already absorb a significant amount of water at humidities much lower than those at which solution formation starts (Pruppacher and Klett, 1978). This uptake of water results in a more rapid deliquescence process than expected by theory. In the specific case under investigation where the particles are produced by a pyrotechnic flare burning at several hundred degrees Celsius, this effect is assumed to be negligible.

A model was developed to investigate the time evolution of a single particle for which the initial size and temperature, pressure and relative humidity to which it is exposed can be prescribed. It is assumed that the particle is spherical, totally composed of KCl and that the diffusional growth equation applies even during the deliquescence phase. The aim of this excercise is to investigate the time needed for hygroscopic particles of different sizes to form solution droplets under given conditions and to compare the growth of these droplets diffusion with the growth of pure water droplets of comparable initial sizes. Furthermore, the time needed to grow to equilibrum is also determined.

(b) Model description

A general subroutine was written in Fortran for diffusional growth. The equation from Pruppacher and Klett (1978) has the following form:

$$dr/dt = (A/r)(S_{vw}-B+C-D)$$

where r is the radius, S_{vw} is the supersaturation.

This implicit equation has the advantage that the droplet temperature is also determined. Although more computer time consuming than simpler methods, the solution and curvature effects are treated in detail. Assumptions were minimized and each term treated fully.

During the initial deliquescence of the KCl particle, it is assumed that an infinitesimal layer of saturated solution forms on the surface of the particle. As vapour diffusion continues the solution part of the particle remains saturated until all KCl has dissolved. During this phase the mixed particle size is computed. After all the KCl has dissolved, the normal treatment with decreasing molality continues.

Mathematically this phase is handled as follows:

1. The size of a saturated solution droplet is determined using the following.

$$r' = (A' r_s^3 p_s / p_w)^{0.33}$$

where r' is the saturated solution droplet radius, A' is the solution ratio (100/34.7 in the case of KCl as 34.7g can be dissolved in 100g of water), r_s is the radius of the salt particle, p_s the salt density and p_w the density of water.

2. Initially it is assumed that a saturated solution droplet with the same size as the KCl particle is allowed to grow. During this phase, which continues until the size determined in 1 is reached, the mass of KCl in solution is computed by

$$M'_{KCl} = (100/34.7) M_w$$

where M_w is the mass of condensed water.

As the mass of KCl not dissolved is now known, the radius of the undissolved particle can be determined.

$$r_{KCl} = (3(M_{KCl} - M'_{KCl})/4\pi p_s)^{0.33}$$

where M_{KCl} is the total mass KCl

Now the radius of the mixed particle can be determined using

$$r_{mix} = (3(V_w + (4/3)\pi r_s^3)/4\pi)^{0.33}$$

where V_w is the volume of the solution portion which is the same as the volume of the condensed water. Furthermore the size of a KCl particle that would cause a saturated solution droplet of radius r_{mix} must also be determined using:

$$r'_{KCl} = ((34.7\ r_{mix}^3\ p_w)/100 p_s)^{0.33}$$

3. As soon as r_{mix} = r' as determined in 1, normal growth occurs and increasing dilution takes place.

(c) Results

Model runs were done to investigate the growth of 10 and 100 micron KCl particles at relative humidities of 80, 95, 100 and 102%. For comparison the size evolution of similarly sized pure water droplets were also computed at 95% and above. As input in all the runs a temperature of 10°C and a pressure of 700 hPa were prescribed. These conditions are representative of the average seeding level.

At 80% relative humidity no growth was seen on the KCl particles and pure water droplets evaporated rapidly. In Figure 8.0(a) the results from the run with a 10 µm diameter KCl particle and a pure water droplet with an initial diameter of 10 µm are shown. Whereas the pure water droplet evaporated in little more than 2 seconds the solution droplet grew, all the KCl dissolved at about 3.5 seconds and it reached its equilibrium size of 26 µm after 12 seconds. Figure 8.0(b) shows the results for particles with initial diameters of 100 µm. In this case complete evaporation of the pure water droplet happened after more than 110 seconds. The hygroscopic particle took about 130 seconds for the deliquescence phase, at which time the solution droplet had reached a diameter of about 175 µm. Continued growth occurred and the equilibrium size was not yet reached at 1000 seconds.

Figures 8.1(a) and (b) show the results of 10 and 100 µm diameter particles at a relative humidity of 100%. As can be expected, the water droplets survived longer, the growth on the KCl particles was faster, especially after deliquescence, and equilibrium sizes were bigger and took longer to be reached.

In Figure 8.2(a) and (b) the results at 102% relative humidity are depicted. In this case the tendency noticed in the previous figures is even more pronounced; even the water droplet grows and as can be seen in the 10 µm case, the marked size difference around 10 seconds becomes negligible towards the end of the run. The same tendency will be observed with the 100 µm particles after much longer growth times than those shown here.

It is interesting to note that the length of the deliquescence phase of the KCl particles under investigation does not vary significantly at the different humidities used. Furthermore a more marked increase in the sizes of the solution drops is seen just after the deliquescence phase. This is caused by the almost saturated solution that still applies at this stage in addition to the cessation of the relative volume decrease caused by the solution of the solid KCl particle during the deliquescence phase.

This theoretical study was done to investigate the expected properties of the hygroscopic flare particles after burning. The results shown here can only be seen as a guideline as the real particles are not composed of KCl only. However it is unlikely that any significant deliquescence could have taken place before

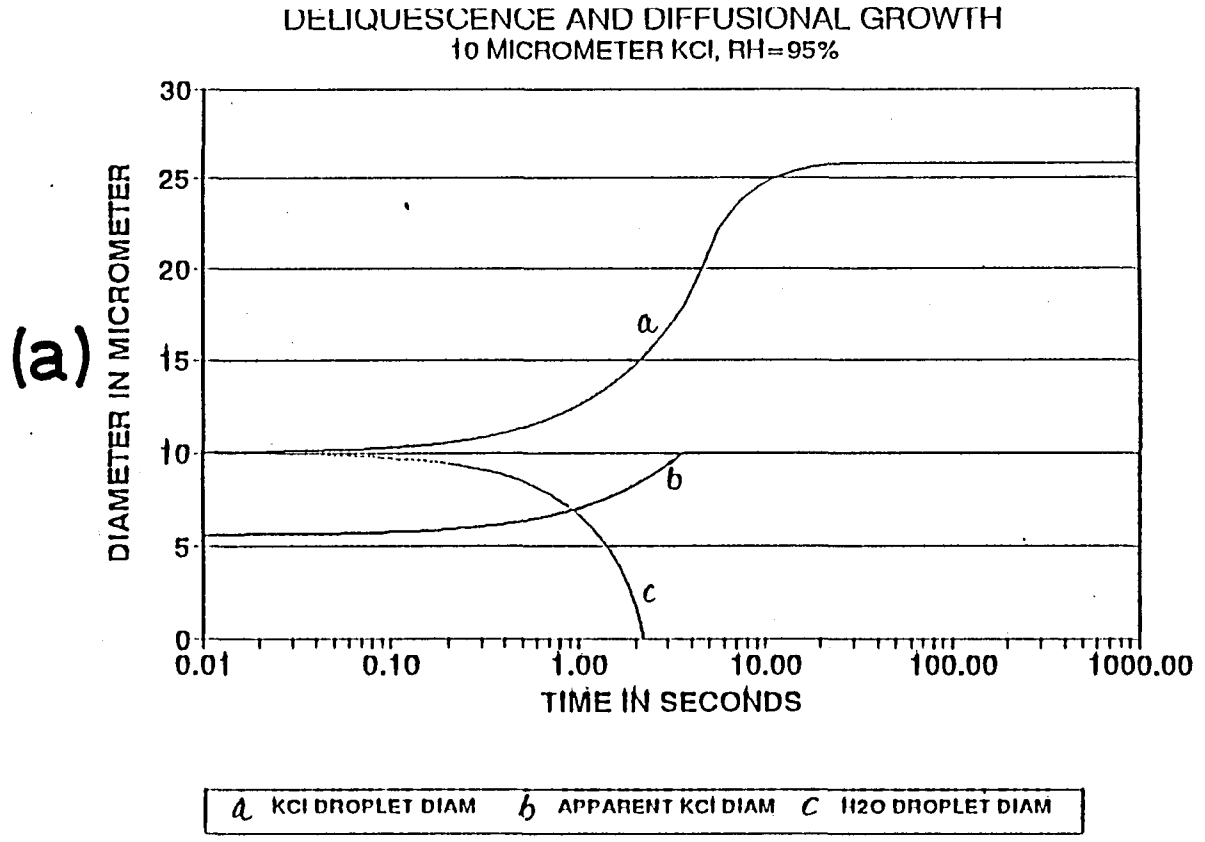

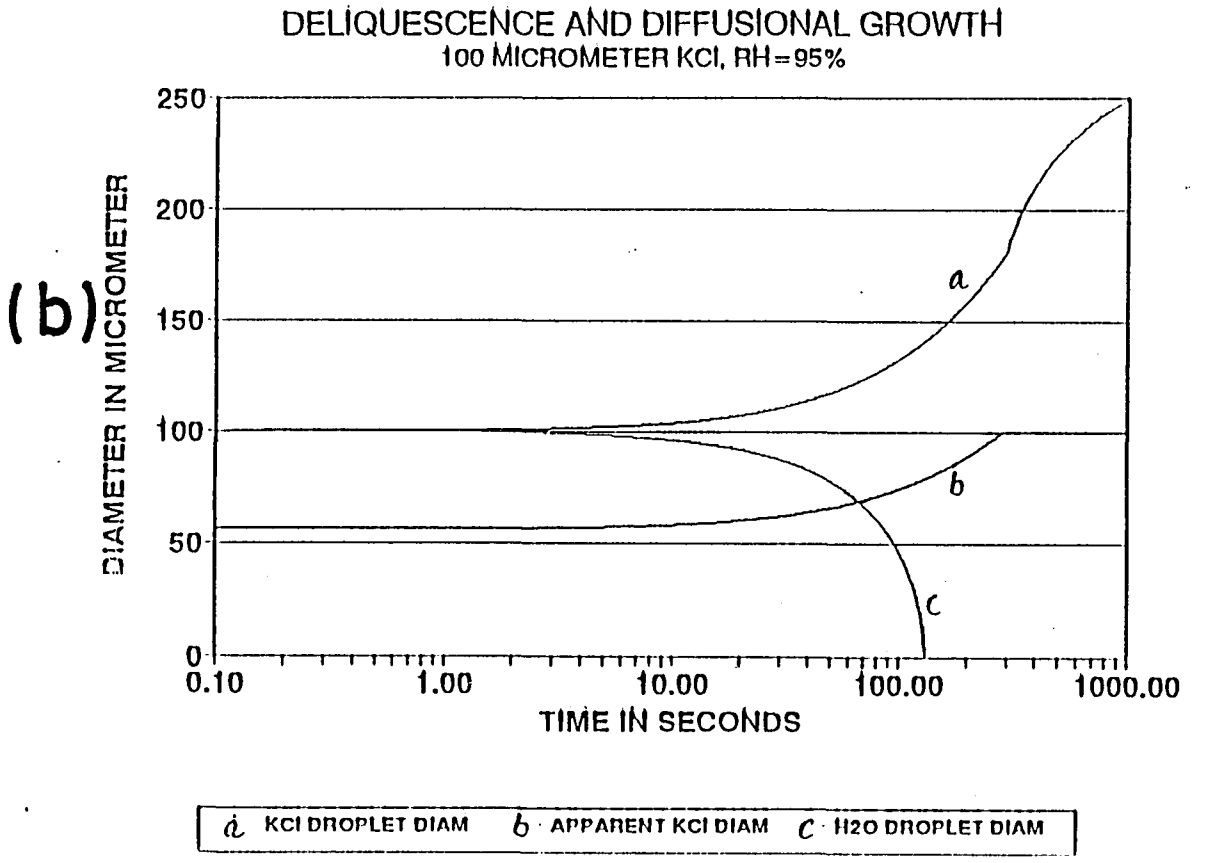

Fig. 8.0 Deliquescence and growth on KCl particle compared to pure water droplet at 95% RH.
(a) 10 μm particle
(b) 100 μm particle

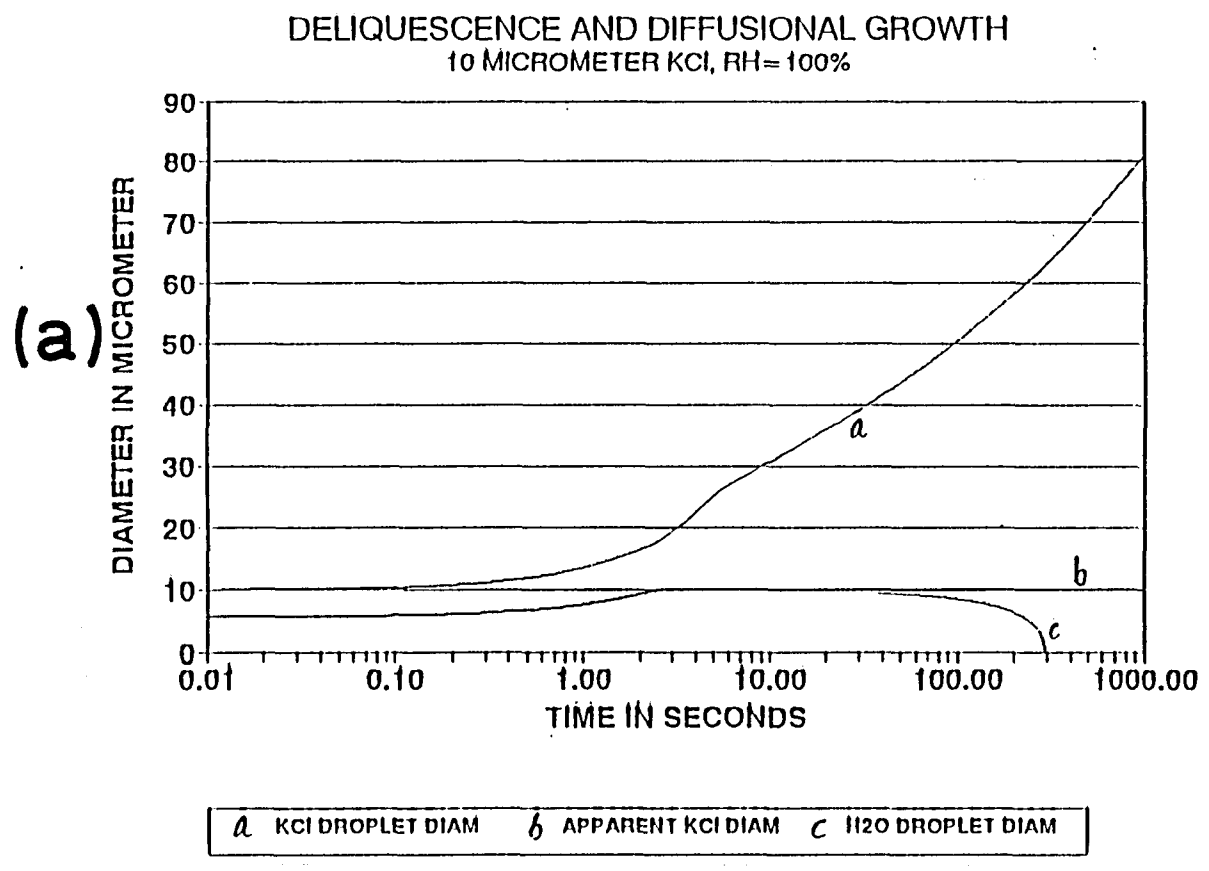

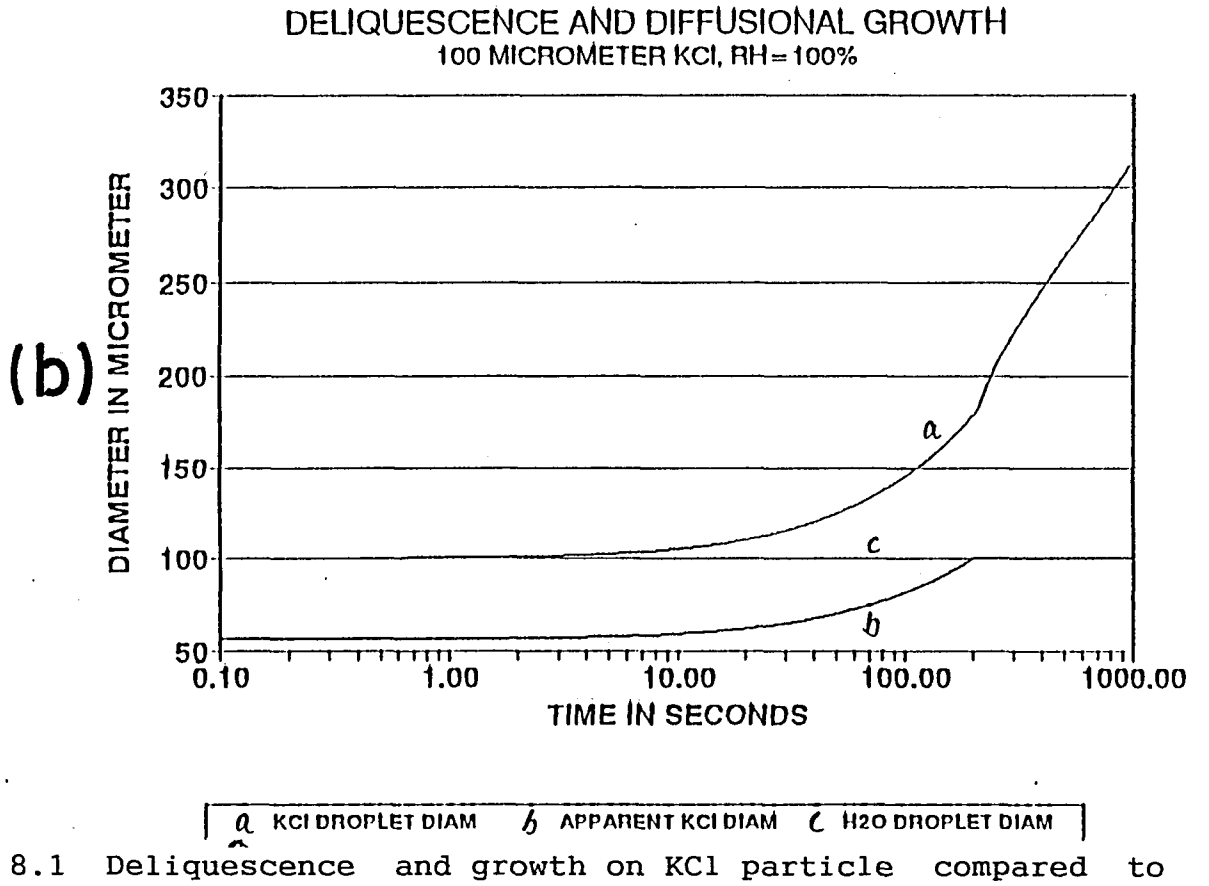

Fig. 8.1 Deliquescence and growth on KCl particle compared to pure water droplet at 100% RH.
(a) 10 μm particle
(b) 100 μm particle

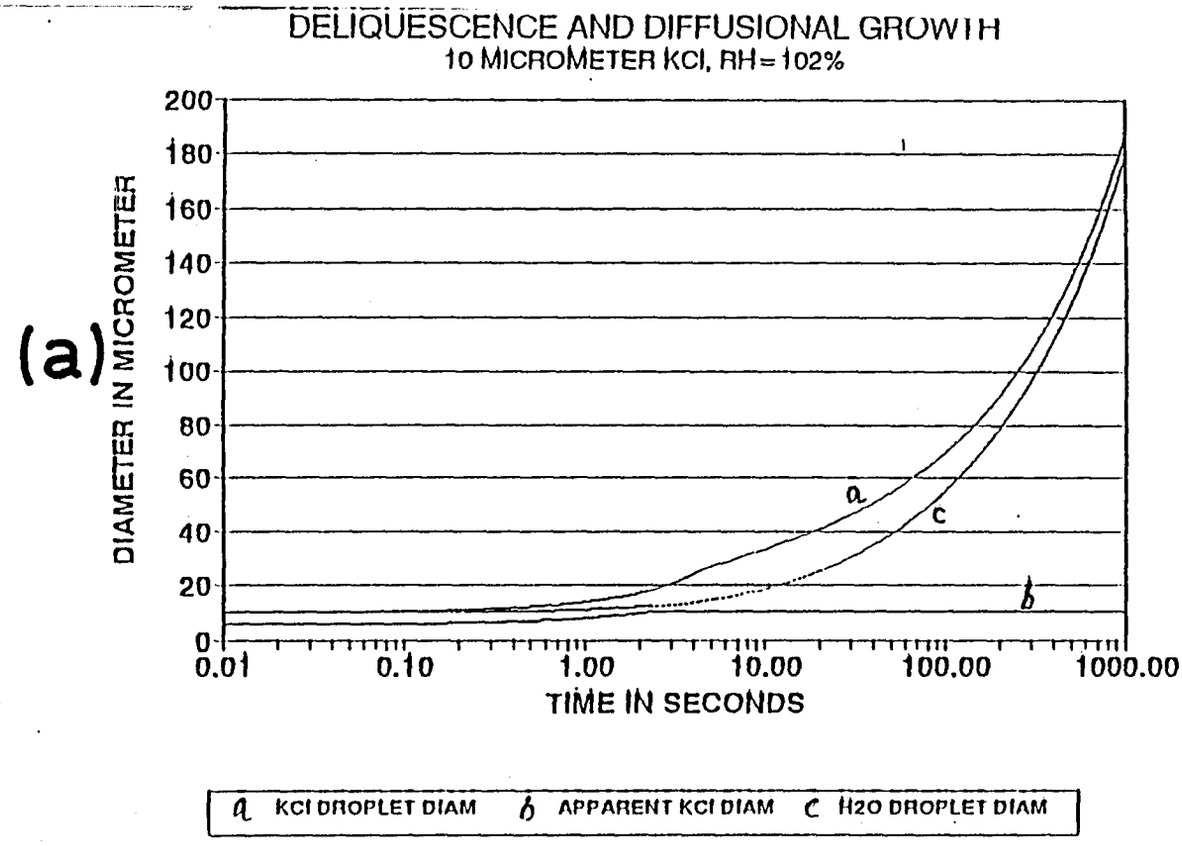

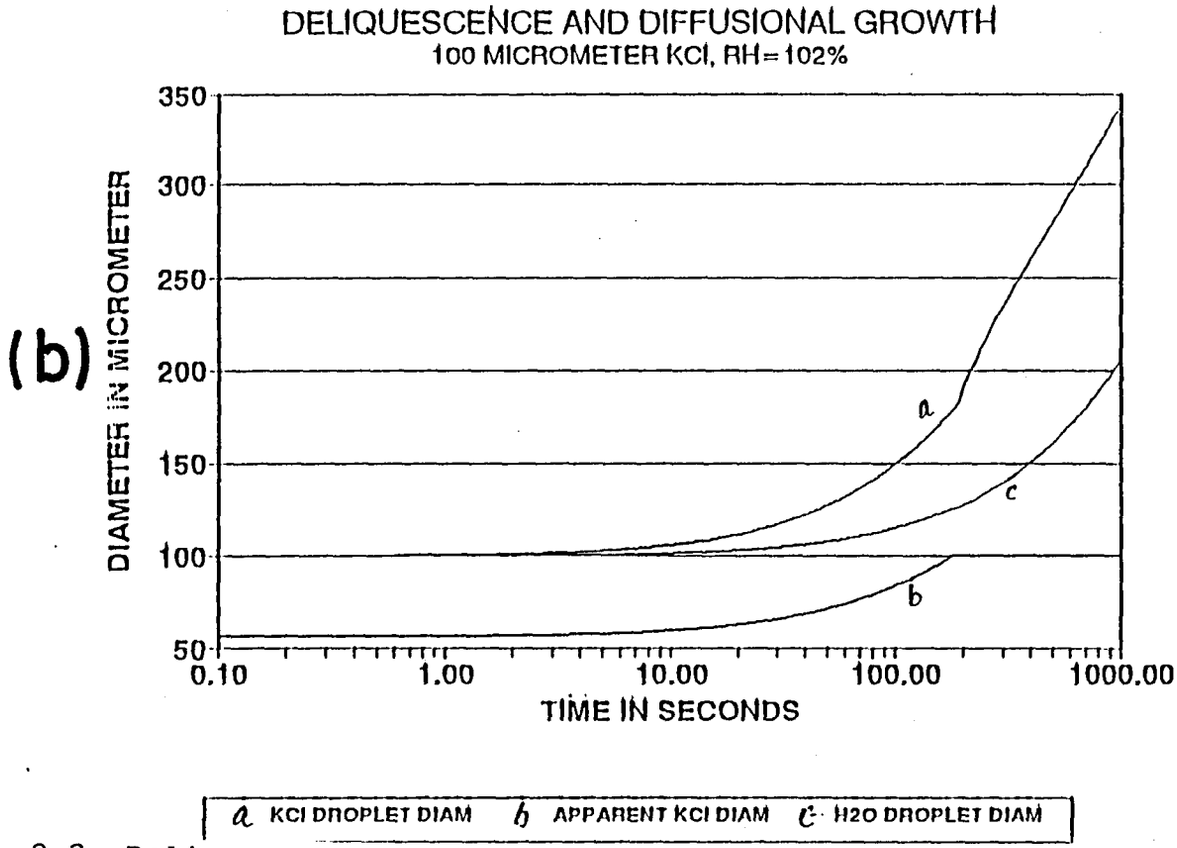

Fig. 8.2 Deliquescence and growth on KCl particle compared to pure water droplet at 102% RH.
(a) 10 μm particle
(b) 100 μm particle

sampling during the airborne tests conducted on 3 October and 14 November 1991. The relative humidity on both occasions was in the region of 80% and the sampling took place less than 2 seconds after the release of the particles.

8.1 Modelling the growth of a population of droplets by diffusion and coalescence

During the diffusional growth of a population of droplets the interaction between the production of supersaturation by the ascending motion and the depletion thereof by condensation plays a crucial role. The level of supersaturation reached determines the number concentration of natural CCN activated and the size growth tempo of these particles. It can therefore be anticipated that changes made to the CCN spectrum ingested by clouds could have effects on the supersaturation profile and therefore also on the droplet population.

A model utilizing the general subroutine already described was developed to investigate these factors numerically. Cloudbase temperature, pressure and a constant updraft are prescribed. Using a constant time step of 1 second the following equations are used to determine the relevant parameters.

1. As a first approximation determine temperature on next level by

$$dT/dz = -g/c_p$$

where T is temperature, z altitude, g acceleration due to gravity and c_p the specific heat. Now the effect of condensational heat is introduced:

$$dT/dw = L/c_p$$

where L is latent heat of condensation and w the condensed water. Initially dw is zero but it will converge to a finite value during the iteration process that follows.

2. Fukuta (1990) described a scheme to determine the supersaturation. The production of supersaturation by condensation is determined by

$$dS/dz = (\epsilon Lg/R^2)(1/c_p - T/(\epsilon L))$$

and the depletion of supersaturation by

$$dS/dw = -(p\epsilon L^2/(c_p R T^2 \epsilon e))$$

where $\epsilon = 0.622$, R is the specific gas constant and e is the vapour pressure.

3. The natural CCN concentration activated is determined using

$$N = aS^b$$

where the parameters a and b can be varied to characterize the CCN spectrum. Each droplet formed is assumed to be at the critical radius for the given supersaturation.

4. Diffusional growth is allowed using the general subroutine. The total mass of water condensed is determined and iteration through steps 1 to 4 is done until convergence occurs.

The determined temperature, supersaturation, droplet sizes and concentration are therefore all in equilibrium for the given conditions.

(a) Coalescence growth

A stochastic coalescence subroutine using the Monte Carlo scheme as suggested by Gillespie (1975) was obtained from NCAR. The only modification made to this routine was to introduce the option to keep track of the transfer of soluble nuclei during coalescence events. The main programme was also adapted to provide all the input needed by the subroutine. This routine is very computer time consuming therefore limiting the volume of the parcel that can be considered.

(b) Model runs

Model runs were done to simulate the evolution in the droplet spectrum formed on a typical continental CCN spectrum and one that was seeded with a number of hygroscopic nuclei. Only a cubic centimetre of cloud was considered and therefore the larger flare particles' effects, produced in low concentrations, could not be realistically considered. The only aim of these runs was to investigate the expected interaction between supersaturation, and droplet characteristics.

In Figure 8.3 the size distribution of the 20 KCl nuclei used for the seeded run is shown. Figure 8.4 depicts the supersaturation profiles above cloudbase of the natural and seeded cases. As the hygroscopic particles causes an increased flux from the vapour to the liquid phase, the peak supersaturation reached in the seeded case is lower. It occurs at a slightly higher elevation above cloudbase which also assists in broadening of the droplet spectrum nucleated on the natural CCN, as there is a longer time span between the activation of the first drops and the last drops activated at the level of maximum supersaturation.

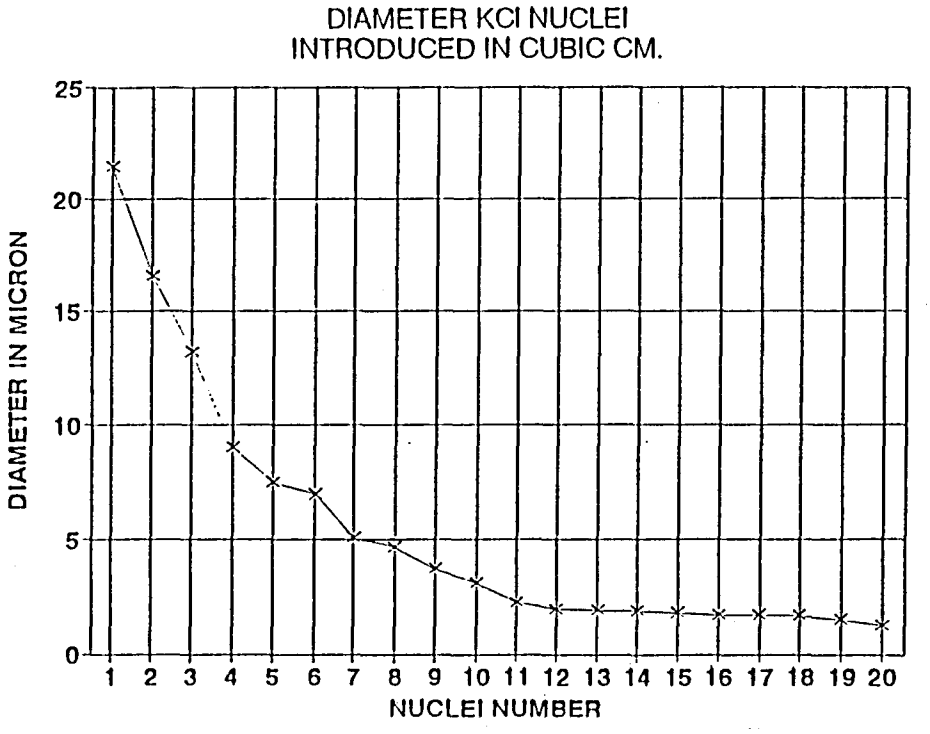

Fig. 8.3 Diameter in micron of KCl particles introduced for seeded run.

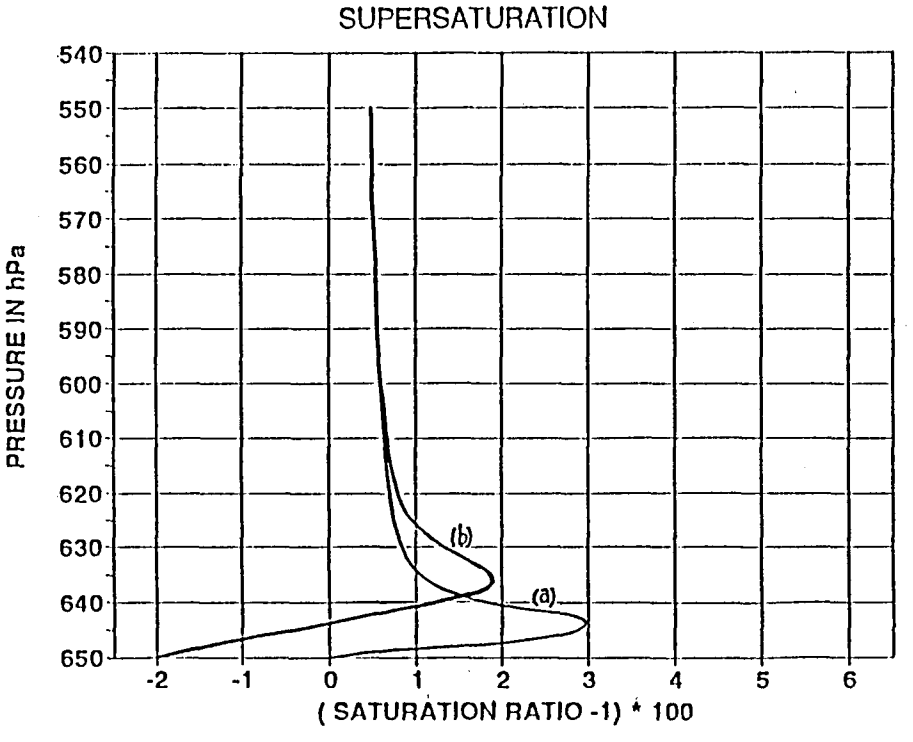

Fig. 8.4 Supersaturation profiles above cloudbase.
(a) Natural CCN
(b) Natural CCN and 20 KCl particles

The droplet number concentrations as a function of height above cloudbase is shown in Figure 8.5. Significantly less drops are activated in the seeded case as a result of the modified supersaturation profile. The present 20 artificial nuclei caused about 80 less natural CCN to be activated. As a constant updraft of $5ms^{-1}$ was prescribed in both cases, the liquid water content was the same. This secondary effect also assisted in creating bigger drops on average. Also shown in this figure are the coalescence events indicated by discontinuities on the two number concentration profiles. A significantly more active coalescence process is present in the seeded case.

From this theoretical study some important secondary effects caused by the introduction of hygroscopic particles at cloudbase in an updraft are indicated. These effects should be considered in a detailed hygroscopic seeding hypothesis and verified with physical measurements.

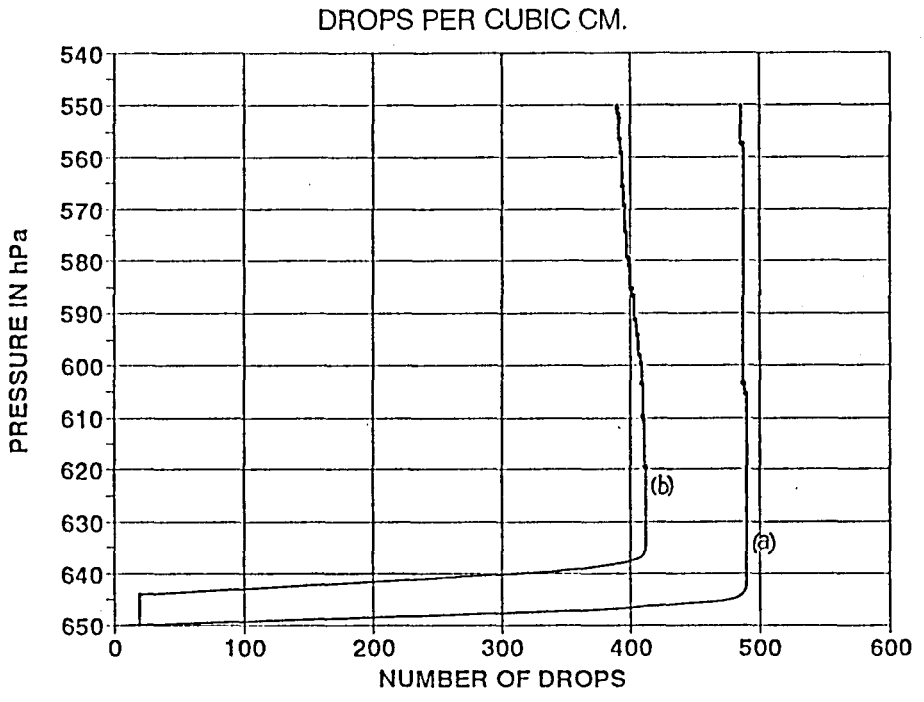

Fig. 8.5 Droplet concentration above cloudbase.
(a) Natural CCN
(b) Natural CCN and 20 KCl particles

9.0 CONCLUSIONS

This section of the report will review progress in terms of the objectives stated at the beginning of the contract period (Section 2.2).

A comprehensive understanding of the precipitation formation processes active in the summer thunderstorms that produce most of the rainfall in the study areas has been achieved. This understanding is the product of the combined use of sophisticated meteorological radars and instrumented aircraft. The development of innovative instrumentation, hardware and software has played a vital role in reaching this goal.

The realization that the precipitation processes in most of the storms that populate the study areas are inefficient (about 30% of the water vapour processed by a storm reaches the ground as precipitation) has led to a search for a method(s) for artificially increasing storm rainfall efficiency by cloud seeding. That precipitation efficiency can be increased inadvertently has been demonstrated by measurements of storms that have ingested the hygroscopic emissions from a local Kraft paper mill. This observation led to the development of a pyrotechnic flare whose combustion product is a broad spectrum of hygroscopic particles. When released into updrafts feeding convective storms, these particles deliquesce, forming relatively large droplets which alter the natural cloud base droplet spectrum. Modelling studies and observations indicate that this early intervention accelerates the coalescence process leading to earlier development of rain drops which more effectively scavenge the available supercooled water, leading to a more efficient rainfall formation process.

The new technology has been tested experimentally on isolated convective storms in the Bethlehem and the Carolina areas. Although the number of experiments is small (about 50 randomly selected seeded and control storms), initial results indicate a doubling of radar-measured rainfall from seeded storms 30 to 40 minutes after decision time (the time at which an experiment, either seed or no-seed, is declared).

This data base must be strengthened by at least one more season of experimental seeding. An expanded data base will allow studies aimed at separating those conditions (thermodynamic, mesoscale forcing, etc) under which storms best respond to treatment from those in which little if any response is detected.

Modelling studies will play an essential role in leading towards an understanding and eventual fine tuning of this new technology. Although not reported here, such studies are well under way. A link between the NPRP and the National Centre for Atmospheric Research (NCAR), has been formed. Drs. Cooper and Bruintjes are using data acquired at Nelspruit in an advanced coalescence model run on the NCAR super computer. Early results are already producing valuable insights into the mechanisms

responsible for the apparent increases in rainfall, and are also indicating areas where additional measurements are required. Tapes of microphysical measurements made in local storms are being routinely sent to NCAR for comparison with model outputs. This valuable feedback loop between field measurements and laboratory modelling should reveal the links in the chain of events leading to the apparent rainfall increases, as well as leading towards optimization of the choice of seeding materials and techniques.

Further field experiments should now proceed in parallel with the planning of an area experiment, the next and most crucial step in the development of a cloud seeding technology aimed at increasing South Africa's water resources. Steps that have been taken in this direction have shown that:

- we can measure rainfall over an area with a carefully calibrated meteorological radar (Section 3)

- modest (8 to 10 percent) increases in rainfall over model-calibrated catchment areas can produce a fourfold increase in streamflows

- a major public relations effort will be required in and around any areas selected for an experiment.

Next, the potential users of additional water must be pursuaded to become actively involved in the planning of an area experiment. The choice of the area, the design of the experiment, the measurements that will be required (streamflow, rain gauges, radar etc), must be agreed upon since it will be up to these users to evaluate the benefits accruing from the application of a rainfall augmentation capability.

ACKNOWLEDGEMENTS

The research described in this report was jointly funded by the Water Research Commission and the Department of Environmental Affairs.

The Steering Committee responsible for this project, consisted of the following persons:

Dr. G C Green	Water Research Commission (Chairman)
Mr. F P Marais	Water Research Commission (Secretary)
Mr. H Maaren	Water Research Commission
Mr. P S du Toit	Weather Bureau
Mr. C G Groenewald	Weather Bureau
Dr. J F Eloff	Agricultural Research Council
Dr. D vd S Roos	EMATEK, CSIR
Dr. A Seed	Department of Water Affairs and Forestry
Prof. P J T Roberts	Institute for Commercial Forestry Research
Prof. J M de Jager	University of the Orange Free State
Dr. J A Lindesay	University of the Witwatersrand
Prof. J van Heerden	University of Pretoria

The financing of the project by the Water Research Commission and the Department of Environmental Affairs and the contribution of the members of the Steering Committee are acknowledged gratefully.

The authors also wish to record their sincere thanks to the following:

Drs. W A Cooper and R T Bruintjes of the National Centre for Atmospheric Research, Boulder, Colorado, U S A.

Special thanks are accorded to Dr. G C Green for his sage advice during the final stages of the preparation of this report.

REFERENCES

Braham, R.R., Jr., 1964: What is the role of ice in summer rain showers? J. Atmos. Sci., 21, 640-645.

Dixon, M., and G.K. Mather, 1986: Radar evaluation of a randomized rain augmentation experiment. Preprints: 10th Planned and Inadvertent Weather Modification Conference, AMS Boston, 139-141.

Doneaud, A.A., P.L. Smith, A.S. Dennis, and S. Sengupta, 1984: The area-time integral as an indicator for convective rain volumes. J. Clim. Appl. Meteor., 23, 555-561.

Fukuta, N., 1990: Water supersaturation in convective clouds. Preprints: Conference on cloud physics, San Francisco. Amer. Met. Soc., 80-85.

Gillespie, D.T., 1975: An exact method for numerically simulating the stochastic coalescence process in a cloud. J. Atmos. Sci., 32, 1977-1989.

Hindeman, E.E., 1978: Water droplet fogs formed from pyrotechnically generated condensation nuclei. J. Wea. Mod., 10, 77-96.

Kraus, T.W., R.T. Bruintjes, J. Verlinde and A Kahn, 1987: Microphysical and radar observations of seeded and nonseeded continental cumulus clouds. J. Climate Appl. Meteor., 26, 585-606.

Mader, G.N., 1979: Numerical study of storms in the Transvaal. S. African Soc. J. 61, No. 2.

Mather, G.K., D. Treddenick and R. Parsons, 1976: An observed relationship between the height of the 45 dBz contours in storm profiles and surface hail reports. J. Appl. Meteor., 15, 1336-1340.

------- 1989: Estimates of precipitation embryo densities using measurements from an aircraft radar. J. Appl. Meteor., 28, 1089-1097.

-------, 1991: Randomized cloud seeding experimentation for assessing potential for rainfall augmentation in the Nelspruit district. PhD Thesis, Department of Atmospheric Science, University of the Orange Free State, Bloemfontein.

--------, 1991: Coalescence enhancement in large multicell storms caused by emissions from a Kraft paper mill. J. Appl. Meteor., 30, 1134-1146.

Mielke, P.W., Jr., Cooper, W.A., Holroyd, E.W., III, Super A.B., Silverman, B.A., Dennis, A.S., Smith, P.L., Berry, K.J., Orville, H.D., and J.R. Miller, Jr., 1987: HIPLEX-1: Experimental design and response variables. J. Climate Appl. Meteor., 23, 497-512.

Morgan, G., B.J. Morrison and G.K. Mather, 1989: Measurements of total and condensed water mixing ratios in warm-based cumulus clouds by a jet engine evaporation technique. Theor. Appl. Climatol., 40, 187-199.

PAWS - Phase 1, 1983-1986, 4 Volumes. Report Nos. 133/1-4/88.

PAWS - Phase 2, 1987-1989, 3 Volumes. Report Nos. 133/5-7/90.

Pruppacher, H.R., and J.D. Klett, 1978: Microphysics of clouds and precipitation. D. Reidel, Dordrecht, Holland, 714pp.

Simpson, J., 1980: Downdrafts as linkages in dynamic cumulus seeding effects. J. Appl. Meteor., 19, 477-487.

Smith, P.L., and D.E. Cain, 1983: Use of sequential analysis methods in adjusting radar rainfall estimates on the basis of rain gage data. Report 83-2, Institute of Atmospheric Science, S. Dakota School of Mines and Technology, 84pp.

Steyn, P.C.L., and R.T. Bruintjes, 1990: Convective cloud characteristics for the Bethlehem area. Water SA, Vol. 16, No. 2, 115-118.

Wilson, J.W., and D.M. Pollock, 1970: Rainfall measurements during hurricane Agnes by three overlapping radars. J. Appl. Meteor., 13, 835-844.

Woodley, W.L., A.G. Barriston, J.A. Flueck and R. Brondini, 1983: The Florida area cumulus experiment's second phase (FACE-2), Part II: Replicated and confirmatory analysis. J. Climate Appl. Meteor., 22, 1529-1540.

APPENDIX 1 - AIRCRAFT MEASUREMENTS

(a) Vertical velocity system

Vertical velocity measurements play a vital role in the analysis and interpretation of microphysical measurements at cloud base, especially in the case of rain rate and reflectivity calculations derived from the 2D-P probe observations. The results of the development and calibration of the vertical velocity system (VVS) are shown. The system consists of the following components:

- a rate gyro, to determine aircraft pitch
- the angle of attack vane, and
- an accelerometer to determine aircraft acceleration.

The equation for the vertical velocity is:

$$w = -TAS \sin\alpha + w_a \qquad (1)$$

where w is the vertical velocity, TAS is the corrected True Air Speed in metres per second, α the instantaneous angle of attack, and w_a is the vertical velocity of the aircraft (determined from the pitch rate and vertical acceleration).

For α small and in radians:

$$w = -TAS\alpha - \int_0^\tau (- TAS\ p + a)dt \qquad (2)$$

where dt is the time interval between data records for the Data Acquisition System (DAS), i.e. 0.1 s in fast mode and 1 s in slow mode, p is the pitch rate in radians per second, and a is the vertical acceleration.

For sinusoidal oscillations in the aircraft flight path ("roller coasters"), the vertical velocity in (2) is zero. To ensure this, the angle of attack requires an upwash coefficient u, due to airflow interference about the airframe, and (2) becomes:

$$w = - u\ TAS\alpha - \int_0^\tau (-TAS\ p + a)\ dt \qquad (3)$$

The upwash coefficient for an angle of attack vane far away from the airframe should be close to one, with the coefficient decreasing as the vane nears the airframe.

To calibrate the VVS, the aircraft is flown in a vertical sinusoidal pattern ("roller coasters"). Two corrections are then applied to the vertical velocity profile. The first correction assumes that the aircraft is in balanced straight and level flight once fast mode is entered prior to actual penetration of the cloud. All the values are averaged over one second, and the angle of attack, rate gyro, and accelerometer values for the

first second are "frozen", and are subtracted from the values that follow, i.e. the values that follow are all relative to the first values:

$$w_{fi} = w_i - w_f$$

$$= - u \, TAS \, (\alpha_i - \alpha_f - (- TAS \, (p_i - p_f) + a_i - a_f) \quad (4)$$

for i = 1, N where N is the number of observations for the penetration, and the subscript f refers to the "frozen value", that is i = 1. We therefore have $w_{f1} = 0$ (since $w_1 = w_f$).

The second is a slope correction: since the aircraft resumes balanced straight and level flight after the roller coasters, the vertical velocity in (4) is zero. This is done by applying a slope correction to the values to "force" the last point on the right hand side of the curve to zero:

$$w_{si} = w_{fi} - \alpha_i \, (w_N - w_1)/N \quad (5)$$

for i = 2, N; where N is the number of observations, and s refers to the slope correction. Note that i begins at 2 since w_{f1} is already zeroed from the first correction. Fig. A1.0 shows the various components that make up the vertical velocity, once the above mentioned corrections have been applied, gathered during a test flight on 1990-12-12.

In practice, the procedure differs slightly from that above in that the freeze and slope corrections are applied first and the upwash coefficient determined last. Fig. A1.1 gives a comparison of the vertical velocity values before and after the calculation of the upwash coefficient (1 and 0.262 respectively) for the same test flight as Fig. A1.0.

(b) Measurements of cloud liquid water

The water content of a cloud is as important a measurement as vertical velocity (updraft). The two, of course, are related since it is the vertical ascent which leads to the condensation of the water vapour in the cloud volume. On the Learjet, cloud water is measured using 3 instruments;

- the CSIRO-King liquid water content probe
- the engine-temperature sensor (E.T.)
- the Lyman-alpha sensor (LA).

All these instruments have been described in previous reports. Here, we present an comparison from a recent flight in which all the cloud water around the -10°C level was contained in cloud droplets (< 100 µm in diameter) i.e. precipitation had not started to form. These comparisons are presented in Figs. A1.2(a) (b) and (c) and the coefficients from the linear regressions, in which one of the points is (0, 0), are listed in Table A1.1. Both

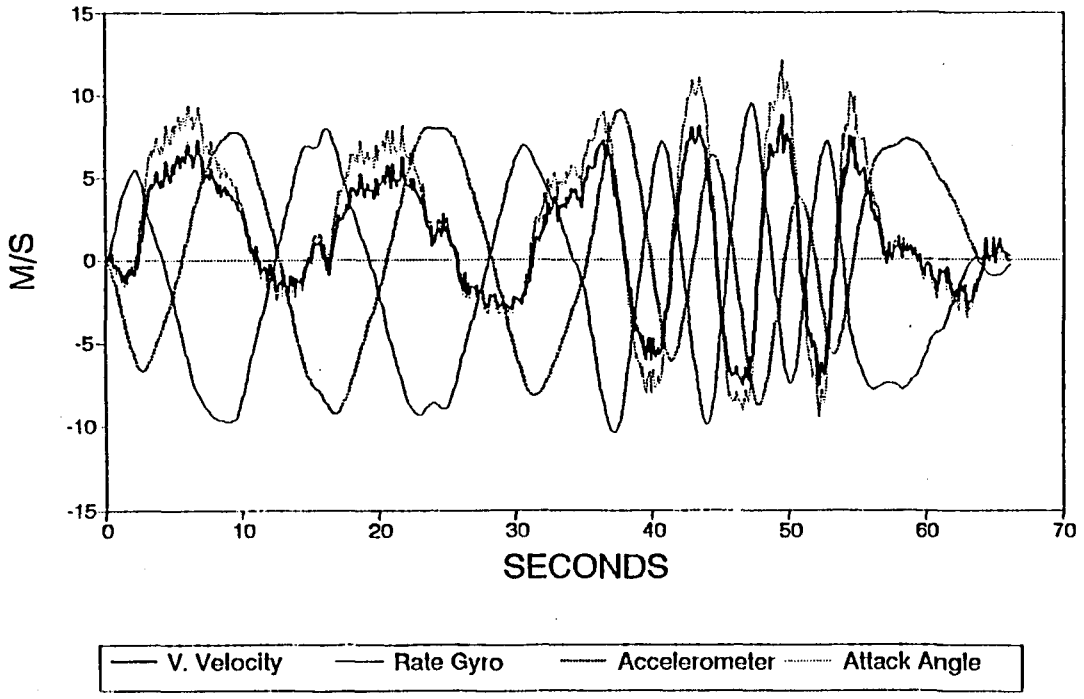

Fig. A1.0 Outputs from accelerometer and angle of attack sensors in "roller-coaster" tests in still air, December 12, 1990.

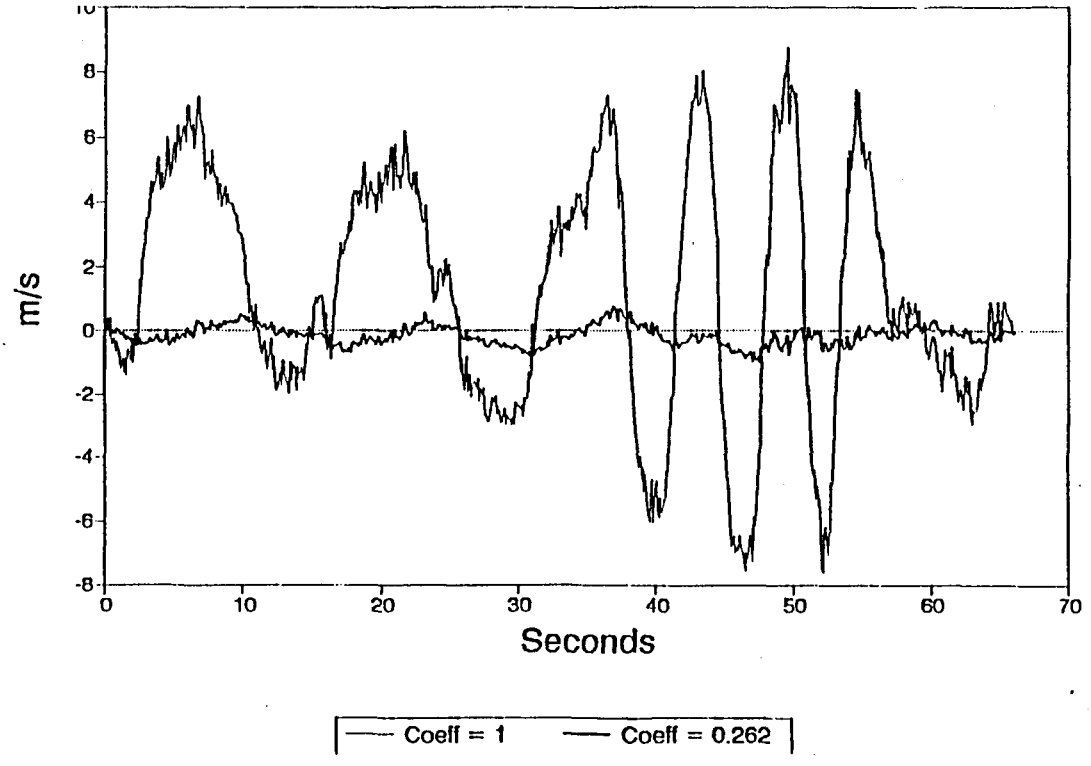

Fig.A1.1 Gust velocity before and after the application of an upwash correction.

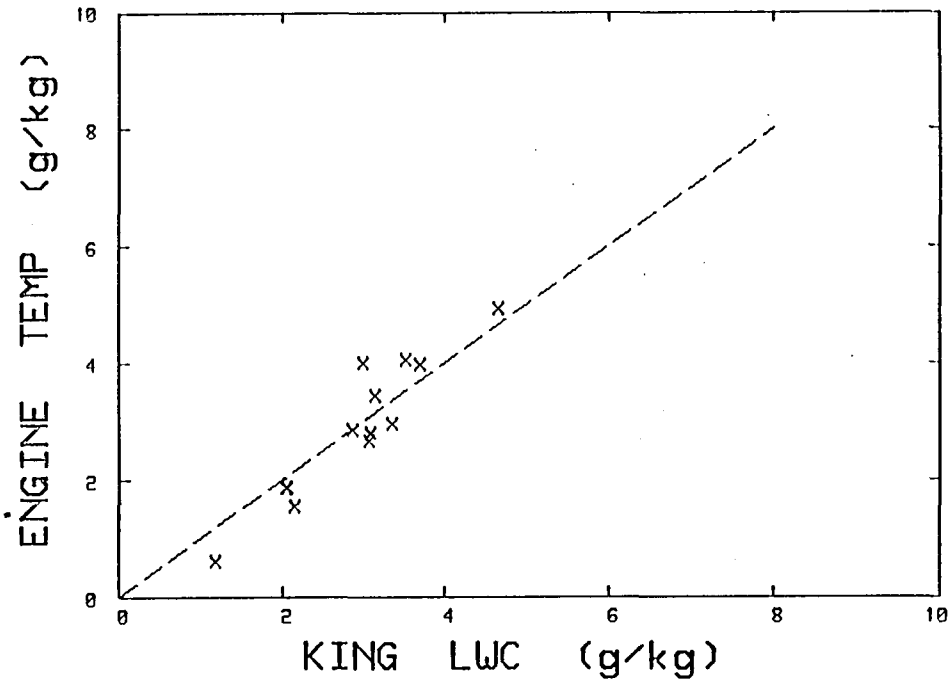

Fig. A1.2(a) Engine temperature (E.T.) and King comparisons of liquid water measurements.

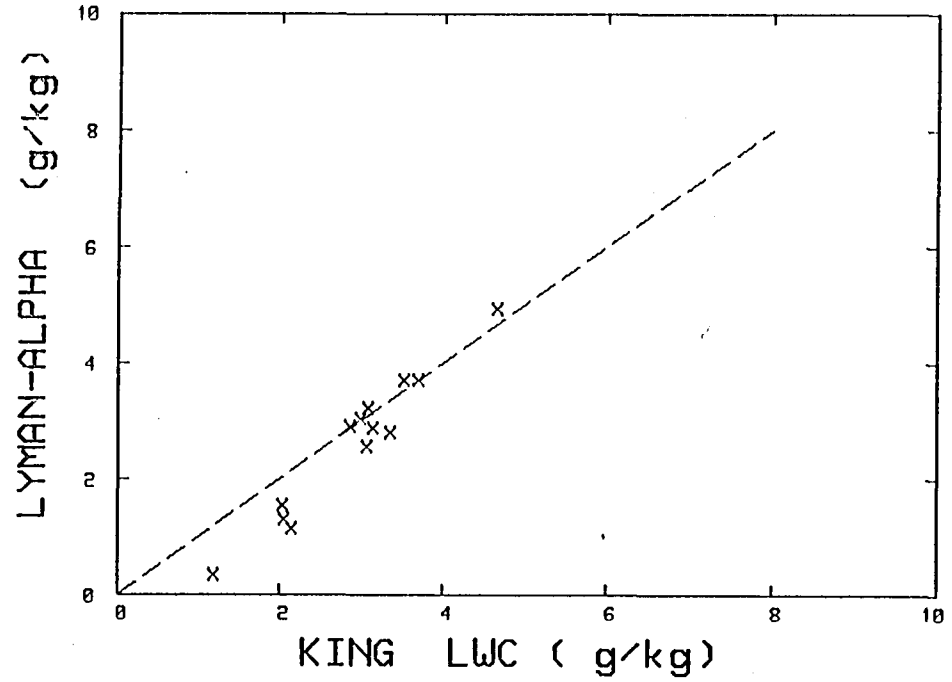

Fig. A1.2(b) Lyman-alpha (LA) and King comparisons.

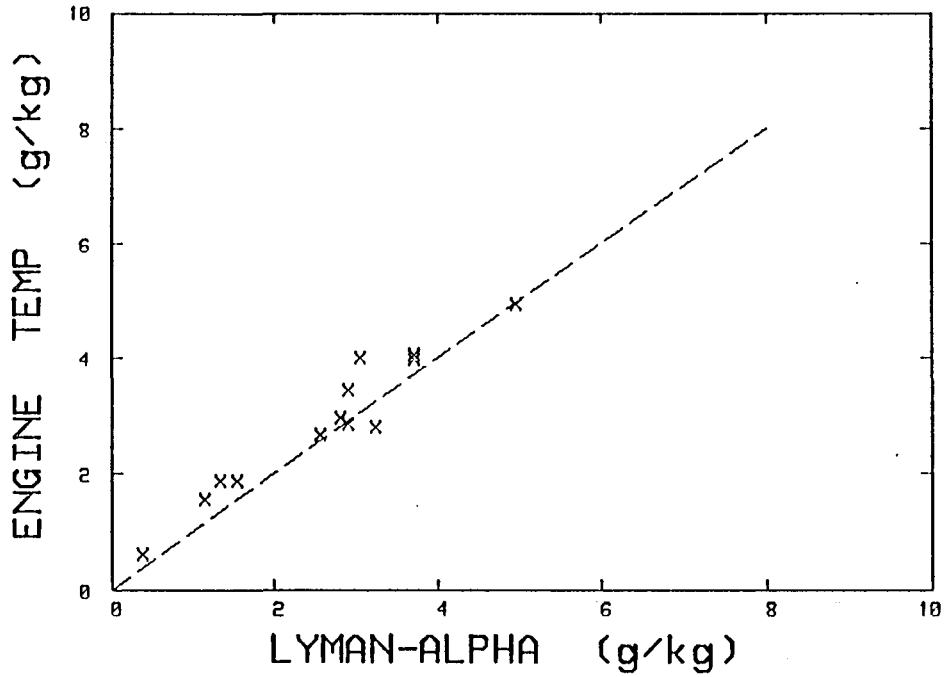

Fig. A1.2(c) E.T. and LA comparisons. See Table 6.0 for regression coefficients.

the E.T. and LA comparisons with the King are similiar. The King device appears to read high in conditions of low liquid water. The comparison between the LA and E.T. measurement looks reasonable over the range from 0 to about 6 g/kg. Standard deviation of the LA from the E.T. is 1.34 g/kg (66% of the LA values are within 1.34 g/kg of the E.T. values).

Table A1.1 Linear regression values for cloud water instrument comparisons

y	x	a	b	r
E.T.	King	-0.42	1.15	0.95
LA	King	-0.69	1.16	0.96
E.T.	LA	0.31	0.97	0.97

Key : $y = a + bx$
r = correlation coefficient

These comparisons indicate that reasonable estimates of the higher total water content (10 - 12 g/kg) routinely encountered in clouds containing cloud water and precipitation can be obtained by a simple linear extrapolation of the E.T. and LA calibrations.

(c) Bethlehem aircraft instrumentation - JRA

The instrumentation on the two Aerocommander 690A's is described in terms of the type of instrument used to measure certain parameters, the calibration of the various instruments (where applicable), and also the relevant equations and calculations to produce the parameters.

(i) Accelerometer

The accelerometer used is a Schaevitz linear accelerometer LSBC2 (s/n 11016). The range of counts is from 32770 to 65482. Measurement range is from -2 to +2 g, and the output voltage from 0.001 to 9.984 volts.

The acceleration (ms^{-2}) is given by:

$$ACCEL = -9.81 * (a_{14} - 32767) / (3282 * 2.496)$$

where a_{14} is the system count of analogue channel 14.

(ii) Angle of attack

The angle of attack vane is the standard aviation vane fitted to the fuselage of the Rockwell Aerocommander 690A. The range of counts is from 32767 to 65534. Measurement range is from 0.0 (fully down) to 54.6 (completely up) degrees and the output voltage from 0.0 to 10.0 volts.

The angle of attack is given by:

$$AOA = -27.3 + (a_{15} - 32767) / 600.13$$

where a_{15} is the system count of analogue channel 15.

The angle of attack formula is calculated as follows:

54.6 degrees gives a voltage range of 10 volts
10.0 * 3276.7 = 32767 gives the system counts range
Therefore the number of system counts per degree is:
32767 / 54.6 = 600.13 (This is the inverse of the gradient)
System counts for 0.0 volts 32767 + 0.0 * 3276.7 = 32767
System counts for 10. volts 32767 + 10.0 * 3276.7 = 65534
We apply a correction of half the range of the angle of attack to give us zero degrees for straight and level.
Therefore -27.3 + (a_{15} - 32767) / 600.13 is the equation.

(iii) Navigation

A Trimble Navigation model TNL-2000 GPS navigator (s/n 21273) is installed and used to record aircraft position in latitude (in the format N#dd#mmhh#) and longitude (in the format W#ddd#mmhh), track (degrees magnetic), groundspeed (knots) and annunciators and errors. The latitude and longitude is converted to give the aircraft range and heading from the ground-based radar.

(iv) Heading

The heading is taken from the standard aircraft instrumentation in synchronous form. The heading in degrees is:

$$HDG = s_2 / 182.04$$

(v) Humidity

The Vaisala 1518 HM humidity sensor is fitted to the Vaisala HMP 14 reverse flow temperature/humidity probe in a housing developed at the BPRP. The range of counts is from 32767 to 36044. Measurement range is from 0 to 100% and the output voltage is from 0 to 1 volt.

The relative humidity (%) is given by:

$$RH = (a_6 - 32767) / 32.767$$

where a_6 is the system count for analogue channel 6.

The humidity is calibrated prior to every flight using one of two Vaisala HMK 11 humidity calibrators (s/n 15704 and 14923) with calibration points of 13 and 97%.

The humidity formula is calculated as follows:

100 percent gives a volt range of 1.0
3276.7 gives the system counts range
Therefore the number of system count per percent is:
3276.7 / 100 = 32.767 (This is the inverse of the gradient)
System counts for 0 % are 32767
System counts for 100 % are 32767 + 1.0 * 3276.7 = 36044
Therefore (a_6 - 32767) / 32.767 is the equation.

(vi) Liquid water content

Two probes are in use, the Johnson-Williams (JW) and the CSIRO King.

The King lwc probe model KLWC-5 (s/n 17849-1189-38) uses a PMS sensor model HW03. The range of counts is from 32767 to 65534. Measurement range is from 0.0 to 5.0 gm^{-3} or 0.0 to 1.0 gm^{-3} and the output voltage from 0.0 to 10.0 volts (we have to date only operated the sensor in the 0 to 5 mode).

The King lwc is given by:

While flying through clear air prior to an in-cloud run:

$$P_{DRY} = 10.0\ |V|_{A(DRY)}$$

$$P_{WET} = P_{TOTAL} - P_{DRY}$$

$$= 10.0 * (|V|_{A(TOTAL)} - |V|_{A(DRY)})$$

$$KLWC = P_{WET} / (0.099 * v)$$

where KLWC is the liquid water content in gm^{-3}, V is the analogue value in volts, P is the power in Watts, and v is the true airspeed in m/s.

The analogue equation while in-cloud sampling is:

$$KLWC = (10.0 * (a_{11(total)} - a_{11(dry)}) / 3276.7) / (0.099 * TAS)$$

where a_{11} is the system count of analogue channel 11.

The King lwc formula is calculated as follows:

0.0 to 5.0 gm^{-3} gives a voltage range of 10.0
10.0 * 3276.7 = 32767 gives the system counts range
Therefore the number of system counts per volt is:
32767/10.0 = 3276.7 (This is the inverse of the gradient)
System counts for 0.0 volts 32767 + 0.0 * 3276.7 = 32767
System counts for 10.0 volts 32767 + 10.0 * 3276.7 = 65534
Therefore (a_{11} - 32767) / 3276.7 is the basic equation to give the probe output in volts (so that it can be converted to power and then corrected for the dry term to give lwc).

The JW lwc comprises a sensor (s/n 177), power supply (s/n 7105) and a Johnson-Williams dummy sensor head (s/n 7105) model LWH calibrated for 100 knots.

The range of counts is from 32767 to 38505. Measurement range is from 0.0 to 2.0 gm^{-3} and the output voltage from 0.0 to 1.751 volts.

The JW lwc is given by:

$$JWLWC = 51.48 * (a_4 - 32767) / 2869.0 / TAS$$

where a_4 is the system count of analogue channel 4.

The JW lwc formula is calculated as follows:

2 gm^{-3} gives a voltage range of 1.751 volts
1.751 * 3276.7 = 5737.5 gives the system counts range
Therefore the number of system counts per gm^{-3} is:
5737.5 / 2.0 = 2868.75 (This is the inverse of the gradient)
System counts for 0.0 volt 32767 + 0.0 * 3276.7 = 32767
System counts for 1.751 volt = 38504.5
The basic equation is therefore: (a_4 - 32767) / 2868.75
A correction factor for TAS needs to be added for the 100 knots (51.49 ms^{-1}) calibration of the dummy sensor head.
Therefore 51.49 * (a_4 - 32767) / 2869 / TAS is the equation.

(vii) Pressure

Static pressure is measured using a Rosemount Model 1201FA1B2B pressure sensor (s/n 1398). The range of counts is from 32773 to 65554. Measurement range is from 0 to 32 in-Hg and the output voltage is from 0.002 to 10.006 volts.

The static pressure in millibars is given by:

$$STP = 1083.64 - (65535 - a_7) / 30.235$$

Pitot pressure is measured using a Rosemount Model 1221F2VL18B2A sensor (s/n 389). The range of counts is from 32767 to 49151. Measurement range is from 0.000 to 1.000 psi and the output voltage is from 0.000 to 5.000 volts.

The pitot pressure in millibars is given by:

$$PTP = (a_3 - 32767) / 237.63$$

(viii) Radar

The aircraft has a Bendix RDS82V, 3 cm radar, with 90 degrees horizontal scan and 30 degrees vertical scan capability.

(ix) Rate gyro

Northrop Rate Gyro (s/n 1534) part no. 6459-301. The range of counts is from 33684 to 64420. Measurement range is from 30 (nose down) to -30 degrees per second (nose up) and the corresponding output voltage from 0.28 to 9.66 volts.

The pitch rate ($deg.s^{-1}$) is given by:

$$RG_{(volts)} = (a_5 - 32767) / 3276.7$$

and

$$RG = -6.521 * RG_{(volts)} + 32.399$$

where a_5 is the system count of analogue channel 5.

The rate gyro formula is calculated as follows:

-60 degrees per second gives a voltage range of 9.38
9.38 * 3276.7 = 30735.4 gives the system counts range
Therefore the number of system counts per volt is:
30735.4 / 9.38 = 3276.695 (The inverse of the gradient)
System counts for 0.28 volt 32767 + 0.28 * 3276.7 = 33684
System counts for 9.66 volt 32767 + 9.66 * 3276.7 = 64420
Therefore (a_5 - 32767) / 3276.695 gives the voltage.
The linear regression on the calibration data, for volts vs degrees/second is y = -6.521 * x + 32.399

(x) Temperature

The Vaisala HMP 14 reverse flow temperature/humidity probe uses a housing developed at the BPRP and a thermistor YSI 44203 temperature sensor. The range of counts is from 37046 to 34418. Measurement range is from -30 to +50°C and the output voltage from 1.306 to 0.504 volts.

The reverse flow temperature is given by:

$$RFT = 50.0 - (34418 - a_1) / 32.85$$

where a_1 is the system count of analogue channel 1.

The reverse flow temperature sensor is calibrated prior to each flight at points -15 and +50°C.

The reverse flow formula is calculated as follows:

80 degrees gives a voltage range of (1.306 - .504) 0.802
0.802 * 3276.7 = 2628 gives the system counts range
Therefore the number of system counts per degree is:
2628 / 80 = 32.85 (This is the inverse of the gradient)
System counts for -30 deg. 32767 + 1.306 * 3276.7 = 37046
System counts for 50 deg. 32767 + 0.504 * 3276.7 = 34416
Therefore 50.0 - (34416 - a_6) / 32.85 is the equation.

The total temperature is measured using a Rosemount Model 102 AU1AF de-iced probe with a Rosemount Model 510BF148 amplifier (s/n 478). The range of the counts is from 32768 to 49150. Measurement range is from -50 to +50°C and 0.0004 to 4.9997 volts.

The Rosemount temperature is given by:

$$RMT = (a_0 - 32768) / 163.81 - 50.0$$

where a_0 is the system count of analogue channel 0.

The Rosemount formula is calculated as follows:

100 degrees gives a volts range of (4.9997 - 0.0004) 4.9993
4.9993 * 3276.7 = 16381 gives the system counts range
Therefore the number of system counts per degree is:
16381 / 100 = 163.81 (This is the inverse of the gradient)
System counts for -50 deg. 32767 + 0.0004 * 3276.7 = 32768
System counts for 50 deg. 32767 + 4.9997 * 3276.7 = 49150
Therefore (a_0 - 32768) / 163.81 - 50.0 is the equation.

(d) Bethlehem aircraft instrumentation - JRB

(i) Accelerometer

The accelerometer used is a Schaevitz linear accelerometer LSBCG2 (s/n 6386).

(ii) Angle of attack

The angle of attack vane is the model 861 fuselage mounted flow angle sensor.

(iii) Navigation

Trimble GPS as for JRA.

(iv) Heading

The heading calculation is the same as for JRA.

(v) Humidity

The Vaisala 1518 HM humidity sensor is fitted to the Vaisala HMP 14 reverse flow temperature/humidity probe in a housing developed at the BPRP. The range of counts is from 32767 to 36044. Measurement range is from 0 to 100% and the output voltage is from 0 to 1 volt.

The relative humidity (%) is given by:

$$RH = (a_6 - 32767) / 32.767$$

where a_6 is the system count for analogue channel 6.

The humidity is calibrated prior to every flight using one of two Vaisala HMK 11 humidity calibrators (s/n 15704 and 14923) with calibration points of 13 and 97%.

(vi) Liquid water content

Two probes are in use, the Johnson-Williams (JW) and the CSIRO King.

The King lwc probe model KLWC-5 (s/n 17849-1189-41) uses a PMS sensor model HW03. The range of counts is from 32767 to 65534. Measurement range is from 0.0 to 5.0 gm^{-3} or 0.0 to 1.0 gm^{-3} and the output voltage from 0.0 to 10.0 volts (we have to date only operated the sensor in the 0 to 5 mode). The King lwc is given by following the same procedure as for JRA.

The JW lwc comprises a sensor (s/n 175), power supply (s/n 7107) and a Johnson-Williams dummy sensor head (s/n 7107-8) model LWH calibrated for 100 knots. The range of counts is from 32767 to 38505. Measurement range is from 0.0 to 2.0 gm^{-3} and the output voltage from 0.0 to 1.751 volts. The JW lwc is given by the same equation as for JRA.

(vii) Pressure

Static pressure is measured using a Rosemount Model 1201FA1B A pressure sensor (s/n 949). The range of counts is from 32783 to 49164. Measurement range is from 0 to 32 in-Hg and the output voltage is from 0.005 to 5.004 volts.

The static pressure in millibars is given by:

$$STP = 1083.65 - (49164 - a_7) / 15.12$$

Pitot pressure is measured using a Rosemount Model 1221F2VL18B2A sensor (s/n 390). The range of counts is from 32767 to 49164. Measurement range is from 0.000 to 1.000 psi and the output voltage is from 0.000 to 5.004 volts.

The pitot pressure in millibars is given by:

$$PTP = (a_3 - 32767) / 237.81$$

(viii) Radar

The aircraft has a Bendix RDS81, 3 cm radar, with 90 degrees horizontal scan capability.

(ix) Rate gyro

The range of counts is from 34438 to 63896. Measurement range is from 30 (nose down) to -30 degrees per second (nose up) and the corresponding output voltage from 0.51 to 9.5 volts.

The pitch rate (deg.s^{-1}) is given by:

$$RG_{(volts)} = (a_5 - 32767) / 3276.7$$

and

$$RG = -6.816 * RG_{(volts)} + 34.148$$

where a_5 is the system count of analogue channel 5.

The rate gyro formula is calculated as follows:

-60 degrees per second gives a voltage range of 9.38
9.38 * 3276.7 = 30735.4 gives the system counts range
Therefore the number of system counts per volt is:
30735.4 / 9.38 = 3276.695 (The inverse of the gradient)
System counts for 0.28 volt 32767 + 0.28 * 3276.7 = 33684
System counts for 9.66 volt 32767 + 9.66 * 3276.7 = 64420
Therefore (a_5 - 32767) / 3276.695 gives the voltage.
The linear regression on the calibration data, for volts vs degrees/second is y = -6.521 * x + 32.399

(x) Temperature

The Vaisala HMP 14 reverse flow temperature/humidity probe uses a housing developed at the BPRP and a thermistor YSI 44203 temperature sensor. The range of counts is from 34418 to 37046. Measurement range is from +50 to -30°C and the output voltage from 0.504 to 1.306 volts.

The reverse flow temperature is given by:

$$RFT = 50.0 - (34418 - a_1) / 32.85$$

where a_1 is the system count of analogue channel 1.

The reverse flow temperature sensor is calibrated prior to each flight at points -15 and +50°C.

The reverse flow formula is calculated as follows:

80 degrees gives a voltage range of (1.306 - .504) 0.802
0.802 * 3276.7 = 2628 gives the system counts range
Therefore the number of system counts per degree is:
2628 / 80 = 32.85 (This is the inverse of the gradient)
System counts for -30 deg. 32767 + 1.306 * 3276.7 = 37046
System counts for 50 deg. 32767 + 0.504 * 3276.7 = 34418
Therefore 50.0 - (34418 - a_6) / 32.85 is the equation.

The total temperature is measured using a Rosemount Model 102 AU1AF de-iced probe (s/n 13577E) with a Rosemount Model 510BF148 amplifier (s/n 477). The range of the counts is from 32767 to 49146. Measurement range is from -50 to +50°C and 0.0000 to 4.9987 volts.

The Rosemount temperature is given by:

$$RMT = (a_0 - 32767) / 163.79 - 50.0$$

where a_0 is the system count of analogue channel 0.

The Rosemount formula is calculated as follows:

100 degrees gives a volts range of (4.9987 - 0.0000) 4.9987
4.9987 * 3276.7 = 16379 gives the system counts range
Therefore the number of system counts per degree is:
16379 / 100 = 163.79 (This is the inverse of the gradient)
System counts for -50 deg. 32767 + 0.000 * 3276.7 = 32767
System counts for 50 deg. 32767 + 4.9987 * 3276.7 = 49146
Therefore (a_0 - 32767) / 163.79 - 50.0 is the equation.

(e) Laser diode for aircraft probes

The Helium-Neon lasers used in the PMS particle imaging and measuring probes have several disadvantages: they are expensive, require careful handling, have a relatively short lifespan (between one and two years), need a high voltage power supply, and need to be imported as required. A diode laser on the other hand is comparatively cheap, does not need careful handling, requires only a five volt power supply, and has a lifetime of up to ten years. In view of these advantages the possibility of using a diode laser in the PMS two dimensional probes was investigated through the Atomic Energy Corporation's (AEC) Optical Energy Systems (OES) section. Preliminary testing of the diode laser has shown it to be a possible candidate for replacing the conventional Helium-Neon laser.

(f) Ground-based software

The Aircraft System is used to analyse the aircraft data. The research team uses the information produced to assist with the cloud research project.

The data sets have been standardized so that the system can process data without differentiation having to be made between the Bethlehem aircraft used or the area where the data have been recorded (Bethlehem or Nelspruit). The output has also been standardized and differentiation is made between the probes used. All duplication in the programmes as well as the output has been removed to create a more streamlined package that is easier to use. A programme has been written to edit the data set of the old aircraft data (1980 - 1989) for processing by the new system.

A user interface has been developed that enables the user to specify a few parameters by which processing and output of the system can be controlled. The user can determine if only a specific time range must be processed and which output reports and files are needed. A date other than the current date can be specified for processing and the system will search for the file

and check if the data set must be edited before processing.

A normal data run will produce an event, picture, history , and sounding report, statistical reports of 2D, pms and air data, time history plots of 2D, air and PMS data and plots of the 2D images. A file with statistical information is created for UNISA. Other reports such as 2D image and buffer analysis reports can be created on request. An in-cloud data file can also be created but is not part of a normal data run.

Error control has been built into the system to ensure ease of use both for users and the maintenance staff. A user manual with full documentation, flow charts, etc. has been written to ensure that the system can be used and understood should the Data Processing staff change in future.

The processing of the aircraft data is done as follows :

Before analysis is done the raw data are calibrated by means of calibration constants that are verified every season. These constants also differ for each aircraft and are stored in a file to keep record of the changes for every season. This file makes programme maintenance a lot easier because it's not necessary to change the programmes every season to make provision for the change in constants.

In the calibration programme (AIRCALIB) these constants are read and used as needed. The fast mode data are processed to get an average per second that is written to a file which serves as input to the analysis programme. The calibrated data are stored in a file and kept on the data base.

In the analysis programme in-cloud averages, minima, maxima and standard deviations are done. Time history plots are drawn and reports with statistical summaries are printed.

(g) Aircraft systems

Development on the aircraft systems is effectively complete, but because of new additions to the systems, development is ongoing.
Additions to the systems were:

1. Trimble GPS navigation systems to replace the Litton INS
2. Synchro to Digital interface for heading, pitch and roll
3. System racks were made to order
4. Bus extenders were added.

The presentation and driver software were extensively updated, with most technical manuals on the interfaces completed. To date the aircraft systems comprise the following:

1. Rack mounted components:
   a. HP Vectra host computer,
   b. Bus extender, allowing up to 12 extra interfaces,
   c. Colour EGA monitor,
   d. Exabyte cassette tape streamer (CTS),
   e. Signal conditioning unit for instruments and low pass filters,
   f. Slide-out keyboard,
   g. Power Supply unit;
2. Cockpit mounted components:
   a. colour EGA monitor,
   b. mini keypad;
3. Interfaces:
   a. PMS 2D probe,
   b. PMS FSSP or 1D probe,
   c. Mini keypad and I/O,
   d. Sixteen channel Analogue to Digital converter for analogue instruments,
   e. RS422 for GPS,
   f. SCSI (for Exabyte CTS),
   g. Synchro to Digital (for aircraft heading);
4. Software for driving the interfaces, and for real-time display and control.

Additions to the aircraft system envisaged for 1992/1993 are:

1. RF telemetry system for real-time transfer of aircraft data to the radar control room,
2. Upgrading the 2D interface to DSP-based card,
3. Digitizing the aircraft radars.

The following ongoing tasks were performed:

1. documenting system changes as they are made,
2. adding new instrumentation and interfaces,
3. upgrading software to accommodate new instrumentation and interfaces, and
4. upgrading and improving present software code and methodology.

THE NATIONAL PRECIPITATION RESEARCH PROGRAMME

FINAL REPORT
1990 - 1992

by

G. K. Mather
CloudQuest (Pty) Ltd

and

D. E. Terblanche
South African Weather Bureau

Report to the
Water Research Commission
Pretoria

March, 1993

WRC Report No. 133/8/93
ISBN 1 874858 96 9

TABLE OF CONTENTS

LIST OF TABLES

LIST OF FIGURES

1. EXECUTIVE SUMMARY

The central objective of the research carried out by the National Precipitation Research Programme (NPRP) has been to evaluate the potential for beneficial modification of summertime convective rainfall. It has been estimated that local water demand will exceed the total available supply around the year 2020. Rainfall augmentation, if feasible, has been identified as an attractive source of good quality water.

The search for rainfall augmentation opportunities must begin with a comphrehensive study of the natural rainfall processes. This has been accomplished in the study areas using sophisticated meteorological radars and instrumented aircraft. These studies have recognized that many of the region's convective storms are inefficient in terms of rainfall production, i.e. only about 30 percent of the atmospheric water vapour entering the storms reaches the ground as precipitation. Thus, the search for augmentation opportunities has centred around a means of increasing rainfall production efficiency. The research has also recognized the efficiency of rainfall formation via a collision-coalescence process which has been shown to occur in certain storms in both the Carolina and Bethlehem study areas. Observations in storms growing over a Kraft paper mill west of Nelspruit raised the possibility that coalescence could be enhanced or accelerated by the addition of hygroscopic nuclei into the storm updraft at cloud base. To investigate the efficiency of hygroscopic nuclei, a hygroscopic cloud seeding flare was designed and manufactured by Swartklip Products, Cape Town. Racks for the flares were designed, constructed and mounted on the aft end of the engine nacelles of one of the project's Commander 690s. Each rack holds a total of 10 flares, which are electrically ignited from switches in the cockpit. Initial seeding trials were so promising that a formal randomized seeding experiment was designed with the aid of the Applied Statistics group at UNISA after one season of trials.

At this point, the strong prospect that pursuit of the hygroscopic seeding approach might accelerate progress towards the goal of developing a viable cloud seeding technology, caused the discontinuation of experiments with dry ice as a seeding material. The dry ice pulse seeding experiment, designed to confirm elements of seeding hypotheses based on previous research at Bethlehem and Nelspruit, had by then produced only promising but as yet inconclusive results.

The results of the hygroscopic randomized seeding experiment show statistically significant increases in radar-measured rainfall after just one experimental season. To our knowledge, no formal convective cloud seeding experiment has ever shown significant increases in rainfall after a single season's experimentation. We believe this new approach to convective cloud seeding can be hailed as a breakthrough in the field of weather modification.

Verifying the efficiency of the new hygroscopic seeding flare required the coordination and application of skills and knowledge that have taken years to develop. The complete report contains many examples of the application of these skills. Coordinating two aircraft, the seeding and the cloud physics sampling aircraft on an experimental storm within range of a project radar is but one example of the exercise of these skills. The knowledge required to analyse and interpret the acquired radar data and cloud physics measurements is another. The in-house skills required to maintain, and when required, to update the hardware and software that is the core of the data gathering capability is yet another. It is the acquired depth of this knowledge and these skills that has bred the confidence required to embark on a novel and, we believe, a more appropriate approach to cloud seeding in South Africa.

The hygroscopic seeding hypothesis which has been formulated should be relatively easily verified by a combination of microphysical and radar measurements supported by numerical cloud models. An additional season of the randomized cloud seeding experiment should supply sufficient additional experiments to reinforce the conclusions of the statistical studies.

The primary objectives set by the contract covering the past 3 years of research were to:

- investigate both natural and artificially modified precipitation process in multicellular convective clouds and to gain a better understanding of the physical mechanisms of precipitation development in the larger cloud systems

- use the knowledge gained to identify those conditions in which precipitation efficiency may be increased by intervention

- develop a viable technology that can be applied operationally to artificially enhance rainfall.

The first two of these objectives have been addressed with a considerable measure of success. Results to date support the contention that, with the new hygroscopic approach to convective cloud modification, the third objective also is well on the way to being accomplished. The ultimate test of the viability of this new technology will be an area experiment in which the first deliberate attempts to produce more rainfall on the ground will be objectively evaluated.

The planning of this next stage should start immediately, and should proceed in parallel with the seeding experiment and further observational and modelling studies. Many of the methodologies required for an area experiment are already in place, having been developed through the NPRP as well as independent research. For instance, rapid progress is being made

with the accurate measurement of rainfall over an area with a calibrated meteorological radar. Catchment modelling studies geared to assessing the impacts of cloud seeding on water resources are well under way. Societal impact studies are indicating that a major public relations effort in and around a chosen experimental area should be an integral part of early planning for the area experiment.

The users of a potentially successful rain augmentation technology must be drawn into the planning from the outset. These include Forestry, Water Affairs and Agriculture. Their participation will be required in the design of the experiment, to specify the measurements (rain gauges, stream flow, radar etc) and the confidence levels that they will require before recommending the use of the technology as an effective means of augmenting South Africa's water resources.

2.0 THE NATIONAL PRECIPITATION RESEARCH PROGRAMME

2.1 Introduction - a historical review

The purpose of this historical review is to place in perspective the aims, procedures and achievements of the National Precipitation Research Programme (NPRP) during the contract period 1990 to 1992. Consolidation of rainfall augmentation research in South Africa was achieved in early 1990 by the amalgamation of the Bethlehem and Nelspruit research projects under the NPRP banner.

Research at Bethlehem and Nelspruit had since 1983 been focussed on the search for a rain augmentation hypothesis, which if successfully tested, would lead to the ability to augment South Africa's water resources by putting more water on the ground. Initially, the research was led by results from major research programmes overseas, mainly in the United States. These well-designed projects were evaluated by a combination of physical measurements and sophisticated experimental techniques using the randomized allocation of treatment. The experimental hypotheses dictated the anticipated outcome, which was clearly stated before the experiment commenced. Any statistical result had to be supported by physical measurements, using instrumented aircraft and radars. There were two favoured hypotheses. The Florida Area Cumulus Experiment (FACE) was based on the dynamic seeding concept, the theory that massive seeding of convective clouds with artificial ice nuclei, in this case silver iodide, would lead to increased buoyancy through the sudden release of the heats of fusion, deposition and condensation, thereby producing taller, wider and longer lasting clouds (Simpson, 1980).

The second hypothesis rested on the assumption that there are insufficient precipitation embryos in the supercooled regions of convective clouds, which results in an inefficient natural precipitation formation process. The introduction of additional precipitation embryos via glaciogenic seeding was expected to redress this deficiency. This hypothesis was thoroughly tested in isolated cumulus congestus clouds in the HIPLEX I experiment in the United States (Mielke et al., 1984) and at Bethlehem in South Africa (Kraus et al., 1987). In both experiments, massive increases in ice crystals were documented, but the linkage between increases in precipitation embryos and more rainfall at cloud base was missing. Measurements in the experimental clouds showed that the available supercooled water was being lost to entrainment (cloud air mixing with dry environmental air) before the artificially produced precipitation embryos had reached their riming threshold, i.e. grown large enough to collect the available supercooled water droplets. Both experiments concluded that future convective cloud experiments should move upscale to the larger, isolated convective complexes where entrainment would not be such an impediment.

The Nelspruit dry ice seeding experiment commenced 1 October, 1984, (Programme for Atmospheric Water Supply, 1990) and chose the isolated convective complex as the experimental unit. Since it was not clear what response to seeding (if any) could be expected from convective complexes, the Nelspruit experiment was designed to test for radar-measured differences between seeded and control storms. In this sense, the experiment was exploratory, since response variables were not specified before the experiment commenced.

There are two mechanisms which produce precipitation embryos, or graupel in the supercooled regions of convective clouds. The first involves the growth of ice crystals via vapour diffusion followed by riming growth, the freezing of supercooled water droplets on the surfaces of the ice crystals. This mechanism was well documented in both the HIPLEX and Bethlehem experiments. In the second, drizzle drops grow by coalescence, which is the collection of smaller cloud droplets via collisions with a few larger drops. If these freeze, then growth continues via the riming process. This second mechanism can be a more efficient precipitation growth process than the ice crystal mechanism because of the greater density of the frozen drop (0.9 g/cm^3 versus 0.2 for ice crystals). The presence and importance of the coalescence growth mechanism was recognized and documented using the cloud physics Learjet at Nelspruit and a simple classification technique developed, based upon cloud base temperature and potential cloud buoyancy, which appears to adequately separate clouds in which ice crystal growth dominates from those in which precipitation is initiated via the coalescence or coalescence-freezing mechanism (Mather et al., 1986). This thermodynamic classification technique was used to stratify the storms collected during the Nelspruit dry ice seeding experiment, eliminating those storms from the radar data base which were unlikely to develop precipitation via the coalescence process. The analysis with this partitioned data set revealed significant and physically realistic differences between the seeded and control storm groups. These differences were consistent with a seeding hypothesis based on an observation by Braham (1964) that drops growing via coalescence will grow faster by riming if they can be frozen by the seeding. The design, analysis and results of the Nelspruit dry ice seeding experiment are fully reported in Mather (1991).

The next step was to run a confirmatory dry ice seeding experiment at Nelspruit, in which the anticipated response variables were specified in advance. This experiment was interrupted after the Review Workshop on Rainfall Stimulation Research in South Africa, held in the Kruger Park in August 1989. Expert overseas scientists at this workshop asserted that unless the physical mechanisms responsible for the apparent radar-inferred increases in rainfall were understood, the results of any number of confirmatory experiments would not be accepted. It was at this stage that the Nelspruit and Bethlehem research groups were amalgamated and the research continued under the

banner of the NPRP, the aims of which are set out below (Section 2.2). The Nelspruit and Bethlehem research bases remained unaltered, operations being conducted from whichever base showed the most potential for storm development. The combined group has made good progress, including the in-house development of hardware and software for radar and aircraft systems. One of the major initial thrusts of the NPRP was to attempt to clarify certain of the postulated mechanisms whereby dry ice seeding led to apparently enhanced precipitation development. For this purpose, the pulse seeding experiments were designed and executed in 1989/90 and 1990/91. More specifically, this was an attempt to resolve the links in the chain of events between the creation of massive amounts of ice crystals at seeding levels and more rainfall on the ground.

The experiment yielded interesting, but inconclusive results. Regretfully, the experiment was abandoned prematurely in favour of an intensive research effort in what was proving to be a much more promising direction; the possible early enhancement of precipitation growth via coalescence through hygroscopic seeding. This alteration of the course of rain augmentation research by the NPRP was prompted by a chance event on 20 December 1988. A storm selected during the normal course of the dry ice seeding experiment departed so radically from what experience had taught us to expect, that some explanation had to be found for the apparent anomalous behaviour of this storm. Huge drops were encountered at the penetration level ($-10^{o}C$), indicating an active coalescence precipitation formation mechanism. Subsequent analyses showed that this unusual storm was growing over a Kraft paper mill west of Nelspruit. Follow-on measurements in cumuli growing near the paper mill showed a broadening of the cloud-drop spectra caused by the hygroscopic material in the emissions from the mill stacks. It was the broadening of the spectra at cloud base that was leading to the enhanced coalescence observed at the $-10^{o}C$ level (Mather, 1991). These observations led to the development of a hygroscopic seeding flare. The idea was to free the research from the geographical restraints of the paper mill, allowing experiments on selected clouds anywhere within the experimental area. Although the flare output is small compared to the paper mill, the hope was that placing the hygroscopic material at exactly the right place and at the right time would compensate for this deficit.

Trial seeding experiments with the new flares commenced in October 1990. These trials were so promising that a randomized experiment was designed and initiated just a year later in October 1991. This experiment was designed and evaluated with the help of the Centre of Applied Statistics at UNISA. The anticipated response variable, rain flux, was specified in advance. A total of 51 experiments were conducted, 21 in the Bethlehem area and 30 around Carolina. This experiment reached acceptable levels of statistical significance in a single season! Contrast this result with that of the dry ice seeding experiment which took three seasons to reach acceptable levels of

statistical significance and then only after the radar data had been partitioned using the coalescence criterion. It was the excitement generated by these results that led to the termination of the dry ice pulse seeding experiment.

The hygroscopic seeding hypothesis is already on firmer ground than the dry ice seeding equivalent. Future work will concentrate on filling in the remaining gaps in this new hypothesis and on strengthening the statistical analysis by continuing with the randomized seeding experiment.

In summary, work at Nelspruit and Bethlehem identified the inefficient rainfall formation process in the convective storms that bring most of the rainfall to the eastern Transvaal and Free State. To redress this inefficiency, attempts have been focussed on placing more and larger precipitation embryos into the strong updraft regions of these storms, to collect more of the available supercooled water before it is swept up into the large anvil clouds that are a characteristic of the summertime skies in the region. At this stage, the most promising method of increasing precipitation efficiency appears to be the addition of hygroscopic nuclei to the updraft feeding the storm at cloud base.

For this reason, it was generally agreed by all those directly involved with the NPRP that the decision to prematurely terminate experimentation with dry ice and concentrate on hygroscopic seeding was fully justified. The results achieved during the course of the dry ice pulse seeding experiments will nevertheless be documented in Section 4.

2.2 Aims of the NPRP

The primary objectives of the rainfall stimulation research project are:

(a) To investigate both natural and artificially modified precipitation processes in multicellular convective clouds and to attain a better understanding of the physical mechanisms of precipitation development in the larger cloud systems.

(b) To use the knowledge gained in (a) to identify those environmental (synoptic) conditions in which the precipitation efficiency of larger cloud systems may be increased by human intervention, should there be any reason to believe that the natural processes are inefficient at times.

To achieve these objectives the following broad research avenues have been identified:

1. Comprehensive field studies to document the fundamental cause and effect relationships during each step of the physical chain of events, in natural and artificially modified clouds, in order to quantify the physical processes and develop an adequate physical understanding of such processes.

2. Numerical cloud modelling to provide a framework for comparisons between observations and theory, and to test and/or refine an underlying hypothesis. Computer technology is now available to develop sophisticated models to test the concepts of rainfall stimulation. Laboratory, theoretical and numerical modelling studies should go hand-in-hand with the field studies.

3. Development and application of technology, instrumentation and data handling systems to ensure that measurements and analytical capabilities are adequate for needed field and modelling studies. Since research is at the forefront of science, developments overseas will have to be monitored diligently and where necessary, incorporated locally with the minimum of delay. For this reason, it is extremely important for the relatively small local research team to interact regularly with researchers in other parts of the world.

4. Development of local expertise in every facet of the research should be a primary goal at all stages of the research effort.

2.3 Personnel

The personnel employed at each site are listed in Tables 2.0 and 2.1. The many skills and disciplines that are required to pursue the programme's objectives become evident after a quick scan of these tables. Meteorological skills must be supplemented by knowledge of radars, computers and sophisticated measuring systems including laser imaging probes. Software must be developed to analyse the outputs from the radars and aircraft measuring systems. These data must be processed and stored in easily accessible data bases.

Statistical techniques must then be employed to assess the significance of the measurements. The assistance of Professor Francois Steffens at UNISA has been elicited for this purpose. The group at UNISA is also consulted about the design of any experiments, especially those that include randomization in their design.

A qualitative rather than a quantitative advantage of the consolidation of the two projects has emerged. The youthful and enthusiastic Bethlehem group blends well with the older, more experienced Nelspruit group. Also, a comparison of past research efforts indicates that both groups have been moving in roughly the same direction. This sharing of common goals has meant that the combined group has been able to agree on plans for future research with much more confidence.

Table 2.0 List of Bethlehem Personnel

Personnel		Responsibilities
D. Terblanche	-	project leader and research director
F. Adam	-	assistant project leader
E. Loftus	-	pilot and aircraft data
F. Hiscutt	-	aircraft and radar systems development
S. Edwards	-	aircraft instrumentation, calibration and development
K. de Waal	-	computers and system software
Z. Botha	-	software development
H. Pienaar	-	radar and radar data
G. van de Hoven	-	forecasting, mesonetwork, surface and upper air observations
H. Ihlenfeldt		
D. Wannenburg		
R. Bindeman		
J. McKerry		
E. Visser		
T. Maseko		
A. Navarro	-	administration
L. Masangana	-	assistant
I. Malan	-	rainfall
S. Mokoena	-	assistant
G. Corroyer	-	aircraft maintenance
P. Mokoena	-	assistant

Table 2.1 List of Nelspruit Personnel

Personnel		Responsibilities
G. Mather	-	project leader and pilot
R. Parsons	-	deputy project leader, pilot, radar analysis software and data base
F. van der Westhuizen	-	chief pilot, surface rain gauge network
C. Wightman	-	pilot, aircraft analysis software and data bases
K. Young	-	electronics engineer, project radars and computers
P. McNaught	-	electronics technician, project radars
I. Ross	-	electronics technician, aircraft instrumentation systems
E. Botha	-	Nelspruit-Weather Bureau computer link, rain gauge data collection, software development
M. Schormann	-	temporary assistant, software development, radar and aircraft
M. Dreyer	-	secretary and comptroller
J. Segage	-	driver
P. Ngobeni	-	site maintenance

2.4 Equipment

The combined equipment of both projects makes an impressive list, making the NPRP one of the best equipped convective cloud research group in the world. A partial list of this equipment follows:

- Learjet 24, instrumented for cloud physics research, has a dry ice seeding capability

- turboprop Aero Commander 690 (JRA), instrumented for cloud physics research and rainfall measurements at cloud base

- turboprop Aero Commander 690 (JRB), instrumented for cloud physics research, has a dry ice seeding capability and is equipped with wing racks for end-burning flares

- Aero Commander 500S (IZN) instrumented for making measurements of rainfall at cloud base, also has an isokinetic particle sampling capability

- twin Commanche, at this stage used for communication flights

- 5 cm meteorological radar with a 1^{o} beam width and volume scan capabilities (Bethlehem)

- a second 5 cm meteorological radar with 1.6^{o} beam width, volume and sector scan capabilities (Carolina)

- mesoscale network of rain gauges and automatic weather stations

- upper air sounding equipment at both sites

- aircraft maintenance and hangar facilities.

Each radar is supported by a computer system which displays, digitizes and records the reflected radar signals. Each radar tracks the project aircraft, displaying (for purposes of control) and recording the position of the aircraft. Each aircraft is equipped with a computer which displays and records the aircraft measurements. Both the radar and aircraft data must be further processed and stored in data bases by large computers. The data bases are accessed for study purposes by cloud physicists at both sites. In the process, valuable analysis software is created.

During the course of experiments, measurements from the data bases are extracted and sent to statisticians at UNISA for analysis.

These data bases are a valuable scientific asset for South Africa since they describe in detail the radar and microphysical climatology of clouds in the Bethlehem and Nelspruit areas.

(a) The Bethlehem Radar

The 5 cm Enterprize radar at Bethlehem was converted to PC based antenna control, data acquisition and storage during the past three years. The prototype designs in this system were upgraded during the past year and the present system is summarized below.

The upgrade to a PC based system was done to replace the Enterprize DVIP for the acquisition real-time display and storage of data by a more flexible system. The hardware based antenna scan sequence was also replaced with a flexible software controlled system and data storage moved from 9 track tapes to miniature video cassettes. The whole system is an improvement on the original system as it uses the latest high speed digital technology, and it is easily upgradable and flexible.

The PC based system and its interfaces with the radar are shown schematically in Figure 2.0.

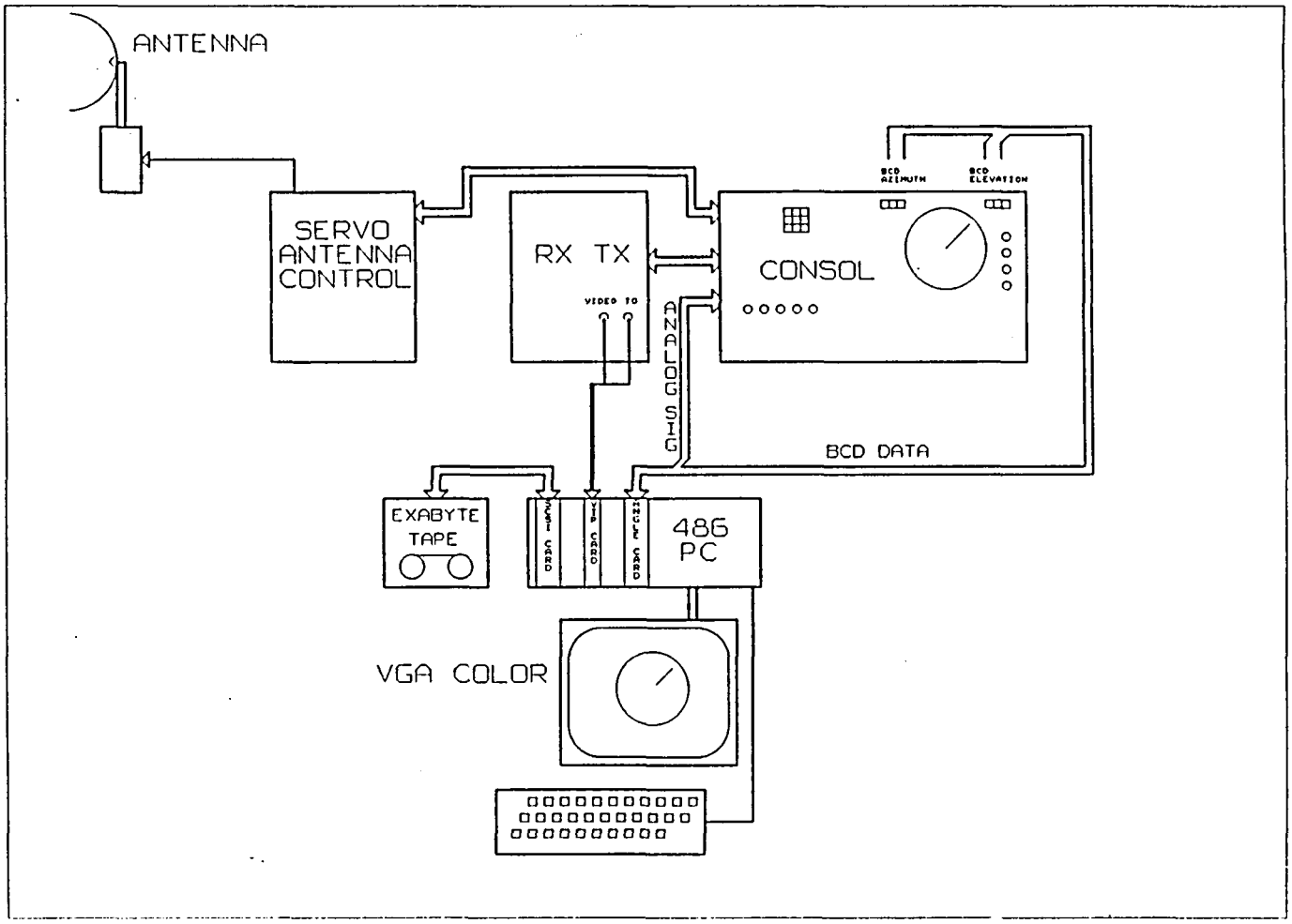

Fig.2.0 PC based system and its interfaces with the radar.

(i) DVIP board

The DVIP interface is a high speed 16 bit ISA bus DSP based Digital Video Integrator Processor card customized for acquisition of radar video data.

The card is capable of a sample rate of up to 1.25 mHz of 12 bit data and performs a real-time integration in range and azimuth producing a 16 bit averaged Bin buffer.

The card is fully user programmable and configurable for sample rate, bin size, integrations per bin and other setup parameters via a 16 bit port between the PC and DSP bus. High speed memory chips and FIFO buffers are implemented to store and prepare the Bin data for downloading to the PC bus.

The card accepts a TRIGGER and VIDEO Input signal from the radar system. The DVIP digitizes the video signal in sync with the master trigger from the radar and when a full buffer of integrated data is available an interrupt is generated signalling the PC to unload the data. The card has 32k words of memory and 4k words of FIFO buffering organized in a ping-pong fashion.

An on-card communications chip allows direct connection to external systems such as Transputers and other DSP based systems. The card uses only 4 I/O ports on the PC bus and makes use of interrupts and I/O to signal when data are ready for unloading into PC memory.

The interface can occupy any expansion slot in a PC AT 286, 386 or 486 compatible computer enclosure and is jumper and dip switch configurable allowing several cards in one system.

A simplified diagram of this card is shown in Figure 2.1.

(ii) Angle board

This PC based interface makes use of a closed loop digital to analogue system which allows the main programme to position the radar antenna to an accuracy of 0.1^{o} in elevation. The present azimuth and elevation position in BCD is read into the PC via this card. The card outputs an analogue signal to the servo driver of the antenna.

The amplitude of this analogue signal is determined by the difference between the present elevation position and the required elevation position. This results in a fast slew in antenna elevation with minimal overshoot. After reaching the required elevation the closed loop system maintains this elevation without main programme intervention.

Figure 2.2 shows the main features of this card.

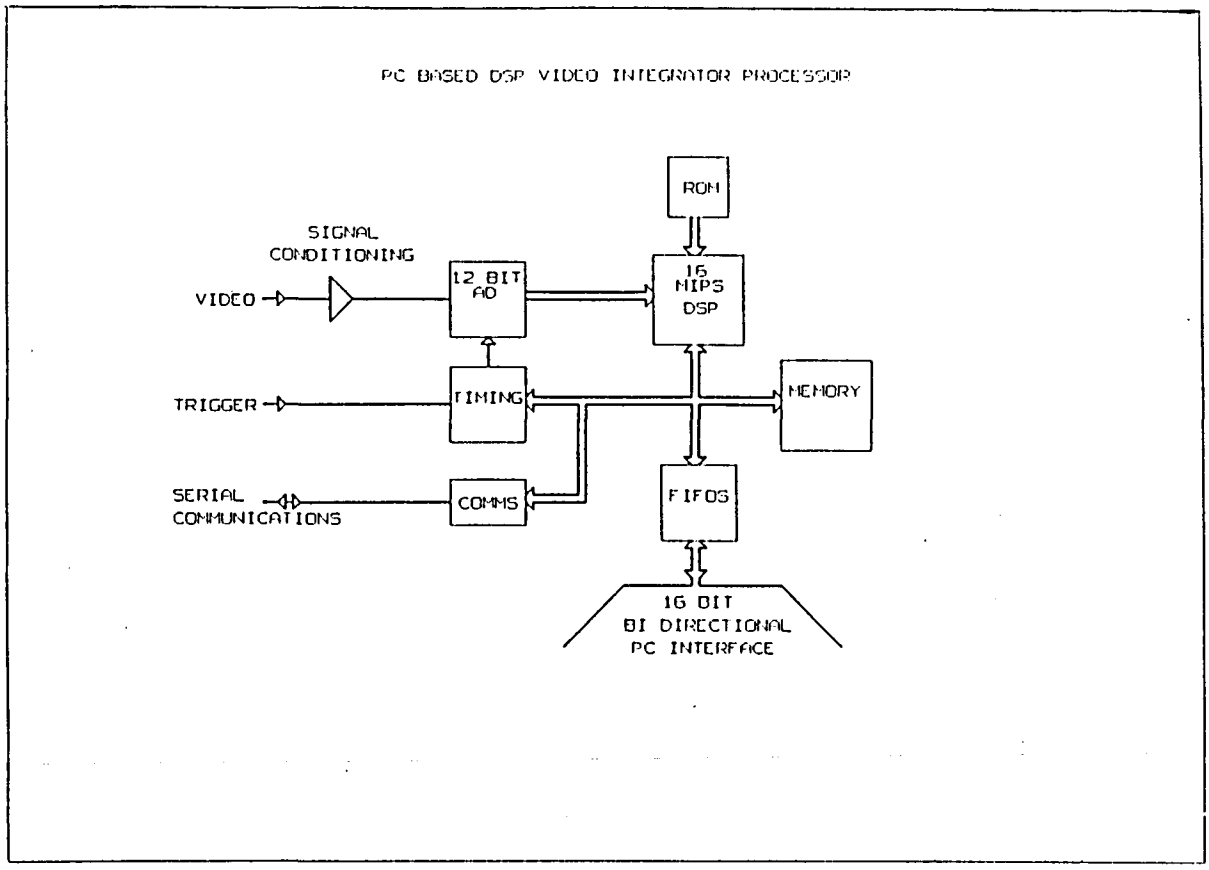

Fig. 2.1 Simplified diagram of DVIP board.

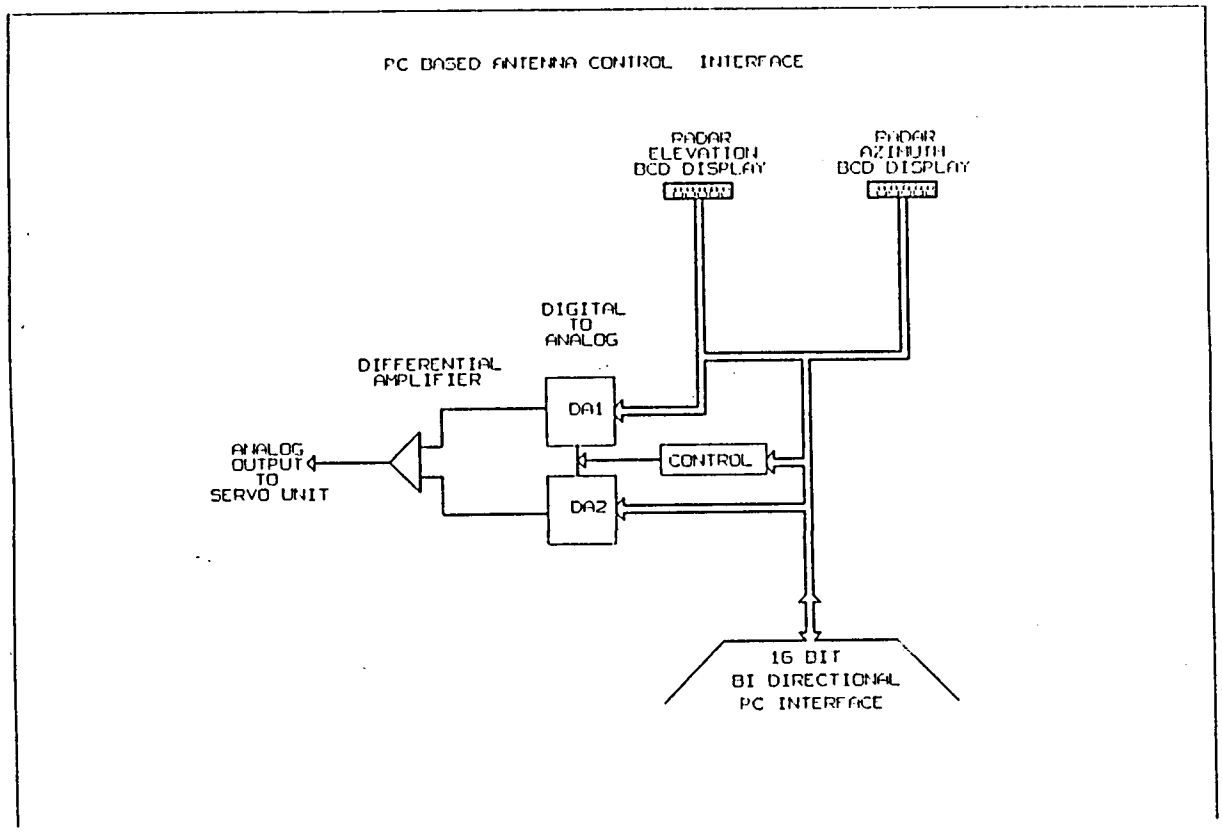

Fig. 2.2 Simplified diagram of angle board.

(iii) Data storage

Data are stored in real-time on miniature video cassette tape by a helical scanning technique on an Exabyte Cassette Tape System. Each cassette can store 2.3 Gigabytes of data allowing extended sustained operation. The Exabyte is interfaced to the PC via a Small Computer System Interface.

As drivers are not commercially available, they were developed to enable real-time data transfer from the PC to Exabyte and error monitoring.

(iv) General

Upon initiation the main radar programme reads a configuration file to set up all the site specific parameters and uploads configuration parameters to the DVIP card for sample rate, bin size, number of bins and number of integrations per bin.

The main programme sends the base scan elevation to the angle board which slews the antenna to this elevation. As soon as this elevation is reached, the main programme starts the DVIP process. Once the DVIP has collected 8 rays (8 PRF pulses) of data it generates an interrupt signalling to the PC that data are available for unloading. The PC will then unload the data into memory and onto Exabyte tape. These data are stored with a header containing date, time, elevation, azimuth, etc. The data in memory are processed for display purposes by the main program.

While the PC is processing and storing the data the DVIP card accumulates the next block of data resulting in a multi-tasking acquisition system which prevents data loss.

The antenna rotation speed is set such that 8 rays of bin data represents 1° of rotation. Once data from 360° have been collected the main program puts the DVIP card in a hold state and slews the antenna via the angle board to the next elevation in the configuration file. This whole process is repeated until the maximum required elevation is reached. On completion of this elevation, the antenna is slewed down to the base scan. This process, producing a complete volume scan, takes about 4 minutes.

(b) The Carolina Radar

Repairing the Carolina radar and site after the fire in early January, 1991 proved to be a major effort. All electronic equipment had to be removed and taken to Johannesburg for cleaning because of smoke damage. Advantage was taken of an opportunity to purchase a full set of critical spare parts for the Carolina radar from a sister radar that was being scrapped in the United States. This will significantly prolong the useful life of this radar.

The Carolina radar was off line from January 14 to March 4, 1991. The combined resources of the NPRP meant that the research could continue, shifting to the Bethlehem area, using the Bethlehem radar, which became operational at the beginning of January, 1991.

(c) Radar software

New software was developed for controlling the Bethlehem radar (in azimuth and elevation), for recording antenna position, radar and aircraft returns on an Exabyte tape recorder. Also developed was software for displaying the low level scan and project aircraft tracks on a colour VGA monitor in almost real time. As the antenna steps up from the lowest scan, the display of this scan is held on the VGA monitor, but the positions of the aircraft are updated each scan so the radar operator has a history of all aircraft tracks. The display is refreshed each time the radar completes a volume scan.

The basic operating, recording and display software are in place. Future plans included manufacturing common boards for both radars and implementing a real-time storm tracking scheme.

The Nelspruit radar analysis software was transferred to Bethlehem. Initially, the first part of the analysis was completed and recorded on magnetic tape at Bethlehem. This tape was then sent to Nelspruit for storm track analysis and display and storage in a radar database. By mid 1991 all storm analyses and displays could be accomplished at Bethlehem. Identical radar data bases for both radars are currently held at both sites. Plans for updating this software include the use of new storm tracking software that is being developed at NCAR by Mike Dixon who was also responsible for installing the original tracking software at Nelspruit in 1983.

(d) Aircraft measuring systems

The new PC based aircraft instrumentation system was installed in both JRA and JRB. New permanent racks to house the hardware, built locally, were installed. It should be emphasized that this system, which includes boards for the laser probes (an FSSP board and a 2D board), analogue to digital converters, a computer, an Exabyte tape recorder, analogue filters and surge protectors and displays has been designed and built in-house. Fig. 2.3 shows the results of a test in which the output from the FSSP probe was fed to the new interface and to the PMS data acquisition system in parallel. There is no discernable difference between the two outputs. These achievements mean that the NPRP has achieved a major goal; almost complete self-sufficiency in terms of hardware and software. Products in use that need outside support receive this support locally. All aircraft will eventually be converted to this new instrumentation

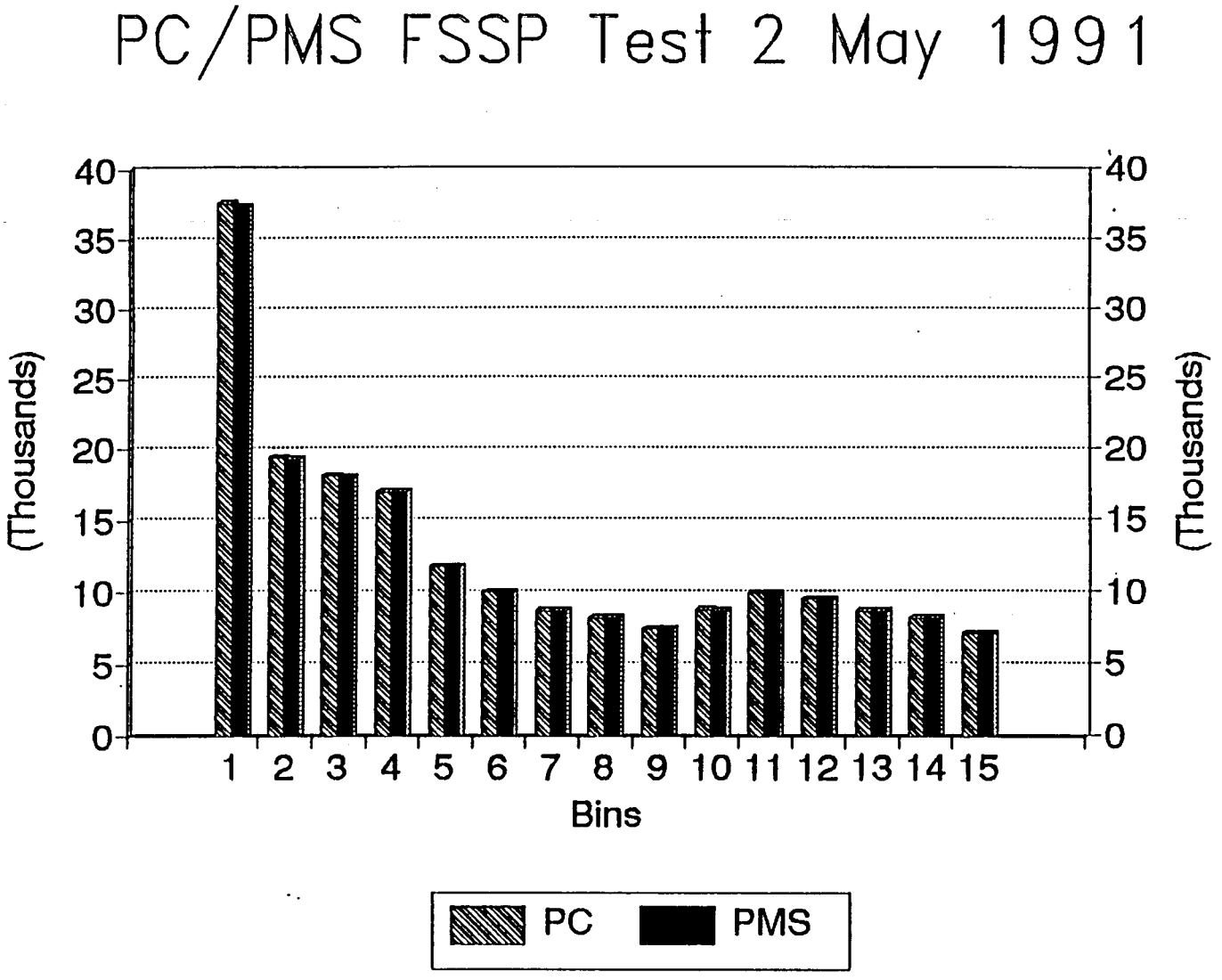

Fig. 2.3 Results from a test in which the output from an FSSP probe was fed in parallel into a PMS commercial data acquisition system and an interface developed in-house. Comparisons in all 15 bins are excellent.

system. A detailed description of aircraft measurements is provided in Appendix 1.

The new hardware requires new software. Software has been developed for recording and displaying in real time chosen variables measured by the aircraft system. Aircraft data analysis and display software is being developed at Bethlehem. At this stage, there are large differences between the aircraft analysis and display hardware at Bethlehem and Nelspruit. These differences are expected to blur as time passes but it is unlikely that the software will ever become identical, since the aircraft measure different variables with different instruments.

(e) Mesoscale network

The Bethlehem mesoscale network of 50 automatic weather stations has been reduced to 12, which are kept operational for monitoring surface conditions in the project area and for transferring data to Central Forecasting. The reasons for this reduction are :

- the 10 year old Diel data loggers and several of the sensors have reached the stage where spares are no longer available

- the NPRP has defined other priorities and staff transfers had to be made

- the limited use of data from the network no longer warranted the cost of its upkeep.

3.0 RADAR/RAIN GAUGE COMPARISONS OF RAINFALL MEASUREMENTS

(a) Introduction

There is a need to begin to consider the design of an area rainfall augmentation experiment, in anticipation of a successful outcome from the current seeding experiments. It is unlikely that an area rainfall experiment will be conducted over an area of less than 10 000 km^2. The most likely statistical design will be random seeding of the target area using the rainfall day or part of a rainfall day as the evaluation unit, or a design using two areas with highly correlated rainfalls for the experiment, choosing randomly one of the areas for treatment and using the other as a control. In any event, the measurement of rainfall, upon which the evaluation of the experiment will depend, will have to be measured as accurately as possible. There are two accepted methods of measuring rainfall over an area; with recording rain gauges, or using a well-calibrated meteorological radar. The problem with gauges is the number required to adequately measure rainfall over an area of 10^4 km^2. Work in Florida (Woodley et al., 1975) indicates that a gauge density of 143 km^2 per gauge would be required to measure the rainfall over an area of that size, i.e. roughly 70 evenly spaced gauges. The logistics of setting up, servicing and taking readings from a gauge network of this size would be formidable.

The use of radar also presents problems, but of a different sort. It seems necessary to prove that rainfall measured aloft by radar corresponds closely to rainfall measured on the ground. This is the purpose of this study.

Studies over the past 30 years have all shown poor correlations between radar and gauge measurements of precipitation. These correlations also seem to be relatively insensitive to the rain rate (R) to reflectivity (Z) relationships used in the analyses. It should be clear by now that these poor correlations are not going to be solved by a 'better' Z-R relationship. What is required is the following:

- accept the low correlation in comparisons of radar and gauge estimates of rainfall as an inherent characteristic of such comparisons
- try to understand the origins and properties of the variability
- develop approaches for handling the comparisons based upon this understanding (Smith and Cain, 1983).

Hodson (PAWS - Phase 2, 1987-1989 Vol. 3) has thoroughly studied this subject and concludes that agreement between measurements aloft and gauge measurements at the ground is only possible when the area-time integral of the rain is compared aloft and at the ground.

This approach is followed here, in a four-season comparison between radar and rain gauge measurements of rainfall from a 1000 km^2 area west of Ermelo.

(b) Measurements

Fig. 3.0 shows the location of the network and its distance from radar. Fig. 3.1 is a close-up of the 20 gauge network. Each gauge is assumed to adequately sample the rainfall for each area shown and each area is about 50 km^2 for a total network area of 1000 km^2. The gauges have a resolution of 0.25 mm (one tip) and total tips are recorded at 5 minute intervals on solid state recorders mounted inside the gauge housing.

(c) Results

The results of measurements over four seasons are summarized in Table 3.0. The familiar Marshall-Palmer relationship was used to convert the measurement of effective radar reflectivity, Z_e, into rainfall,

where $Z_e = 200\ (R)^{1.6}$
R = rain rate (mm/hr)
Z_e = effective radar reflectivity (mm^6/m^3).

The unit used in the following comparisons is a partial rain day. It started when the radar was turned on and ended when the radar was turned off. The biggest discrepancy between the gauges and the radar occurred on December 1, 1989. Cumulative totals of gauge/radar rainfall amounts up to this day are within 100 ktons of each other (28360 versus 28453). A scan-by-scan analysis of December 1 shows that the discrepancy between the gauge and radar measurements of rainfall was caused by attenuation of the radar beam by storms between the radar and the gauge network. Successive lines of storms on this day moving in from the southwest moved over the gauge network, then between the gauge network and the radar, blocking the radar view over the gauges. For example, Fig. 3.2 (a) shows the low level (1.5^o) scan for 15:31. Fig. 3.2 (b) shows the rain rates recorded by the network between 15:25 and 15:30. Only those equivalent radar reflectivities that are greater than 30 dBz are displayed. Rain rates of 3, 6 and 9 mm/hr correspond to reflectivities of 30.6, 35.5 and 38.3 dBz respectively using the Marshall-Palmer relationship of $Z = 200\ (R)^{1.6}$. While the correspondence between radar echo and rainfall looks reasonable over the northern edge of the network, there is a complete absence of echo over the southwestern part of the network, where rain rates of 5 mm/hr (35.5 dBz) were recorded by the gauges. The radar was not seeing storms that were breaking out over the network behind the squall line.

Cumulative gauge totals are commenced again on December 4, 1989. The cumulative totals are close until December 6, 1990 when another attenuation event takes place. The exercise is repeated

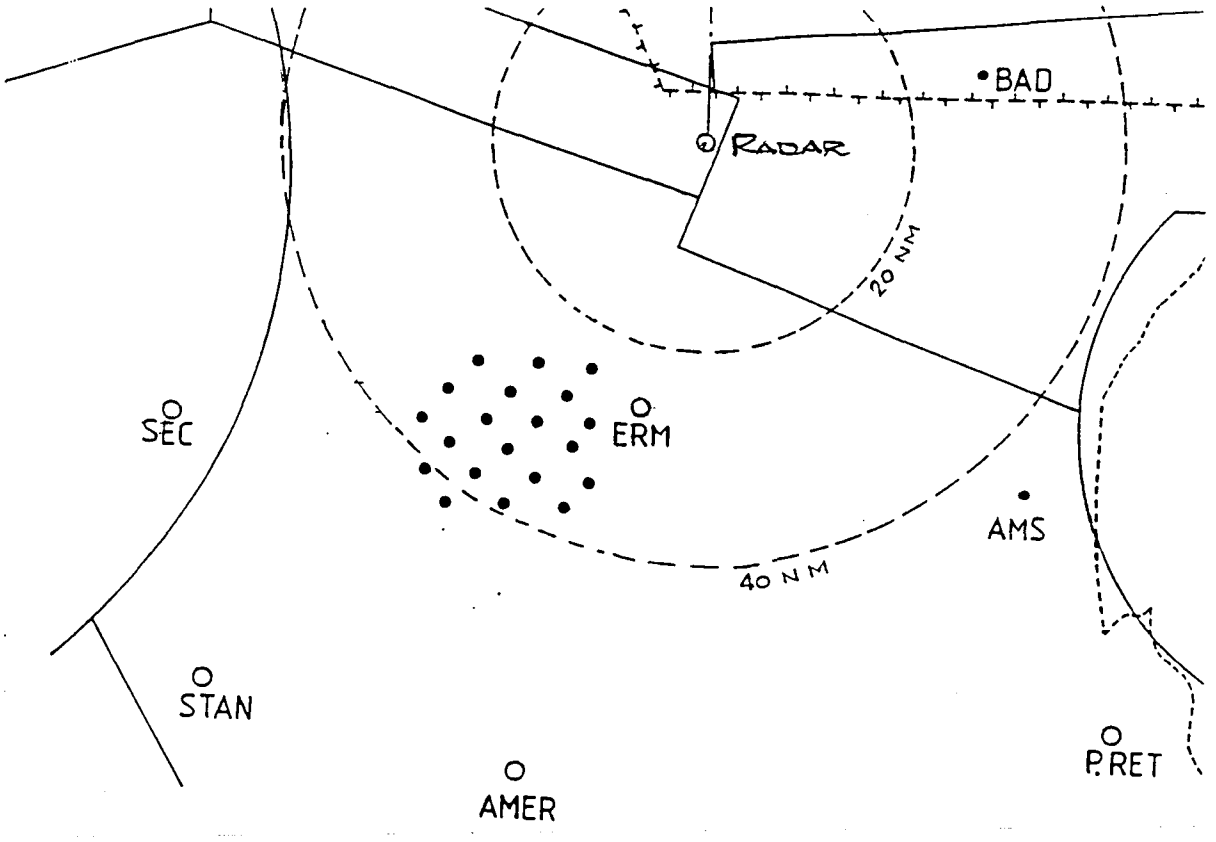

Fig. 3.0 Location of rain gauge network west of Ermelo in relation to the 5 cm radar at Carolina.

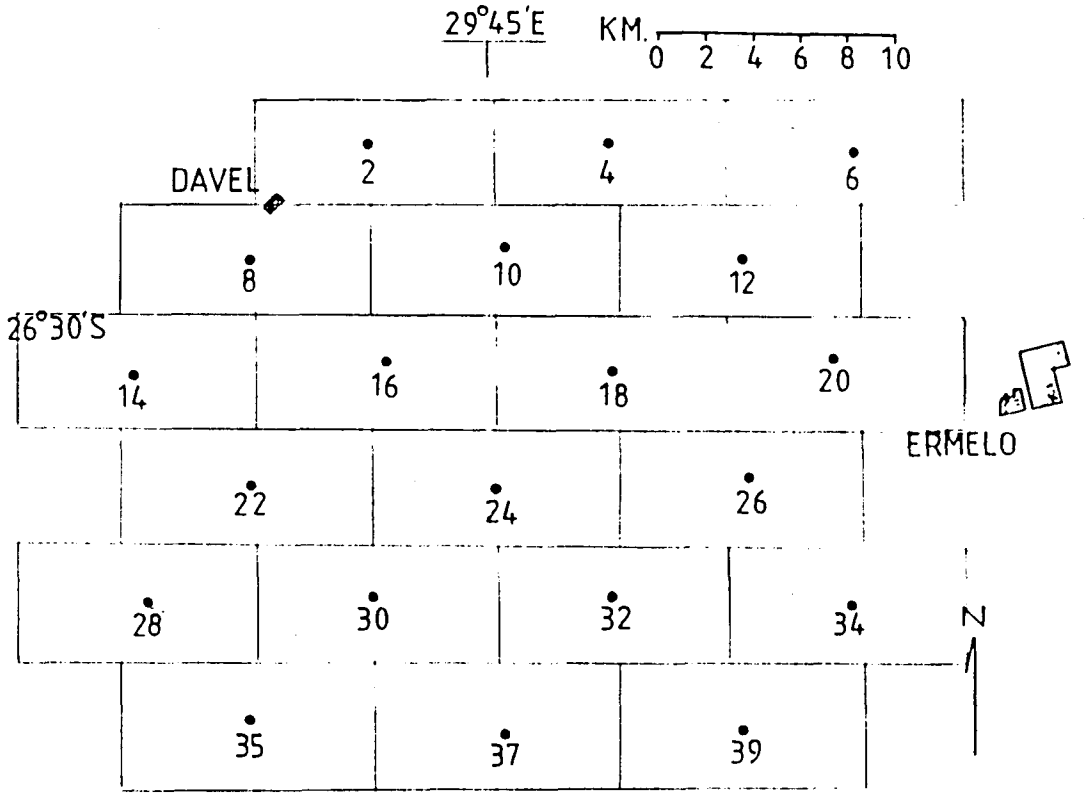

Fig. 3.1 A close up of the network. Each rain gauge is assumed to adequately sample the rain falling in each area shown in the figure.

Table 3.0 Comparison of radar/rain gauge measurements of rainfall.

Date	Time	Gauges (KTONS)	Radar (KTONS)	Cum. Gauges (KTONS)	Cum. Radar (KTONS)	Log G/R
3/11/88	1042/1654	1988	1983	1998	1983	0.001
9/11/88	1314/1730	683	2868	2681	4851	-0.623
26/11/88	1128/1714	1688	2302	4369	7153	-0.135
28/11/88	1038/1554	554	638	4923	7791	-0.061
5/12/88	1101/1519	3303	3796	8226	11587	-0.060
12/12/88	1129/1604	0	2	8226	11589	-
15/12/88	1137/1605	29	1	8255	11590	1.462
20/12/88	1316/1803	0	20	8255	11610	-
21/12/88	1100/1726	384	791	8639	12401	0.314
9/01/89	1223/1851	5221	3641	13850	16042	0.156
10/01/89	1230/1822	15	1	13865	16043	1.176
11/01/89	1158/1608	117	274	13982	16317	-0.369
14/02/89	1051/1449	189	48	14171	16365	0.595
1/03/89	1612/1747	607	492	14778	16857	0.091
2/03/89	0955/1801	24	8	14802	16865	0.477
13/03/89	1252/1559	171	345	14973	17210	-0.305
19/10/89	1204/1542	114	709	15087	17919	-0.794
25/10/89	1304/1638	934	804	16021	18723	0.065
10/11/89	1429/1759	6034	5749	22055	24472	0.021
29/11/89	1338/1520	1016	1140	23071	25612	-0.050
30/11/89	1133/1650	5289	2841	28360	28453	0.270
1/12/89	1051/1620	14768	3584	43128	32037	0.615
4/12/89	1319/1631	145	333	143	333	-0.361
9/01/90	1320/1627	317	0	462	333	-
10/01/90	1434/1641	930	1001	1392	1334	-0.032
20/01/90	1247/1647	23	8	1415	1342	0.459
23/01/90	1153/1521	1235	1454	2650	2796	-0.071
27/01/90	1227/1443	0	4	2650	2800	-
30/10/90	1136/1729	1254	1141	3904	3941	0.041
5/11/90	1408/1539	903	733	4807	4674	0.091
20/11/90	1223/1523	0	362	4807	5036	-
21/11/90	1121/1805	317	457	5124	5493	-0.159
22/11/90	1314/1651	660	587	5784	6080	0.051
5/12/90	1159/1539	456	944	6240	7024	-0.316
6/12/90	1429/1600	4712	1144	10952	8168	0.615
12/12/90	1200/1732	10244	8067	21196	16235	0.104
15/12/90	1118/1414	0	7	21196	16242	-
1/03/91	1448/1646	0	57	21196	16299	-
4/03/91	1217/1545	65	0	21261	16299	-
21/03/91	1142/1555	2804	1384	24065	17683	0.307
5/03/91	1528/1816	498	966	24563	18649	-0.288

Continuation of Table 3.0

Date	Time	Gauges (KTONS)	Radar (KTONS)	Cum. Gauges (KTONS)	Cum. Radar (KTONS)	Log G/R
31/10/91	1224/1555	73	191	73	191	-.418
1/11/91	1116/1545	1077	1434	1150	1625	-.124
11/11/91	1243/1706	52	227	1202	1852	-.640
12/11/91	1037/1617	302	196	1504	2048	.188
13/11/91	1127/1356	399	678	1903	2726	-.230
19/11/91	1304/1643	37	153	1940	2879	-.616
21/11/91	1115/1448	0	120	1940	2999	-
26/11/91	1233/1611	209	635	2149	3634	-.483
28/11/91	1148/1542	15	133	2164	3767	-.949
29/11/91	1129/1634	13	7	2177	3774	.269
2/12/91	1315/1603	922	557	3099	4331	.219
11/12/91	1530/1807	3601	2966	6700	7297	.084
13/12/91	1316/1546	5017	3330	11717	10627	.178
16/12/91	1153/1558	986	481	12703	11108	.312
6/01/92	1103/1611	2373	2150	15076	13258	.043
10/01/92	1248/1801	2224	2622	17300	15880	-.071
14/01/92	1535/1849	1085	1134	18385	17014	-.019
15/01/92	1057/1818	0	4	18385	17018	-
17/01/92	1249/1716	0	2	18385	17020	-
21/01/92	1050/1747	1788	3823	20173	20843	-.330
24/01/92	1251/1559	12	498	20185	21341	-1.618
30/01/92	1340/1824	2820	2370	23005	23711	-.076
3/02/92	1238/1759	3819	3909	26824	27620	-.010
4/02/92	1338/1657	473	238	27297	27858	0.298
13/02/92	1320/1615	0	143	27297	28001	
20/03/92	1254/1559	184	138	27481	28139	.125
23/03/92	1243/1651	106	366	27587	28505	-.538
17/02/92	1236/1532	2123	1294	29710	29799	.215
21/02/92	1203/1527	829	631	30539	30430	.119
2/03/92	1356/1508	4852	1781	35391	32211	.435
18/03/92	1305/1559	602	800	35993	33011	-.123

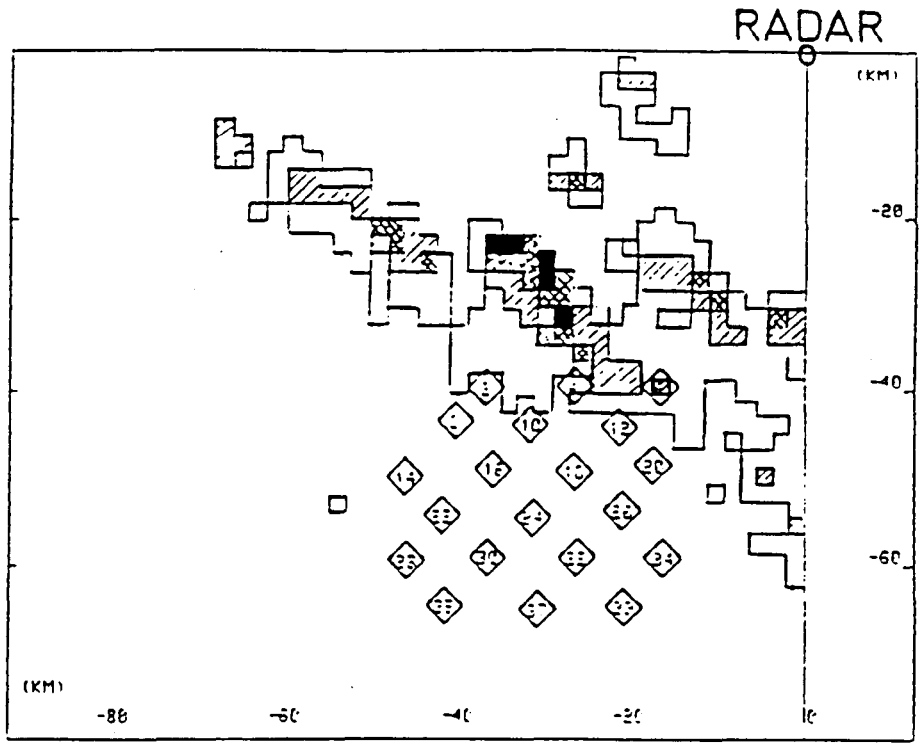

Fig. 3.2 (a). Schematic of radar echo over the rain gauge network at 15:31.

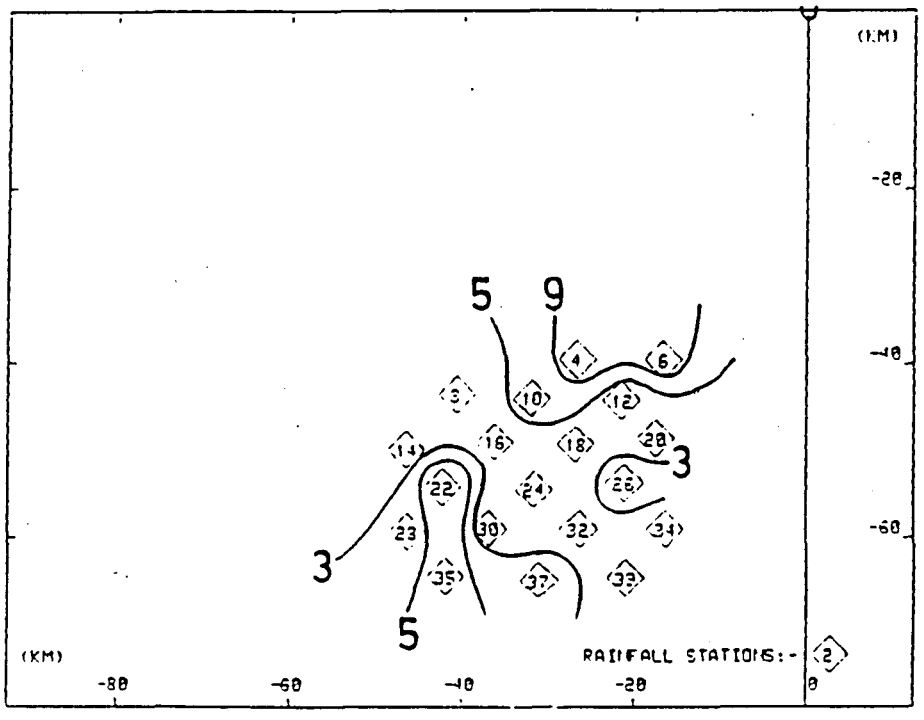

Fig. 3.2 (b). Contours of rain rates measured by the rain gauge between 15:25 and 15:30. Units are in millimeters per hour.

yet again, commencing on October 31, 1991. Here, the comparison between the two measurements is excellent until March 2, 1992 when attenuation again affects the radar measurement of rainfall over the gauge network. Attenuation of the radar beam at 5 cm wavelength is the single biggest source of error between the radar and gauge measurements. This type of error can be eliminated by careful attention to radar patterns, or perhaps an algorithm could be developed for objectively eliminating such events.(The best cure, of course, would be to use a 10 cm radar).

The two measurements of rainfall are compared by analysing the ratios of the log of the gauge rainfalls to the log of the radar measurements (log G/R). Studies have shown that this ratio has a normal distribution (Smith and Caine, 1983), which permits the use of normal distribution statistics. The agreement between gauges and radar can be improved by eliminating the smaller rainfall events. Table 3.1 lists the mean and standard deviations of log G/R for all gauge measurements and those measurements that exceed 100, 250, 500 and 1000 ktons. The 3 attenuation events, underlined in Table 3.0, have been omitted for these comparisons.

There are two features from this table that should be noted:

- for all values of rain events, mean gauge and radar measurements of rainfall are very similar. For instance, for those events over the network that exceed 250 ktons, the two estimates differ by about 2% (antilog of 0.010)

- the standard error of log (G/R) or log G - log R decreases almost exponentially at first, then more gradually as the rain over the network increases. This is not a new result. The Florida work (Woodley et al., 1975) showed that the accuracy of gauge measurement of rainfall is a function of the gauge density and the size of the rain event.

For those gauge measurements that exceed 250 ktons, the standard error of 0.198 corresponds to a factor of difference between the daily gauge/rainfall measurements of $10^{.198}$ which equals 1.58. Another way of stating this is that the radar and gauge measurements differ by less than 58 percent for 66 percent of the comparisons (plus and minus 1 standard error). Most studies show about a factor of difference of about 2 in radar and gauge comparison studies (Wilson, 1970).

Table 3.1 Comparsion of radar/rain gauge rainfall estimates in terms of log G/R for all measurements, those gauge events larger than 100, 250, 500 and 1000 Ktons. The 3 attenuation cases, underlined in Table 3.0, have been omitted for this comparison.

Class	Mean	Standard Error	Cases
All	-0.037	0.456	57
> 100 Ktons	-0.037	0.267	50
> 250 Ktons	0.010	0.198	42
> 500 Ktons	0.018	0.180	35
> 1000 Ktons	0.023	0.146	24

For our purposes, the mean of log G/R is of most importance, since in an area experiment, seeded and control rainfall will be compared whether measured by gauges or radar. Here, after 4 seasons, the gauge and radar measurements for those cases that exceed 250 ktons differ by just 2 percent. This convergence of the two estimates is a result of the long integration period, and indicates that the scatter of the individual (daily) gauge and radar measurements of rainfall are random. Other studies (Woodley et al., 1975) indicate that gauge errors of about 25 percent are likely with a gauge density of one per 50 km^2 for network events that exceed 250 ktons and a radar error of around 25 percent seems reasonable (leaving only 8 percent unaccounted for). We wish to stress here that there is no evidence of systematic errors in these measurements. No amount of "fine tuning" of the Z-R relationship will improve this analysis.

(d) Conclusions

A four season comparison of rain gauge and radar measurements of rainfall in a 1000 km^2 area west of Ermelo has shown that:

- the biggest single source of error is attenuation of the 5 cm wavelength radar beam. This may restrict an area experiment relying on radar measurements of rainfall to isolated storms, eliminating squall lines and fronts from the experiment

- although the daily gauge/radar measurements of rainfall show scatter around a perfect correlation (1 to 1), summing of these events over time leads to almost perfect agreement between the mean radar and gauge measurements of rainfall, provided that attenuation events are avoided and the analysis is restricted to looking at the bigger rain events over the network. Since it appears that radar can measure rainfall over an area within a few percent of gauge readings, radar rainfall measurements, summed over time can be used in an area experiment

- these results show that there were no systematic biases in either measurement and clearly indicate the success of the area-time integral approach to gauge/rainfall comparisons.

Perhaps the best compromise for an area experiment will be to nest a manageable rain gauge network (about 20 gauges) within the experimental area(s). This might satisfy the need for "ground truth" rainfall measurements. Another reason for some sort of a gauge network is the possibility that seeding may change the rain drop spectra at cloud base. Because equivalent radar reflectivities are proportional to the sixth power of drop diameters, it is possible to imagine a redistribution of drop diameters which causes an increase in radar reflectivity without a concomitant increase in rain mass.

4.0 CONTINUATION OF RESEARCH ON DRY ICE SEEDING

4.1 The Pulse Seeding Experiment

The concept of the pulse seeding experiment was to seed a large turret growing on the flank of a multicell storm (convective complex) only once with dry ice, then to try to trace the resulting physical changes (if any) from the time of seeding to the appearance of rainfall at cloud base. Changes were monitored by the seeding aircraft which penetrated the target turret while seeding (pre-seed pass) and attempted to repenetrate the seeded volume some 3 to 6 minutes later (post-seed pass). The target cloud was within range of a ground based radar (at Carolina or Bethlehem) operating in volume scan mode. A second aircraft at cloud base made serial passes through the precipitation falling from the target cloud for a period of 30 minutes after the seeding run. The experiment was randomized so that the significance of any measured changes could be assessed.

The experiment was designed to thoroughly test the seeding hypotheses that had been formulated at Bethlehem and Nelspruit. These hypotheses can be stated as follows:

Two hypotheses were formulated for the Bethlehem area; the so called "static" and "dynamic" modes of cloud seeding. Briefly stated, the first assumes that an injection of a moderate amount of seeding material leads to the formation of earlier and more precipitation. The latter intends to invigorate clouds by altering their water and heat budgets through the injection of large amounts of glaciogenic material (Kraus et al., 1987).

The seeding hypothesis under test at Nelspruit proposed that the early freezing of drops by glaciogenic seeding would speed up the precipitation growth process, since frozen drops would grow faster by rimming than unfrozen drops via collision and coalescence.

The significance of the rainfall measurements at cloud base cannot be overemphasized. Both hypotheses, if correct, should result in a change in rainfall, brought about by an increase in rain drop concentration and/or size, i.e. an increase in <u>rain rate</u>.

The design of the pulse seeding experiment was arrived at after exploratory seeding trials, conducted during the 1989/90 season. The randomized experiment commenced with the 1990/91 season.

(a) Seeding trials

Only once during the 1989/90 trials was the cloud base aircraft successfully manoeuvred beneath a test cloud chosen for a pulse seed experiment. A case study of this experiment follows:

(1) Pulse seeding case study - 12 January 1990.

The atmospheric sounding for 12 January 90 showed some positive buoyancy, 1.2 degrees at 500 mb, and a warm cloud base, 12.8^{o}C, the type of sounding that experience has shown leads to a coalescence and/or a coalescence freezing precipitation formation process.

A relatively small storm, radar cloud tops about 5500 m above sea level, was chosen and seeded at 14:00 SAST. The time history of the penetration indicated that the seeded turret was almost 7 km across. The total cloud water mixing ratio (10.7 g/kg) was close to the cloud base mixing ratio of 12.1 g/kg, indicating an adiabatic (unmixed) cloud core. The seeding time was 39 seconds for a total of 7.8 kg of dry ice (0.2 kg/s seeding rate).

(i) Microphysical measurements

Averages of measurements made on the first (seed) and second (post seed) pass through the cloud selected for an experiment on January 12 are listed in Table 4.0. Pertinent observations from the table are:

- weak updraft, consistent with the weak thermal buoyancy (4)

- King liquid water content decreased slightly between first and second pass (6)

- cloud water mixing ratio decreased (7)

- radar reflectivity increased

- particle concentrations increased but diameters decreased between passes (9 and 11)

- assuming that all 2D images are water, the mass of this water increased (12)

- the cloud was large and almost symmetrical as shown by the lengths of the two almost orthogonal passes (13 and 14).

Table 4.0 Cloud physics measurements from the passes made through the test cloud - 12 January 1990.

Measurement	1st Pass	2nd Pass	Units
1 Time	14:00	14:06	SAST
2 Pressure	469.3	482.2	mb
3 Temperature	-10.9	-9.6	^{o}C
4 Updraft	2.3	2.4	m/s
5 True air speed	164.1	150.8	m/s
6 King LW mix ratio	3.9	3.2	g/kg
7 Engine CW mix ratio	7.1	5.9	g/kg
8 Radar reflectivity	10.8	14.9	dBz
9 2D Total conc.	0.9	5.7	l^{-1}
10 2D > 1068 µm	0.02	0.04	l^{-1}
11 2D MW Mean dia.	1.48	1.05	mm
12 2D liquid water	0.19	0.46	g/kg
13 Pass length	6878	7075	m
14 Heading	081	190	^{o}M

There is no strong evidence that the Lear intercepted the seeded plume in this comparison. While concentrations increased from 0.9 to 5.7 l^{-1}, the mass-weighted mean diameter decreased from 1.48 to 1.05 mm, a result not consistent with the Nelspruit seeding hypothesis, which calls for rapid growth in particle diameters following seeding.

This illustrates one of the problems of post-seed sampling using aircraft. The volume sampled by the aircraft is so small compared to the storm volume that it is unrealistic to expect consistent interception of the seeded volume. This problem becomes more acute when dealing with the larger storm complexes. Tracing microphysical changes much past 10 minutes after seeding cannot be accomplished with any regularity using aircraft sampling at seeding levels. The use of additional aircraft is of little value because of the co-ordination problem in a multicell storm environment.

A total of 13 pulse seed experiments took place from January to mid April 1990. The in-cloud measurements from these experiments (13 first and 13 second passes) were stored in a prototype microphysical data base. Averages of some of these measurements are listed in Table 4.1.

Table 4.1 In-cloud averages of measurements from first (pre-seed) and second (post-seed) passes from 13 exploratory pulse seed experiments. Second pass was 3 to 6 minutes after 1st pass.

Measurement	1st Pass	2nd Pass	Units
1 Pressure	462.4	459.8	mb
2 Temperature	-10.2	-10.2	^{o}C
3 Updraft	3.2	4.1	m/s
4 True Airspeed	143.1	138.7	m/s
5 King LW mix ratio	3.4	2.5	g/kg
6 Engine CW mix ratio	5.5	4.9	g/kg
7 Radar reflectivity	12.5	17.8	dBz
8 2D Total conc	63	206	l^{-1}
9 2D > 1068 μm	0.5	1.3	l^{-1}
10 2D MW mean dia.	0.566	0.745	mm
11 2D LW mix ratio	4.5	14.3	g/kg
12 Cloud dimension	3916	3846	m

Note from this table that, on average:

- updrafts have increased slightly (dynamic effect?) between first and second passes (3)

- liquid water measurements by the King hot wire have decreased (5)

- total cloud water mixing ratios have also decreased but not as much as cloud liquid water (6)

- radar reflectivities have increased by about 5 dBz (7)

- particle concentrations measured by the laser imaging probe have increased (8)

- mass-weighted mean diameters have increased (10)

- assuming a particle density of one (water), precipitation mass in the cloud has increased dramatically (11)

- the average diameter of the clouds selected for this experiment was around 4 km (12).

The cloud physics measurements from this short experiment are promising. Both the Nelspruit and Bethlehem seeding hypotheses require an increase in particle diameters following seeding. On average, this seems to be occurring. Clearly, it is not possible to assess the significance of the trends shown in Table 4.1 without recourse to a randomized experiment.

(ii) Radar measurements

The experiment on 12 January was conducted within about 45 km of the 5 cm radar at Carolina. The radar was placed in a sector scan mode shortly before seeding so that a complete volume scan of the storm was acquired every 3.5 minutes. Three relevant storm track properties are plotted in Fig. 4.0. Some 30 minutes before the cloud was seeded, the radar storm top exceeded 8 km and the rain flux 300 m^3/s. Recall that this storm was seeded at 14:00. Some 26 minutes after seeding, the rain flux again peaked around 300 m^3/sec, but this time, radar storm tops barely exceeded 6 km.

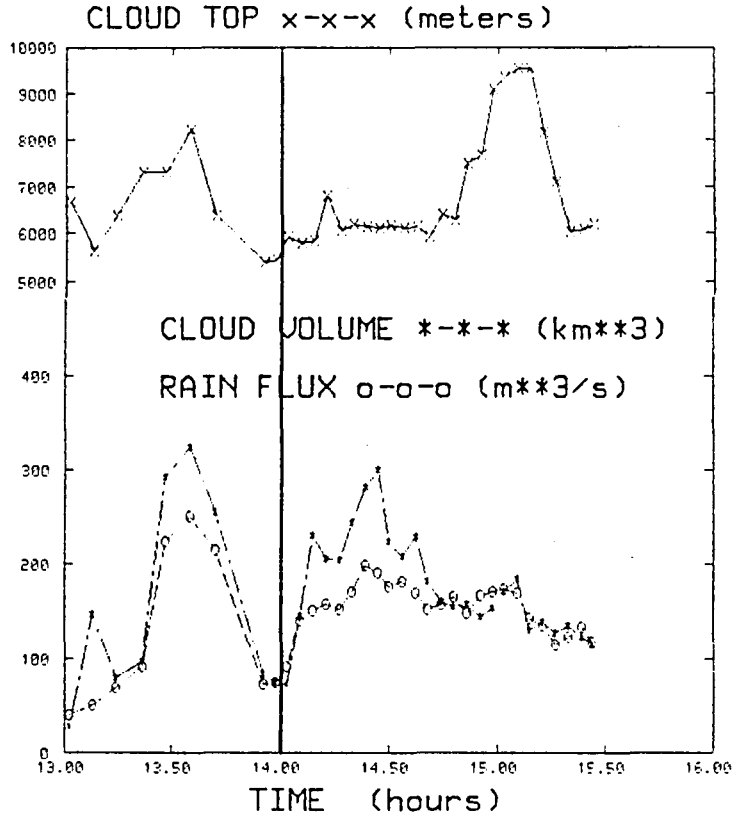

Fig. 4.0. Plot of cloud top height, volume and rain flux versus time measured by radar. This cloud was seeded once at 14:00.

If the additional rain following seeding was caused by the treatment, it was coming from a cloud whose observed top rose only slightly after seeding, indicating a microphysical rather than a dynamical enhancement of the rainfall process.

Another type of analysis that may be useful in a pulse seeding experiment uses time-height plots of peak radar reflectivity. Such a plot is depicted in Fig. 4.1. The positive slope of the peak reflectivity contours after seeding (time = 0) may be indicative of heightened particle trajectories caused by the freezing, then rapid riming, of small drops, a crucial part of the Nelspruit seeding hypothesis.

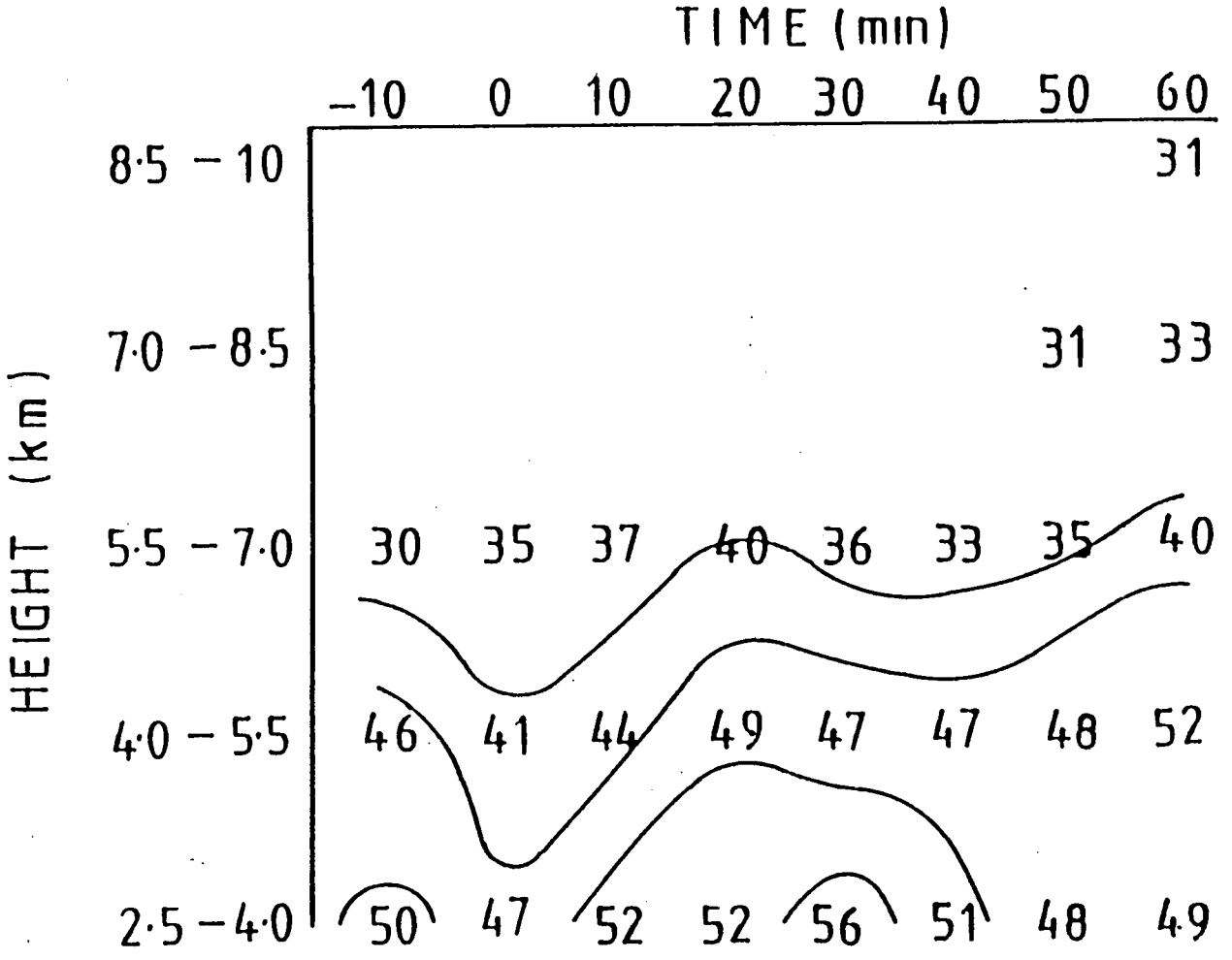

Fig. 4.1. Time-height plots of peak reflectivity of "pulse" seeded storm, 12 January 1990. Contours are fitted by eye.

(iii) Rainfall measurements at cloud base

On January 12, 1990 the cloud base aircraft (ZS-IZN) was positioned underneath a test cloud. Orthogonal penetrations commenced at 14:10 (ten minutes after seeding). Figure 4.2 shows time histories of the rain rates calculated from the 2D-P drop images, corrected for large drop distortion and up and downdrafts. A sudden increase in rain rate appears on the 14:27 panel. Rates increased to more than twice the values recorded before or after this event and persisted for about 1.2 km. A comparison of the aircraft (Table 4.2) and radar measurements (Table 4.3) of rainfall for this event follows.

The storm was located 45 km from the radar. The beam width at this range is 1.3 km wide. The precipitation shaft of interest was about 1.2 km in diameter, assuming symmetry, so there was a beam filling problem that would lead to an underestimation of the radar return. The best radar measurement for detecting such a small scale feature is the maximum reflectivity measured in the scan closest to the event. In fact, the maximum reflectivity jumped almost 4 dB between 14:26 and 14:30. The maximum recorded radar reflectivity at 14:30, 56.4 dBz is within about 2 dB of the average reflectivity calculated from the 2D-P probe measurements through the intense rain shaft (58.3 dBz). However, both measurements fall far short of the calculated rain rates that take into account the downdraft that was associated with the intense shower. The average rain rate calculated for this event, 435 mm/hr, corresponds to an equivalent radar reflectivity of 65.2 dBz, using the Marshall-Palmer reflectivity-rain rate relationship. Clearly, it was the inability of the radar to "see" the downdraft that led to the radar underestimating the rain rate in this study. If the event was caused by the seeding, then this result has implications in terms of using only a radar to evaluate the results of a seeding experiment.

Of additional interest because of its possible bearing on the seeding hypothesis was the approximate doubling of the particle concentrations measured in the precipitation shaft without a noticeable increase in mass-weighted mean diameters.

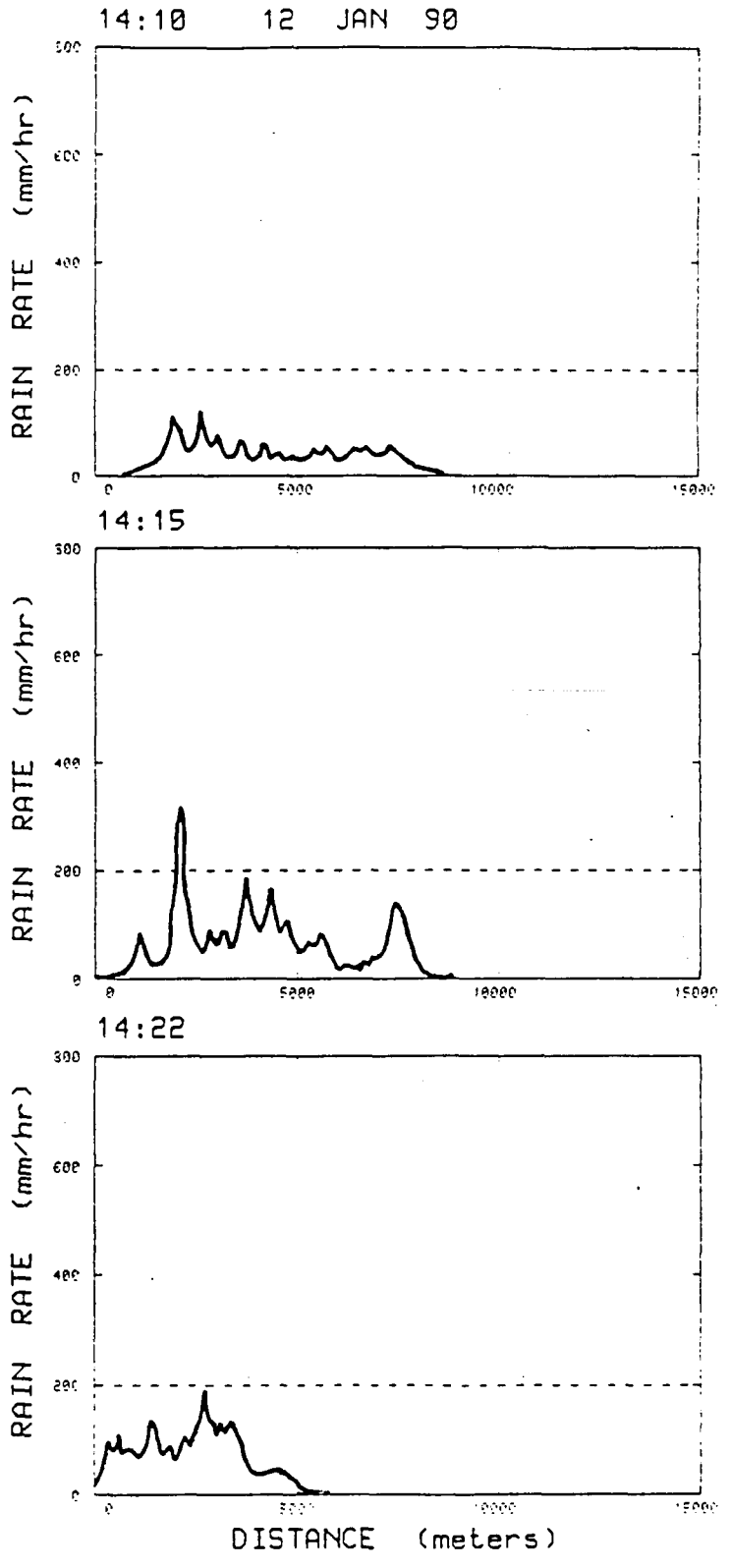

Fig. 4.2 Time histories of rain rates measured with the 2D-P probe on the cloud base aircraft. The cloud was seeded at 14:00.

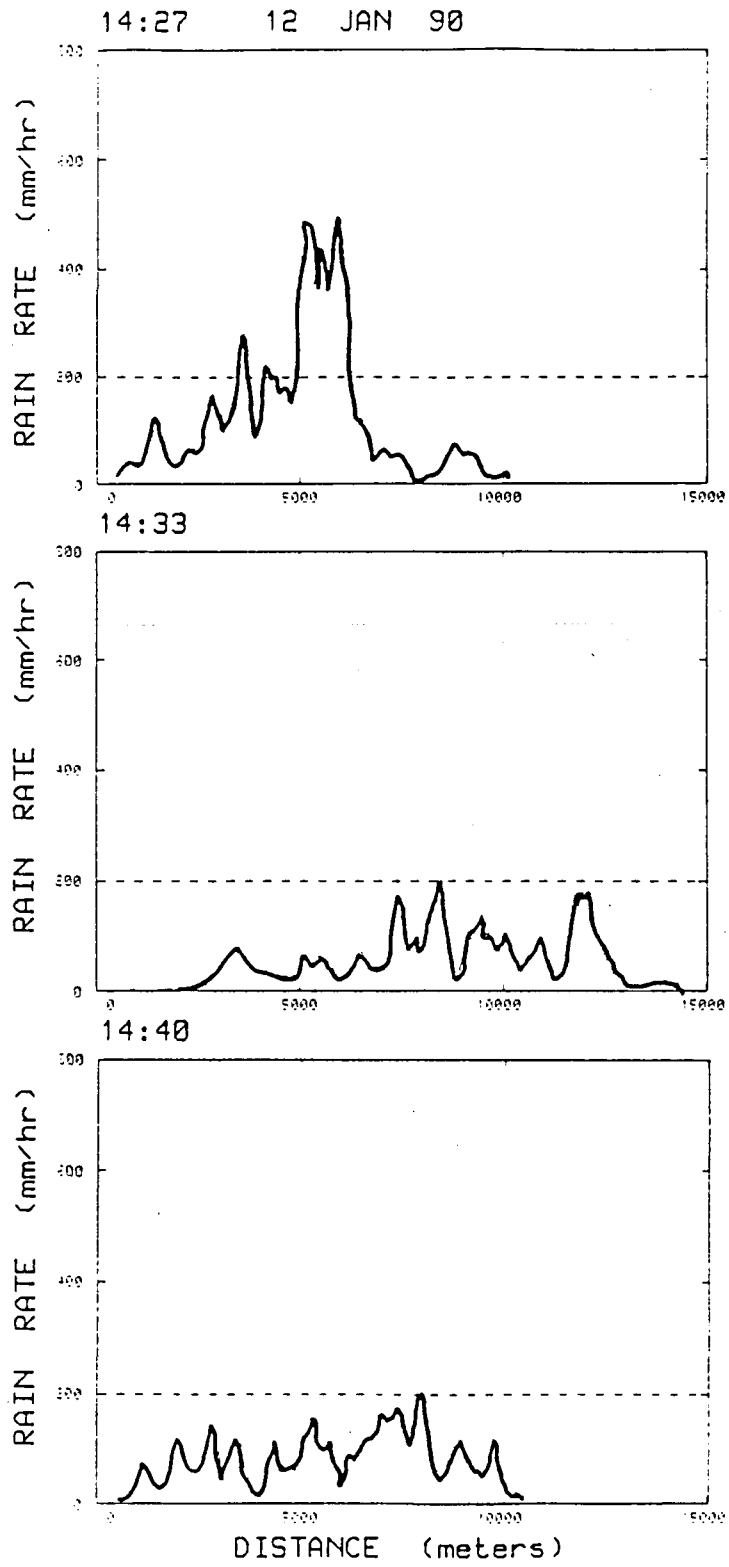

Fig. 4.2 Continued.

Table 4.2 Detailed aircraft measurements through rain shaft, 12 January 1990.

Time	Rain rate (mm/hr)	Reflectivity (dBz)	MWD (mm)	Conc (m^{-3})	Distance (m)	Vertical wind (m/sec)
	140	52.9	2.4	5842		.5
	206	50.6	2.1	4020		- .7
	235	56.9	2.9	4333		-1.8
	85	46.4	1.8	3470		- .7
	197	55.8	2.9	5446		-1.7
	240	56.0	2.9	4997		- .9
	96	50.1	2.2	4413		-1.6
	84	43.3	0.8	4700		-1.4
14:29	254	57.5	3.2	5053	5806	-2.8
	694	61.7	3.4	8533		-4.7
	451	55.2	2.5	6643		-5.1
	581	57.8	2.6	*		-4.1
	101	42.4	1.3	8527		-4.8
	513	64.0	4.5	9327		-4.3
	577	59.2	2.8	*		-5.1
	396	59.7	2.9	8912		-1.9
	103	41.2	1.2	8781		-3.3
	610	58.1	2.8	7545		-4.5
	568	55.0	2.2	*		MSG
	446	52.7	2.0	*		-7.2
	447	57.2	2.7	8521		-7.3
14:29:12	353	56.8	2.7	7181	6977	-5.0
	198	45.5	1.5	8393		-6.2
	107	47.5	2.2	2726		-5.5
	76	42.0	1.5	3675		-6.1
MEAN	435	58.3	2.6			-4.6

Table 4.2 Notes:

1. MWD is the mass-weighted mean diameter
2. * in concentrations column indicates that the drop concentrations have exceeded 10 000 m^{-3}
3. Means are calculated across the precipitation shaft, from 14:29 to 14:29:12.

Table 4.3 Track properties computed from the radar data acquired for the experimental storm - 12 January 1990.

Time (SAST)	Volume (km^3)	1.5^o Area (km^2)	Rain Flux (m^3/s)	R (mm/hr)	Ze max (dBz)
14:02	92	35.2	74	7.6	44.8
14:05	140	56.4	146	9.3	50.3
14:09	151	70.1	231	11.9	51.8
14:12	158	65.7	206	11.3	52.4
14:16	152	60.2	204	12.2	53.9
14:19	171	70.3	245	12.6	52.1
14:23	199	81.0	282	12.5	53.2
14:26	191	91.1	300	11.8	52.9
14:30	177	72.7	225	11.1	56.4

4.2 The randomized pulse seed experiment

The 1989/90 exploratory seeding trials were sufficiently encouraging to lead to the design and execution of a randomized experiment that commenced at the beginning of the 1990/91 season.

The design of the experiment was as follows. Two sets of cards containing randomized seed/no-seed instructions were prepared by UNISA; one set for the Bethlehem area, the other for the Carolina area. The seeding aircraft, in this case the Learjet, held a set of cards for the Carolina and Bethlehem areas. The Learjet crew would select a suitable test case, an isolated multicell convective storm and declare an experiment (decision time). The respective radar operator would open an envelope and instruct the crew to seed or not to seed. The Lear crew would then open the envelope that corresponded to that test case and area (Bethlehem or Carolina). The envelope would contain either a "yes" or "no" instruction. The instructions and actions appear below.

RADAR	LEARJET	ACTION
Seed	No	No-Seed
Seed	Yes	Seed
No-Seed	Yes	No-Seed
No-Seed	No	Seed

The procedure in the event of a seed decision was to penetrate and seed an active turret growing on the flank of a selected target storm. A second sampling penetration would take place 3 to 6 minutes later, if possible orthogonal to the seeding run. For no-seed outcomes, the Lear merely simulated the seeding pass and the subsequent sampling run, keeping clear of all cloud. This procedure kept both the radar operator and the aircraft sampling the rain at cloud base "blind" as to treatment, preventing any biases from creeping into the collection of the radar and rainfall measurements.

The pulse seed missions are summarized in Table 4.4. All of the early experiments took place in the Carolina area because the Bethlehem radar was not fully serviceable until the middle of January, 1991. A total of 31 experiments were conducted. Good radar data were acquired on all experiments except for the first Bethlehem experiment (16 January 1991). Measurements of rainfall at cloud base were not made in a consistent manner and led to an inadvertent bias towards the number of seed cases. Of 10 measurements of rainfall below cloud base, 7 were seed cases and just 3 were no-seed. Since just three no-seed storms were sampled, it may not be possible to judge the significance of these events.

Table 4.4 Summary of Pulse Seed Experiments 1990/91

Carolina Area

Exp No	Cloudbase a/c	Date	D.T.	Treatment
P.S. 1	-	30 Oct 90	13:13	S
2	-	" "	13:30	S
3	IZN	3 Nov	14:55	NS
4	-	21 Nov	16:21	NS
5	-	5 Dec	13:03	NS
6	IZN	" "	13:26	S
7	-	" "	13:50	S
8	IZN	12 Dec	13:02	S
9	-	" "	13:32	S
10	-	" "	13:47	NS
11	IZN	5 Mar 91	16:16	S
12	-	" "	16:35	NS
13	IZN	21 Mar	13:36	S
14	-	21 Mar	14:48	S
15	-	31 Oct	13:14	NS
16	-	31 Oct	13:47	NS
17	-	11 Nov	13:38	S
18	-	11 Nov	14:06	NS
19	-	11 Nov	14:26	S
20	JRA	12 Nov	12:43	S
21	JRA	13 Nov	12:48	S
22	JRA	13 Nov	13:26	NS
23	IZN	19 Nov	15:08	NS

Bethlehem Area

1	JRA	16 Jan 91	14:11	S
2	-	23 Jan	15:18	NS
3	2D-Probe U/S	7 Feb	13:12	S
4	-	14 Feb	12:14	S
5	-	14 Feb	13:05	NS
6	-	" "	16:30	NS
7	-	15 Feb	13:11	NS
8	-	8 Mar	12:10	S

(a) Gushers or unusual rainfall events

A "gusher" is defined as an unusually heavy rain rate, usually associated with a downdraft, encountered at cloud base by either of the instrumented aircraft (IZN, JRA). The first such event was recorded in the seeding trials on 12 Jan 1990.

Table 4.5 summarizes the gusher events to date. Recall that all these clouds were seeded once and once only with dry ice. The gusher events occur between 15 and 27 minutes after decision time, i.e. in the time range in which the effects of seeding at cloud top might be expected to appear at cloud base.

The most impressive event occurred on December 5, 1990. Fig. 4.3 shows the computed rain rates (unsmoothed) captured by the 2D-P probe. The downdraft that was associated with this event is shown in the same figure.

It is again instructive to compare the cloud base aircraft and radar measurements. Table 4.6 lists some of the pertinent radar measurements collected during this experiment, with the radar in sector/volume scan mode. Rain flux divided by storm area (column 5) is a measure of average storm rain rate. Note that this radar-measured variable does peak at 13:51 (the scan closest to the aircraft pass at 13:52), but the relative magnitude of the increase is small compared to the aircraft measurements. However, a peak reflectivity of 62 dBz corresponds to a rain rate of 273 mm/hr (using $Z = 200\ (R)^{1.6}$) which would be a pretty good average for the gusher depicted in Fig. 4.3.

Listed in column 6 is another ratio; rain flux divided by storm volume. This can be viewed as a measure of rainfall "efficiency", i.e. the rain flux per unit storm volume. This ratio also peaks at 13:51.

The rain rates measured by the instrumented aircraft are summarized in Fig. 4.4, for the 7 seed and 3 no-seed cases. Four out of the 7 seeded cases show rain rates that exceed 100 mm/hr some 15 to 26 minutes after decision time (t=0). None of the no-seed cases exceeds this threshold.

In summary, unusual rainfall events have been recorded by instrumented aircraft beneath seeded storms. These events are characterised by sudden increases in rain rate, often associated with a strong downdraft. It is too early to state that these events are unique to seeded storms, but if further measurements prove this to be true, this is the sort of "strong" seeding signature that experimenters search for.

Since the radar does not "see" downdrafts, radar measurements underestimate the rain rates associated with these events, a result that should be considered when designing rain augmentation experiments.

Table 4.5 Summary of Gusher Statistics

Date	D.T.	Time	Conc (m^{-3})	MWD (mm)	R (mm/hr)
12/1/90	14:00	14:10	443	2.69	18
		14:15	873	2.33	25
	(:27)	14:22	1150	2.19	23
		14:27	1851	2.84	61
		14:33	767	2.34	22
		14:40	1437	2.40	42
5/12/90	13:26	13:38	1687	0.82	42
		13:45	1351	0.76	30
	(:26)	13:52	12202	3.05	128
12/12/90	13:02	13:06	1420	4.41	53
	(:16)	13:18	1489	4.33	74
		13:24	680	3.27	28
		13:33	937	2.84	28
		13:36	800	3.64	32
		13:41	1280	3.79	51
16/1/91	14:10	14:14	512	1.72	9
		14:17	1625	1.74	18
		14:20	1054	1.73	14
	(:19)	14:25	1528	2.00	26
		14:29	3609	1.91	81
		14:35	2071	1.94	37
		14:40	2812	1.86	49
21/3/91	13:36	13:36	1255	1.02	42
		13:43	2150	1.85	58
	(:15)	13:51	4521	2.20	99
		13:58	1080	1.36	17
		14:05	1667	1.93	23
		14:13	1928	1.76	20
		14:21	1066	0.77	22

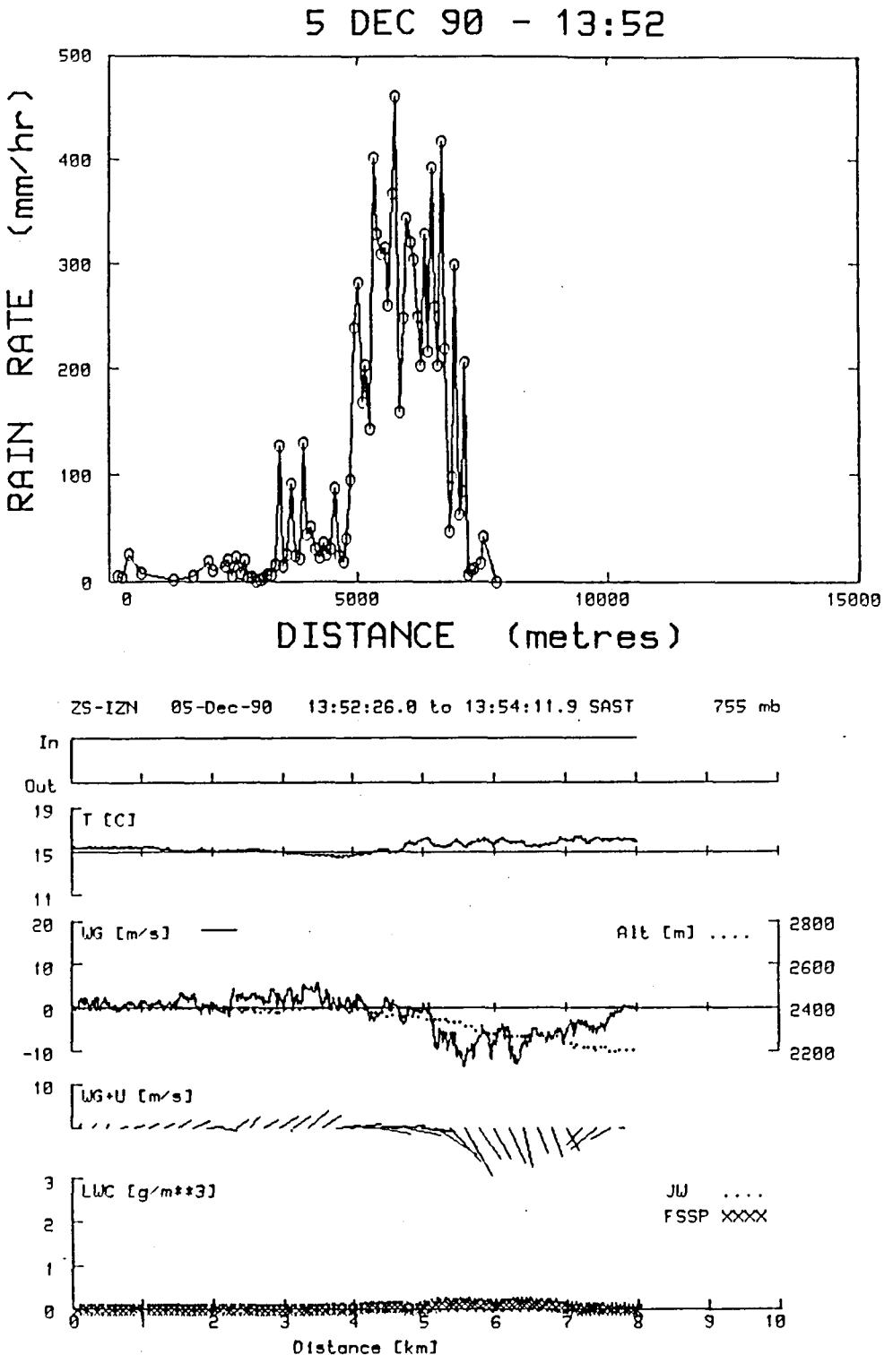

Fig. 4.3 Measurements of rain rates by the cloud base aircraft (IZN) on December 5, 1990. Note the downdraft measured by the aircraft in the lower portion of the figure.

Table 4.6 Radar data - 5 December 1990
Decision time - 13:26

Scan time	Storm Area (km^2)	Rain Flux (m^3/s)	Peak Ze (dBz)	Flux / Area	Flux / Vol
13:25	107	395	57	3.70	0.9
13:29	98	442	53	4.53	1.1
13:32	112	517	55	4.60	1.2
13:36	117	501	55	4.27	1.1
13:40	121	585	56	4.83	1.2
13:44	120	467	60	3.89	1.0
13:47	135	598	59	4.41	1.3
13:51	123	645	62	5.25	1.5
13:55	108	486	57	4.49	1.3
13:59	94	304	52	3.24	0.8

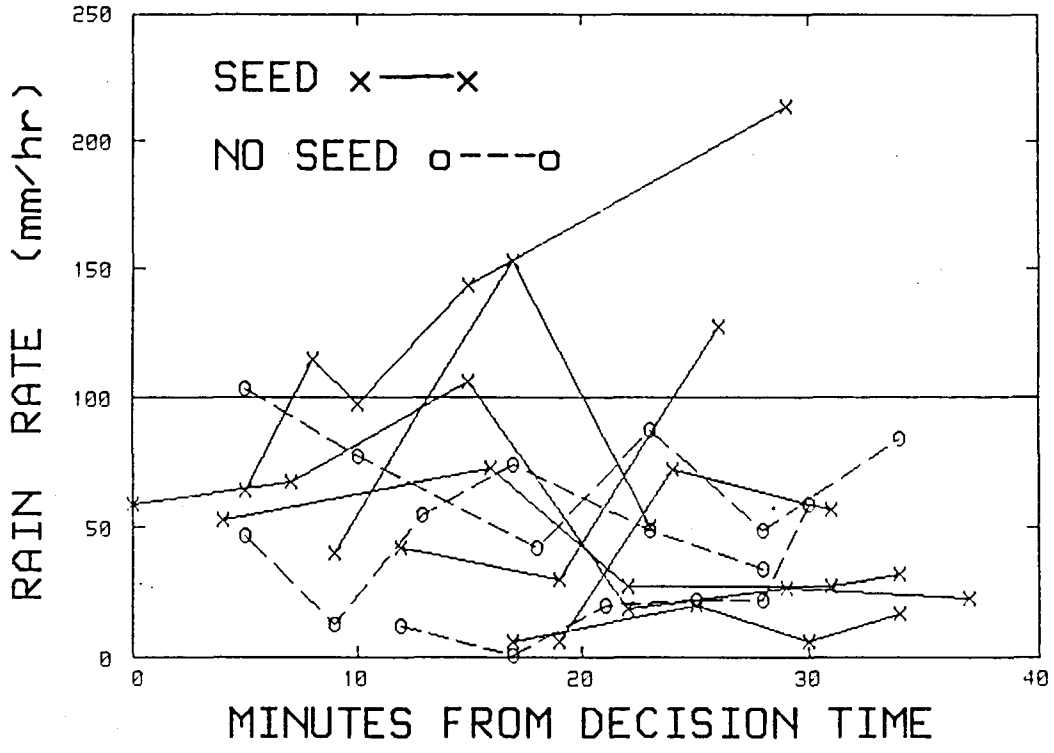

Fig. 4.4 Time histories of average rain rates measured at cloud base in the randomized pulse seed experiment - 7 seed and 3 no-seed cases.

(b) Statistical results

Of the 31 pulse seeding experiments, radar data were not available for one of the cases (16 Jan 91) and two failed to fall within the range limitations (10 - 90 km radius from the radars). Past experience has shown that 28 cases is not sufficient for the type of analysis used here - an examination and comparison of storm track characteristics in 10 minute time windows from decision time. The analysis is presented here for two reasons. First, it is unlikely that the pulse seed experiment will continue, since the results from the seeding experiments using the hygroscopic flares are showing more promise than the dry ice seeding experiments. Second, the analysis shows what can go wrong with an experiment having too few cases. In our experience, the statistics acquire stability (admittedly a subjective judgement) when case numbers reach about 50.

The results of the statistical analyses, using a re-randomization or a permutation analysis are listed in Table 4.7 and show an apparent decrease in rainfall 20 to 30 minutes after decision time. Listed in Table 4.8 are the individual rain masses from each experiment calculated over 10 minute time intervals from decision time (t = 0). Track 10, a no-seed case, increases its rain mass 16 times by the third time interval, completely dominating the analysis. This track merged with a large storm mass shortly after decision time. If this track is deleted from the analysis and arithmetic means computed (including zeros) both seed and no-seed cases show about a 10 percent decrease in rain mass 20 to 30 minutes after decision time. The only other feature of note in this analysis is that more of the no-seed cases dissipate than in the seeded case.

(c) Aircraft microphysical measurements

The Lear samples the characteristics of the treated cloud on the seeding pass and then penetrates the same cloud some 3 to 6 minutes later. In this experiment, no-seed cases are not sampled, because of the concern that aircraft-produced ice particles (APIPS) may affect the unseeded clouds. Thus Table 4.9 is a summary of microphysical measurements from the Lear database for the seeded cases from the 1990/91 experimental season and, for purposes of comparison, the results from the previous season's exploratory seeding trials.

The microphysical implications of these observed gushers are important. Under what thermodynamic conditions do they occur? Does the time between treatment and appearance of the gusher at cloud base have any significance?

Table 4.5 suggests that the increases in rain rates are caused by increases in both drop concentrations and diameters. This observation impacts upon the formulation of a seeding hypothesis. For instance, if the dry ice seeding is freezing drops that are already present which now proceed to grow faster as graupel, how does one explain the increase in concentrations? Is it possible that some of the drops that are frozen would have been collected via coalescence in an untreated cloud? These and other matters must be settled with further observations. The pulse-seeding experiment appears to have taken us a lot closer to one of our goals - a seeding hypothesis validated through observations.

Table 4.7 Results of statistical analysis of the pulse seed experiment

	MINUTES		
	0 - 10	10 - 20	20 - 30
GEOM. MEAN OF:	Seed/No-Seed	S/NS	S/NS
Volume (km^3)	258/186	244/327	214/547
Area (km^2)	53/41	60/76	54/119
Rain Mass (ktons)	97/56	94/107	83/253
1.5°			
Rain flux (m^3/s)	172/97	177/226	141/422
Rain mass (ktons)	62/35	38/62	35/154
6 km			
Rain flux (m^3/sec)	103/61	72/131	58/258

% DIFFERENCE (SEED - NO-SEED/NO-SEED) x 100

	%	%	%
Volume (km^3)	39	- 25	- 61
Area (km^2)	29	- 21	- 54
Rain mass (ktons)	75	- 12	- 67
1.5°			
Rain flux (m^3/s)	77	- 22	- 67
Rain mass (ktons)	75	- 38	- 77
6 km			
Rain flux (m^3/s)	68	- 45	- 77

Table 4.8 Rain Masses (ktons) @ 1.5°

Track No.	0 - 10	10 - 20	20 - 30
	SEED CASES (N = 15)		
26	264	350	272
43	37	53	49
201	285	315	346
35	182	76	86
114	208	92	36
229	80	93	88
28	24	18	0
183	42	80	22
6	26	20	5
5	203	44	0
45	207	197	392
48	330	363	273
99	300	254	368
244	391	545	380
150	2	8	6
ARITH MEAN	172	167	155
	NO-SEED CASES (N = 13)		
10	59	296	952
205	573	467	549
133	143	128	171
217	18	0	0
72	2	0	0
243	1	0	0
27	8	1	0
226	157	23	0
1	354	357	259
32	289	269	274
68	180	217	273
83	129	190	140
41	57	58	69
ARITH MEAN	159	142	144

Table 4.9 Microphysical measurements - Pulse Seeding Experiment

	1989/90		1990/91		
Measurement	1st Pass	2nd Pass	1st Pass	2nd Pass	Units
Pass length	3916	3846	3085	3110	m
Pressure	462	460	455	451	mb
Temperature	-10.2	-10.2	-10.8	-11.0	^{o}C
Updraft	3.2	4.1	4.3	11.3	m/s
True air speed	143	139	143	141	m/s
Radar reflectivity	12.5	17.8	15	19	dBz
King LW mix ratio	3.4	2.5	2.2	1.6	g/kg
La CW mix ratio	2.1	2.3	5.7	5.3	g/kg
E.T. CW mix ratio	5.5	4.9	4.9	5.0	g/kg
2D LW mix ratio	4.5	14.3	1.9	3.4	g/kg
2D Total conc	63	206	16	85	l^{-1}
2D > 1068 μm	0.5	1.3	.2	0.3	l^{-1}
2D MWD	566	745	718	818	μm
Temp @ CCL	12.8		10.9		^{o}C
ΔT_{500}	3.8		4.3		^{o}C

Notes from Table 4.9

- updraft increases between pass 1 and 2 in both seasons; possible dynamic reaction from the release of the latent heat of freezing

- radar reflectivity increases about 4-5 dB between pass 1 and 2, both seasons; an increase in particle size and/or number

- King LW decreases between pass 1 and 2, both seasons; depletion of cloud liquid water by growing hydrometeors

- La and E.T. cloud water (CW) contents stay roughly the same between passes in both seasons; no decrease in cloud water contents, which is the sum of supercooled cloud water and precipitation particles. (La values are low; there were problems with this instrument during the 1989/90 season).

- 2D calculated liquid water contents (precipitation) increase; expectations are for increases after seeding

- 2D concentrations go the right way, showing large average increases by the second pass after seeding

- large particles (> 1 mm) show an increase in concentrations in the first season, but on average, remain constant in the second; expectations are for increases

- mass-weighted mean diameters (MWD) increase from passes 1 to 2;

Generally, the statistics are showing increases in the expected variables in the expected directions. What plagues all measurements of this sort is the inescapable sample volume limitations of all aircraft microphysical measurements; the clouds are so big and the aircraft is so small.

(d) Summary

The pulse seed experiment, designed to validate the Bethlehem and Nelspruit dry ice seeding hypotheses, was not conclusive. Intriguing observations of gushers, or sudden increases in rain rates at cloud base were observed in some of the seeded cases. Because of the inability to obtain reliable measurements of rainfall at cloud base using instrumented aircraft, the significance of this observation cannot be assessed. We were warned that a single dry ice seeding run would not produce a sufficient signal to be detected by radar in the noisy convective storm environment. This appears to be the case, as the radar analysis of the 15 seed and 13 no-seed cases does not detect a seeding effect.

The statistical analysis was useful in the sense that an apparent negative result was shown to be the result of a single case which completely dominated the routine analysis, a circumstance encountered all to often in convective cloud experiments.

This experiment, while constructive, was not carried through to a conclusion. Hopefully, the reasons for the early termination of the experiment are adequately expounded in the historical review that introduces this report.

5.0 NEW HYGROSCOPIC SEEDING FLARES

(a) Introduction

In an attempt to mimic the effects of the Kraft paper mill on storms, an experimental hygroscopic flare was designed and subsequently manufactured by Swartklip Products in Cape Town. Initially a batch of 25 flares was ordered, each flare about the size of a beer can, containing 500g of the seeding mixture (see Fig. 5.0).

The flare racks originally used for silver iodide end-burning flares on the Commander JRB were modified to accept 4 of the new hygroscopic flares on each rack (for a total of 8). Since both flares were fired electrically, the original firing mechanism was used.

Tests performed on the combustion products of the new flares were carried out by Dr. Mark van der Riet at the engineering laboratory at ESKOM. These tests determined the chemical composition of combustion products and provided some information on particle sizes (spectra). Further static tests were conducted at Nelspruit. An FSSP-100 probe was positioned behind JRB and a flare was lit while the engine was running. Airborne tests at Bethlehem cast doubts on the spectra obtained from the ground runs. Additional ground runs were performed collecting particles in the plume on sticky glass slides. Particles of over 100 μm in diameter were collected on these tests, supporting the airborne measurements. The particles collected on the glass slides were analysed at the University of the Witwatersrand, using a scanning electron microscope and an X-ray diffractometer.

Fig. 5.0 The two sizes of hygroscopic seeding flares manufactured in Cape Town by Swartklip Products (Pty) Limited.

The first test of these new flares on a relatively small convective storm produced spectacular results. Observational systems used in this test (October 9, 1990) were the Learjet and the 5 cm radar at Carolina in sector scan mode. This test is described in detail in a later section. This and a second test were sufficiently encouraging to warrant the placing of an order for additional flares. The second version of the flare was twice as long, containing around 1 kg of the seeding mixture. A total of 200 of the longer version was ordered.

Further seeding tests with the longer flares, both at Nelspruit and at Bethlehem were very encouraging. On most tests, a solid radar and/or microphysical signature was detected shortly after seeding commenced, and the signals were commensurate with the seeding hypothesis which states that the coalescence rainfall formation process can be enhanced by the introduction of hygroscopic materials into the storm updraft at cloud base. This clearly represents a breakthrough in weather modification. Based upon a solid knowledge of the microphysics of the local precipitation mechanisms, a seeding device, designed to increase the efficiency of the precipitation process by encouraging (accelerating) coalescence, has been manufactured and subsequent tests have indicated that the new device achieves the desired effect.

(b) Analyses of combustion products

(1) ESKOM tests

A flare was supplied to ESKOM for an investigation into the combustion residue (chemical composition and particle size distribution). The composition of the flare, according to the manufacturer was:

- 65% potassium perchlorate ($KClO_4$)
- 10% sodium chloride (NaCl)
- 2% lithium carbonate ($Li_2 CO_3$)
- 5% Magnesium (Mg)
- 18% hydrocarbon binder

The mixture was combusted in 3 ways. The method closest to actual flight conditions was the use of a wind tunnel. The residues from the wind tunnel tests were analysed by a scanning electron microscope. The chemical composition is similar to the one deduced by Hindeman (1978).

	Hindeman (%)	Eskom (%)
Sodium chloride (NaCl)	19	21
Potassium chloride (KCl)	65	67
Lithium Carbonate (Li_2CO_3)	1	-
Magnesium oxide (MgO)	15	12

It is of interest to note that no trace of lithium was detected in any of the measurements.

The particle size measurements were probably not representative. Following combustion in the wind tunnel, the residue was collected on a filter paper and some agglomeration occurred. Undoubtably, agglomeration also occurred during the cooling phase, before the particles struck the filter face. Ultrasonic vibration was used to attempt to disperse the impacted agglomerates and leave the "fused" agglomerates intact. Unfortunately no experimental technique can disperse one type of agglomerate to the total exclusion of the other.

(2) Nelspruit and Bethlehem ground and airborne tests

The FSSP probe on the wing of IZN was placed about 2 m behind the flare rack mounted on the rear end of JRB's engine nacelle. JRB's engine was started and, when a suitable RPM had been reached, the flare was ignited. Airflow past the FSSP was measured using a pitot tube that was connected to IZN's pitot-static system. Knowing the speed of the flow past the FSSP ($\sim$37 m/s), the approximate diameter of the plume ($\sim$ 30 cm) and the length of the burn (220 s), particle concentrations measured by the FSSP (120 cm^{-3}) could be used to estimate the total number of particles produced by the flare. This estimate produced a total particle production of around 10^{11}, or about 10^{8} particles per gram of flare mix.

The largest particle sensed by the FSSP was 13 μm in diameter. This result was somewhat contradicted by airborne tests conducted at low level early in the morning in calm conditions and relative humidities exceeding 80%. The first Commander (JRB) was trailed by the second Commander (JRA) equipped with an FSSP-100 probe and a 2D cloud probe. Two flares were ignited, and JRA trailing JRB by about 30 to 40 m, made measurements in the plume. Unexpectedly, the 2D probe recorded images of what appeared to be drops with diameters between 80 and 300 μm in concentrations of about 8 l^{-1} (Fig 5.1).

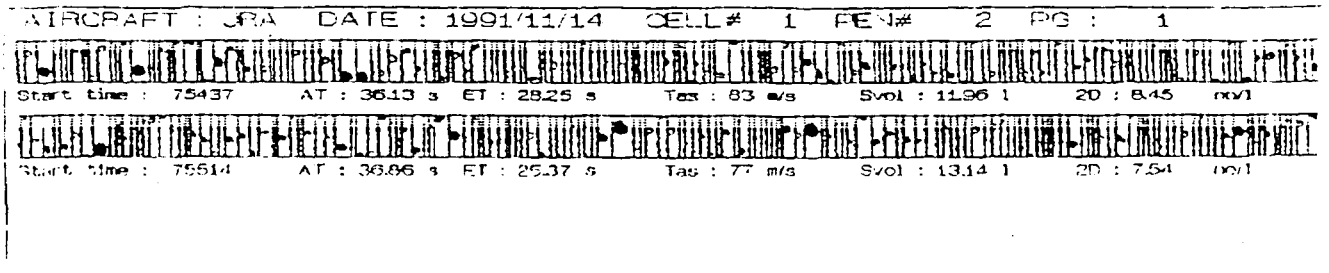

Fig. 5.1 2D images recorded by an aircraft flying in the plume from 2 flares burning on the seeding aircraft. Vertical time bars are 800 microns long.

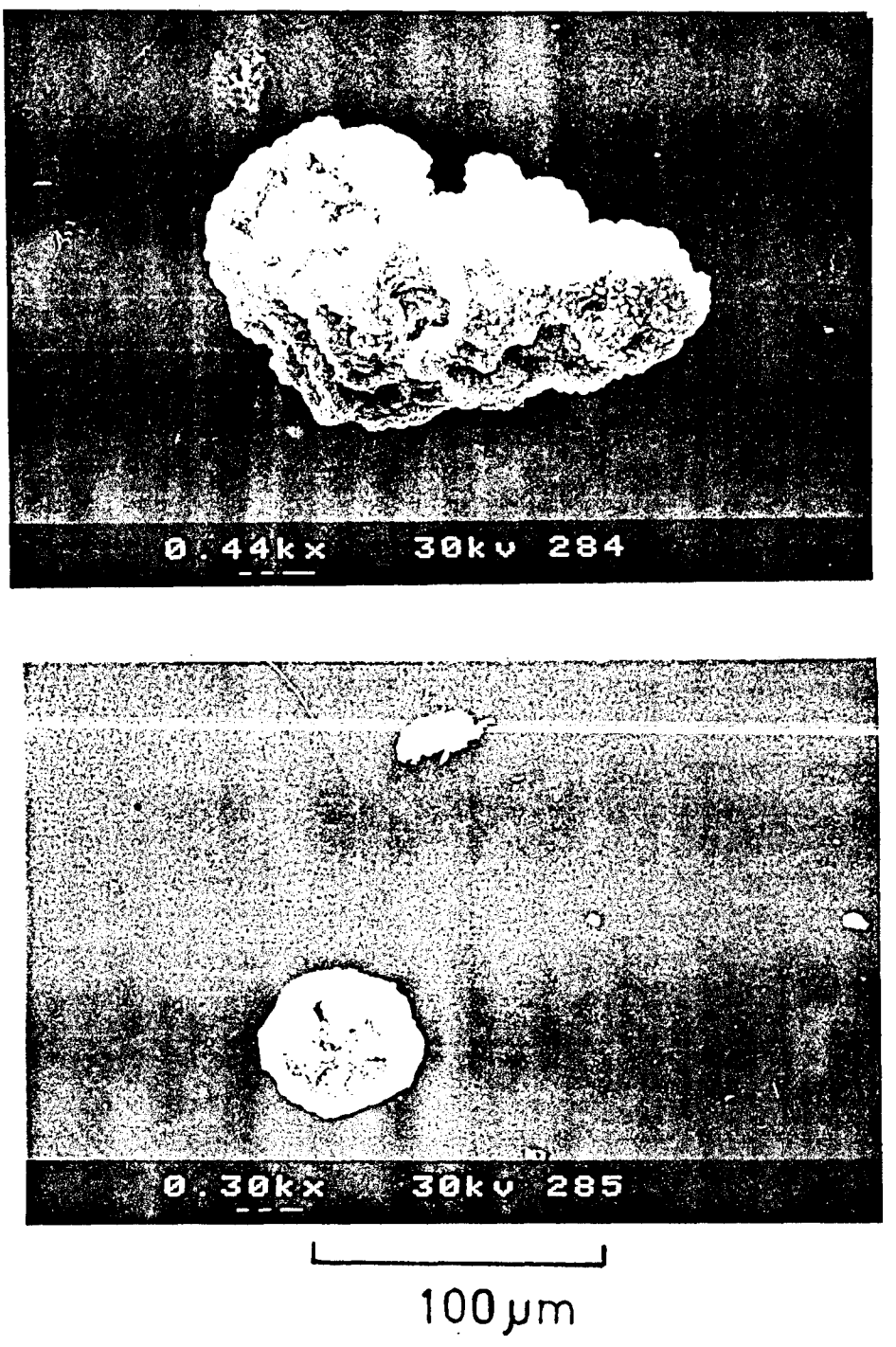

Fig. 5.2 Electron microscope photographs of large particles collected on sticky slides held in the plume of a flare burning on the seeding aircraft on the ground, engine running.

A second ground run was conducted in which sticky glass slides were used to collect particles in the plume of a burning flare. The slides were examined by Mrs. Pat Sterling at the University of the Witwatersrand, using a scanning electron microscope and X-ray diffraction. These tests identified the elements potassium and chlorine in some of the particles whose diameters exceed 100 µm (see Fig 5.2), confirming the presence of large particles in the plume that were detected in the airborne tests. The small sample volume of the FSSP 100 may explain why this probe missed the larger particles.

The ground and airborne tests are compared in Fig. 5.3, and agree within an order of magnitude. Differences between the measurements can be attributed to:

- underestimation of the concentrations in the airborne tests, since it was not possible to keep probes in the plume from the flares at all times

- the deliquescence of the larger hygroscopic particles causing the "knee" in the airborne spectrum.

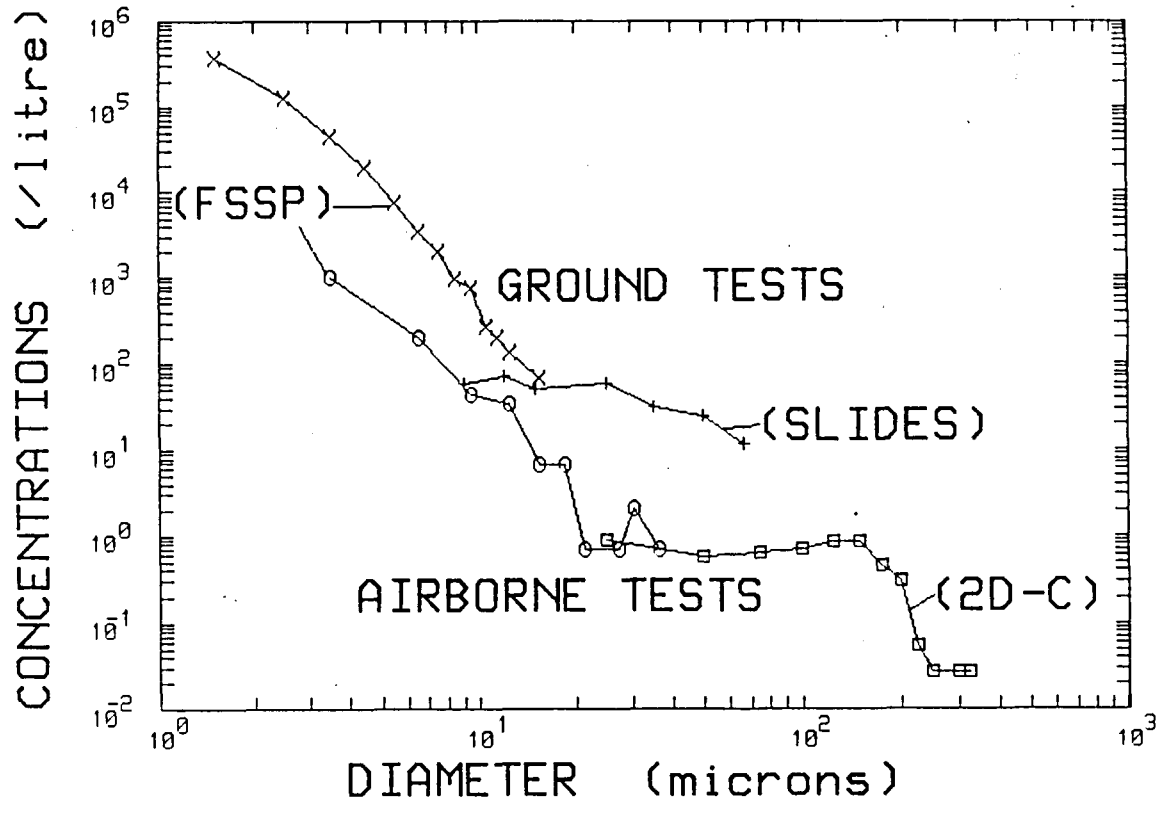

Fig. 5.3 Measured dry particle combustion spectra from ground and airborne tests of hygroscopic flares. See text for details.

(c) Cloud seeding tests

The first trial on clouds took place on October 9, 1990. Observational systems used were the Learjet and the 5 cm radar in volume scan mode. The flares, mounted on the Aero Commander, were ignited at cloud base under a small isolated storm at 15:56. The Learjet had commenced sampling cloud turrets rising on the northwestern flank of this storm at 15:54. Updraft speed was measured at 8.2 m/s. The second pass was at 15:58, and an updraft speed of 9.4 m/s was measured. The Learjet first encountered the seeded plume at 16:02, some six minutes after seeding commenced. This is clearly shown in Table 5.0 and illustrated in Fig. 5.4. The Commander was seeding at about 3000 m and the Lear was sampling at 5900 m, an altitude difference of 2900 m. To reach the altitude of the Lear in the available 6 minutes, the seeding material would have to travel vertically at a speed of 8 m/s which is close to the observed updraft speeds.

There is a dramatic difference in FSSP measurements between pass 2 and 3, most pronounced in the 1 km averages around the updraft maxima. The number of drops with diameters greater than 32 um increases almost seven times from 0.55 to 3.68 cm^{-3}. Note that the mean particle diameter decreases but the mass-weighted mean diameter increases (Table 5.0). Fig. 5.4 portrays time histories of FSSP concentrations and updraft profiles for passes 2 to 4. The tick marks on the X axes are 1 km apart. The spectra show the size distributions of water mass up to the probe size limit of 47 μm. The second spectrum in each group (2) is the 1 km average around the updraft maximum. It is this spectrum that changes radically from pass 2 to pass 3. The updraft peak coincides with the peak in concentrations >32 μm confirming that the updraft is carrying the seeding material. By 16:06, the material appears to be pretty well spread throughout the cloud. The mass density spectra around the liquid water and updraft maxima look similar. Concentrations have almost doubled (Table 5.0) and computed liquid water contents peak on this pass. By 16:10, values have fallen back to pre-treatment levels.

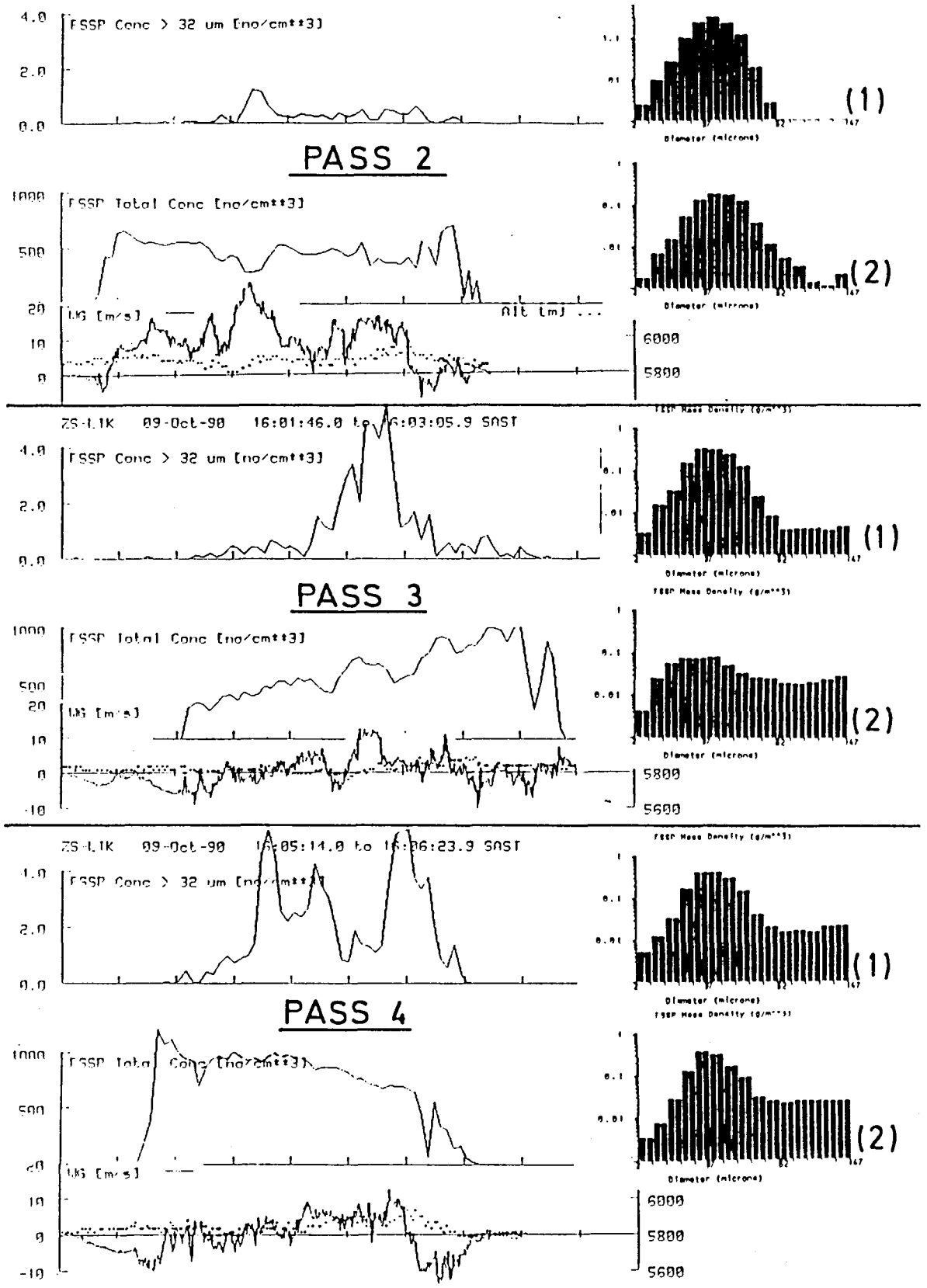

Fig. 5.4 Time histories of FSSP concentrations, FSSP concentrations of droplets >32 μm and vertical velocities measured on 3 passes through a cloud seeded with hygroscopic flares, October 9, 1990. The spectra show how the mass of water is distributed between 2 and 47 μm and is measured over a distance of 1 km around the maximum concentrations (1) and the maximum updrafts (2).

Table 5.0 Comparisons of 1 km averages of FSSP measurements around the maximum liquid water content and the maximum updraft speed.

		Pass:	1	2	3	4	5
		Time:	15:54	15:58	16:02	16:06	16:10
1 km averages around max. FSSP	conc (cm^{-3})		470	589	808	965	595
	conc >32 μm (cm^{-3})		0.20	.02	0.70	3.00	1.13
	LWC (g/m^3)		0.92	1.00	1.26	1.63	1.00
	mean dia. (μm)		13.20	12.30	11.90	12.00	12.30
	MW mean dia.(μm)		19.10	18.40	18.40	19.50	18.70
1 km averages around max updraft	conc (cm^{-3})		413	393	649	703	391
	conc >32 μm(cm^{-3})		0.39	0.55	3.68	3.77	0.57
	LWC (g/m^3)		0.76	0.77	0.57	1.22	0.58
	mean dia. (μm)		12.70	12.60	8.50	12.20	11.60
	MW mean dia. (μm)		19.00	19.90	21.80	19.90	18.20

Aircraft tracks and returns from the target storm were recorded by the project's 5 cm radar, operating in volume scan mode. Objective storm tracking software is used to process the raw radar data. Thus storms are described or characterized in terms of their track properties. Time-height plots of peak equivalent reflectivities appear to be one of the most revealing ways of presenting storm time histories. This technique is used here and portrayed in Fig. 5.5. The trajectory of the seeding material, released at time = 0, arcing up into the cloud to produce a maximum aloft (46 dBz at t+10), the downward cascade of the growing precipitation particles reaching cloud base at t+20 (51 dBz); these can easily be visualized when presented in this manner.

We believe that this seeding event has been well documented; from the release of the material at cloud base to the first interception of the plume by the Learjet to the formation of a reflectivity maximum aloft to rainfall, at least at cloud base. These observations are completely consistent with a seeding-induced acceleration of the coalescence process leading to the early development of large precipitation particles (recall the spreading of the FSSP spectra) in a cloud that might otherwise not have rained at all.

The exploratory seeding trials that were conducted during the 1990/91 season are listed in Table 5.1. Data from the Bethlehem radar was not retrievable until after 16 January 1991. "No data" under aircraft response refers to instrument failure.

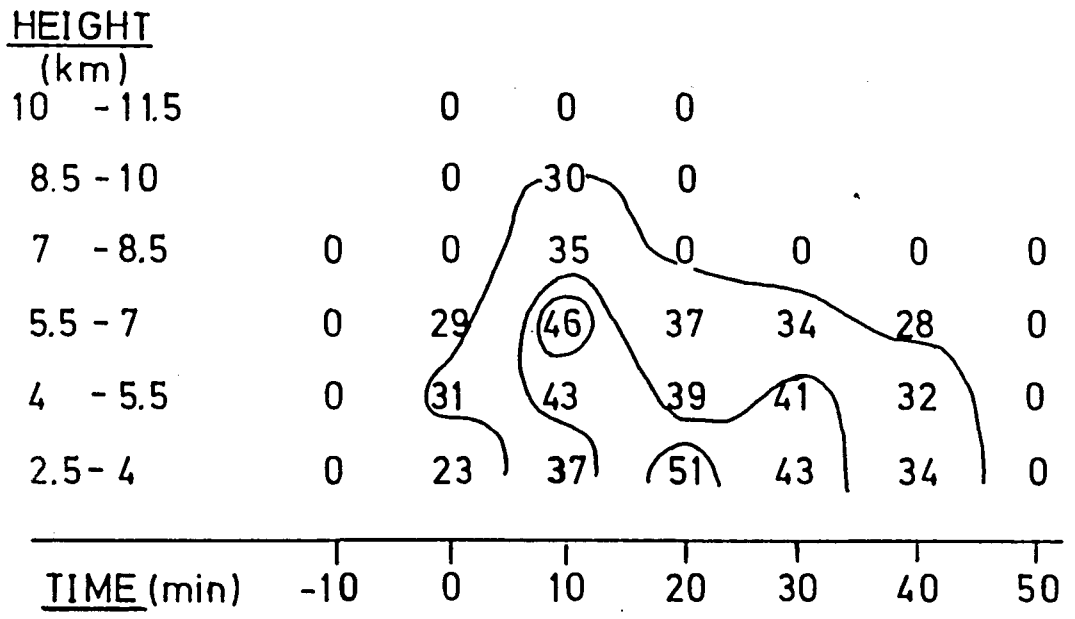

Fig. 5.5 Height-time profile of peak reflectivities measured in a small storm treated with hygroscopic flares on October 9, 1990. The numbers in this figure are in dBz. Contours were drawn by hand.

On December 13, a storm was seeded at cloud base with 7 flares. This storm located just west of the Braam Raubenheimer dam, produced 80 mm of rain in less than an hour, but no hail, despite the fact that the 45 dBz contours exceeded 9000 m (Mather et al., 1976). The time-height profile of this storm is presented in Fig. 5.6. Note the behaviour of the maximum reflectivity profile between about 14:50 and 15:07. Treatment of this storm commenced at 14:20.

Table 5.1 Summary of Flare Tests

Date	Exp	Fired	Radar response	Cloud response
9 Oct	F1	2(S)	Yes *	Yes *
13 Oct	F2	5(S)	Yes	No
20 Nov	F3	2	No, small storm	No
21 Nov	F5	4	Yes *	No
28 Nov	F6(B)	1	No radar	No
13 Dec	F7	6	Yes *	No
15 Dec	F8	4	Yes	Possible
	F9	1	No, small storm	No
4 Jan	F10	4	No data	No data
	F11	4	No data	No data
5 Jan	F12	8	Yes	Yes *
16 Jan	F13(B)	4	No data	Yes *
	F14(B)	2	No data	No data
14 Feb	F15(B)	3	No	No
	F16(B)	2	No	No
	F17(B)	8	No	Yes *
15 Feb	F18	6	No	Yes *
1 Mar	F19	7	Yes *	No
4 Mar	F20	4	Yes	Yes *
	F21	4	No	No
8 Mar	F22(B)	4	Yes	Yes *
	F23(B)	4	Yes	Yes *

NOTES:

1. (S) refers to short flare.
2. (B) experiments conducted at Bethlehem.
3. * further analyses in text and tables.

Two examples of storm track alterations that may have been caused by the seeding are presented next. A storm was seeded east of Carolina on a day when winds at storm steering levels were light. Fig. 5.7 shows all the storm tracks recorded by the Carolina radar on that day. Only one storm exhibits any significant movement (the circled storm). Fig. 5.8 is a blowup of the storm track and the storm time-height profile. Seeding commenced at 15:23 and the last two flares were ignited at 15:38. The first significant jump of the storm position westward occurred between 15:33 and 15:40, some 10 to 15 minutes after seeding commenced. The storm stopped its westward propagation between 16:15 and 16:22, about 30 minutes after the last flare was extinguished. Note the now familiar arc in the time-height plot of maximum reflectivity in Fig. 5.8. Assuming that this traces the seeding effect, the altered precipitation should be reaching the ground some 20 minutes after seeding commences, which coincides closely with commencement of the storm's westward

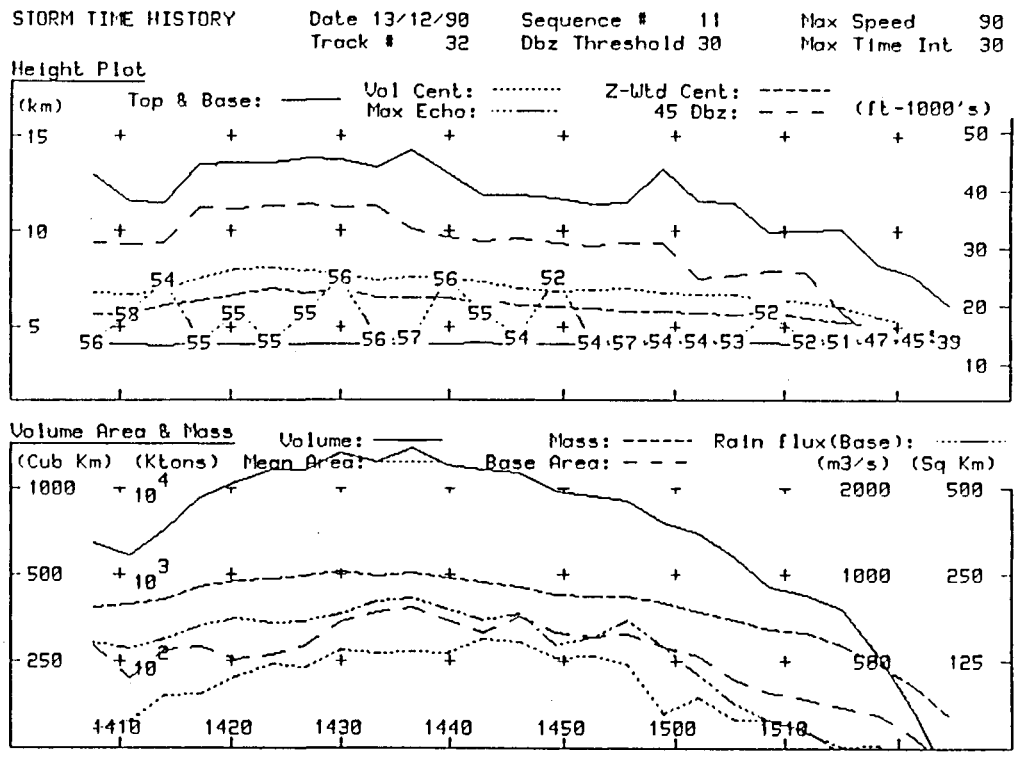

Fig. 5.6 Storm seeded with hygroscopic flares at 14:20 on December 13, 1991. Note the height of the 45 dBz contour (exceeds 10 km). There were no traces of hail from this storm.

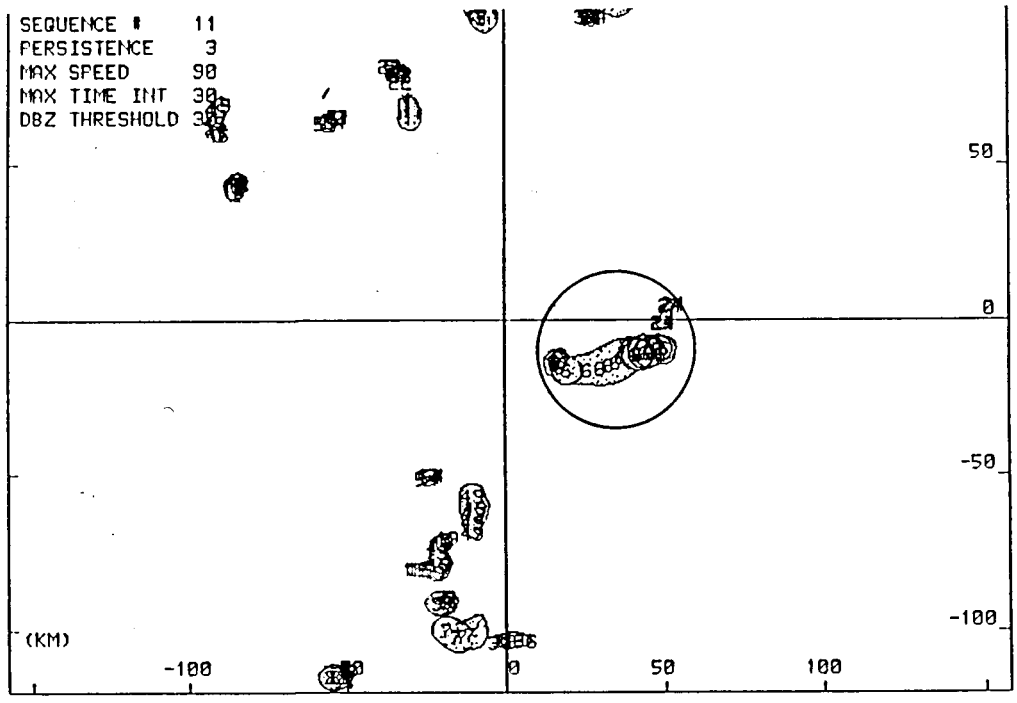

Fig. 5.7 Map of storms tracked on March 1, 1991 within a 120 km radius of the Carolina radar. Note lack of movement except for the storm directly ESE of the radar.

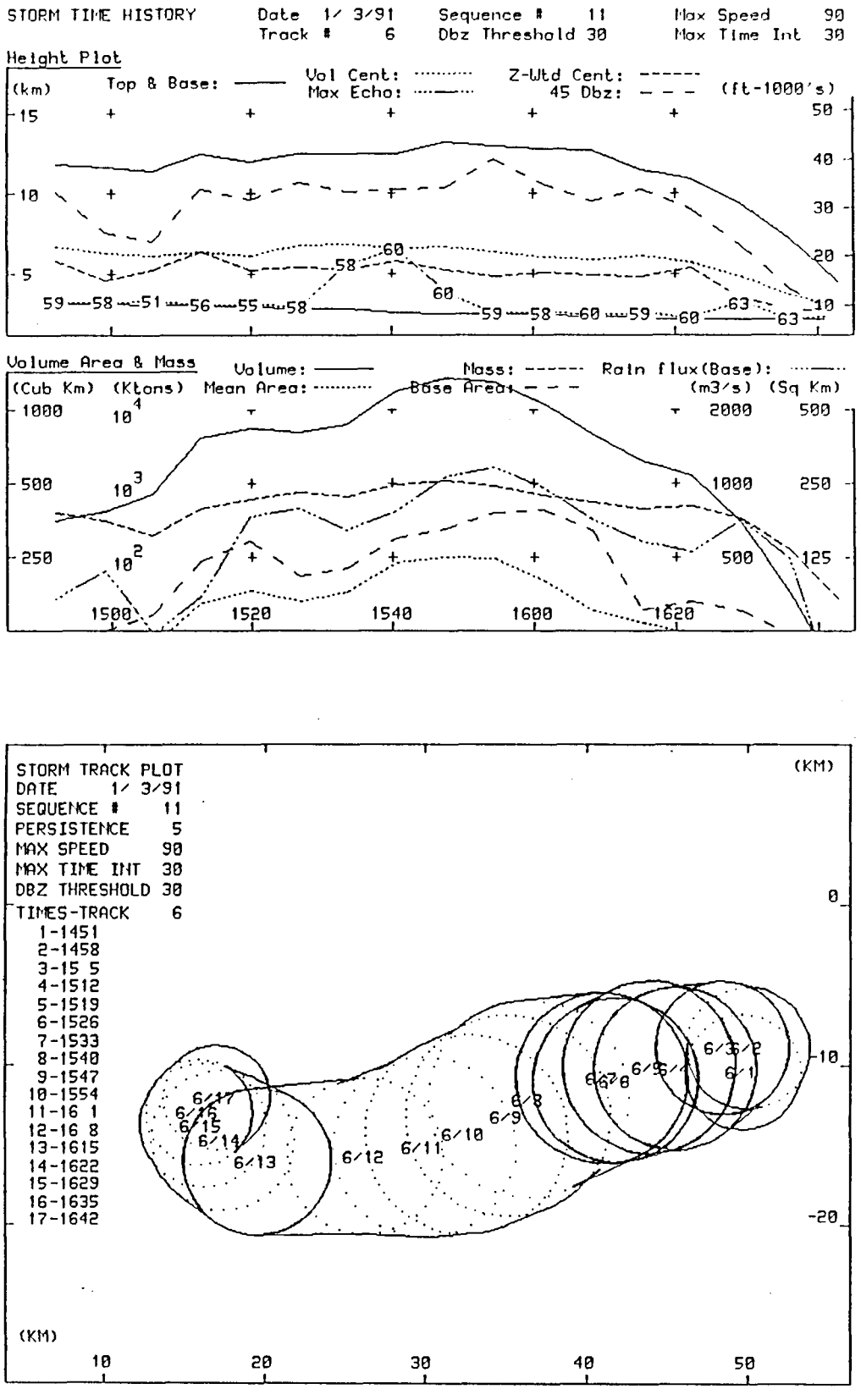

Fig. 5.8 Track and height-time profile of storm seeded on March 1, 1991. Note trajectory of max reflectivity between 15:20 and 16:00 (top).

propagation.

A flare seeding mission in Bethlehem on March 8, 1991 produced curious results. Two adjacent storms were seeded and both exhibited a " dog leg" in their plotted storm tracks which coincided with the seeding. Fig. 5.9 is a plot of storm tracks acquired by the Bethlehem radar on that day. Most of the storms are tracking smoothly to the southeast, except for two tracks, track 46 and 90 which exhibit a sudden lurch westward before continuing their southeast bound tracks. This "lurch" occurs shortly after seeding commences on both tracks. Fig. 5.10 shows the seeding track of JRB and the two apparently altered storm tracks. Fig. 5.11 shows the time-height profiles of both storms. The familiar maximum reflectivity signature is evident in the profile of storm track 90 after seeding commences. Track 46 appears to reflect the commencement of seeding in an upward pulse in the height of the 45 dBz contour (around 13:20).

In summary then, from the exploratory seeding conducted to date, the radar seeding signature appears to be:

- a parabolic trajectory described by the time-height plots of the maximum reflectivities. The trajectory reaches its peak height about 10 minutes after seeding commences

- possible changes in storm tracks, especially notable in light storm steering wind conditions.

The last observation is most intriguing. Microphysical changes of sufficient magnitude to affect the rainfall are likely to have dynamic consequences. Intuitively any significant changes in storm dynamics are most likely to show up as changes in storm track behaviour.

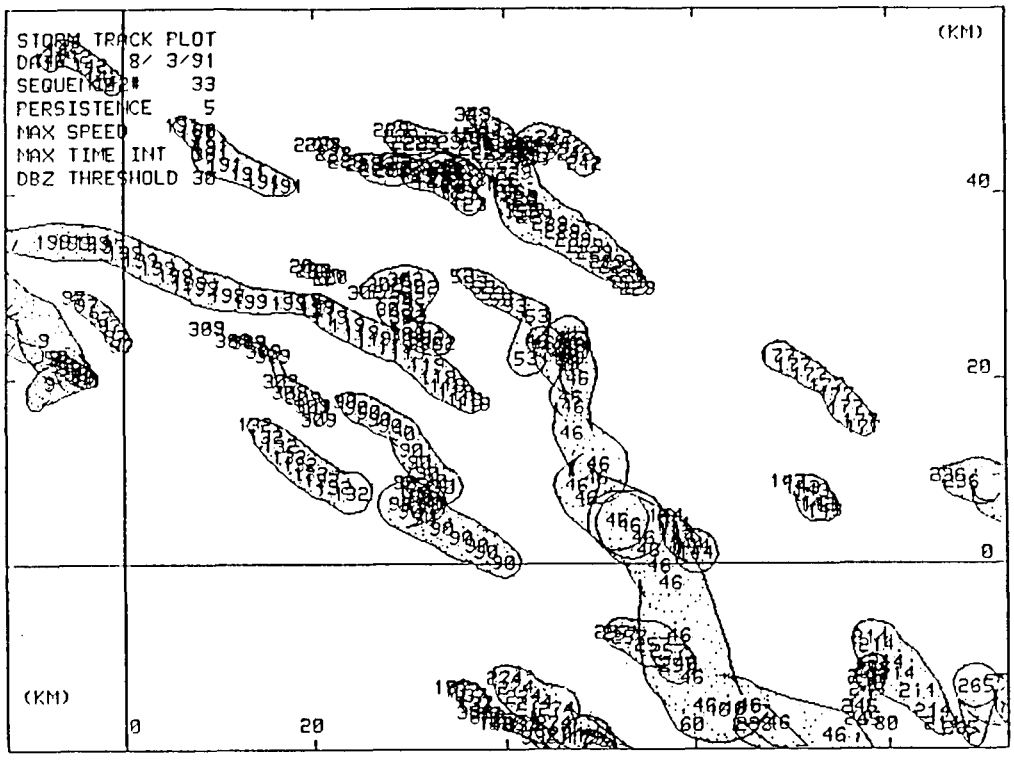

Fig. 5.9 Storms tracked by the Bethlehem radar on March 8, 1991.

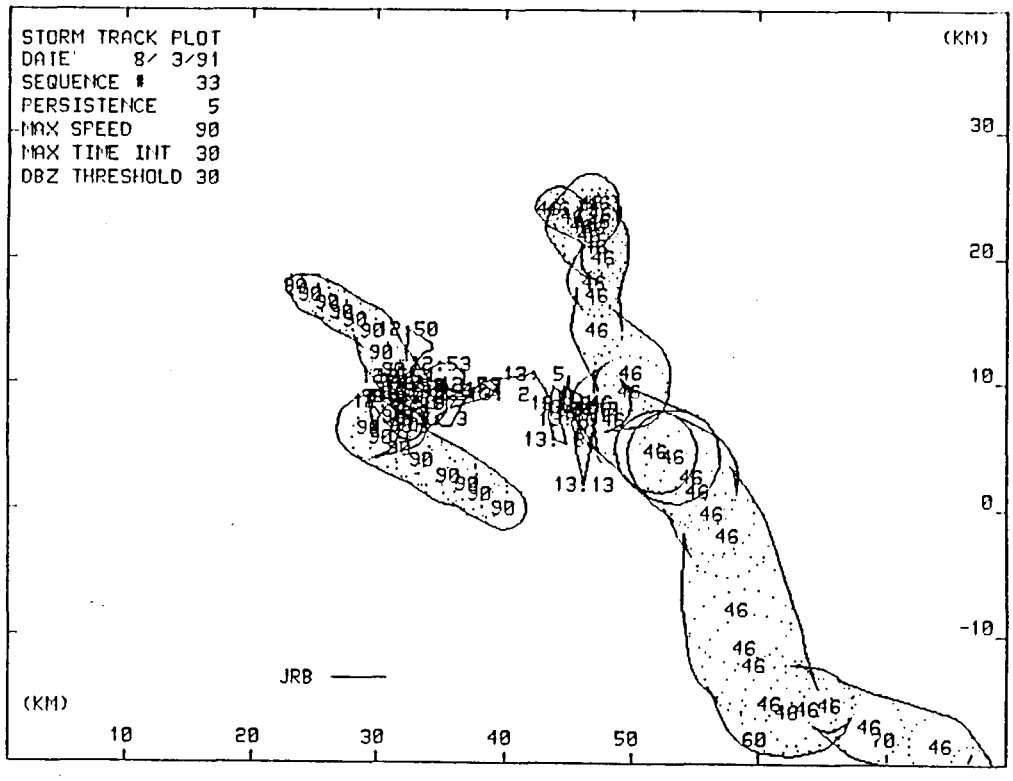

Fig. 5.10 Tracks of storms seeded on March 8, 1991 with hygroscopic flares. The track of the seeding aircraft (JRB) is also shown in this figure. Note that the seeding locations coincide with the storm track shifts westward.

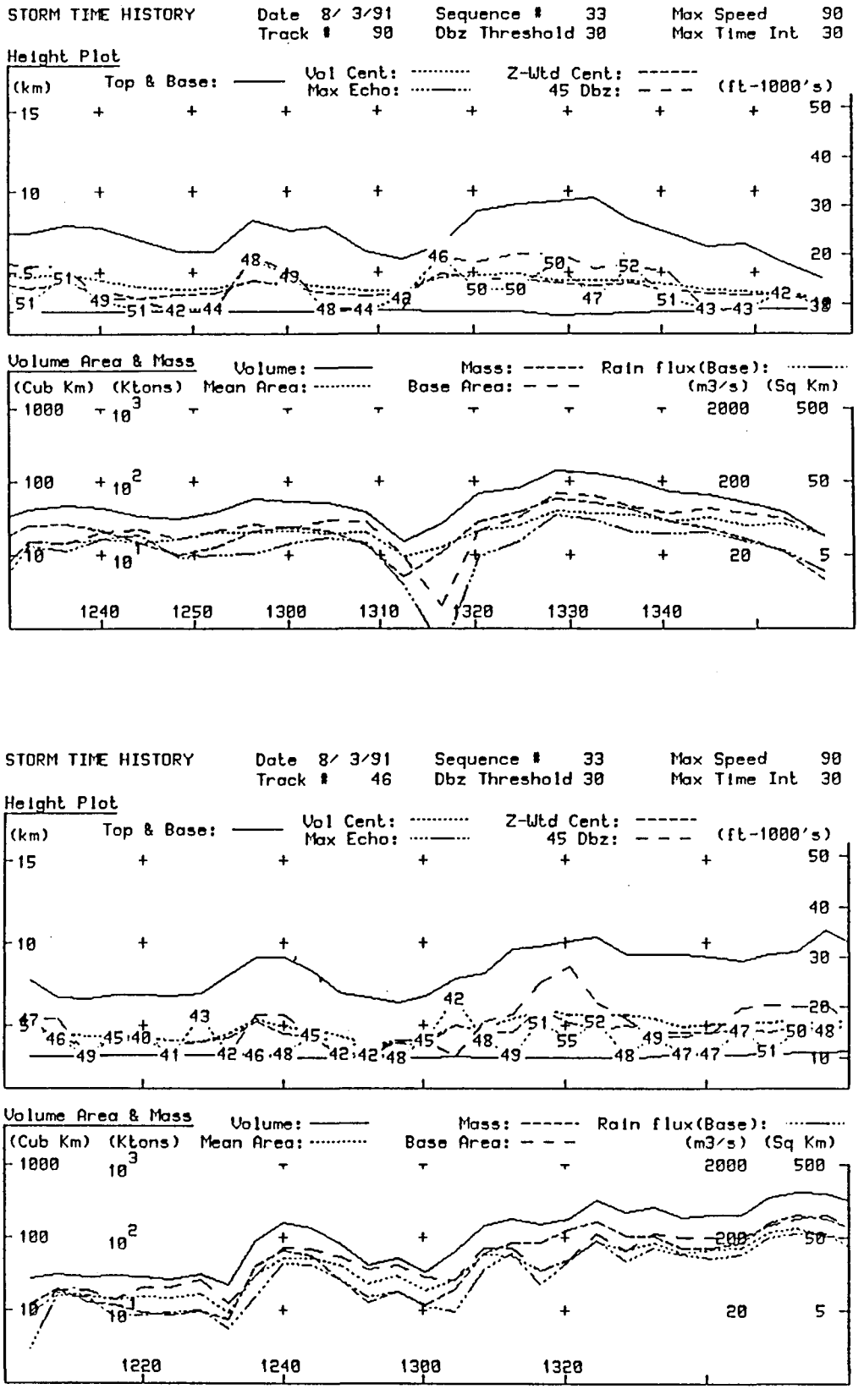

Fig. 5.11 Height-time profiles of the 2 storms seeded with hygroscopic seeding flares in the Bethlehem area on March 8, 1991. Storm track 90 (top) was seeded at 12:50 and track 46 at 13:06.

(d) Microphysical evidence

Table 5.2 is a summary of Lear measurements from clouds judged to be showing a response to hygroscopic seeding. Listed are the times of the sampling pass, the mean 2D-C particle concentrations and mass-weighted mean diameters, the mean and maximum equivalent reflectivities recorded by the aircraft radar and an estimated particle density based on a comparison of reflectivity computed from the 2D-C measurements to that measured by the aircraft radar (Mather, 1989).

Consider January 5, 1991 from Table 5.2. Seeding commenced at cloud base at 13:52. The Lear started sampling at 13:58. Although some ice was present, mass-weighted mean diameters (MWD) are small and radar reflectivities are barely above noise levels. All this changed at 14:07. Particle concentrations jump and MWD increase by almost a factor of 10. Radar reflectivities jump to a mean of 24 and a maximum of 40 dBz. Radar and 2D-C calculated reflectivities match best if the sampled particles are assumed to be water drops.

The 2D-C images from 2 passes on February 14 (Table 5.2) are presented to illustrate the development of drops, frozen drops and dense graupel, presumably as a result of the seeding, in a storm in the Bethlehem area. Fig. 5.12(a) is a pass through a cloud unaffected by the seeding. The images show "streaking" (caused by water running off the probe) and some small images less than 300 μm in diameter, probably small ice crystals. The line of pass-averaged variables, immediately above the images indicate a high liquid water content and a poor "conversion efficiency", i.e. very little of the cloud water has been converted to precipitation at the sampling level. Contrast Fig. 5.12(a) with (b) which shows images of large frozen drops and graupel. The line of pass-averaged variables for this figure indicates that in this case, 57 percent of the cloud water has been converted into precipitation. The engine temperature measurement of cloud water content, which is the water content in the precipitation plus the cloud supercooled liquid water content (measured by the King hot wire), has been used in the conversion efficiency computation (Morgan et al., 1989).

In summary then, both the radar and the microphysical measurements in many of the clouds that have been seeded experimentally with the new hygroscopic seeding flares are showing strong signatures that are compatible with the seeding hypothesis. (Hygroscopic seeding at cloud base should produce more and larger particles sooner in the life cycle of the treated storm, thereby harvesting more of the available supercooled water, i.e. increasing the efficiency of the rainfall process).

Table 5.2 Summary of Lear Measurements

Time (SAST)	2D-C CONC (l^{-1})	2D-C MWD (mm)	Radar MEAN (dBz)	Radar MAX (dBz)	Est. Density (g/cm^3)	Remarks
5 JANUARY 1991 - NELSPRUIT						
13:58	13.5	0.14	6	13	-	Flares
14:02	7.7	0.12	4	7	-	2 x 13:52
14:07	37.1	1.14	24	40	1.0	2 x 13:56
14:10	15.2	0.89	21	36	-	2 x 14:02
14:14	8.3	0.28	14	28	-	2 x 14:08
14:21	11.8	0.44	12	25	-	
14:28	48.5	0.33	15	26	1.0	
14:34	20.3	1.30	18	33	0.2	
16 JANUARY 1991 - BETHLEHEM						
13:36	2.1	0.06	3	4	-	2 x 13:35
:38	0.9	0.12	3	4	-	
:41	5.6	0.40	6	14	0.2	
:44	2.5	0.18	4	6	0.8	2 x 13:44
:49	25.7	1.41	20	37	1.0	
:51	5.8	0.23	24	34	1.0	
14 FEBRUARY 1991 - BETHLEHEM						
15:37	38.4	0.95	13	21	0.4	2 flares
15:42	2.3	0.18	4	5	-	
15:46	2.2	0.57	6	13	-	2 flares
15:52	13.3	1.56	17	30	0.8	2 flares
15:54	4.4	0.29	6	18	-	
15:56	17.5	1.07	10	23	0.2	
15:59	13.0	0.85	12	24	0.4	2 flares
16:06	16.8	1.56	24	32	1.0	
16:12	9.3	2.18	24	40	-	Drops
15 FEBRUARY 1991 - BETHLEHEM						
13:24	1.7	0.26	6	14	-	2 x 13:22
13:31	2.6	0.27	5	11	0.2	2 x 13:26
13:36	1.3	0.71	14	24		2 x 13:38

- abandoned because of generator failure

Table 5.2 continued/

Time (SAST)	2D-C CONC (l^{-1})	2D-C MWD (mm)	Radar MEAN (dBz)	Radar MAX (dBz)	Est. Density (g/cm^3)	Remarks
			4 MARCH 1991 - NELSPRUIT			
13:29	0.3	0.35	3	4	-	2 x 13:35
13:42	0.9	0.09	4	4	-	2 x 13:41
13:44	3.9	2.57	21	30	1.0	
13:51	20.4	1.40	25	35	-	
			8 MARCH 1991 - BETHLEHEM			
12:51	1.9	1.28	6	31	0.6	2 x 12:50
	9.2	0.77	16	27	0.4	
12:56	14.2	1.67	19	30	1.0	2 x 12:56
12:59	48.1	0.51	27	34	0.8	
13:02	1.0	0.08	3	5	-	
			8 MARCH 1991 - BETHLEHEM			
13:04	1.7	0.33	4	7	0.8	
	2.2	0.35	6	9	0.6	
13:06	1.4	0.21	7	14	-	2 x 13:06
13:09	17.0	1.02	29	40	1.0	2 x 13:10
13:12	27.7	1.12	31	45	-	
13:15	4.7	1.56	15	25	-	
13:18	36.5	0.91	28	36	1.0	

Fig. 5.12(a)

Time (SAST)	Alt (m)	Temp (°C)	Updraft (m/s)	King La (g/kg)		E.T.	C.E. (%)
15:42	5905	-6.0	5.1	4.32	5.43	4.78	10

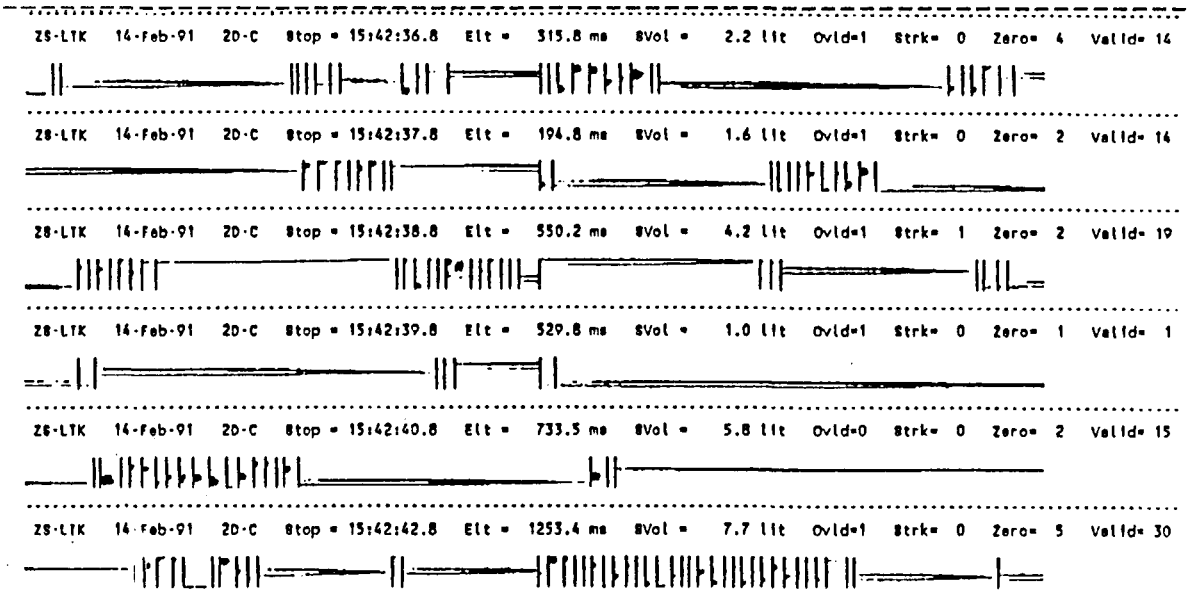

Fig. 5.12(b)

Time (SAST)	Alt (m)	Temp (°C)	Updraft (m/s)	King La (g/kg)		E.T.	C.E. (%)
16:12	5844	-7.0	3.0	2.03	7.29	4.77	57

Notes: (1) Vertical time bars separating images are 1.2mm long
(2) C.E. is defined as (1 - King/E.T.) x 100.

The results from this one season of experimental seeding justified the design and execution of a randomized seeding experiment, which was conducted during the 1991/92 season.

6.0 THE RANDOMIZED HYGROSCOPIC CLOUD SEEDING EXPERIMENT

(a) Introduction

The decision to conduct a randomized seeding experiment was based upon the promising results of the 1990/91 seeding trials. The experiment was proposed only after the NPRP researchers had achieved confidence in their seeding hypothesis.

Flare racks were built by Atlas Aircraft Corporation to carry ten 1 kg flares mounted behind each engine nacelle. These were electrically fired from a selector switch and a firing button in the aircraft cockpit. First tests of the racks (Oct 3, 1991) indicated that flow reversal around the rear of the nacelles was burning the plastic connectors holding the ignition wires. The racks were returned to Atlas for modification. The first randomized seeding experiment took place on October 15. Two flares were ignited on the left hand rack. These set alight the rest of the flares in the rack. The resulting conflagration severely damaged the seeding rack. At this stage, Atlas proposed a completely new design. Each flare receptacle was mounted on a small pylon which placed the burning flare well above the boundary layer into the air flow around the nacelle. To ensure streamline flow, the nacelle rear faring was replaced.

The new flare racks were successfully tested on November 14, and no further troubles were encountered with the new system.

(b) Experimental design

The experimental design was worked out in conjunction with Professor F E Steffens and his team at UNISA.

1. Two sets of paired envelopes were prepared at UNISA, one for Bethlehem experiments, the second for Nelspruit. One set of the pairs was held at the Carolina and Bethlehem radars. Matching pairs were held in the seeding aircraft (JRB).

2. Launch criterion was the appearance on radar of two separate echoes that simultaneously exceeded 40 dBz.

3. The seeding aircraft was directed to the storm of interest by radar. The cloud top sampling aircraft, either the Learjet or the other Commander, was directed to the same storm.

4. JRB's pilot chose the experimental storm on the basis of a seedable updraft before declaring an experiment (decision time).

5. An experiment was performed if

- JRB's transponder was visible on radar
- the storm was clearly identified on radar
- the cloud top aircraft was in position. However, experiments were permitted in the absence of an available cloud top aircraft.

Once JRB's pilot declared an experiment, and it was determined that the above conditions were fulfilled, the radar operator opened the appropriate envelope, broadcast the decision to JRB who then opened his matching envelope. The combinations and outcomes were as follows:

RADAR	JRB	ACTION
Seed	No	No-seed
Seed	Yes	Seed
No-seed	Yes	No-seed
No-seed	No	Seed

Since the pilot did not announce his action, and stayed with the chosen storm for 15 minutes whatever the outcome (seed or no-seed), both the radar operator and the cloud top aircraft were "blind" as to treatment. This prevented any biases creeping into the collection of the radar and microphysical observations.

JRB was equipped with 20 flares of which a maximum of 10 were used per experiment (storm). Since two successive cases could both be "seed", no more than 2 experiments took place per flight, thus preserving blindness as to treatment. A second experimental storm had to be at least 20 km distant from the first case.

Daily forecasts of the best area for operations were made by the Bethlehem group. Telephone briefings took place each day at 10:30 and operations were planned based upon the forecast and equipment availability (aircraft, radars).

(c) The experiment

The design of the experiment remained unchanged throughout the season. The breakdown of case numbers by month and area are shown in Table 6.0.

Table 6.0 Experiments tabulated by month and area.

Month	Bethlehem		Nelspruit	
Oct			201	(1)
Nov	501	(1)	202 - 209	(8)
Dec	502 - 504	(3)	210 - 214	(5)
Jan	505 - 506	(2)	215 - 225	(11)
Feb	507 - 514	(8)	226	(1)
Mar	515 - 521	(7)	227 - 230	(4)
	Totals	21		30

Most of the Bethlehem storms were acquired in the last two months of the season, whereas the experiments at Nelspruit took place in the first four months of the season.

At a farmers meeting in Carolina on February 4, 1992, it was agreed to suspend operations in that area for one month (Feb 4 to Mar 4). This accounts for the sudden drop off in experiments in that area.

The 1991/92 season was one of the driest summers on record, resulting in fewer storms and the usual public relations problems attendant with droughts. This may also have affected storm characteristics in other ways (smaller storms, higher cloud bases, etc). Comparison of results from future experimental seasons will be needed to resolve this question.

The radar data were collected by the Bethlehem and Carolina 5 cm radars operating in volume scan mode. Both radars used identical software to collect storm reflectivities. Calibration of both radars was checked on a daily basis. Initially the radar tapes at Bethlehem were processed using Nelspruit software and the "storms" file sent to Nelspruit for storm track analyses. By the end of the season, the storm tracking software had been implemented on the Bethlehem computer, and track identification and analysis could be carried out at both sites. This had the advantage of allowing all personnel to participate in the track selection process, thereby increasing our confidence in the correct selection of case tracks. For details on the storm and track analysis software, see Programme for Atmospheric Water Supply, Volume 4, (1986). All tracks from all experimental days are stored on both computers, so it would be possible for the analysis to be re-run by individuals that were unaware of treatment. Here, most of the tracks were selected by staff who were aware of the treatment.

(d) Results

The core of the statistical analysis of the experiment is being carried out at UNISA by Professor Steffens and his group, and results to date are included as appendices to this report (Appendix 2 and 3). Presented here is a brief analysis of the experiment carried out at Nelspruit using the re-randomization software that is available in our radar software package. This analysis differs from UNISA's since geometric rather than arithmetic means were used in the storm track property comparisons. However, the results of the two analyses are almost identical. In both, storm track properties are averaged over 10 minute segments from decision time (t=0). This follows the procedure that was developed to analyse the Nelspruit dry ice seeding experiment, which led to insights into physical mechanisms that could have led to the observed increases in radar-measured rainfall. Table 6.1 is a summary of the relevant mean storm track properties.

Table 6.1 Mean storm track properties

Property	0 - 10 Seed/No-seed	10 - 20 Seed/No-Seed	20 - 30 Seed/No-seed	30 - 40 Seed/No-seed	
Mean storm:					
Volume	203/222	171/239	211/250	319/224	(km^3)
Area	45/48	41/48	49/60	69/55	(km^2)
Rain flux (1.5^o)	106/126	91/123	111/143	172/166	(m^3/s)
Rain mass (1.5^o)	63/73	49/60	57/72	101/46	(ktons)
Rain mass (6 km)	29/39	23/32	36/27	65/16	(ktons)
Rain mass (6 km) / Rain mass (1.5^o)	0.46/0.53	0.47/0.53	0.63/0.38	0.64/0.35	
CASES	24/24	25/24	22/20	16/17	

PERCENTAGE DIFFERENCES $\frac{\text{SEED - NO-SEED}}{\text{NO-SEED}} \times 100$

Mean Storm:	%	%	%	%
Volume	- 9	- 28	- 16	42
Area	- 6	- 16	- 18	27
Rain flux (1.5^o)	- 25	- 26	- 22	48
Rain flux (6 km)	- 25	- 33	30	185
Rain mass (1.5^o)	- 14	- 19	- 20	117
Rain mass (6 km)	- 27	- 28	35	298

Pertinent observations from this table are :

1. The radar data from Bethlehem and Nelspruit have been combined since this is a relatively small data set. The combined geometric means show a negative bias (against a seeding effect) which is dramatically reversed in the 30 - 40 minute time interval.

2. All the data have been used. No attempts were made to stratify the data on the basis for example, of cloud base temperature, location etc. The only restriction was that the average storm positions had to be contained in a range interval of between 10 and 90 km from the radars. All case tracks passed this restriction.

3. The statistics are well behaved. For example, the average seed versus no-seed rain masses parallel each other for the first 3 time windows. Only in the fourth (30 - 40 minutes after seeding commences) do they diverge, the average seeded storm rain mass exceeding the no-seed by 117 percent.

4. Of great importance here is that the first seed/no-seed differences appear in the third time window (20 - 30 min) at 6 km. Radar-measured changes between the seeded and control group of storms are appearing first aloft, then later at the surface (more correctly at 6 km then on the low level scan). This observation is depicted in Fig. 6.0 and perfectly matches the seeding hypothesis.

5. The ratio of the seeded rain mass at 6 km to that at 1.5^{o} becomes significantly greater than the unseeded storm mass ratio 20 to 30 minutes after decision. This ratio was previously used to stratify those storms allegedly altered by the Kraft paper mill west of Nelspruit from other storms in the area (Mather, 1991). This previous study showed that certain storms growing close to the paper mill were showing enhanced growth of drops aloft, interpreted as clear evidence of an accelerated or amplified coalescence growth process presumably caused by the hygroscopic emissions from the mill. Table 6.1 shows this ratio jumping from 0.47 to 0.63 from the second to the third time window for the seeded storms, whereas the control group mean drops from 0.53 to 0.38 over the same period. This top heavy structure revealed by the radars is believed to be a characteristic of storms in which precipitation formation via coalescence dominates.

6. Remarkably, this experiment has reached acceptable levels of statistical significance in a single season, without the use of covariates or data stratification. Given the noisy environment characteristic of convective cloud research, this means that the seeding signal is a strong one.

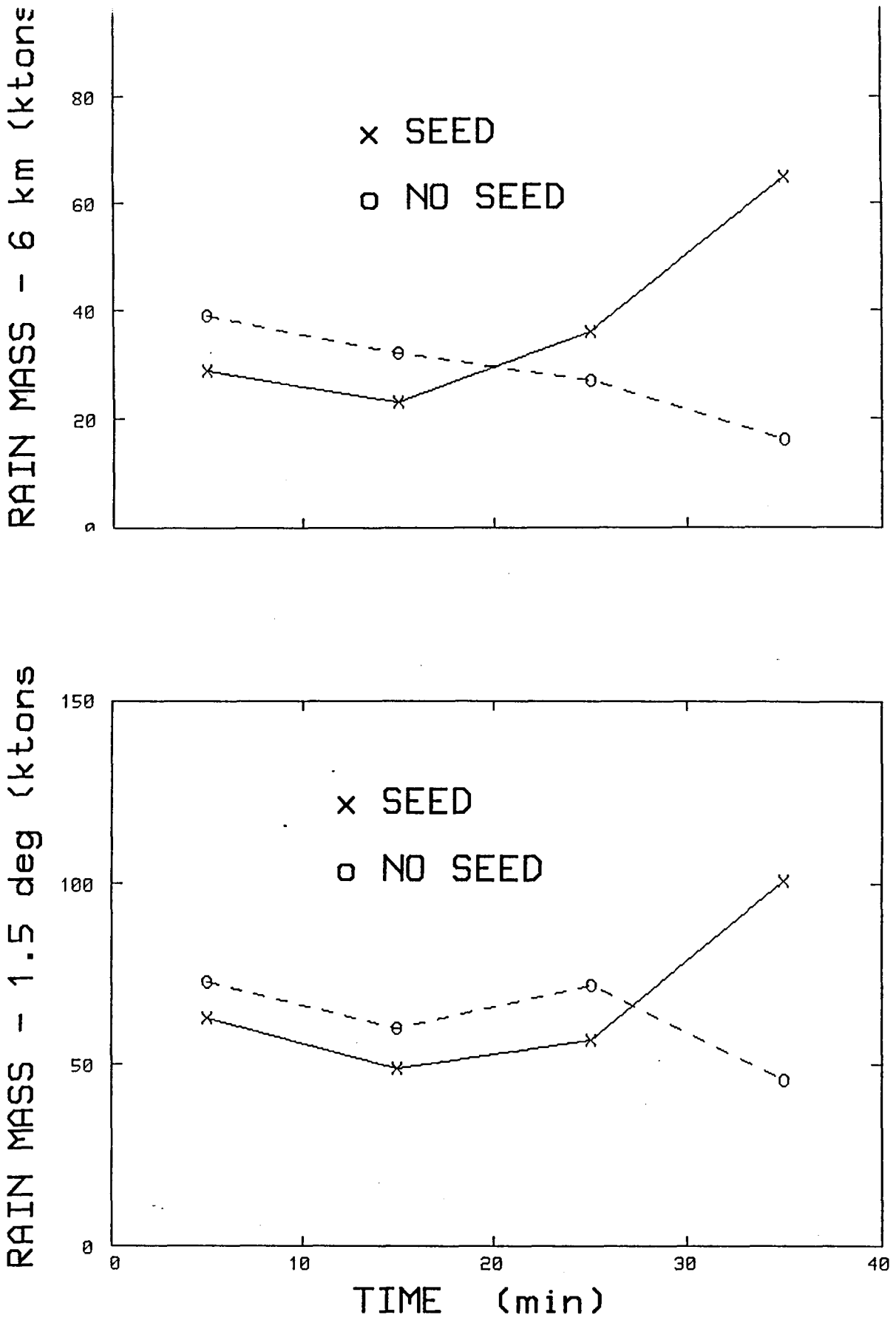

Fig. 6.0. Comparison of seed versus no-seed rain mass in 10 minute time windows from decision time (t=0) at 6 km and lowest scan (1.5°).

It is prudent to examine the distributions of the key variables to make sure that the results are not dependent upon outliers or some other quirk in the data. A comparison of relative frequency distributions is one of the best ways of obtaining a feel for the way the variables are behaving. Fig. 6.1 compares the relative frequency distributions of seed versus no-seed radar-estimated storm rain mass at 6 km. In the first time window, there is a clear bias here in favour of the control storms. As time passes, the no-seed distributions show only minor changes whereas the seeded distributions increase steadily, overtaking then surpassing the control distribution.

The radar-measured increases in rainfall from seeded storms are coming from an increase in storm area and rainfall rate. Average rain rates can be obtained by dividing the rain flux by storm area and multiplying by 3.6 (units of mm/hr)

Table 6.2 Comparative average rain rates

	0 - 10 Seed/no-seed	10 - 20 S/NS	20 - 30 S/NS	30 - 40 min S/NS
Rain rates (mm/hr)	8.5/9.4	8.0/9.2	8.2/8.6	9.0/7.6

Both the seeded and control storms are showing decreases in rain rates in the second time window. The unseeded storms continue this trend whereas the seeded storms begin an increase in the third time window which is carried through to the 30 - 40 min. time interval. Convective storms all have a finite life span, and normal behaviour after selection would be a decrease in intensity with time. The dry ice experiment suggested that seeding led to a reduction in this rate of decline. Initial results from this experiment show a reversal of this trend; apparent increases in storm sizes. Corroboration of this result from an extended experimental data set would provide convincing indications of storm invigoration through alterations of storm dynamics.

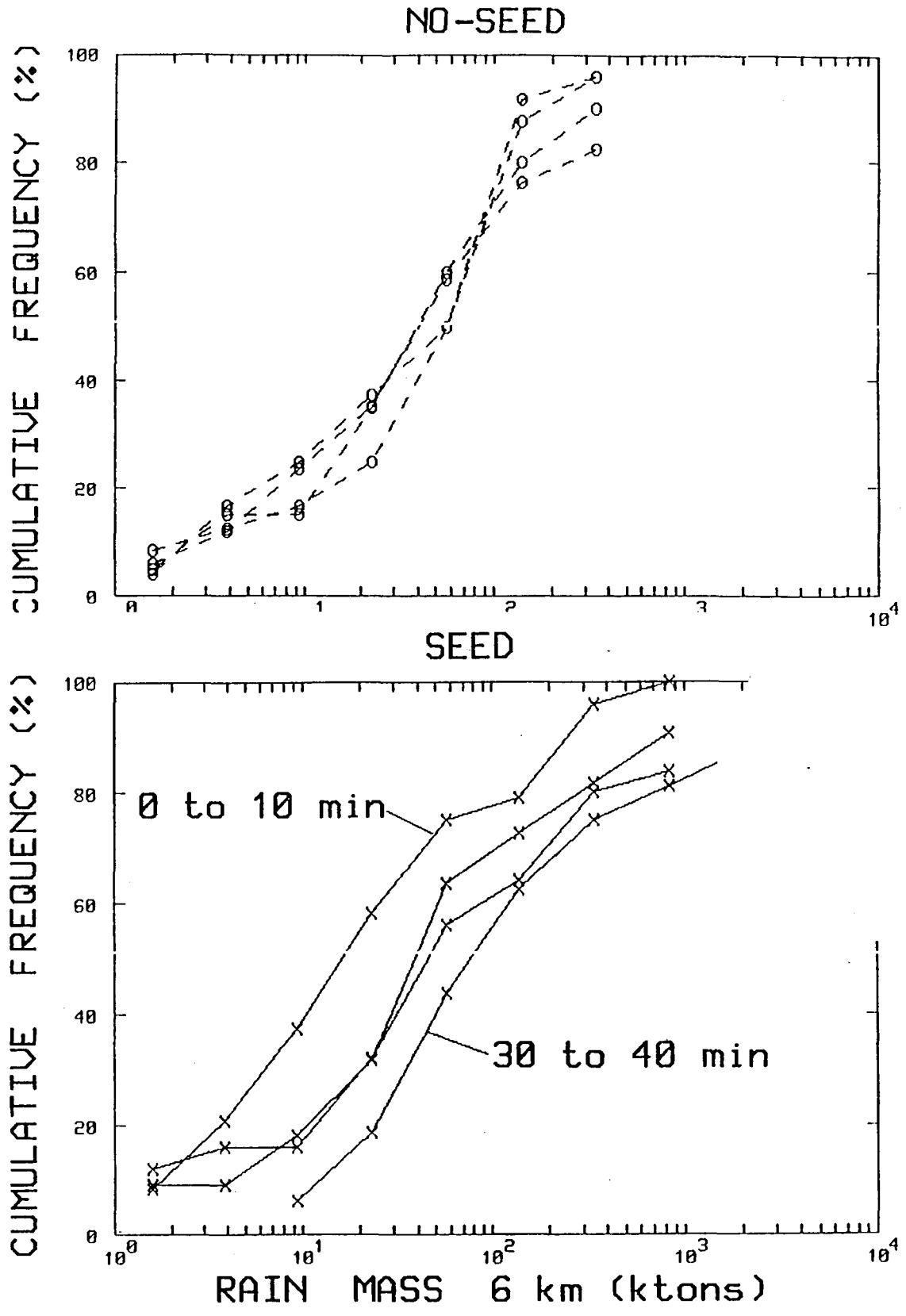

Fig. 6.1. Cumulative frequency distribution of storm rain mass at 6 km for seeded and control storms in four 10 minute time windows from decision time.

7.0 RADAR CLIMATOLOGY

(a) Introduction

With the Nelspruit storm tracking software implemented on the Bethlehem radar, it now becomes possible to compare the storm climatology of the two areas. This comparison serves two purposes; it checks on the performance of the radars, determining for example range limitations (how far from the radars can an experiment take place), and it compares the characteristics of the storms in the two areas.

(b) Analysis methods and results

Volume scan data from the 2 radars were analysed in the following manner. The average storm track positions for the 1991/92 season were stratified into 20 km annuli as shown in Table 7.0. Because of different scan angle sequences determined by the different radar beam widths (Bethlehem 1.0 deg, Nelspruit 1.6 deg.) the analysis at Nelspruit starts 10 km from the radar, while the Bethlehem analysis commences at 20 km. The normalized tracks (normalized by dividing the track numbers by the number of tracks in the first annulus) are compared to the normalized areas (divided by the area of the first annulus). Based upon geometry alone, these two normalized values should compare closely and do up to about a range of 80 km from both radars. Thereafter, the normalized track values decrease even though the areas of the annuli are increasing. We believe that this behaviour is caused by attenuation of the radar signal by storms in the inner annuli.

Storms only partially filling the radar beam, leading to overestimation of storm volumes, areas and rain masses, is apparent after about 80 km from both radars. This effect should begin to appear at a greater range at Bethlehem because of the narrower beam width, but is probably offset by the smaller storms that were recorded in this area. The averages (storm volumes, areas and rain masses) shown in Table 7.0 are all geometric means except for the values shown in parenthesis under "Averages" at the bottom of this table. These arithmetic averages indicate that Bethlehem storms are 3 to 4 times smaller on average than the storms acquired by the Carolina radar over the period in which this study took place. It is interesting to compare the arithmetic averages of the storms chosen as cases for the randomized seeding experiment. Although larger than the rain mass averages in the climatic study, the ratio of about 4 (Carolina rain mass/Bethlehem rain mass) found in the climatology study is preserved in the experiment. This suggests that the cases chosen for experiments in both areas are representative of the overall storm populations.

The relation between radar-estimated rain masses (R_b and R_c) and area-time-integrals is listed at the bottom of Table 7.0, and is similar for both areas (and both radars). Storms with area-time-integrals larger than 2 km^2.hr on average produce more

rainfall in the Carolina area than in Bethlehem. Also, larger storms in the Carolina area rain harder (a Bethlehem exponent of 1.10 versus 1.16 for Carolina).

This study will have an impact upon future planning of an area experiment, given that the sample used in this study is representative of the average storm climatologies in both areas.

Table 7.0 Bethlehem and Carolina radar comparisons

CAROLINA

Range Annulus	10/30	20/40	30/50	40/60	50/70	60/80	70/90	80/100	90/110 km
Mean Range	20	30	40	50	60	70	80	90	100
TRACKS	385	593	790	937	1069	1053	928	834	717
NORM AREA	1	1.5	2.0	2.5	3.0	3.5	4.0	4.5	5.0
NORM TRACKS	1	1.7	2.1	2.4	2.8	2.7	2.4	2.2	1.9
MEAN:									
Echo top (m)	6519	6368	6095	5913	5905	6094	6359	6533	6703
Volume(km^3)	26	28	26	24	23	25	29	34	38
Area(km^2)	6.9	8.7	9.8	10.3	10.3	10.5	11.6	12.4	14.5
Rain Mass(1.5^o)	17	19	19	17	16	16	16	19	21
Rain Mass (6.0km)	4	4	3	4	4	5	6	6	10
dBz (1.5^o)	37.1	36.4	35.6	34.9	34.5	34.4	34.3	34.6	34.6

BETHLEHEM

Range Annulus	20/40	30/50	40/60	50/70	60/80	70/90	80/100	90/110 km
Mean Range	30	40	50	60	70	80	90	100
TRACKS	286	323	414	489	520	508	441	411
NORM.AREA	1	1.3	1.7	2.0	2.3	2.7	3.0	3.3
NORM. TRACKS	1	1.1	1.4	1.7	1.8	1.8	1.5	1.4
MEAN:								
Echo top (m)	6187	6239	6196	6203	6172	6377	6873	7235
Volume(km^3)	21	20	19	18	18	21	28	33
Area (km^2)	4.5	5.1	5.2	5.6	6.2	6.9	8.1	9.1
Rain Mass (1.5^o)	8	9	8	9	9	10	11	12
Rain Mass (6km)	2	2	2	2	3	4	5	7
dBz(1.5^o)	34.7	34.7	34.4	34.8	34.2	34.1	34.5	34.4

AVERAGES

Mean	Bethlehem (1456 tracks)		Nelspruit (3172 tracks)	
Echo Tops (m)	6257		6160	
Volume (km^3)	20	(45)	26	(132)
Area (km^2)	5.7	(10.6)	10.0	(31.3)
Rain mass (1.5^o)	9	(43)	17	(160)
Rain mass (6km)	3	(31)	5	(95)
dBz (1.5^o)	34.3		35.1	

$$R_B = 5.04\ (ATI)^{1.10} \qquad R_N = 4.88\ (ATI)^{1.16}$$

Randomized experiment

Rain mass (1.5^o)	(58)	(225)

7.1 Radar storm characteristics at and above the 30 dBz level in the Bethlehem area during December 1991 and January 1992.

(a) Introduction

During the summer of 1991/1992 the National Precipitation Reseach Programme's (NPRP) Bethlehem section participated in a satellite/radar/rainfall study whereby the Enterprize radar was operated on a continuous basis. This study is funded by the Water Research Commission and is known as RASRAIN (RAdar and Satelite RAINfall). The Weather Bureau, the University of Pretoria and the Department of Water Affairs are the participants in this ongoing study.

Steyn and Bruintjes (1990) reported on the characteristics of 3345 echoes observed during during 33 days in the summer of 1988/1989. They concentrated on echoes at and above the 10 dBz level in contrast with the higher reflectivity storms that are considered in the present study.

The radar data collected as part of the RASRAIN project were used to study the storm properties of all storms between 20 and 80 km from Bethlehem at or above the 30 dBz level. The aim of this study is to summarize the characteristics of the more significant clouds which are representative of the experimental units in the present precipitation research effort of the NPRP. An objective tracking procedure was used to calculate storm properties of 826 storms with lifetimes greater than 16 minutes.

(b) Equipment and data

Steyn and Bruintjes (1990) summarized the Enterprize radar's technical specifications. Since 1990 this radar has been upgraded to computer based data assimilation, storage and control of the antenna. The radar is programmed to operate in an 18 step volume scan which takes about 4 minutes to complete. A base scan elevation of 1.5 degrees was chosen. The elevation step size was determined using an optimization scheme which assures constant resolution between steps at the furthest radar bin of interest. Therefore the step sizes at higher elevations are larger than those at low elevations.

The raw video and pulse repetition frequency (PRF) signals are fed directly into the same computer where integration and processing takes place. Thereafter the data are stored on 2.3 Gigabyte Exabyte cassettes for analysis and at the same time a selected elevation is displayed. In addition to the above, the raw IFF (Identify Friend or Foe) position signals of the research aircraft's transponders are processed, displayed and stored by the same system. Parameters including radar bin size (600m), number of integrations per bin (8), and number of elevation steps with the required elevation values, are all software controlled and therefore easily changeable. All the hardware and software

used in this system was developed inhouse by the technical team of the NPRP. Daily calibrations to check the stability of transmitter power and receiver linearity were done.

An objective tracking programme originally devised by Mader (1979) and adapted by Dixon and Mather (1986) to take the three dimensional structure of echoes into account, was used to track the centroids of storms. Thresholds of 30 dBz minimum intensity and 750 km^3 maximum initial echo volume were applied. The translation speed between volume scans was limited to less than 90 kmh^{-1}. Only echoes with lifetimes longer than five consecutive volume scans (+- 16 minutes) were considered. This package is also used routinely to determine storm properties of interest in the precipitation research experiment.

The periods of data collection were between 2 and 19 December 1991 and between 5 and 23 January 1992. The December period was characterized by good convective development. Towards the end of the January period activity decreased and a serious drought set in over most of South Africa, including the Bethlehem area. Although the results of this study cannot be seen as a general climatology, it is characteristic of normal to below normal rain periods over the area of interest. In Table 7.0, a summary of the echo properties is given on a day to day basis. As echo activity reaches a minimum in the morning a day is defined as the 24 hour period ending at 08:00. The date used is that of the day in which the 24 hour period started. On average 29.5 individual 30+ dBz echoes occurred per day excluding the eight days with no activity and one day which was classified as a general rain day.

The absolute maximum reflectivity in the period under investigation was 57.3 dBz on 9 December 1991, a day on which serious hail damage was reported. The maximum 30 dBz echo top of 15 864 m above ground occurred on 2 December.

(c) Storm development and lifetimes

The diurnal distribution of first 30+ dBz echo development is shown in Figure 7.0. The effect of the diurnal cycle in surface heating in the development of convective clouds can be seen. After 12:00 there is a rapid increase in the number of 30+ dBz echoes that develop. The maximum number of storms (17%) developed between 15:00 and 16:00 whereafter a gradual decrease in echo development occurred. About 75% of first development occurred between 14:00 and 20:00. These results agree with the findings of Steyn and Bruintjes although they found a more gradual increase in activity between early morning and maximum activity. Also shown in this figure is the diurnal distribution for storms that developed in the different sectors. First development occurred in the 150 to 180 degree sector with the other sectors lagging and the latest development starting in the sectors to the west.

Table 7.1 Summary of storm echo properties.

DATE	# OF TRACKS	AVG. MAX. dBZ	MEAN VOLUME km^3	AVG. DIR.	AVG. SPEED $km.h^{-1}$	AVG. LIFE
2/12/91	70	43.6	70.7	73.2	9.5	27.5
3/12/91	39	42.5	33.8	114.9	5.6	27.8
4/12/91	11	43.8	109.2	81.5	16.2	22.9
5/12/91	NO WEATHER					
6/12/91	NO WEATHER					
7/12/91	1	40.8	21.0	166.3	11.5	16.9
8/12/91	34	42.7	49.0	128.5	17.5	28.1
9/12/91	3	48.5	24.3	66.4	8.1	40.4
10/12/91	60	43.3	51.0	127.8	9.9	28.2
11/12/91	32	44.9	61.5	102.7	19.4	35.6
12/12/91	33	43.5	46.5	112.8	10.6	28.6
13/12/91	12	43.4	21.2	54.6	5.9	22.7
14/12/91	49	43.8	38.7	91.3	8.8	30.6
15/12/91	33	43.8	44.2	104.8	6.4	26.4
16/12/91	26	46.8	42.6	161.5	5.1	30.1
17/12/91	36	43.6	32.0	67.5	7.9	33.7
18/12/91	44	44.1	39.6	210.0	4.9	32.4
19/12/91	GENERAL RAIN CONDITION					
5/1/92	11	39.8	12.2	103.8	11.3	28.2
6/1/92	54	44.3	78.8	58.1	10.2	31.3
7/1/92	2	42.6	23.0	62.1	8.1	29.2
8/1/92	20	44.1	70.4	85.2	7.9	28.2
9/1/92	33	42.5	23.7	100.3	11.5	23.1
10/1/92	18	44.1	78.6	143.1	10.4	28.6
11/1/92	21	46.5	307.6	107.4	17.0	31.9
12/1/92	45	43.7	43.7	91.2	14.9	29.9
13/1/92	78	44.3	75.2	125.5	12.9	24.3
14/1/92	NO WEATHER					
15/1/92	3	43.8	40.7	91.1	17.1	27.8
16/1/92	5	43.3	15.6	111.8	20.7	27.6
17/1/92	NO WEATHER					
18/1/92	NO WEATHER					
19/1/92	NO WEATHER					
20/1/92	35	45.2	81.1	101.7	20.8	26.6
21/1/92	NO WEATHER					
22/1/92	NO WEATHER					
23/1/92	18	42.5	33.3	92.3	15.2	26.3
AVERAGES	29.5	43.9	59.7	107.2	11.2	28.5

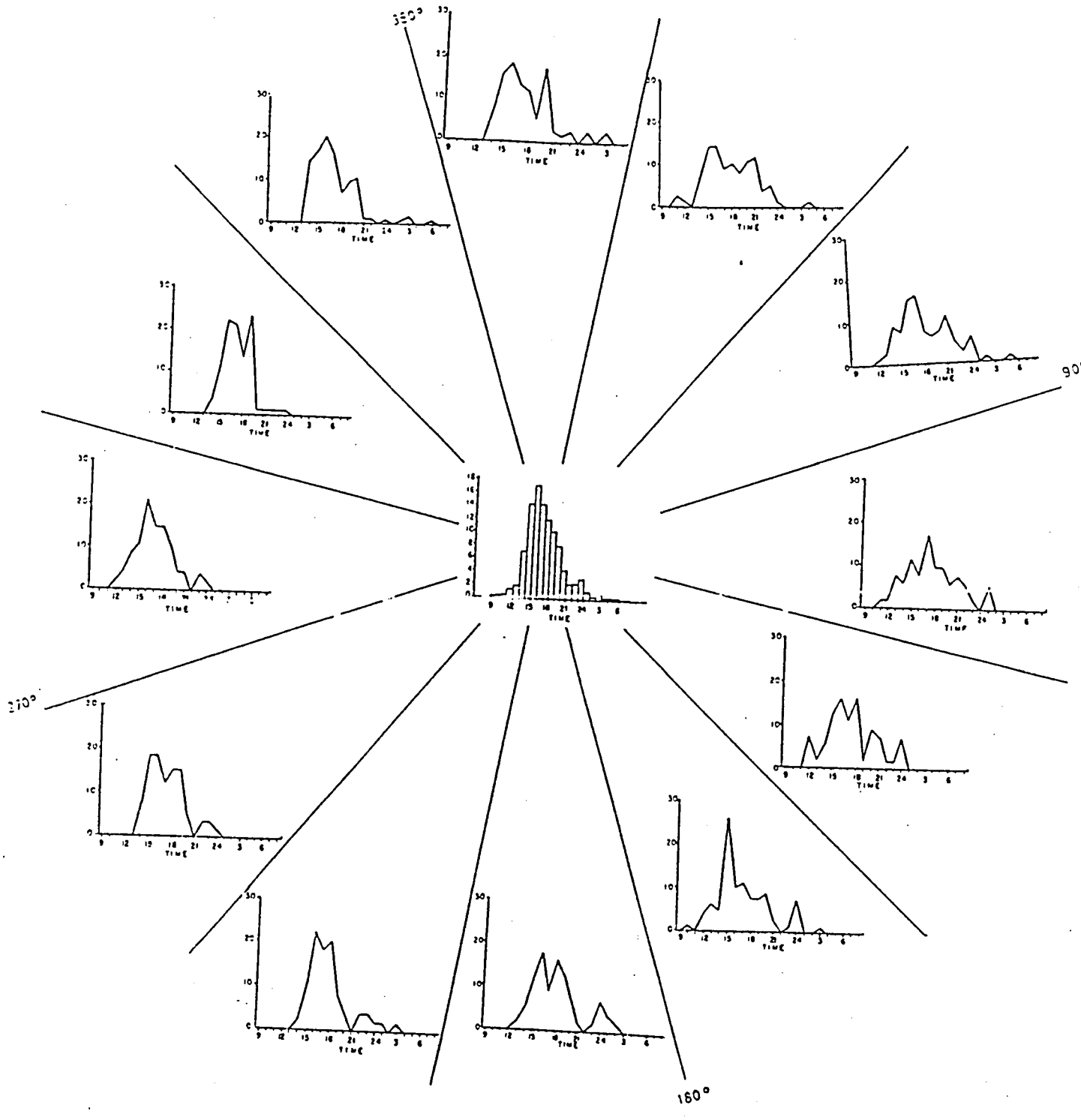

Fig. 7.0 Diurnal distribution of first echo development (inner diagram) and diurnal distribution of first echoes for different sectors.

Figure 7.1 shows the frequency of 30+dBz echo development in the different sectors. The development between 300 and 360 degrees is the most prominent. In contrast to the findings of Steyn and Bruintjes (1990) a marked decrease in development is evident in the south west.

A histogram of the frequency of storm lifetimes is displayed in Figure 7.2 where it is clear that in the period under investigation the 30+ dBz echoes were generally shortlived. Only a quarter of the echoes had lifetimes of more than 30 minutes. Also shown in the figure are the lifetime frequencies of storms in the different sectors. From this it is apparent that storms tend to have longer lifetimes in the eastern sectors.

(d) Storm translation

The average direction of storm movement was generally from west to east as depicted in Figure 7.3. Also shown is the direction of movement of storms that developed in the different sectors.

Of all the storms studied, about 75% had tracks of less than 15 km and only 3.5% of the tracks were longer than 30 km. As shown in Table 1, the average translation speed of all the storms was 11.2 kmh^{-1}.

(e) Echo volumes

The distribution of echo volumes above the 30 dBz threshold is shown in Figure 7.4. It is clear that about half of the storms that occurred during the period under investigation had volumes of less than 25 km^3.

(f) Maximum echo intensities and heights

Figure 7.5 displays the distribution of maximum echo intensity in all the storms under investigation. It is of interest that storms which develop above the 30 dBz level on average tend to develop further into significant storms.

The maximum height of the 30 dBz intensity level in each cloud was investigated. The peak occurrence (20%) was between 9 and 10 km above ground. In only 14% of the cases did the 30 dBz intensity level peak at above 12 km.

(g) Conclusions

This study summarizes the properties of 826 individual 30+ dBz echoes in the Bethlehem radar area that were observed during December 1991 and January 1992. The majority of the storms developed between 14:00 and 20:00 with initial development in the south eastern sector. The north western sector was the area with the most frequent development. Only a quarter of all the echoes had lifetimes of more than 30 minutes and about half of the echoes had volumes of less than 25 km^3. The storms generally

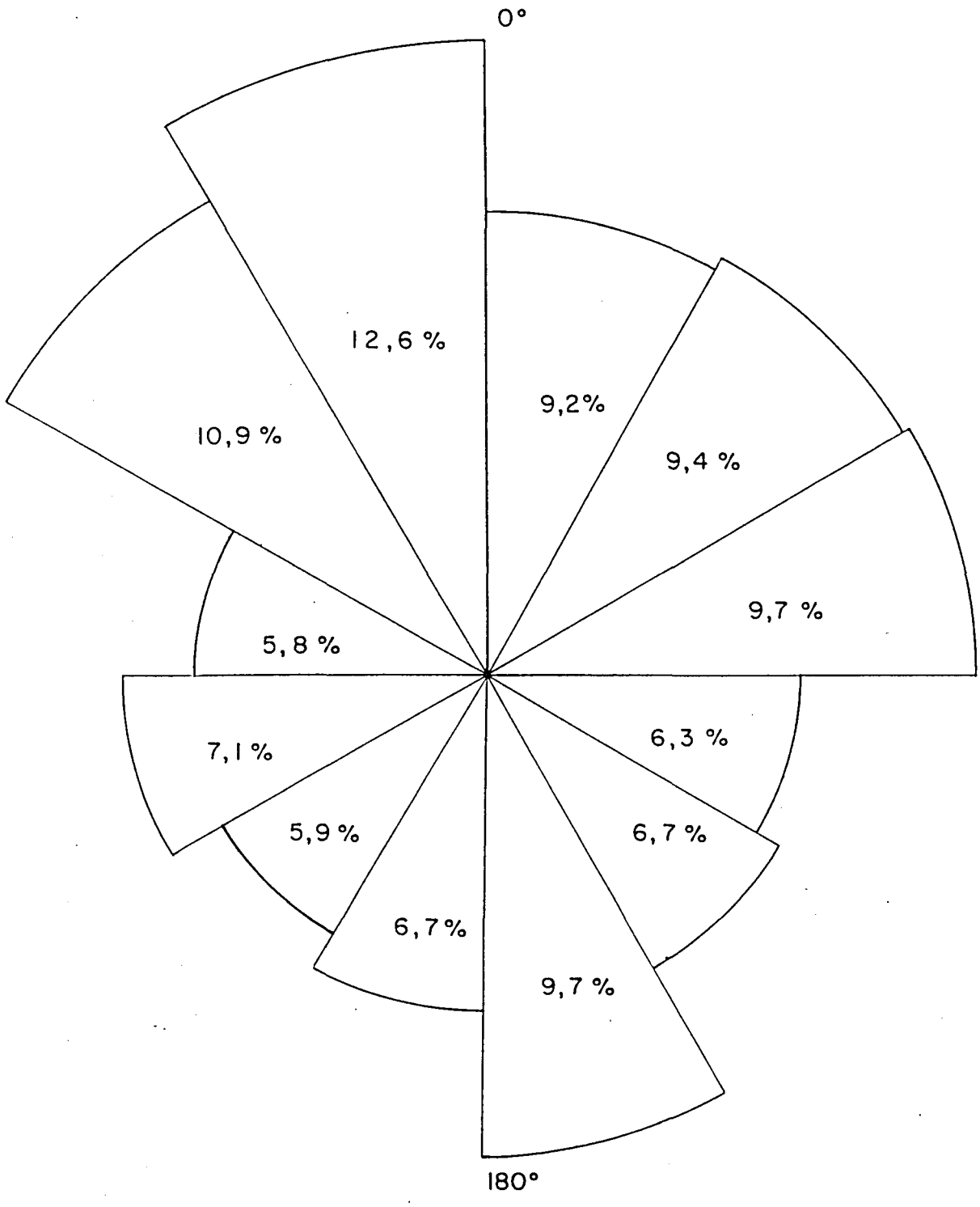

Fig. 7.1 Percentage of first echo development in sectors.

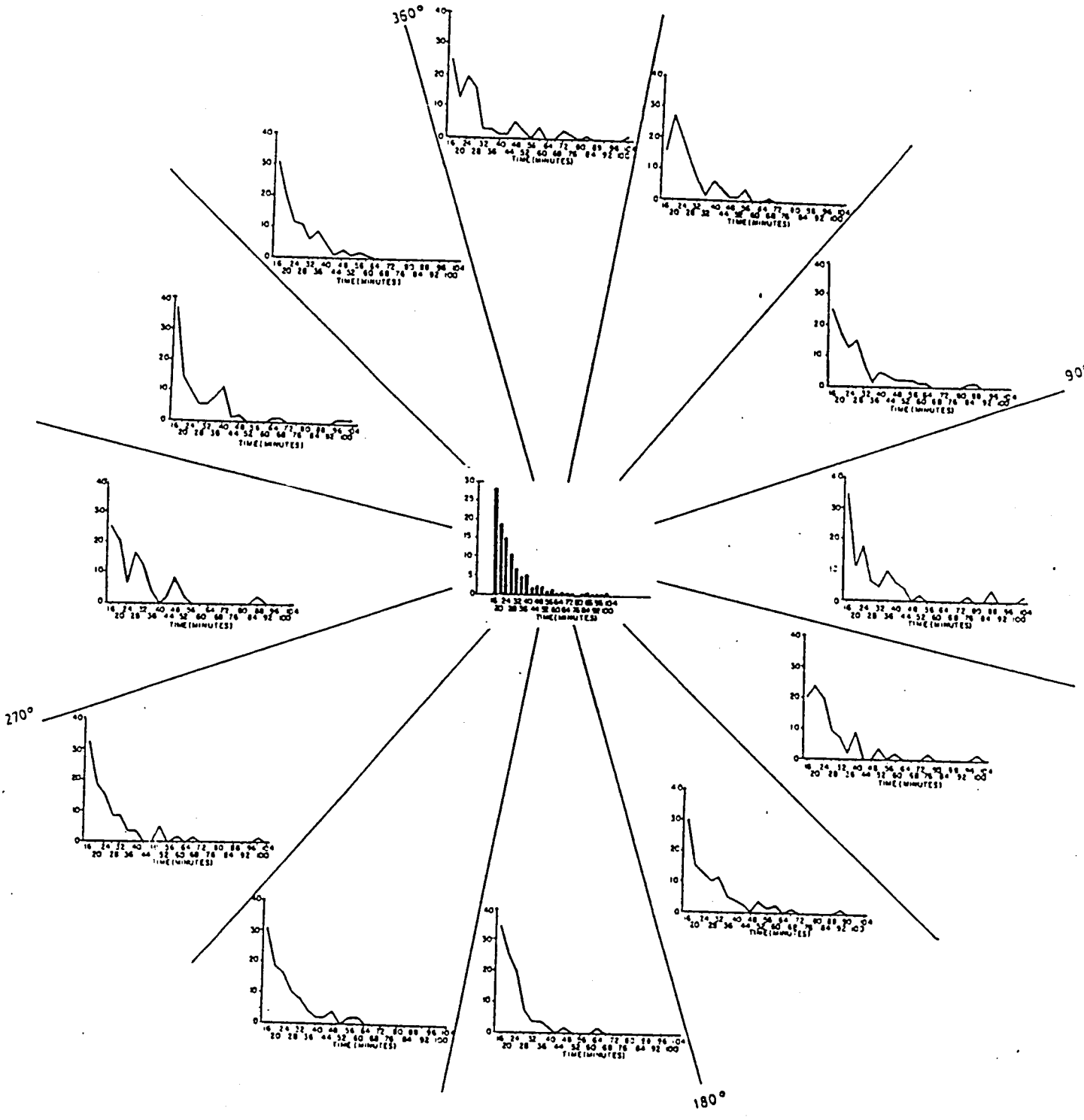

Fig. 7.2 Distribution of storm lifetimes (inner diagram) and the distribution for each sector.

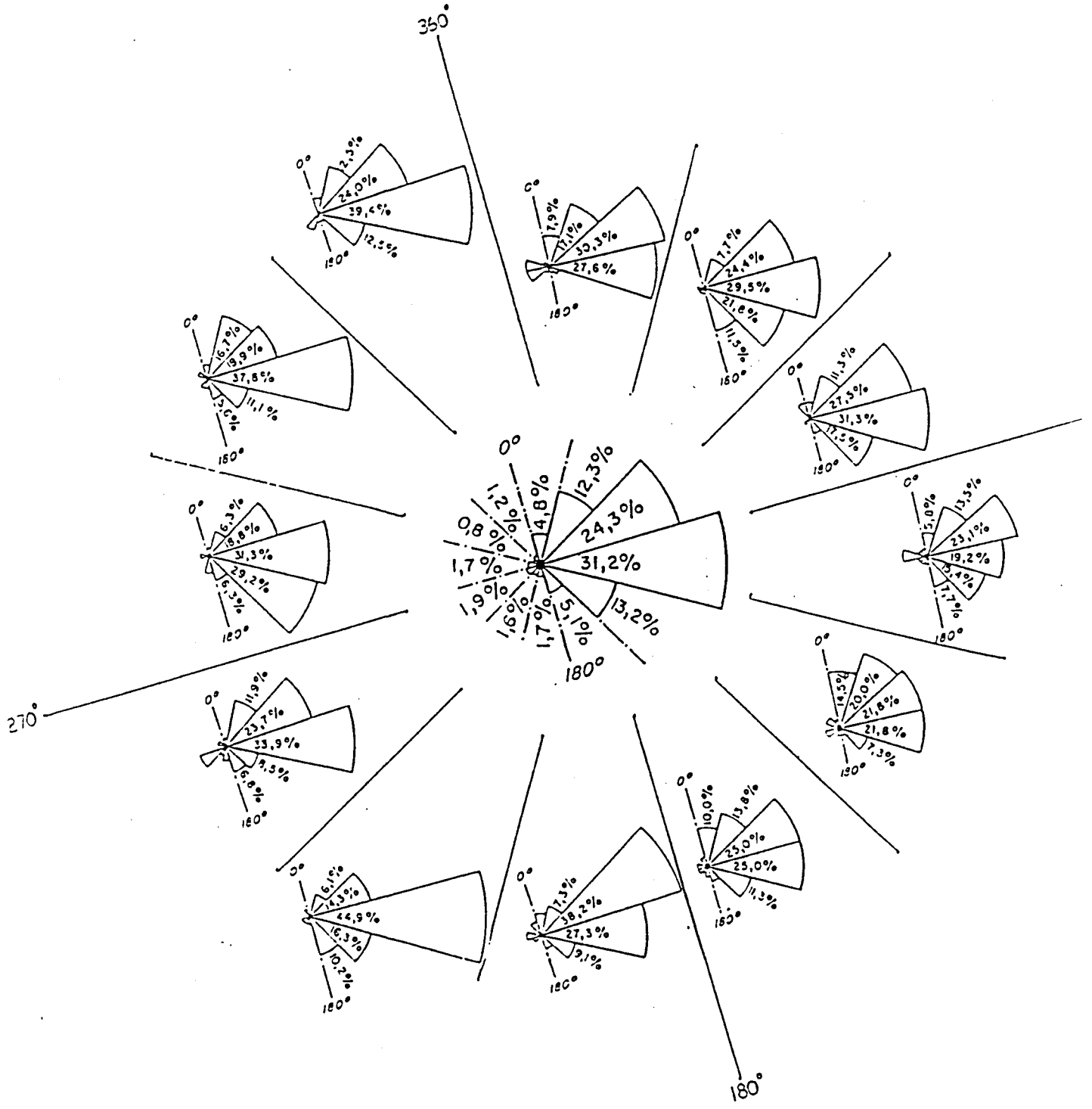

Fig. 7.3 Distribution of storm movement (inner diagram) and the distribution for each sector.

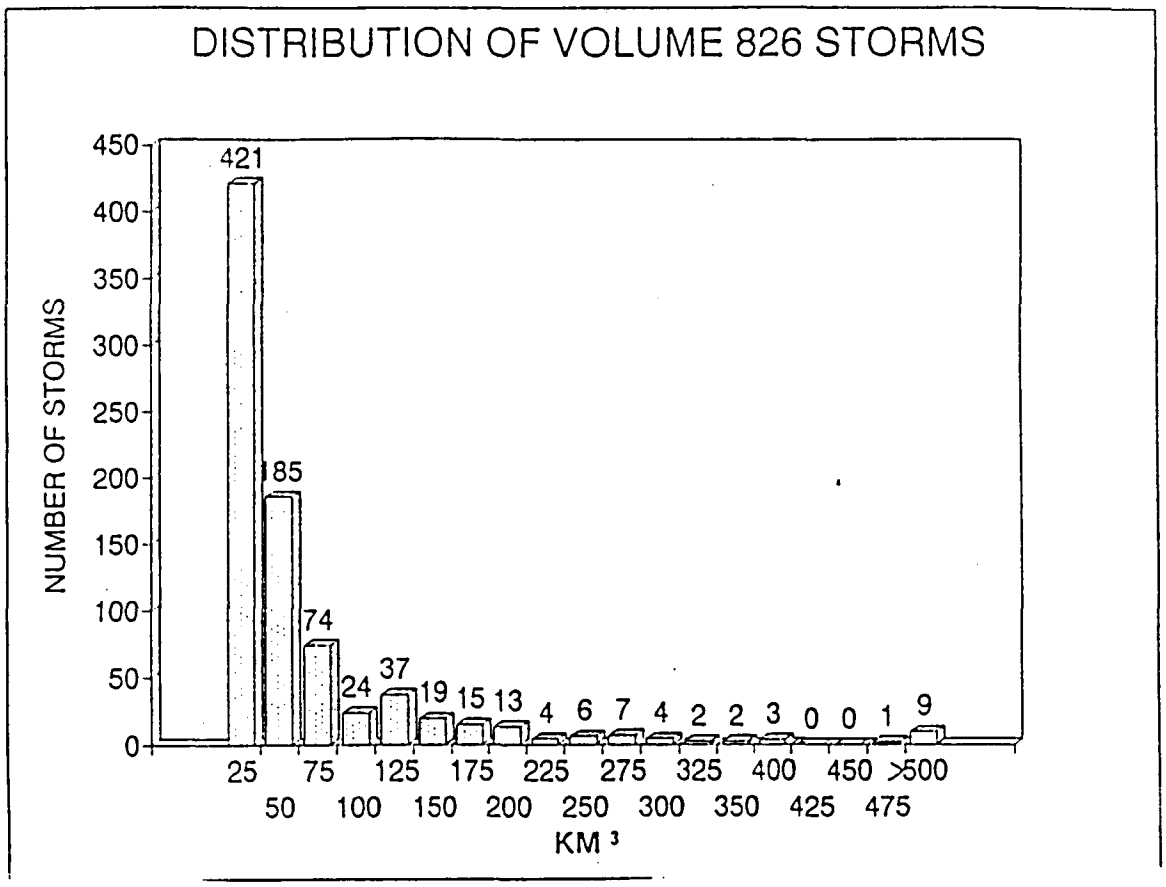

Fig. 7.4 Volume distribution of storms.

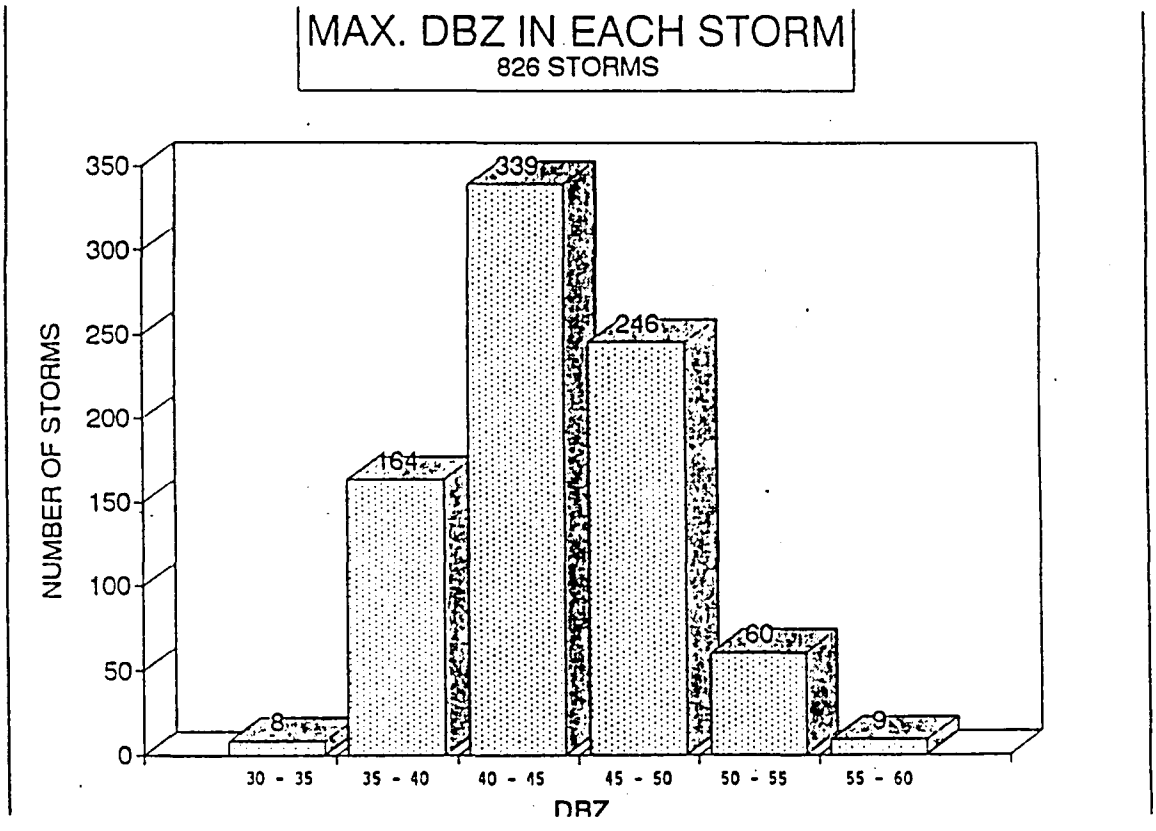

Fig. 7.5 Distribution of maximum dBz.

moved from west to east at an average speed of 11.2 km^{-1}. Storms which developed above the 30 dBz level and lived for longer than 16 minutes generally tended to develop further.

The results show the importance of fast reaction times during aircraft operations, especially in droughts. It is clear that although the clouds are shortlived, there is adequate cloud development above the threshold of interest.

8.0 HYGROSCOPIC MODELLING STUDIES

(a) Deliquescence and initial diffusional growth

A hygroscopic particle exposed to humidity conditions above the value at which solution formation starts, is subject to a process known as deliquescence. During this process vapour from the environment is absorbed, the hygroscopic material goes into solution and the particle grows. This process continues until all the hygroscopic material is in solution. Up to this point the solution part of the particle can be treated as a saturated solution but thereafter dilution takes place.

It has been found that particles exposed to slowly increasing humdities already absorb a significant amount of water at humidities much lower than those at which solution formation starts (Pruppacher and Klett, 1978). This uptake of water results in a more rapid deliquescence process than expected by theory. In the specific case under investigation where the particles are produced by a pyrotechnic flare burning at several hundred degrees Celsius, this effect is assumed to be negligible.

A model was developed to investigate the time evolution of a single particle for which the initial size and temperature, pressure and relative humidity to which it is exposed can be prescribed. It is assumed that the particle is spherical, totally composed of KCl and that the diffusional growth equation applies even during the deliquescence phase. The aim of this excercise is to investigate the time needed for hygroscopic particles of different sizes to form solution droplets under given conditions and to compare the growth of these droplets diffusion with the growth of pure water droplets of comparable initial sizes. Furthermore, the time needed to grow to equilibrum is also determined.

(b) Model description

A general subroutine was written in Fortran for diffusional growth. The equation from Pruppacher and Klett (1978) has the following form:

$$dr/dt = (A/r)(S_{vw}-B+C-D)$$

where r is the radius, S_{vw} is the supersaturation.

This implicit equation has the advantage that the droplet temperature is also determined. Although more computer time consuming than simpler methods, the solution and curvature effects are treated in detail. Assumptions were minimized and each term treated fully.

During the initial deliquescence of the KCl particle, it is assumed that an infinitesimal layer of saturated solution forms on the surface of the particle. As vapour diffusion continues the solution part of the particle remains saturated until all KCl has dissolved. During this phase the mixed particle size is computed. After all the KCl has dissolved, the normal treatment with decreasing molality continues.

Mathematically this phase is handled as follows:

1. The size of a saturated solution droplet is determined using the following.

$$r' = (A' r_s^3 p_s / p_w)^{0.33}$$

where r' is the saturated solution droplet radius, A' is the solution ratio (100/34.7 in the case of KCl as 34.7g can be dissolved in 100g of water), r_s is the radius of the salt particle, p_s the salt density and p_w the density of water.

2. Initially it is assumed that a saturated solution droplet with the same size as the KCl particle is allowed to grow. During this phase, which continues until the size determined in 1 is reached, the mass of KCl in solution is computed by

$$M'_{KCl} = (100/34.7) M_w$$

where M_w is the mass of condensed water.

As the mass of KCl not dissolved is now known, the radius of the undissolved particle can be determined.

$$r_{KCl} = (3(M_{KCl} - M'_{KCl})/4\pi p_s)^{0.33}$$

where M_{KCl} is the total mass KCl

Now the radius of the mixed particle can be determined using

$$r_{mix} = (3(V_w + (4/3)\pi r_s^3)/4\pi)^{0.33}$$

where V_w is the volume of the solution portion which is the same as the volume of the condensed water. Furthermore the size of a KCl particle that would cause a saturated solution droplet of radius r_{mix} must also be determined using:

$$r'_{KCl} = ((34.7\ r_{mix}^3\ p_w)/100 p_s)^{0.33}$$

3. As soon as r_{mix} = r' as determined in 1, normal growth occurs and increasing dilution takes place.

(c) Results

Model runs were done to investigate the growth of 10 and 100 micron KCl particles at relative humidities of 80, 95, 100 and 102%. For comparison the size evolution of similarly sized pure water droplets were also computed at 95% and above. As input in all the runs a temperature of 10°C and a pressure of 700 hPa were prescribed. These conditions are representative of the average seeding level.

At 80% relative humidity no growth was seen on the KCl particles and pure water droplets evaporated rapidly. In Figure 8.0(a) the results from the run with a 10 μm diameter KCl particle and a pure water droplet with an initial diameter of 10 μm are shown. Whereas the pure water droplet evaporated in little more than 2 seconds the solution droplet grew, all the KCl dissolved at about 3.5 seconds and it reached its equilibrium size of 26 μm after 12 seconds. Figure 8.0(b) shows the results for particles with initial diameters of 100 μm. In this case complete evaporation of the pure water droplet happened after more than 110 seconds. The hygroscopic particle took about 130 seconds for the deliquescence phase, at which time the solution droplet had reached a diameter of about 175 μm. Continued growth occurred and the equilibrium size was not yet reached at 1000 seconds.

Figures 8.1(a) and (b) show the results of 10 and 100 μm diameter particles at a relative humidity of 100%. As can be expected, the water droplets survived longer, the growth on the KCl particles was faster, especially after deliquescence, and equilibrium sizes were bigger and took longer to be reached.

In Figure 8.2(a) and (b) the results at 102% relative humidity are depicted. In this case the tendency noticed in the previous figures is even more pronounced; even the water droplet grows and as can be seen in the 10 μm case, the marked size difference around 10 seconds becomes negligible towards the end of the run. The same tendency will be observed with the 100 μm particles after much longer growth times than those shown here.

It is interesting to note that the length of the deliquescence phase of the KCl particles under investigation does not vary significantly at the different humidities used. Furthermore a more marked increase in the sizes of the solution drops is seen just after the deliquescence phase. This is caused by the almost saturated solution that still applies at this stage in addition to the cessation of the relative volume decrease caused by the solution of the solid KCl particle during the deliquescence phase.

This theoretical study was done to investigate the expected properties of the hygroscopic flare particles after burning. The results shown here can only be seen as a guideline as the real particles are not composed of KCl only. However it is unlikely that any significant deliquescence could have taken place before

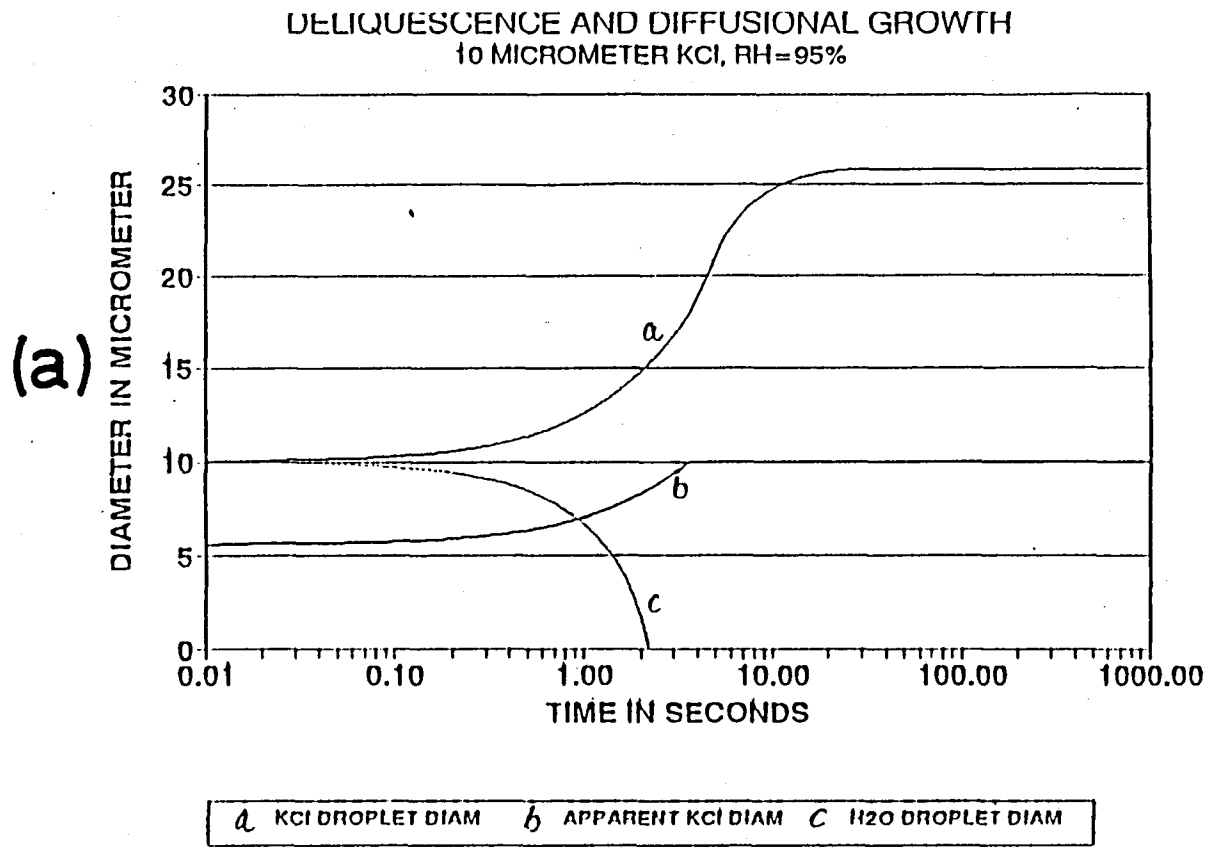

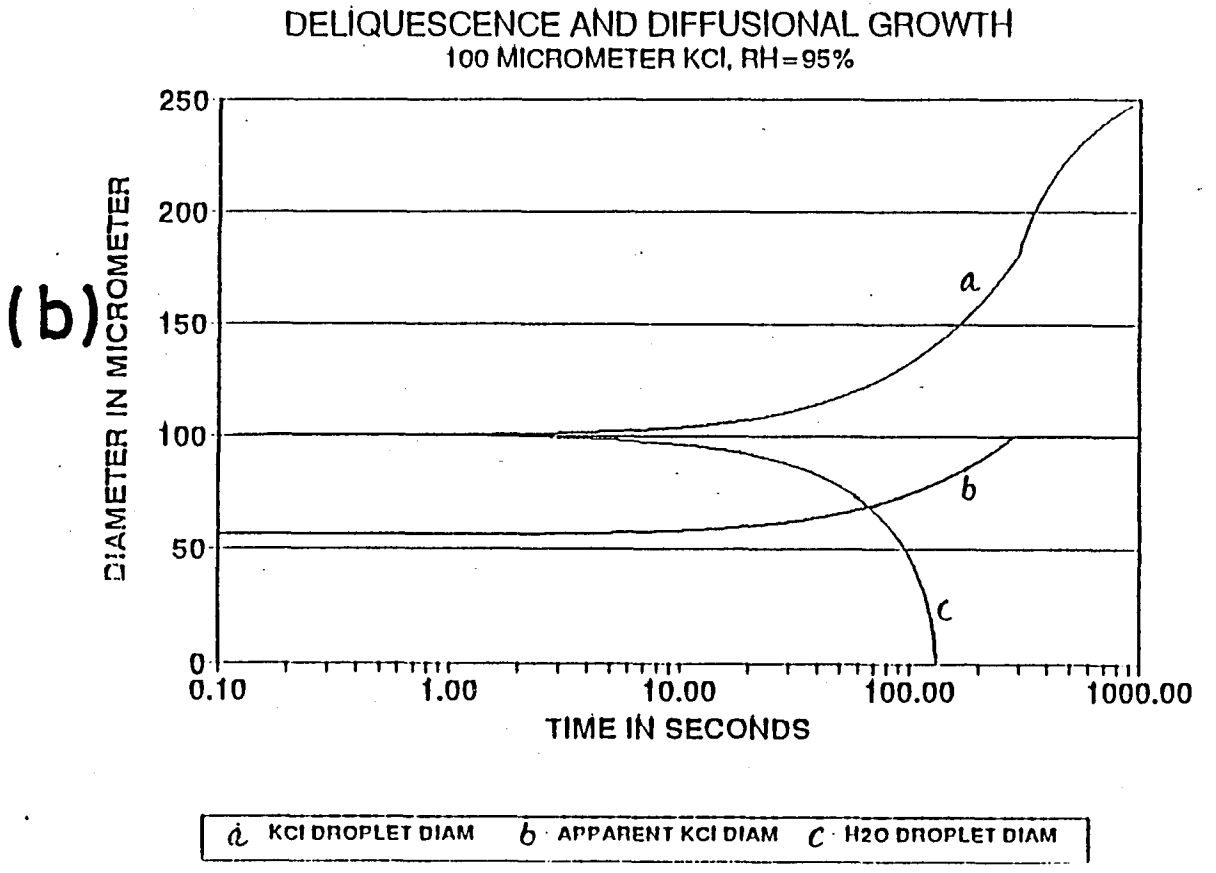

Fig. 8.0 Deliquescence and growth on KCl particle compared to pure water droplet at 95% RH.
(a) 10 μm particle
(b) 100 μm particle

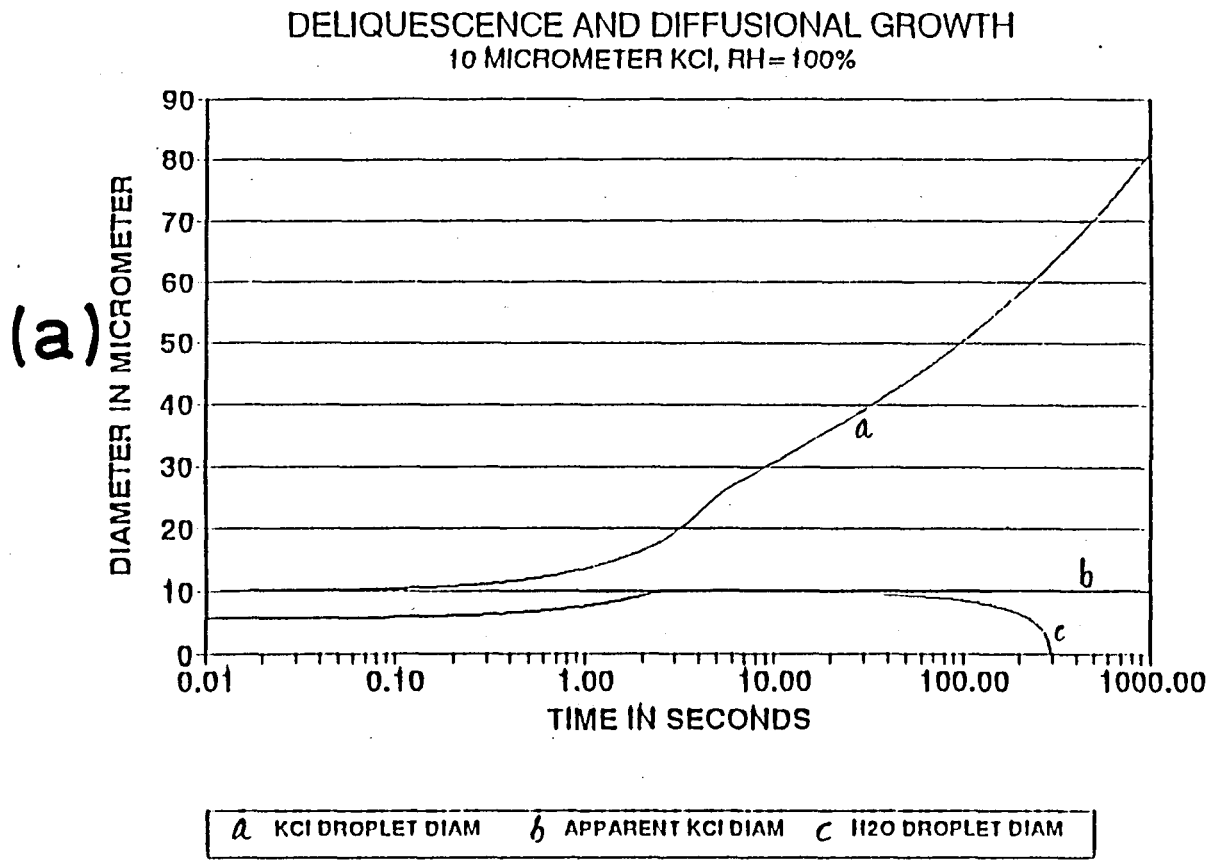

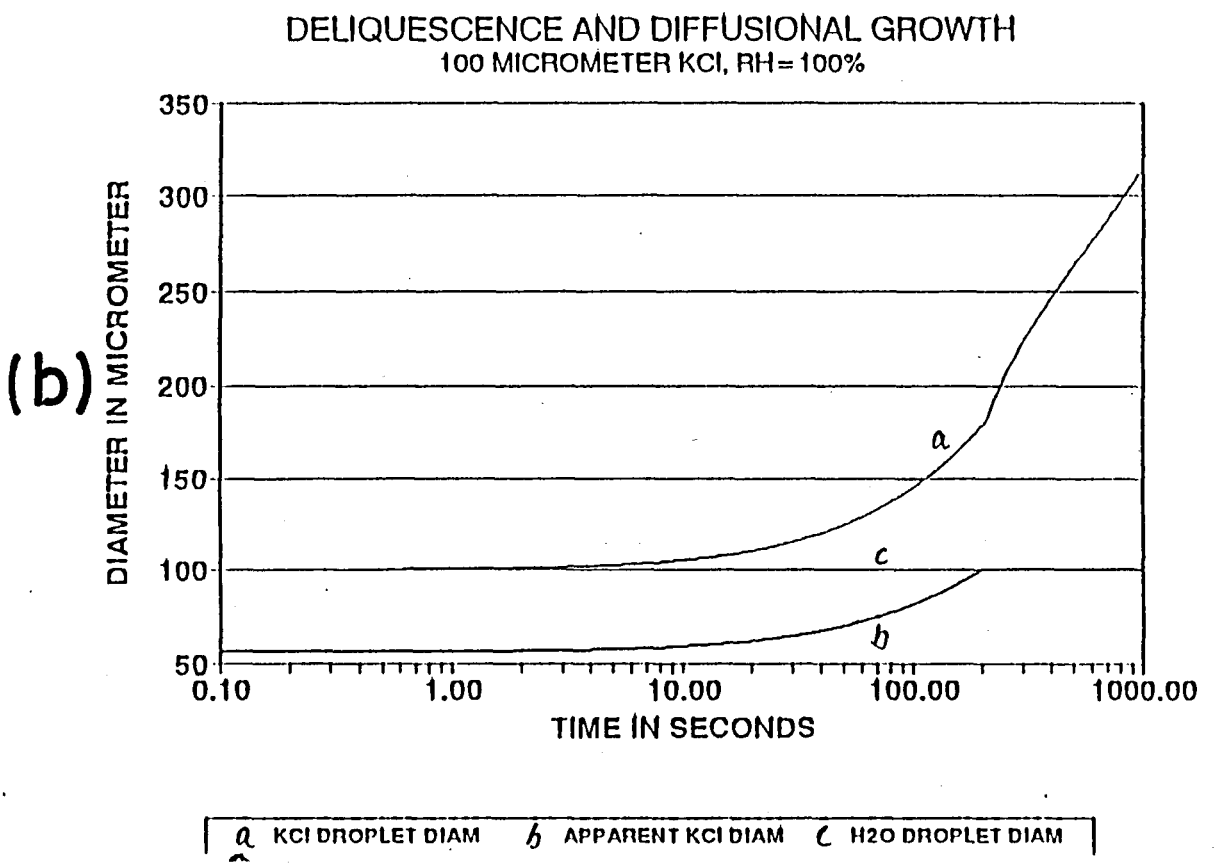

Fig. 8.1 Deliquescence and growth on KCl particle compared to pure water droplet at 100% RH.
(a) 10 μm particle
(b) 100 μm particle

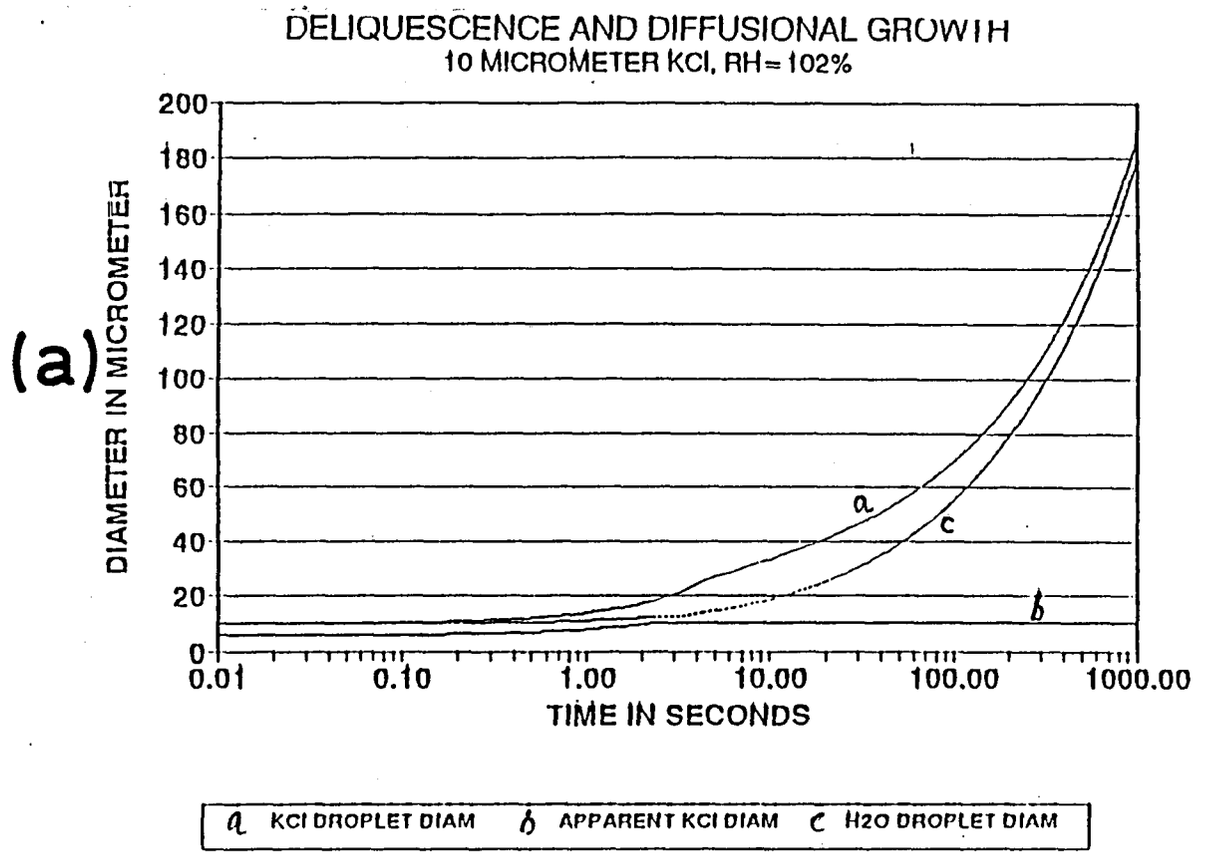

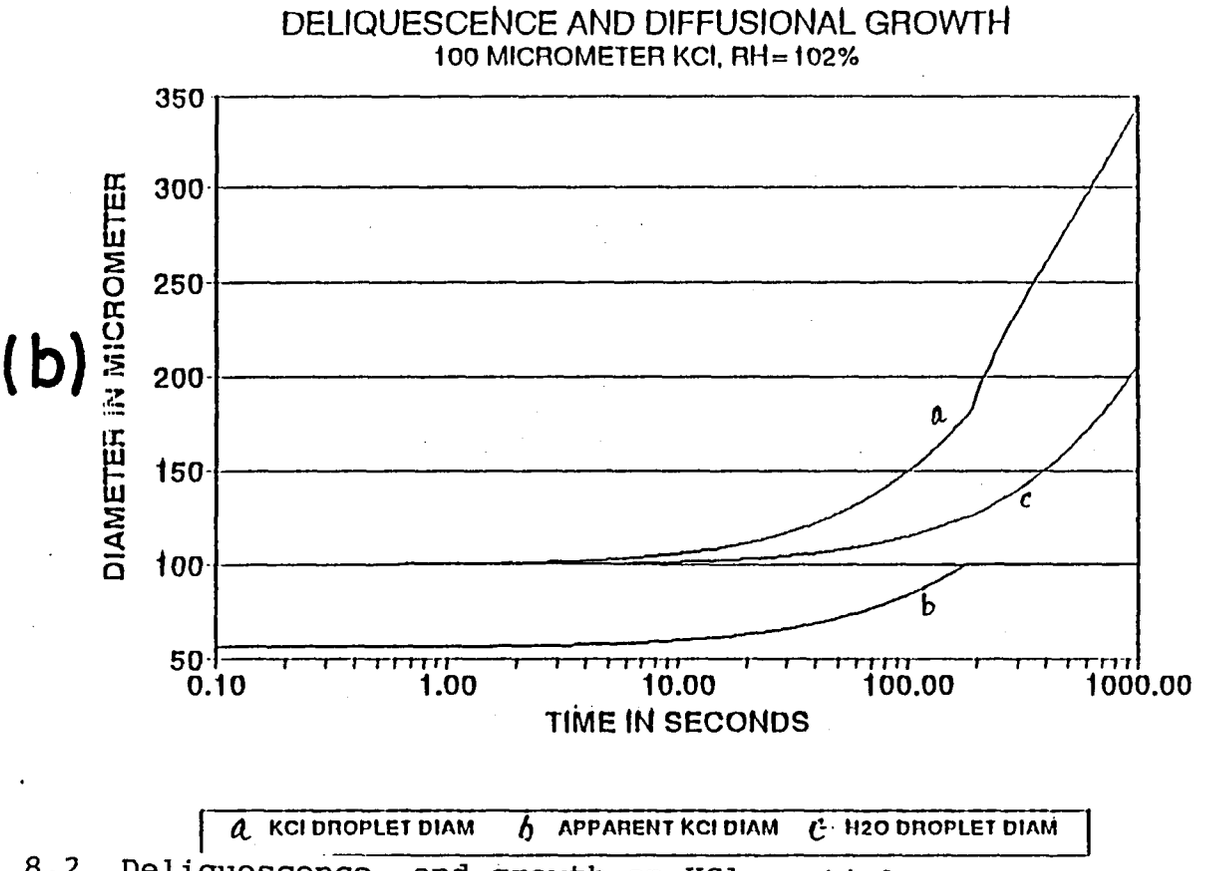

Fig. 8.2 Deliquescence and growth on KCl particle compared to pure water droplet at 102% RH.
(a) 10 μm particle
(b) 100 μm particle

sampling during the airborne tests conducted on 3 October and 14 November 1991. The relative humidity on both occasions was in the region of 80% and the sampling took place less than 2 seconds after the release of the particles.

8.1 Modelling the growth of a population of droplets by diffusion and coalescence

During the diffusional growth of a population of droplets the interaction between the production of supersaturation by the ascending motion and the depletion thereof by condensation plays a crucial role. The level of supersaturation reached determines the number concentration of natural CCN activated and the size growth tempo of these particles. It can therefore be anticipated that changes made to the CCN spectrum ingested by clouds could have effects on the supersaturation profile and therefore also on the droplet population.

A model utilizing the general subroutine already described was developed to investigate these factors numerically. Cloudbase temperature, pressure and a constant updraft are prescribed. Using a constant time step of 1 second the following equations are used to determine the relevant parameters.

1. As a first approximation determine temperature on next level by

$$dT/dz = -g/c_p$$

where T is temperature, z altitude, g acceleration due to gravity and c_p the specific heat. Now the effect of condensational heat is introduced:

$$dT/dw = L/c_p$$

where L is latent heat of condensation and w the condensed water. Initially dw is zero but it will converge to a finite value during the iteration process that follows.

2. Fukuta (1990) described a scheme to determine the supersaturation. The production of supersaturation by condensation is determined by

$$dS/dz = (\epsilon L g/R^2)(1/c_p - T/(\epsilon L))$$

and the depletion of supersaturation by

$$dS/dw = -(p\epsilon L^2/(c_p R T^2 \epsilon e))$$

where ϵ = 0.622, R is the specific gas constant and e is the vapour pressure.

3. The natural CCN concentration activated is determined using

$$N = aS^b$$

where the parameters a and b can be varied to characterize the CCN spectrum. Each droplet formed is assumed to be at the critical radius for the given supersaturation.

4. Diffusional growth is allowed using the general subroutine. The total mass of water condensed is determined and iteration through steps 1 to 4 is done until convergence occurs.

The determined temperature, supersaturation, droplet sizes and concentration are therefore all in equilibrium for the given conditions.

(a) Coalescence growth

A stochastic coalescence subroutine using the Monte Carlo scheme as suggested by Gillespie (1975) was obtained from NCAR. The only modification made to this routine was to introduce the option to keep track of the transfer of soluble nuclei during coalescence events. The main programme was also adapted to provide all the input needed by the subroutine. This routine is very computer time consuming therefore limiting the volume of the parcel that can be considered.

(b) Model runs

Model runs were done to simulate the evolution in the droplet spectrum formed on a typical continental CCN spectrum and one that was seeded with a number of hygroscopic nuclei. Only a cubic centimetre of cloud was considered and therefore the larger flare particles' effects, produced in low concentrations, could not be realistically considered. The only aim of these runs was to investigate the expected interaction between supersaturation, and droplet characteristics.

In Figure 8.3 the size distribution of the 20 KCl nuclei used for the seeded run is shown. Figure 8.4 depicts the supersaturation profiles above cloudbase of the natural and seeded cases. As the hygroscopic particles causes an increased flux from the vapour to the liquid phase, the peak supersaturation reached in the seeded case is lower. It occurs at a slightly higher elevation above cloudbase which also assists in broadening of the droplet spectrum nucleated on the natural CCN, as there is a longer time span between the activation of the first drops and the last drops activated at the level of maximum supersaturation.

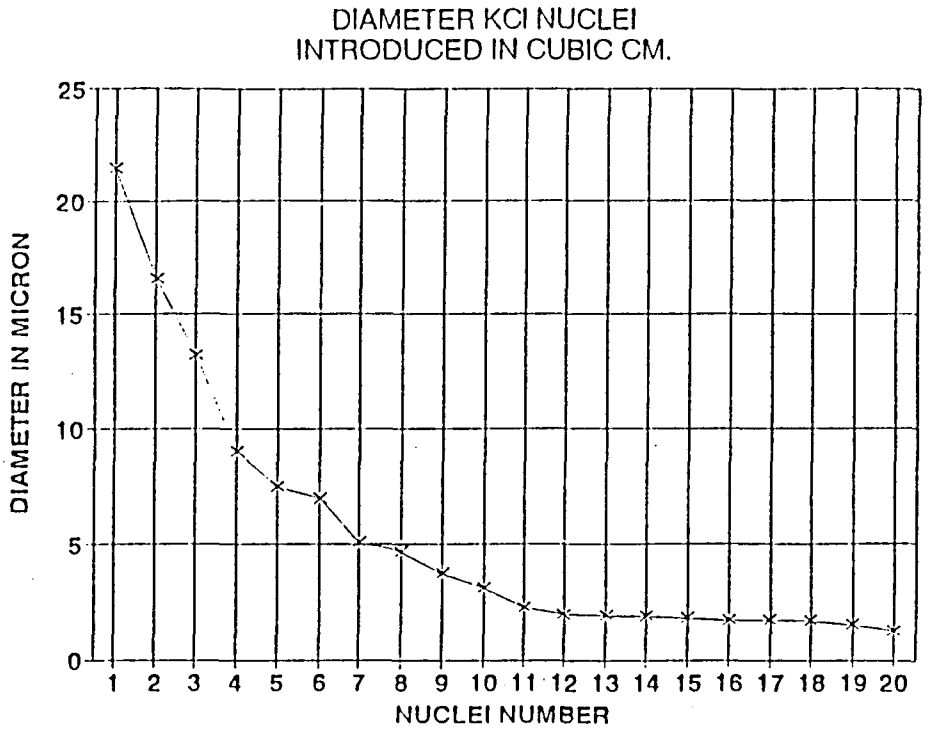

Fig. 8.3 Diameter in micron of KCl particles introduced for seeded run.

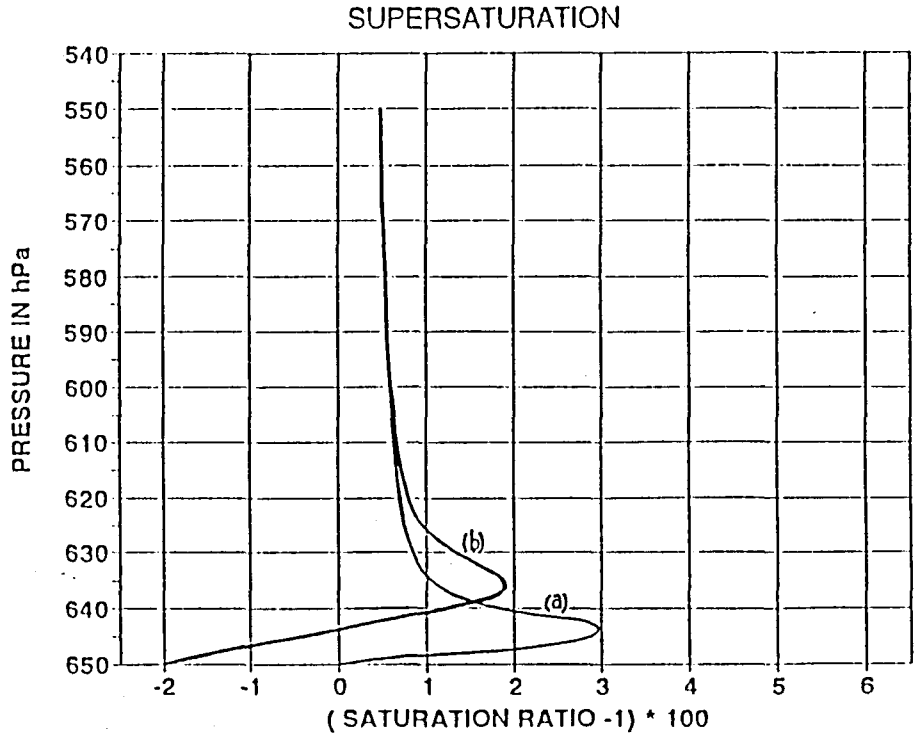

Fig. 8.4 Supersaturation profiles above cloudbase.
(a) Natural CCN
(b) Natural CCN and 20 KCl particles

The droplet number concentrations as a function of height above cloudbase is shown in Figure 8.5. Significantly less drops are activated in the seeded case as a result of the modified supersaturation profile. The present 20 artificial nuclei caused about 80 less natural CCN to be activated. As a constant updraft of $5ms^{-1}$ was prescribed in both cases, the liquid water content was the same. This secondary effect also assisted in creating bigger drops on average. Also shown in this figure are the coalescence events indicated by discontinuities on the two number concentration profiles. A significantly more active coalescence process is present in the seeded case.

From this theoretical study some important secondary effects caused by the introduction of hygroscopic particles at cloudbase in an updraft are indicated. These effects should be considered in a detailed hygroscopic seeding hypothesis and verified with physical measurements.

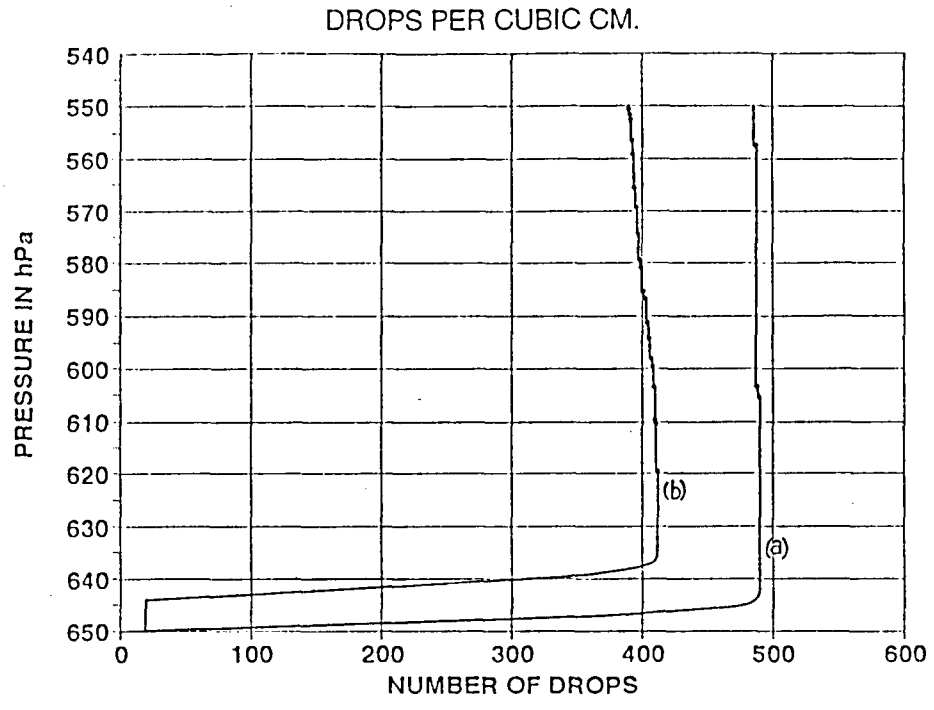

Fig. 8.5 Droplet concentration above cloudbase.
(a) Natural CCN
(b) Natural CCN and 20 KCl particles

responsible for the apparent increases in rainfall, and are also indicating areas where additional measurements are required. Tapes of microphysical measurements made in local storms are being routinely sent to NCAR for comparison with model outputs. This valuable feedback loop between field measurements and laboratory modelling should reveal the links in the chain of events leading to the apparent rainfall increases, as well as leading towards optimization of the choice of seeding materials and techniques.

Further field experiments should now proceed in parallel with the planning of an area experiment, the next and most crucial step in the development of a cloud seeding technology aimed at increasing South Africa's water resources. Steps that have been taken in this direction have shown that:

- we can measure rainfall over an area with a carefully calibrated meteorological radar (Section 3)

- modest (8 to 10 percent) increases in rainfall over model-calibrated catchment areas can produce a fourfold increase in streamflows

- a major public relations effort will be required in and around any areas selected for an experiment.

Next, the potential users of additional water must be pursuaded to become actively involved in the planning of an area experiment. The choice of the area, the design of the experiment, the measurements that will be required (streamflow, rain gauges, radar etc), must be agreed upon since it will be up to these users to evaluate the benefits accruing from the application of a rainfall augmentation capability.

ACKNOWLEDGEMENTS

The research described in this report was jointly funded by the Water Research Commission and the Department of Environmental Affairs.

The Steering Committee responsible for this project, consisted of the following persons:

Dr. G C Green	Water Research Commission (Chairman)
Mr. F P Marais	Water Research Commission (Secretary)
Mr. H Maaren	Water Research Commission
Mr. P S du Toit	Weather Bureau
Mr. C G Groenewald	Weather Bureau
Dr. J F Eloff	Agricultural Research Council
Dr. D vd S Roos	EMATEK, CSIR
Dr. A Seed	Department of Water Affairs and Forestry
Prof. P J T Roberts	Institute for Commercial Forestry Research
Prof. J M de Jager	University of the Orange Free State
Dr. J A Lindesay	University of the Witwatersrand
Prof. J van Heerden	University of Pretoria

The financing of the project by the Water Research Commission and the Department of Environmental Affairs and the contribution of the members of the Steering Committee are acknowledged gratefully.

The authors also wish to record their sincere thanks to the following:

Drs. W A Cooper and R T Bruintjes of the National Centre for Atmospheric Research, Boulder, Colorado, U S A.

Special thanks are accorded to Dr. G C Green for his sage advice during the final stages of the preparation of this report.

REFERENCES

Braham, R.R., Jr., 1964: What is the role of ice in summer rain showers? J. Atmos. Sci., 21, 640-645.

Dixon, M., and G.K. Mather, 1986: Radar evaluation of a randomized rain augmentation experiment. Preprints: 10th Planned and Inadvertent Weather Modification Conference, AMS Boston, 139-141.

Doneaud, A.A., P.L. Smith, A.S. Dennis, and S. Sengupta, 1984: The area-time integral as an indicator for convective rain volumes. J. Clim. Appl. Meteor., 23, 555-561.

Fukuta, N., 1990: Water supersaturation in convective clouds. Preprints: Conference on cloud physics, San Francisco. Amer. Met. Soc., 80-85.

Gillespie, D.T., 1975: An exact method for numerically simulating the stochastic coalescence process in a cloud. J. Atmos. Sci., 32, 1977-1989.

Hindeman, E.E., 1978: Water droplet fogs formed from pyrotechnically generated condensation nuclei. J. Wea. Mod., 10, 77-96.

Kraus, T.W., R.T. Bruintjes, J. Verlinde and A Kahn, 1987: Microphysical and radar observations of seeded and nonseeded continental cumulus clouds. J. Climate Appl. Meteor., 26, 585-606.

Mader, G.N., 1979: Numerical study of storms in the Transvaal. S. African Soc. J. 61, No. 2.

Mather, G.K., D. Treddenick and R. Parsons, 1976: An observed relationship between the height of the 45 dBz contours in storm profiles and surface hail reports. J. Appl. Meteor., 15, 1336-1340.

------- 1989: Estimates of precipitation embryo densities using measurements from an aircraft radar. J. Appl. Meteor., 28, 1089-1097.

-------, 1991: Randomized cloud seeding experimentation for assessing potential for rainfall augmentation in the Nelspruit district. PhD Thesis, Department of Atmospheric Science, University of the Orange Free State, Bloemfontein.

--------, 1991: Coalescence enhancement in large multicell storms caused by emissions from a Kraft paper mill. J. Appl. Meteor., 30, 1134-1146.

Mielke, P.W., Jr., Cooper, W.A., Holroyd, E.W., III, Super A.B., Silverman, B.A., Dennis, A.S., Smith, P.L., Berry, K.J., Orville, H.D., and J.R. Miller, Jr., 1987: HIPLEX-1: Experimental design and response variables. J. Climate Appl. Meteor., 23, 497-512.

Morgan, G., B.J. Morrison and G.K. Mather, 1989: Measurements of total and condensed water mixing ratios in warm-based cumulus clouds by a jet engine evaporation technique. Theor. Appl. Climatol., 40, 187-199.

PAWS - Phase 1, 1983-1986, 4 Volumes. Report Nos. 133/1-4/88.

PAWS - Phase 2, 1987-1989, 3 Volumes. Report Nos. 133/5-7/90.

Pruppacher, H.R., and J.D. Klett, 1978: Microphysics of clouds and precipitation. D. Reidel, Dordrecht, Holland, 714pp.

Simpson, J., 1980: Downdrafts as linkages in dynamic cumulus seeding effects. J. Appl. Meteor., 19, 477-487.

Smith, P.L., and D.E. Cain, 1983: Use of sequential analysis methods in adjusting radar rainfall estimates on the basis of rain gage data. Report 83-2, Institute of Atmospheric Science, S. Dakota School of Mines and Technology, 84pp.

Steyn, P.C.L., and R.T. Bruintjes, 1990: Convective cloud characteristics for the Bethlehem area. Water SA, Vol. 16, No. 2, 115-118.

Wilson, J.W., and D.M. Pollock, 1970: Rainfall measurements during hurricane Agnes by three overlapping radars. J. Appl. Meteor., 13, 835-844.

Woodley, W.L., A.G. Barriston, J.A. Flueck and R. Brondini, 1983: The Florida area cumulus experiment's second phase (FACE-2), Part II: Replicated and confirmatory analysis. J. Climate Appl. Meteor., 22, 1529-1540.

APPENDIX 1 - AIRCRAFT MEASUREMENTS

(a) Vertical velocity system

Vertical velocity measurements play a vital role in the analysis and interpretation of microphysical measurements at cloud base, especially in the case of rain rate and reflectivity calculations derived from the 2D-P probe observations. The results of the development and calibration of the vertical velocity system (VVS) are shown. The system consists of the following components:

- a rate gyro, to determine aircraft pitch
- the angle of attack vane, and
- an accelerometer to determine aircraft acceleration.

The equation for the vertical velocity is:

$$w = -TAS \sin\alpha + w_a \qquad (1)$$

where w is the vertical velocity, TAS is the corrected True Air Speed in metres per second, α the instantaneous angle of attack, and w_a is the vertical velocity of the aircraft (determined from the pitch rate and vertical acceleration).

For α small and in radians:

$$w = -TAS\alpha - \int_0^\tau (- TAS\ p + a)dt \qquad (2)$$

where dt is the time interval between data records for the Data Acquisition System (DAS), i.e. 0.1 s in fast mode and 1 s in slow mode, p is the pitch rate in radians per second, and a is the vertical acceleration.

For sinusoidal oscillations in the aircraft flight path ("roller coasters"), the vertical velocity in (2) is zero. To ensure this, the angle of attack requires an upwash coefficient u, due to airflow interference about the airframe, and (2) becomes:

$$w = - u\ TAS\alpha - \int_0^\tau (-TAS\ p + a)\ dt \qquad (3)$$

The upwash coefficient for an angle of attack vane far away from the airframe should be close to one, with the coefficient decreasing as the vane nears the airframe.

To calibrate the VVS, the aircraft is flown in a vertical sinusoidal pattern ("roller coasters"). Two corrections are then applied to the vertical velocity profile. The first correction assumes that the aircraft is in balanced straight and level flight once fast mode is entered prior to actual penetration of the cloud. All the values are averaged over one second, and the angle of attack, rate gyro, and accelerometer values for the

first second are "frozen", and are subtracted from the values that follow, i.e. the values that follow are all relative to the first values:

$$w_{fi} = w_i - w_f$$

$$= - u\ TAS\ (\alpha_i - \alpha_f - (-\ TAS\ (p_i - p_f) + a_i - a_f) \quad (4)$$

for i = 1, N where N is the number of observations for the penetration, and the subscript f refers to the "frozen value", that is i = 1. We therefore have $w_{f1} = 0$ (since $w_1 = w_f$).

The second is a slope correction: since the aircraft resumes balanced straight and level flight after the roller coasters, the vertical velocity in (4) is zero. This is done by applying a slope correction to the values to "force" the last point on the right hand side of the curve to zero:

$$w_{si} = w_{fi} - \alpha_i\ (w_N - w_1)/N \quad (5)$$

for i = 2, N; where N is the number of observations, and s refers to the slope correction. Note that i begins at 2 since w_{f1} is already zeroed from the first correction. Fig. A1.0 shows the various components that make up the vertical velocity, once the above mentioned corrections have been applied, gathered during a test flight on 1990-12-12.

In practice, the procedure differs slightly from that above in that the freeze and slope corrections are applied first and the upwash coefficient determined last. Fig. A1.1 gives a comparison of the vertical velocity values before and after the calculation of the upwash coefficient (1 and 0.262 respectively) for the same test flight as Fig. A1.0.

(b) Measurements of cloud liquid water

The water content of a cloud is as important a measurement as vertical velocity (updraft). The two, of course, are related since it is the vertical ascent which leads to the condensation of the water vapour in the cloud volume. On the Learjet, cloud water is measured using 3 instruments;

- the CSIRO-King liquid water content probe
- the engine-temperature sensor (E.T.)
- the Lyman-alpha sensor (LA).

All these instruments have been described in previous reports. Here, we present an comparison from a recent flight in which all the cloud water around the -10°C level was contained in cloud droplets (< 100 µm in diameter) i.e. precipitation had not started to form. These comparisons are presented in Figs. A1.2(a) (b) and (c) and the coefficients from the linear regressions, in which one of the points is (0, 0), are listed in Table A1.1. Both

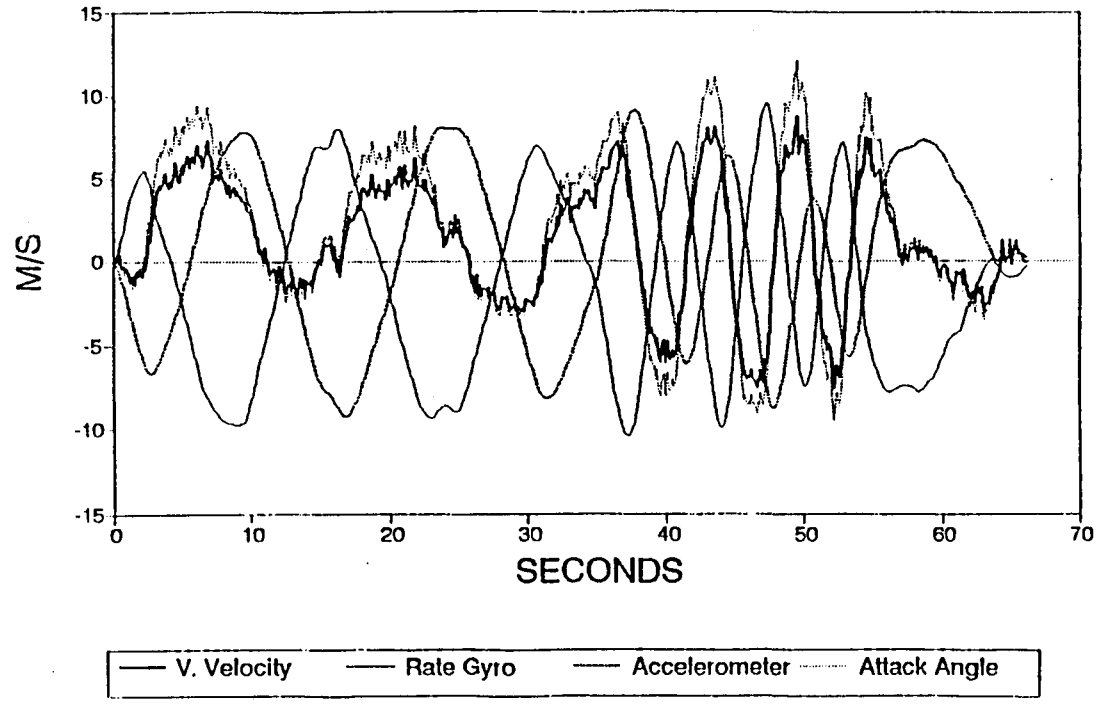

Fig. A1.0 Outputs from accelerometer and angle of attack sensors in "roller-coaster" tests in still air, December 12, 1990.

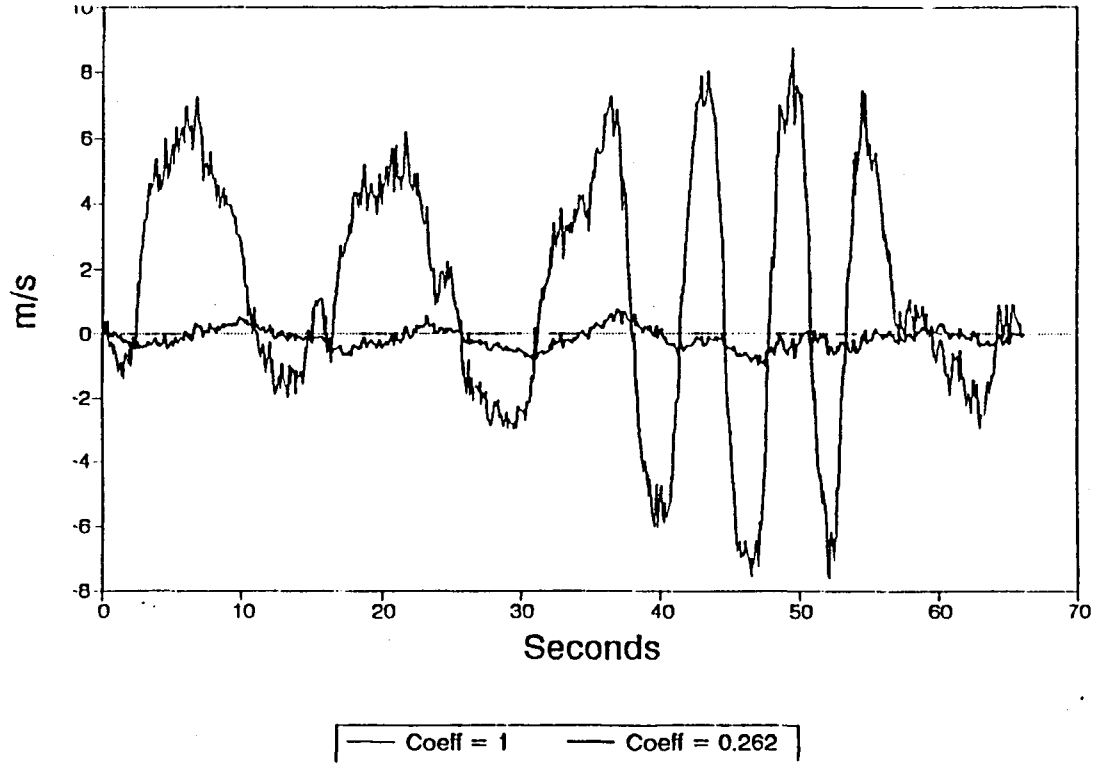

Fig.A1.1 Gust velocity before and after the application of an upwash correction.

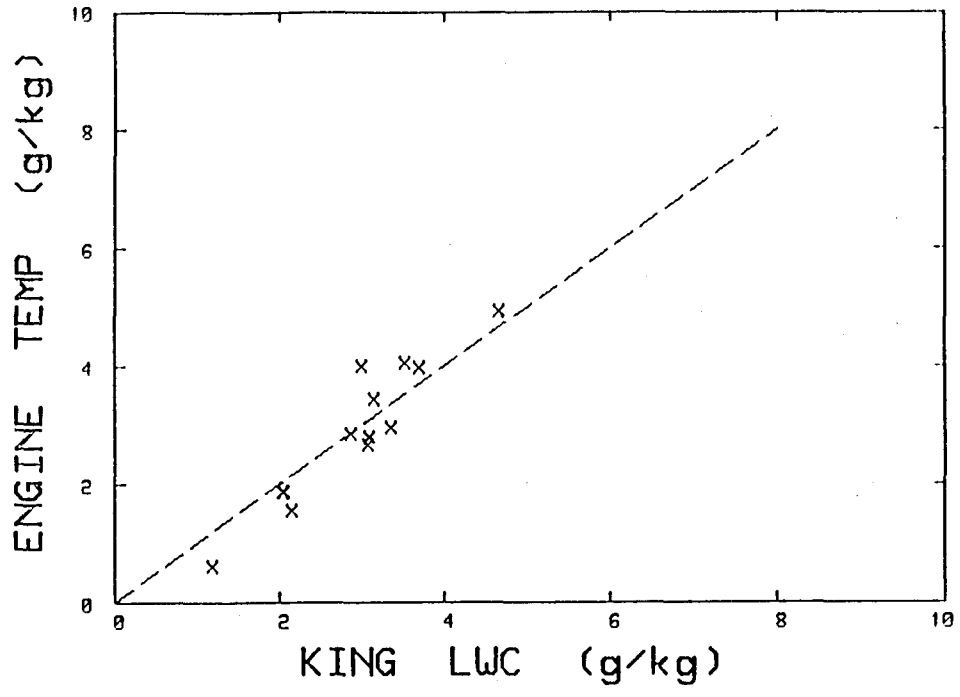

Fig. A1.2(a) Engine temperature (E.T.) and King comparisons of liquid water measurements.

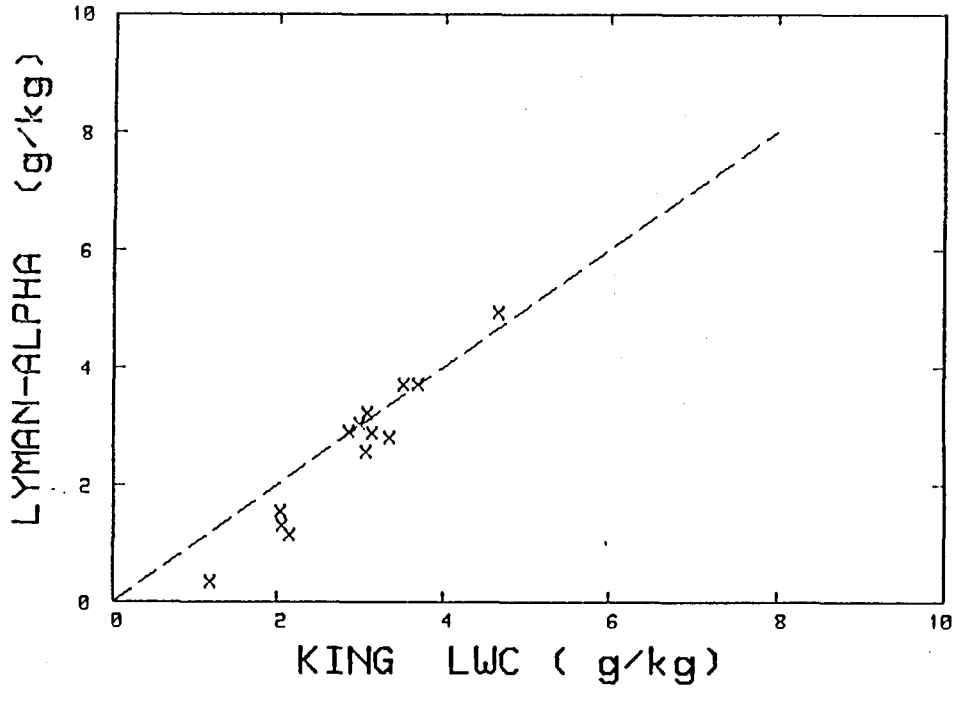

Fig. A1.2(b) Lyman-alpha (LA) and King comparisons.

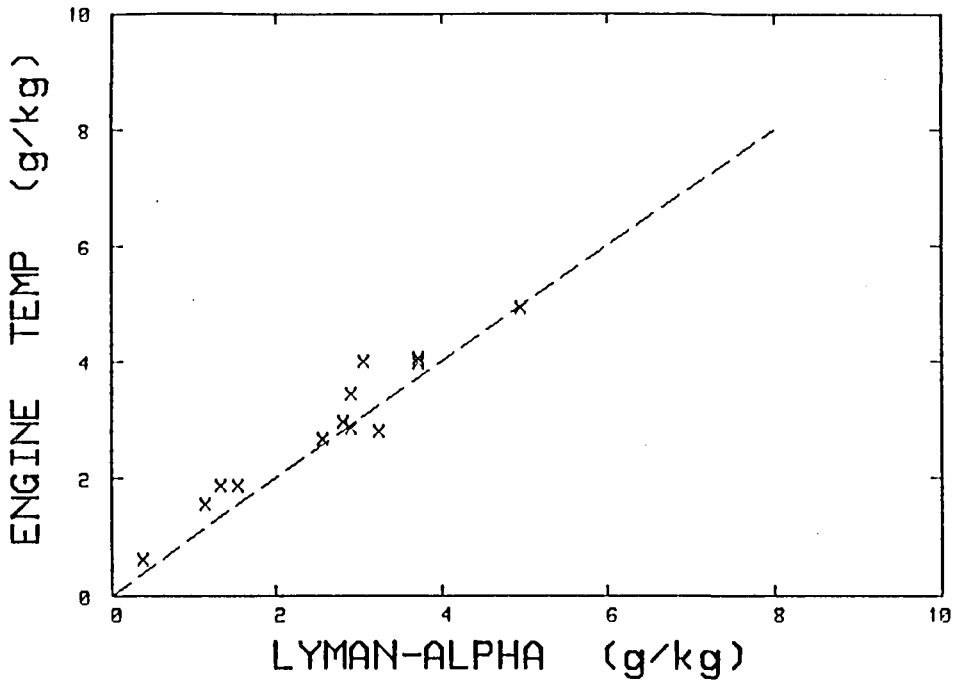

Fig. A1.2(c) E.T. and LA comparisons. See Table 6.0 for regression coefficients.

the E.T. and LA comparisons with the King are similiar. The King device appears to read high in conditions of low liquid water. The comparison between the LA and E.T. measurement looks reasonable over the range from 0 to about 6 g/kg. Standard deviation of the LA from the E.T. is 1.34 g/kg (66% of the LA values are within 1.34 g/kg of the E.T. values).

Table A1.1 Linear regression values for cloud water instrument comparisons

y	x	a	b	r
E.T.	King	-0.42	1.15	0.95
LA	King	-0.69	1.16	0.96
E.T.	LA	0.31	0.97	0.97

Key : $y = a + bx$
r = correlation coefficient

These comparisons indicate that reasonable estimates of the higher total water content (10 - 12 g/kg) routinely encountered in clouds containing cloud water and precipitation can be obtained by a simple linear extrapolation of the E.T. and LA calibrations.

(c) Bethlehem aircraft instrumentation - JRA

The instrumentation on the two Aerocommander 690A's is described in terms of the type of instrument used to measure certain parameters, the calibration of the various instruments (where applicable), and also the relevant equations and calculations to produce the parameters.

(i) Accelerometer

The accelerometer used is a Schaevitz linear accelerometer LSBC2 (s/n 11016). The range of counts is from 32770 to 65482. Measurement range is from -2 to +2 g, and the output voltage from 0.001 to 9.984 volts.

The acceleration (ms^{-2}) is given by:

$$ACCEL = -9.81 * (a_{14} - 32767) / (3282 * 2.496)$$

where a_{14} is the system count of analogue channel 14.

(ii) Angle of attack

The angle of attack vane is the standard aviation vane fitted to the fuselage of the Rockwell Aerocommander 690A. The range of counts is from 32767 to 65534. Measurement range is from 0.0 (fully down) to 54.6 (completely up) degrees and the output voltage from 0.0 to 10.0 volts.

The angle of attack is given by:

$$AOA = -27.3 + (a_{15} - 32767) / 600.13$$

where a_{15} is the system count of analogue channel 15.

The angle of attack formula is calculated as follows:

54.6 degrees gives a voltage range of 10 volts
10.0 * 3276.7 = 32767 gives the system counts range
Therefore the number of system counts per degree is:
32767 / 54.6 = 600.13 (This is the inverse of the gradient)
System counts for 0.0 volts 32767 + 0.0 * 3276.7 = 32767
System counts for 10. volts 32767 + 10.0 * 3276.7 = 65534
We apply a correction of half the range of the angle of attack to give us zero degrees for straight and level.
Therefore -27.3 + (a_{15} - 32767) / 600.13 is the equation.

(iii) Navigation

A Trimble Navigation model TNL-2000 GPS navigator (s/n 21273) is installed and used to record aircraft position in latitude (in the format N#dd#mmhh#) and longitude (in the format W#ddd#mmhh), track (degrees magnetic), groundspeed (knots) and annunciators and errors. The latitude and longitude is converted to give the aircraft range and heading from the ground-based radar.

(iv) Heading

The heading is taken from the standard aircraft instrumentation in synchronous form. The heading in degrees is:

$$HDG = s_2 / 182.04$$

(v) Humidity

The Vaisala 1518 HM humidity sensor is fitted to the Vaisala HMP 14 reverse flow temperature/humidity probe in a housing developed at the BPRP. The range of counts is from 32767 to 36044. Measurement range is from 0 to 100% and the output voltage is from 0 to 1 volt.

The relative humidity (%) is given by:

$$RH = (a_6 - 32767) / 32.767$$

where a_6 is the system count for analogue channel 6.

The humidity is calibrated prior to every flight using one of two Vaisala HMK 11 humidity calibrators (s/n 15704 and 14923) with calibration points of 13 and 97%.

The humidity formula is calculated as follows:

100 percent gives a volt range of 1.0
3276.7 gives the system counts range
Therefore the number of system count per percent is:
3276.7 / 100 = 32.767 (This is the inverse of the gradient)
System counts for 0 % are 32767
System counts for 100 % are 32767 + 1.0 * 3276.7 = 36044
Therefore (a_6 - 32767) / 32.767 is the equation.

(vi) Liquid water content

Two probes are in use, the Johnson-Williams (JW) and the CSIRO King.

The King lwc probe model KLWC-5 (s/n 17849-1189-38) uses a PMS sensor model HW03. The range of counts is from 32767 to 65534. Measurement range is from 0.0 to 5.0 gm^{-3} or 0.0 to 1.0 gm^{-3} and the output voltage from 0.0 to 10.0 volts (we have to date only operated the sensor in the 0 to 5 mode).

The King lwc is given by:

While flying through clear air prior to an in-cloud run:

$$P_{DRY} = 10.0\ |V|_{A(DRY)}$$

$$P_{WET} = P_{TOTAL} - P_{DRY}$$

$$= 10.0 * (|V|_{A(TOTAL)} - |V|_{A(DRY)})$$

$$KLWC = P_{WET} / (0.099 * v)$$

where KLWC is the liquid water content in gm^{-3}, V is the analogue value in volts, P is the power in Watts, and v is the true airspeed in m/s.

The analogue equation while in-cloud sampling is:

$$KLWC = (10.0 * (a_{11(total)} - a_{11(dry)}) / 3276.7) / (0.099 * TAS)$$

where a_{11} is the system count of analogue channel 11.

The King lwc formula is calculated as follows:

0.0 to 5.0 gm^{-3} gives a voltage range of 10.0
10.0 * 3276.7 = 32767 gives the system counts range
Therefore the number of system counts per volt is:
32767/10.0 = 3276.7 (This is the inverse of the gradient)
System counts for 0.0 volts 32767 + 0.0 * 3276.7 = 32767
System counts for 10.0 volts 32767 + 10.0 * 3276.7 = 65534
Therefore (a_{11} - 32767) / 3276.7 is the basic equation to give the probe output in volts (so that it can be converted to power and then corrected for the dry term to give lwc).

The JW lwc comprises a sensor (s/n 177), power supply (s/n 7105) and a Johnson-Williams dummy sensor head (s/n 7105) model LWH calibrated for 100 knots.

The range of counts is from 32767 to 38505. Measurement range is from 0.0 to 2.0 gm^{-3} and the output voltage from 0.0 to 1.751 volts.

The JW lwc is given by:

$$JWLWC = 51.48 * (a_4 - 32767) / 2869.0 / TAS$$

where a_4 is the system count of analogue channel 4.

The JW lwc formula is calculated as follows:

2 gm^{-3} gives a voltage range of 1.751 volts
1.751 * 3276.7 = 5737.5 gives the system counts range
Therefore the number of system counts per gm^{-3} is:
5737.5 / 2.0 = 2868.75 (This is the inverse of the gradient)
System counts for 0.0 volt 32767 + 0.0 * 3276.7 = 32767
System counts for 1.751 volt = 38504.5
The basic equation is therefore: (a_4 - 32767) / 2868.75
A correction factor for TAS needs to be added for the 100 knots (51.49 ms^{-1}) calibration of the dummy sensor head.
Therefore 51.49 * (a_4 - 32767) / 2869 / TAS is the equation.

(vii) Pressure

Static pressure is measured using a Rosemount Model 1201FA1B2B pressure sensor (s/n 1398). The range of counts is from 32773 to 65554. Measurement range is from 0 to 32 in-Hg and the output voltage is from 0.002 to 10.006 volts.

The static pressure in millibars is given by:

$$STP = 1083.64 - (65535 - a_7) / 30.235$$

Pitot pressure is measured using a Rosemount Model 1221F2VL18B2A sensor (s/n 389). The range of counts is from 32767 to 49151. Measurement range is from 0.000 to 1.000 psi and the output voltage is from 0.000 to 5.000 volts.

The pitot pressure in millibars is given by:

$$PTP = (a_3 - 32767) / 237.63$$

(viii) Radar

The aircraft has a Bendix RDS82V, 3 cm radar, with 90 degrees horizontal scan and 30 degrees vertical scan capability.

(ix) Rate gyro

Northrop Rate Gyro (s/n 1534) part no. 6459-301. The range of counts is from 33684 to 64420. Measurement range is from 30 (nose down) to -30 degrees per second (nose up) and the corresponding output voltage from 0.28 to 9.66 volts.

The pitch rate ($deg.s^{-1}$) is given by:

$$RG_{(volts)} = (a_5 - 32767) / 3276.7$$

and

$$RG = -6.521 * RG_{(volts)} + 32.399$$

where a_5 is the system count of analogue channel 5.

The rate gyro formula is calculated as follows:

-60 degrees per second gives a voltage range of 9.38
9.38 * 3276.7 = 30735.4 gives the system counts range
Therefore the number of system counts per volt is:
30735.4 / 9.38 = 3276.695 (The inverse of the gradient)
System counts for 0.28 volt 32767 + 0.28 * 3276.7 = 33684
System counts for 9.66 volt 32767 + 9.66 * 3276.7 = 64420
Therefore (a_5 - 32767) / 3276.695 gives the voltage.
The linear regression on the calibration data, for volts vs degrees/second is y = -6.521 * x + 32.399

(x) Temperature

The Vaisala HMP 14 reverse flow temperature/humidity probe uses a housing developed at the BPRP and a thermistor YSI 44203 temperature sensor. The range of counts is from 37046 to 34418. Measurement range is from -30 to +50°C and the output voltage from 1.306 to 0.504 volts.

The reverse flow temperature is given by:

$$RFT = 50.0 - (34418 - a_1) / 32.85$$

where a_1 is the system count of analogue channel 1.

The reverse flow temperature sensor is calibrated prior to each flight at points -15 and +50°C.

The reverse flow formula is calculated as follows:

80 degrees gives a voltage range of (1.306 - .504) 0.802
0.802 * 3276.7 = 2628 gives the system counts range
Therefore the number of system counts per degree is:
2628 / 80 = 32.85 (This is the inverse of the gradient)
System counts for -30 deg. 32767 + 1.306 * 3276.7 = 37046
System counts for 50 deg. 32767 + 0.504 * 3276.7 = 34416
Therefore 50.0 - (34416 - a_6) / 32.85 is the equation.

The total temperature is measured using a Rosemount Model 102 AU1AF de-iced probe with a Rosemount Model 510BF148 amplifier (s/n 478). The range of the counts is from 32768 to 49150. Measurement range is from -50 to +50°C and 0.0004 to 4.9997 volts.

The Rosemount temperature is given by:

$$RMT = (a_0 - 32768) / 163.81 - 50.0$$

where a_0 is the system count of analogue channel 0.

The Rosemount formula is calculated as follows:

100 degrees gives a volts range of (4.9997 - 0.0004) 4.9993
4.9993 * 3276.7 = 16381 gives the system counts range
Therefore the number of system counts per degree is:
16381 / 100 = 163.81 (This is the inverse of the gradient)
System counts for -50 deg. 32767 + 0.0004 * 3276.7 = 32768
System counts for 50 deg. 32767 + 4.9997 * 3276.7 = 49150
Therefore (a_0 - 32768) / 163.81 - 50.0 is the equation.

(d) Bethlehem aircraft instrumentation - JRB

(i) Accelerometer

The accelerometer used is a Schaevitz linear accelerometer LSBCG2 (s/n 6386).

(ii) Angle of attack

The angle of attack vane is the model 861 fuselage mounted flow angle sensor.

(iii) Navigation

Trimble GPS as for JRA.

(iv) Heading

The heading calculation is the same as for JRA.

(v) Humidity

The Vaisala 1518 HM humidity sensor is fitted to the Vaisala HMP 14 reverse flow temperature/humidity probe in a housing developed at the BPRP. The range of counts is from 32767 to 36044. Measurement range is from 0 to 100% and the output voltage is from 0 to 1 volt.

The relative humidity (%) is given by:

$$RH = (a_6 - 32767) / 32.767$$

where a_6 is the system count for analogue channel 6.

The humidity is calibrated prior to every flight using one of two Vaisala HMK 11 humidity calibrators (s/n 15704 and 14923) with calibration points of 13 and 97%.

(vi) Liquid water content

Two probes are in use, the Johnson-Williams (JW) and the CSIRO King.

The King lwc probe model KLWC-5 (s/n 17849-1189-41) uses a PMS sensor model HW03. The range of counts is from 32767 to 65534. Measurement range is from 0.0 to 5.0 gm^{-3} or 0.0 to 1.0 gm^{-3} and the output voltage from 0.0 to 10.0 volts (we have to date only operated the sensor in the 0 to 5 mode). The King lwc is given by following the same procedure as for JRA.

The JW lwc comprises a sensor (s/n 175), power supply (s/n 7107) and a Johnson-Williams dummy sensor head (s/n 7107-8) model LWH calibrated for 100 knots. The range of counts is from 32767 to 38505. Measurement range is from 0.0 to 2.0 gm^{-3} and the output voltage from 0.0 to 1.751 volts. The JW lwc is given by the same equation as for JRA.

(vii) Pressure

Static pressure is measured using a Rosemount Model 1201FA1B A pressure sensor (s/n 949). The range of counts is from 32783 to 49164. Measurement range is from 0 to 32 in-Hg and the output voltage is from 0.005 to 5.004 volts.

The static pressure in millibars is given by:

$$STP = 1083.65 - (49164 - a_7) / 15.12$$

Pitot pressure is measured using a Rosemount Model 1221F2VL18B2A sensor (s/n 390). The range of counts is from 32767 to 49164. Measurement range is from 0.000 to 1.000 psi and the output voltage is from 0.000 to 5.004 volts.

The pitot pressure in millibars is given by:

$$PTP = (a_3 - 32767) / 237.81$$

(viii) Radar

The aircraft has a Bendix RDS81, 3 cm radar, with 90 degrees horizontal scan capability.

(ix) Rate gyro

The range of counts is from 34438 to 63896. Measurement range is from 30 (nose down) to -30 degrees per second (nose up) and the corresponding output voltage from 0.51 to 9.5 volts.

The pitch rate (deg.s^{-1}) is given by:

$$RG_{(volts)} = (a_5 - 32767) / 3276.7$$

and

$$RG = -6.816 * RG_{(volts)} + 34.148$$

where a_5 is the system count of analogue channel 5.

The rate gyro formula is calculated as follows:

-60 degrees per second gives a voltage range of 9.38
9.38 * 3276.7 = 30735.4 gives the system counts range
Therefore the number of system counts per volt is:
30735.4 / 9.38 = 3276.695 (The inverse of the gradient)
System counts for 0.28 volt 32767 + 0.28 * 3276.7 = 33684
System counts for 9.66 volt 32767 + 9.66 * 3276.7 = 64420
Therefore (a_5 - 32767) / 3276.695 gives the voltage.
The linear regression on the calibration data, for volts vs degrees/second is y = -6.521 * x + 32.399

(x) Temperature

The Vaisala HMP 14 reverse flow temperature/humidity probe uses a housing developed at the BPRP and a thermistor YSI 44203 temperature sensor. The range of counts is from 34418 to 37046. Measurement range is from +50 to -30°C and the output voltage from 0.504 to 1.306 volts.

The reverse flow temperature is given by:

$$RFT = 50.0 - (34418 - a_1) / 32.85$$

where a_1 is the system count of analogue channel 1.

The reverse flow temperature sensor is calibrated prior to each flight at points -15 and +50°C.

The reverse flow formula is calculated as follows:

80 degrees gives a voltage range of (1.306 - .504) 0.802
0.802 * 3276.7 = 2628 gives the system counts range
Therefore the number of system counts per degree is:
2628 / 80 = 32.85 (This is the inverse of the gradient)
System counts for -30 deg. 32767 + 1.306 * 3276.7 = 37046
System counts for 50 deg. 32767 + 0.504 * 3276.7 = 34418
Therefore 50.0 - (34418 - a_6) / 32.85 is the equation.

The total temperature is measured using a Rosemount Model 102 AU1AF de-iced probe (s/n 13577E) with a Rosemount Model 510BF148 amplifier (s/n 477). The range of the counts is from 32767 to 49146. Measurement range is from -50 to +50°C and 0.0000 to 4.9987 volts.

The Rosemount temperature is given by:

$$RMT = (a_0 - 32767) / 163.79 - 50.0$$

where a_0 is the system count of analogue channel 0.

The Rosemount formula is calculated as follows:

100 degrees gives a volts range of (4.9987 - 0.0000) 4.9987
4.9987 * 3276.7 = 16379 gives the system counts range
Therefore the number of system counts per degree is:
16379 / 100 = 163.79 (This is the inverse of the gradient)
System counts for -50 deg. 32767 + 0.000 * 3276.7 = 32767
System counts for 50 deg. 32767 + 4.9987 * 3276.7 = 49146
Therefore (a_0 - 32767) / 163.79 - 50.0 is the equation.

(e) Laser diode for aircraft probes

The Helium-Neon lasers used in the PMS particle imaging and measuring probes have several disadvantages: they are expensive, require careful handling, have a relatively short lifespan (between one and two years), need a high voltage power supply, and need to be imported as required. A diode laser on the other hand is comparatively cheap, does not need careful handling, requires only a five volt power supply, and has a lifetime of up to ten years. In view of these advantages the possibility of using a diode laser in the PMS two dimensional probes was investigated through the Atomic Energy Corporation's (AEC) Optical Energy Systems (OES) section. Preliminary testing of the diode laser has shown it to be a possible candidate for replacing the conventional Helium-Neon laser.

(f) Ground-based software

The Aircraft System is used to analyse the aircraft data. The research team uses the information produced to assist with the cloud research project.

The data sets have been standardized so that the system can process data without differentiation having to be made between the Bethlehem aircraft used or the area where the data have been recorded (Bethlehem or Nelspruit). The output has also been standardized and differentiation is made between the probes used. All duplication in the programmes as well as the output has been removed to create a more streamlined package that is easier to use. A programme has been written to edit the data set of the old aircraft data (1980 - 1989) for processing by the new system.

A user interface has been developed that enables the user to specify a few parameters by which processing and output of the system can be controlled. The user can determine if only a specific time range must be processed and which output reports and files are needed. A date other than the current date can be specified for processing and the system will search for the file

and check if the data set must be edited before processing.

A normal data run will produce an event, picture, history , and sounding report, statistical reports of 2D, pms and air data, time history plots of 2D, air and PMS data and plots of the 2D images. A file with statistical information is created for UNISA. Other reports such as 2D image and buffer analysis reports can be created on request. An in-cloud data file can also be created but is not part of a normal data run.

Error control has been built into the system to ensure ease of use both for users and the maintenance staff. A user manual with full documentation, flow charts, etc. has been written to ensure that the system can be used and understood should the Data Processing staff change in future.

The processing of the aircraft data is done as follows :

Before analysis is done the raw data are calibrated by means of calibration constants that are verified every season. These constants also differ for each aircraft and are stored in a file to keep record of the changes for every season. This file makes programme maintenance a lot easier because it's not necessary to change the programmes every season to make provision for the change in constants.

In the calibration programme (AIRCALIB) these constants are read and used as needed. The fast mode data are processed to get an average per second that is written to a file which serves as input to the analysis programme. The calibrated data are stored in a file and kept on the data base.

In the analysis programme in-cloud averages, minima, maxima and standard deviations are done. Time history plots are drawn and reports with statistical summaries are printed.

(g) Aircraft systems

Development on the aircraft systems is effectively complete, but because of new additions to the systems, development is ongoing.
Additions to the systems were:

1. Trimble GPS navigation systems to replace the Litton INS
2. Synchro to Digital interface for heading, pitch and roll
3. System racks were made to order
4. Bus extenders were added.

The presentation and driver software were extensively updated, with most technical manuals on the interfaces completed. To date the aircraft systems comprise the following:

1. Rack mounted components:
   a. HP Vectra host computer,
   b. Bus extender, allowing up to 12 extra interfaces,
   c. Colour EGA monitor,
   d. Exabyte cassette tape streamer (CTS),
   e. Signal conditioning unit for instruments and low pass filters,
   f. Slide-out keyboard,
   g. Power Supply unit;
2. Cockpit mounted components:
   a. colour EGA monitor,
   b. mini keypad;
3. Interfaces:
   a. PMS 2D probe,
   b. PMS FSSP or 1D probe,
   c. Mini keypad and I/O,
   d. Sixteen channel Analogue to Digital converter for analogue instruments,
   e. RS422 for GPS,
   f. SCSI (for Exabyte CTS),
   g. Synchro to Digital (for aircraft heading);
4. Software for driving the interfaces, and for real-time display and control.

Additions to the aircraft system envisaged for 1992/1993 are:

1. RF telemetry system for real-time transfer of aircraft data to the radar control room,
2. Upgrading the 2D interface to DSP-based card,
3. Digitizing the aircraft radars.

The following ongoing tasks were performed:

1. documenting system changes as they are made,
2. adding new instrumentation and interfaces,
3. upgrading software to accommodate new instrumentation and interfaces, and
4. upgrading and improving present software code and methodology.